



UIT

THE ARCTIC
UNIVERSITY
OF NORWAY

Faculty of Health Sciences

Department of Medical Biology

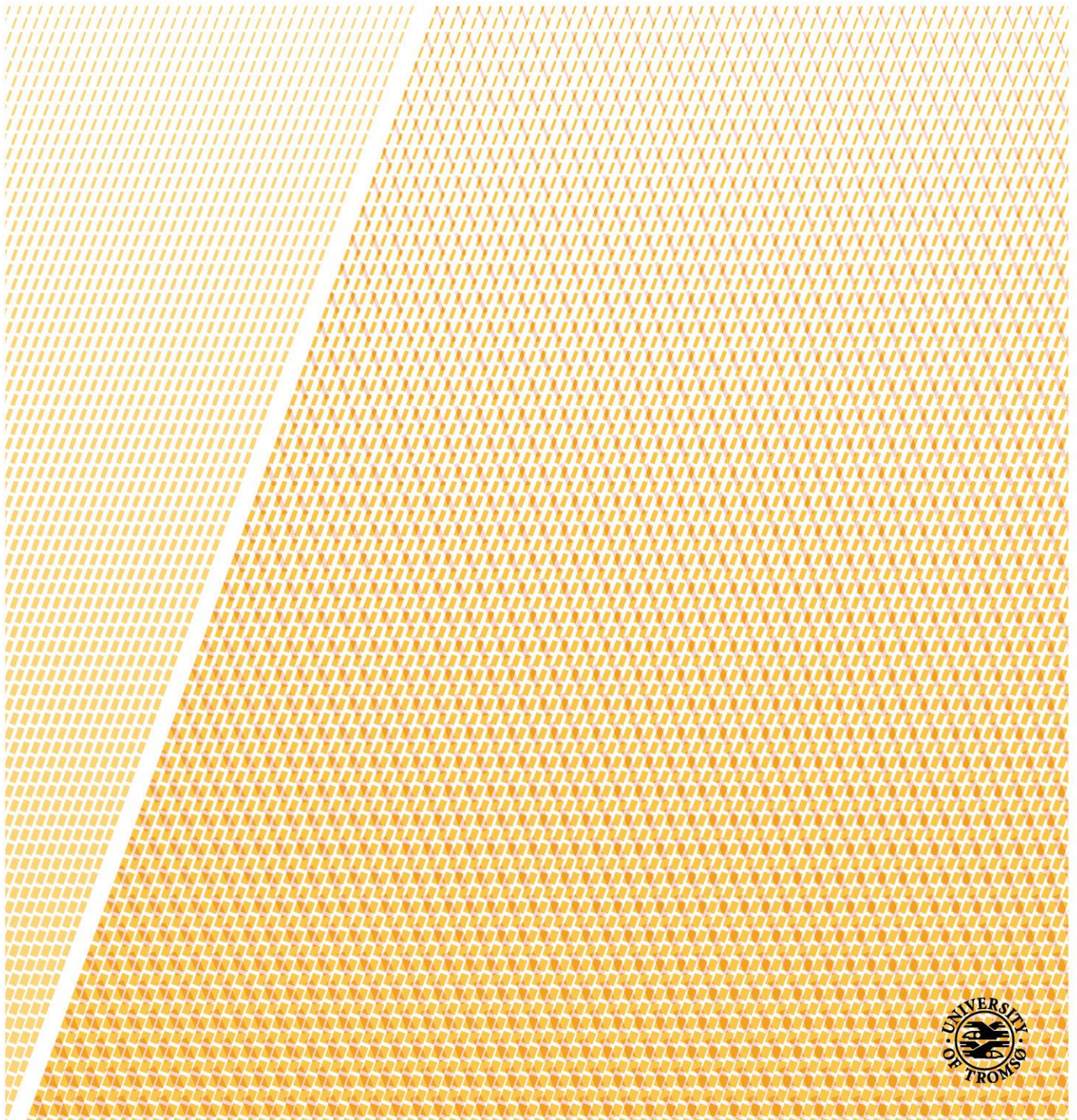
Regulation of Autophagy-related proteins

Roles of post-translational modifications

—

Birendra Kumar Shrestha

A dissertation for the degree of Philosophiae Doctor – September 2019



Regulation of Autophagy-related proteins: Roles of post-translational modifications

By

Birendra Kumar Shrestha



A dissertation for the degree of Philosophiae Doctor

UiT - The Arctic University of Norway

Faculty of Health Sciences

Department of Medical Biology

Molecular Cancer Research Group

September 2019

Table of Contents

| | |
|--|-----|
| Summary | i |
| Acknowledgments | iii |
| List of papers | iv |
| Abbreviations | v |
| Introduction | 1 |
| Ubiquitin Proteasome system (UPS) | 1 |
| Autophagy | 4 |
| Autophagosome biogenesis: Initiation, elongation, closure, and fusion | 6 |
| ATG8 and its LDS and UDS binding surfaces..... | 13 |
| ATG4B | 16 |
| TP53INP1 and TP53INP2 | 17 |
| Regulation of autophagy: Posttranslational modifications | 18 |
| Regulation of autophagy by serine-threonine kinases | 21 |
| STK3/STK4..... | 21 |
| PKC ζ | 22 |
| NIMA-related Kinase 9 (NEK9) | 24 |
| Aims of the study | 26 |
| Summary of papers..... | 27 |
| Discussion | 29 |
| Regulation of the LC3B by phosphorylation of threonine-50 (Paper I)..... | 29 |
| The phospho-mimicking T50E mutant of LC3B regulates LIR-LDS interactions (Paper I) | 31 |
| Acetylation regulates subcellular localization and degradation of TP53INP2 (Paper II)..... | 32 |
| ATG4B-mediated regulation of ATG8s via LIR-mediated binding (Paper III)..... | 35 |
| Methodological considerations..... | 38 |
| References | 40 |

Summary

Autophagy is a cell renovation system that directs almost any type of cell contents for lysosomal degradation and recycling of building blocks. It is fundamental for cellular homeostasis and for determining cell fate in response to stress. Hence, understanding the regulation of autophagy-related proteins is of great importance. This study focuses on the effect of posttranslational modifications on the autophagy proteins LC3B and TP53INP2, and importance of molecular interactions for ATG4B mediated cleavage and delipidation of the ATG8 family proteins.

In the first paper, we shed light on the effect of phosphorylation of LC3B on selective autophagy. LC3B is the most recognized member of the ATG8 family proteins and is used as a readout for autophagy activity. LC3B is enriched in the growing autophagosomal membrane, where it recruits cargo and cargo receptors to the autophagosomes via direct LC3 interacting region (LIR)-LC3 docking site (LDS) interactions. We identified four serine-threonine kinases that phosphorylate LC3B at the threonine 50 (T50) residue. *In vivo* and *in vitro* data show that they interact with LC3B via LIR-LDS mediated interactions. The LC3B T50 residue is adjacent to the LDS motif in LC3B. Importantly, we found that the phospho-mimicking LC3B T50E mutant inhibited the interaction of LC3B with core autophagy proteins and negatively regulated selective autophagy. We showed that NEK9 phosphorylate LC3B T50 and that depletion of NEK9 facilitated autophagic flux. This study thus points to NEK9 as a regulator of selective autophagic flux via phosphorylation of LC3B T50.

In the second paper, we show that subcellular localization of the autophagy protein TP53INP2 is regulated by acetylation. TP53INP2 is previously recognized as a regulator of autophagy, providing nuclear export of LC3B and autophagosome formation by interactions with the ATG8s and VMP1. Here we show that upon mTOR inactivation, nuclear import of TP53INP2 is impaired via acetylation of K187, while its degradation is facilitated by acetylation of K165 and K204. Hence, mTOR dependent re-localization of TP53INP2 is due to enhanced nuclear degradation and cytoplasmic retention.

The functional role of the cysteine protease ATG4B for cleavage and delipidation of ATG8 homologues are well known. In the third paper, we unravel essential residues involved in the ATG4B-ATG8s functional interactions. We identified a canonical LIR motif at C-terminal part of ATG4B and solved the crystal structure of GABARAPL1 in complex with a peptide containing this LIR motif. Our *in vivo* and *in vitro* data showed that the ATG4B C-terminal LIR is important for efficient cleavage of LC3B. Furthermore, it was found to mediate

stabilization of unlipidated GABARAP and GABARAPL1, protecting them from proteasomal degradation.

Acknowledgments

To me, Ph.D. was a learning experience in terms of research, personal life, Norwegian culture, language and most importantly winter at the north. So, I am indebted to everyone that guided me along the journey.

Foremost, this journey of my Ph.D. would be incomplete without continuous love and support from my parents, my wife Neelam and her gift Nirvan.

I would like to thank my supervisor Terje Johansen for providing me an opportunity to explore and understand the field of autophagy. I am thankful for your continuous support, guidance, and freedom to explore without boundaries.

I am in debt to my Co-supervisor Trond Lamark and Eva Sjøttem for sharing scientific knowledge about the field and providing me guidance throughout project work.

My special thanks to Aud, Gry, and Hanne for their hidden works of constantly updating and maintaining lab, thereby helping me work without hindrance. I am also grateful for all those successful and unsuccessful experiments done for my projects.

Mads, Pradip, Steingrim, and Ashish!! thank you for helping me at the early stage of my Ph.D. During my Ph.D., I learned two important things: *on earth there exist only one country Denmark and nothing is as might as ATG4B*. All credit goes to Mads S Rasmussen.

I would like to mention my special thanks to western blot specialist Mutugi “*Blot never looked so beautiful before*”.

Yakubu Princely Abudu “*CRISPR PRINCE*”. Thank you for your help.

Finally, I would like to thank all current and past members of the MCRG group.

List of papers

Paper I

Birendra Kumar Shrestha Mads Skytte Rasmussen, Yakubu Abudu Princely, Jack-Ansgar Bruun, Kenneth Bowitz Larsen, Endalkachew A. Alemu, Eva Sjøttem, Trond Lamark & Terje Johansen (2019)

Phosphorylation of LC3B at threonine-50 inhibits selective autophagy. *Manuscript*

Paper II

Birendra Kumar Shrestha, Eva Sjøttem, Aud Øvervatn, Hanne B Brenne, Jack-Ansgar Bruun, Trond Lamark & Terje Johansen (2019)

Subcellular localization of TP53INP2 is regulated by acetylation. *Manuscript*

Paper III

Mads Skytte Rasmussen, Stéphane Mouilleron, Birendra Kumar Shrestha, Martina Wirth, Rebecca Lee, Kenneth Bowitz Larsen, Yakubu Abudu Princely, Nicola O'Reilly, Eva Sjøttem, Sharon A. Tooze, Trond Lamark & Terje Johansen (2017)

ATG4B contains a C-terminal LIR motif important for binding and efficient cleavage of mammalian orthologs of yeast Atg8. *Autophagy* 13:834-853.

Abbreviations

| | |
|-----------|---|
| ATG | AuTophagy related |
| GABARAP | Gamma-aminobutyric acid receptor-associated protein |
| GABARAPL1 | Gamma-aminobutyric acid receptor-associated protein-like 1 |
| GABARAPL2 | Gamma-aminobutyric acid receptor-associated protein-like 2 |
| MAP1LC3B | Microtubules associated protein 1A/1B light chain 3B |
| FYCO1 | FYVE and coiled-coil domain-containing 1 |
| NDP52 | Nuclear Dot Protein 52 |
| mTOR | Mechanistic target of rapamycin |
| PKA | Protein Kinase A |
| PKC | Protein Kinase C |
| NEK9 | NIMA (Never in mitosis A) -related kinase 9 |
| LIR | LC3 interaction region |
| LIRC | C-terminal LIR of ATG4B |
| LIRN | N-terminal LIR of ATG4B |
| LAMP | Lysosomal-associated membrane protein |
| STK3 | STE20-like kinase 3 |
| PAS | Phagophore assembly site |
| PLEKHM1 | Pleckstrin homology domain containing protein family member 1 |
| AMPK | AMP-activated protein kinase |
| AMBRA1 | Autophagy and BECN1 regulator 1 |
| HOPS | Homotypic fusion and protein sorting |
| ULK | Unc-51-Like Kinase |
| WIPI | WD-repeat protein interacting with phosphoinositides |

| | |
|----------|---|
| SNARE | Soluble <i>N</i> -ethylmaleimide-sensitive factor attachment protein receptor |
| VAMP1 | Vesicle associated membrane protein 1 |
| RB1CC1 | RB1 inducible coiled coil 1 |
| TP53INP2 | Tumor protein p53-inducible nuclear protein 2 |
| UDS | Ubiquitin interacting motif like sequence (UIM) docking site |
| PI3K | Phosphatidylinositol 3-Kinase |
| CMA | Chaperone-mediated autophagy |
| PI3P | Phosphatidylinositol 3-phosphate |

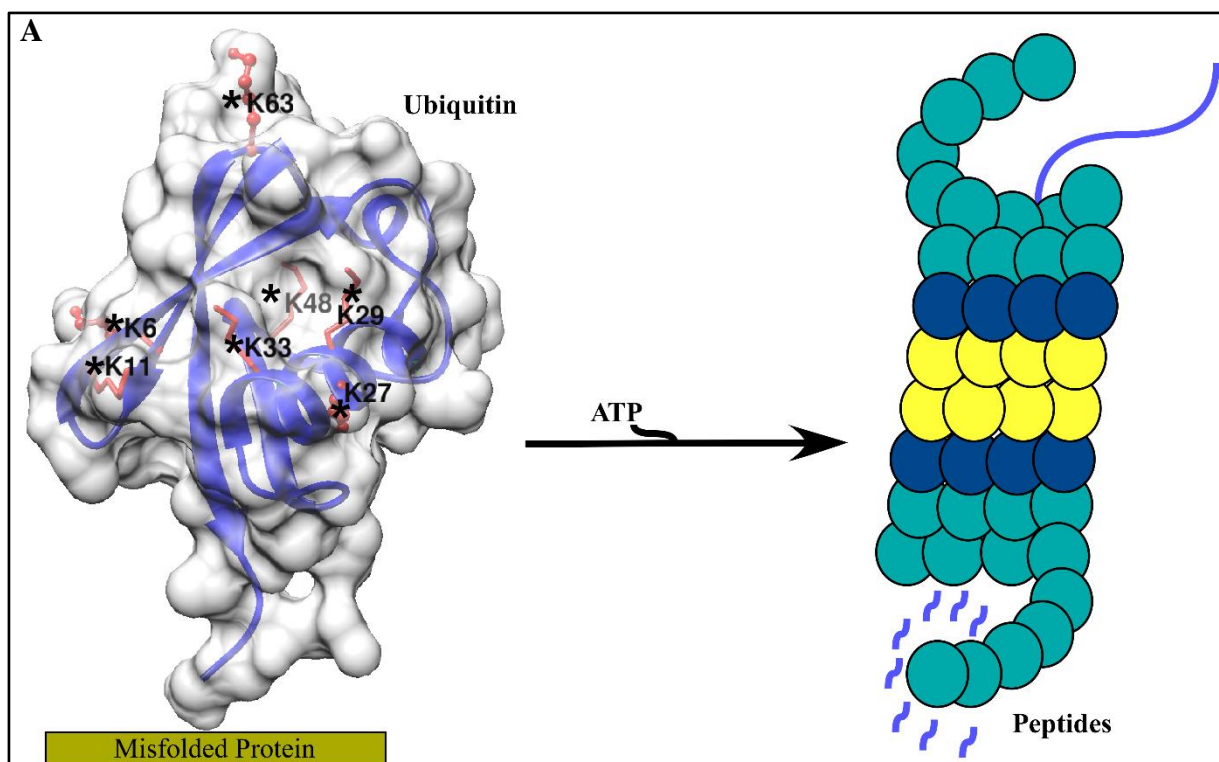
Introduction

Proteostasis is an essential requirement for the maintenance of healthy cells. The cells have a complex network of cellular mechanisms that tightly controls protein stability, folding, its rate of synthesis and degradation. The disturbance of proteostasis has detrimental consequences resulting in accumulation of unfolded proteins, misfolded proteins or damaged proteins that affects cellular functions leading to aging and age-related diseases, cancers, immunological disorders and several other metabolic diseases (Balch et al., 2008). To maintain proteostasis, cells are equipped with a complex protein quality control system, which constantly regulates cellular proteomes via tracking each nascent protein from synthesis to degradation. Each process from mRNA transcription, translation, transportation, and degradation need constant surveillance (Schubert et al., 2000). During mRNA transcription, abnormal mRNA transcripts are degraded before translation. During protein translation, nascent protein requires correct folding which is often mediated by chaperones. Such chaperones also facilitate the degradation of misfolded proteins (McClellan et al., 2005). In addition, cells are exposed to several internal and external stresses, which may lead to the accumulation of protein aggregates. Such protein aggregates are removed by two major complementary degradation systems called the ubiquitin-proteasome system (UPS) and the autophagy-lysosome system.

Ubiquitin Proteasome system (UPS)

Every protein within the cell has a defined half-life ranging from a few minutes to several days, which is tightly regulated. Proteins that are destined to be degraded are first modified by ubiquitin in an ATP dependent manner and later subjected to degradation by a large proteolytic complex called the 26S proteasome (Raynes et al., 2016) (**Figure 1A**). Ubiquitin is a 76 amino acid protein, which is activated by ubiquitin-activating enzymes known as E1 and transferred to the Ub conjugating enzymes E2. Finally, ubiquitin molecules carried by E2 are conjugated to specific substrates by ubiquitin E3 ligase enzymes. Ubiquitin contains internal lysine residues, which can be repeatedly conjugated to another ubiquitin leading to the formation of polyubiquitin chains. The specificity in the process is determined by the E3 ligases (Buetow and Huang, 2016). The E3 ligase recognizes a degradative signal or “degron”, which are either basic or hydrophobic residues in the N-terminal part of a protein. Such residues in the N-terminal part of a protein tend to destabilize it, leading to recognition by E3 enzymes (Ravid and Hochstrasser, 2008). The specificity of E3 ligases is also facilitated by chaperones such as Hsp70 and Hsp90 (Murata et al., 2001). Finally, the mono- or polyubiquitinated substrate

protein is subjected to degradation by the 26S proteasome. The proteasome is a large multi-subunit protease complex, approximately 2.5MDa, composed of two subcomplexes: the catalytic 20S core particle (CP) and 19S regulatory particle (RP) which are attached to either end of the barrel-shaped 20S CP (Voges et al., 1999) (**Figure 1B**). The 20S CP consists of 28 subunits arranged in two outer α -rings and two inner β -rings. The α -rings act as gates for substrate entry into the catalytic chamber formed by the β -rings. These β -ring subunits are associated with caspase-like, trypsin-like, and chymotrypsin-like activities, which digest the substrate protein into peptides ranging from 2-24 amino acids. The 19S RP is composed of lid and base substructures. The base is composed of six AAA' ATPase subunits (Rpt 1-6) which provide ATP energy source for deubiquitinating and unfolding of the substrate. This is essential for the transport of the substrate to the core proteolytic chamber of CP (Smith et al., 2007). In addition to the ATPase subunits, the RP base also contains non-ATPase proteins (Rpn 1, 2, 10, 12 and 13). The Rpn10 and Rpn13 function as receptors for ubiquitinated substrates via their ubiquitin-binding domains (Finley, 2009). Besides recognition of ubiquitinated substrates by Rpn10 and Rpn13, there are also shuttling factors such as Rad23, Dsk2, Ddil and p62 that mediate delivery of ubiquitinated proteins to the proteasome (Finley, 2009). Hence, the delivery of ubiquitinated substrates to the proteasome is a sequential process where first the substrate is recognized by proteasome receptors followed by protein unfolding in an ATPase dependent manner, removal of ubiquitin chains by deubiquitinating enzymes (DUBs) to regenerate free



Ub and finally delivery of unfolded proteins into the core proteolytic chamber for cleavage into short peptides.

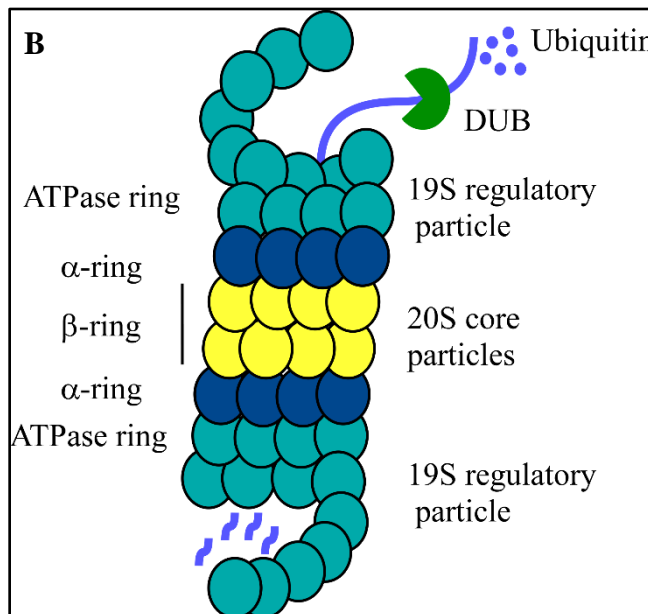


Figure 1: The Ubiquitin-Proteasome pathway (UPS): (A) The proteasomal degradation of misfolded protein by UPS. (B) The 26S proteasome is composed of a 20S core and 19S regulatory core particles. The substrate recognition is mediated by 19S regulatory subunit whereas substrate proteolysis is carried out by β -ring subunits of 20S core particles.

The modes of ubiquitination determine different degradation fates of proteins. The ubiquitin molecules can be linked at K6, K11, K27, K29, K33, K48 and K68 lysine

residues, generating seven various ubiquitin chains. In addition, heterogeneous polyubiquitination chains can be formed (Swatek and Komander, 2016). These homo- and heterogeneous ubiquitin linkages generate different binding surfaces and thereby specificity towards ubiquitin-binding proteins (Hicke et al., 2005; Swatek and Komander, 2016), which may lead to different modes of degradation. Furthermore, ubiquitin chains can be of varying length varying from single ubiquitin (monoubiquitination) or multiple residues (polyubiquitination). For a protein to be directed to proteasomal degradation, the ubiquitin chain must contain a minimum of four ubiquitins (Hicke et al., 2005). The K48 and K11 ubiquitin linkages serve as potent proteasomal degradation signals (Jin et al., 2008; Xu et al., 2009), although a study has also shown specificity towards K29 and K63 linkages (Swatek and Komander, 2016).

It is becoming increasingly clear that proteins also can be subjected to proteasomal degradation in an ubiquitin-independent manner by both the 26S and the 20S core proteasomes (Asher et al., 2005; Hwang et al., 2011). The substrates for such a degradation pathway are native proteins with intrinsically disorder regions (IDRs)(van der Lee et al., 2014). Proteins involved in cell cycle progression, growth and oncogenesis are found to be degraded by this pathway (Dyson and Wright, 2005). It is shown that the same protein can be degraded by both ubiquitin-dependent and -independent pathways (Asher et al., 2005).

The role of the proteasome is not limited to the clearance of proteins within cytoplasm but also extends to the regulation of gene expression. The first evidence of the presence of proteasome systems within the nucleus leads to the identification of several nuclear proteins as substrates for proteasomal degradation (Kleinschmidt et al., 1983). The nuclear proteasomal degradation pathway is associated with regulation of transcription, replication, DNA repair and nuclear protein quality control (Floyd et al., 2001; Krogan et al., 2004; Mendez et al., 2002). Like cytoplasmic proteasomal degradation pathway, studies have shown that the nuclear proteasomal pathway can degrade substrates both by ubiquitin-dependent and-independent pathways. In addition, there is now growing evidence for the existence of a nucleolar ubiquitin-independent proteasomal degradation pathway (Maehama et al., 2014; Murai et al., 2018).

Autophagy

The genesis of the word autophagy started five-decades ago. Christian de Duve and colleagues identified acid phosphatase and other hydrolytic enzymes within membranous structures in the cell. Later, he named these unique organelles lysosome for their lytic function (De Duve et al., 1955). Novikoff working in Christian de Duve's research group further identified organelles such as mitochondria, endoplasmic reticulum, and ribosomes within the acid phosphatase containing membranous compartments (Novikoff et al., 1956). Following studies showed that some membranous compartments contained cellular organelles but not hydrolytic enzymes, indicating the formation of autophagosomes which later fuse with lysosomes (Arstila and Trump, 1968). C de Duve defined this process of delivery of cytoplasmic contents to lysosomes for degradation as "autophagy" (Hanada et al., 2007). The word autophagy is derived from Greek meaning self-eating.

The process of degradation of cytoplasmic contents in lysosomes is subdivided into three categories: microautophagy, chaperone-mediated autophagy (CMA) and macroautophagy. Microautophagy involves the engulfment of cytoplasmic content by direct invagination of the lysosomal membrane (**Figure 2**). The microautophagy pathway is well studied in yeast but studies in mammalian cells are limited. Although several techniques have been developed to study microautophagy, morphological analysis of lysosomal structures by electron microscopy has been the main choice of method (de Waal et al., 1986; Mortimore et al., 1988). This method has some limitations and requires extra caution for interpretation of results. In yeast, microautophagy is constitutively active but can be further induced by Target of Rapamycin (TOR) inactivation (Dubouloz et al., 2005). It can be a nonselective or a selective

process (Li et al., 2012). The selective degradation of mitochondria (Kissova et al., 2007), peroxisomes (Sakai et al., 1998) and nucleus (Krick et al., 2009) is shown to be mediated via microautophagy. No homologous process is identified in mammalian cells. However, recently in mammalian, a degradation pathway similar to yeast microautophagy was identified. In such pathway, cytosolic proteins are rapidly degraded in late endosomes or multivesicular bodies (MVB) instead of lysosome and pathway are termed as endosomal microautophagy (Mejlvang et al., 2018; Sahu et al., 2011). The pathway depends on proteins associated with endosomal sorting complexes required for transport machinery (ESCRT)(Sahu et al., 2011). The endosomal microautophagy involves bulk degradation of cytosolic protein and selective degradation of proteins mediated by HSP70 (Sahu et al., 2011).

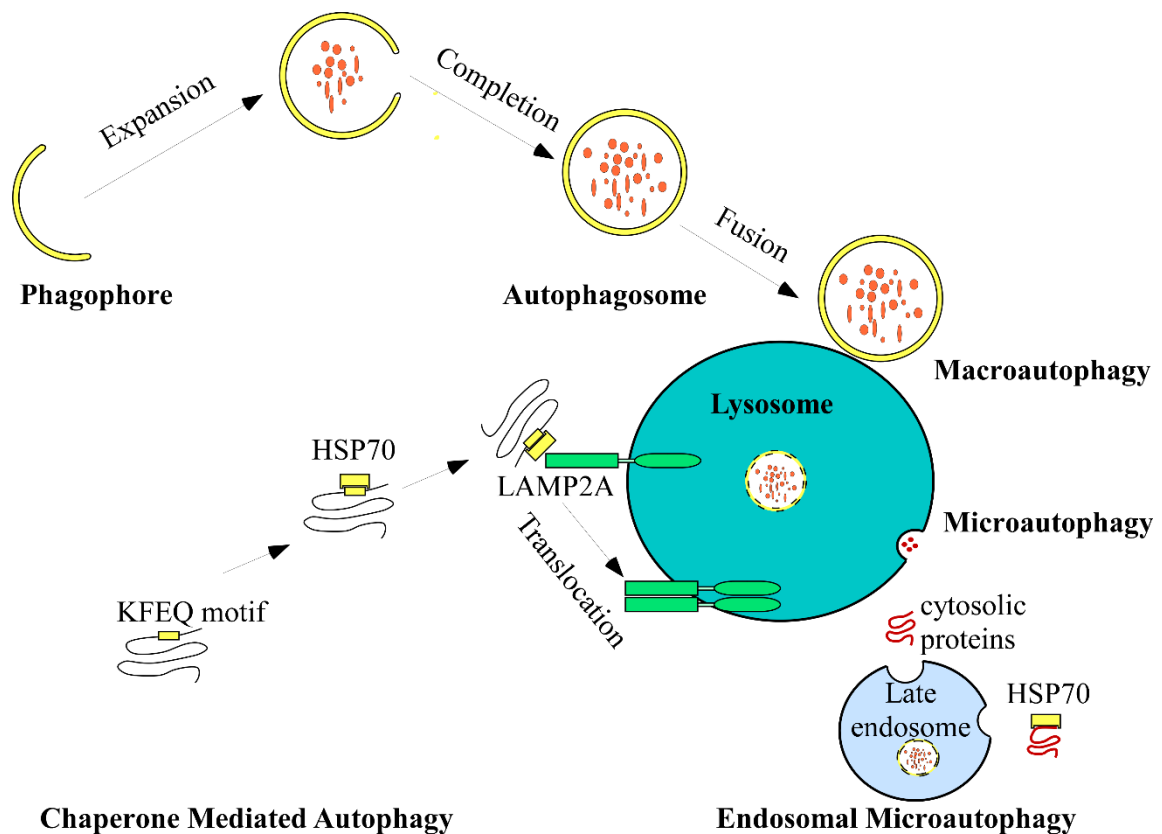


Figure 2: The three autophagy pathways microautophagy, CMA and macroautophagy. Microautophagy involves direct invagination of the lysosomal membrane for engulfment of cytoplasmic contents and its degradation. Endosomal microautophagy involves degradation of cytosolic proteins in late endosomal vesicles. CMA involves lysosomal degradation of its substrate protein via recognition of a specific motif. Macroautophagy involves sequestration of cargo within the double-membrane structure called autophagosome which fuses with the lysosome for its degradation.

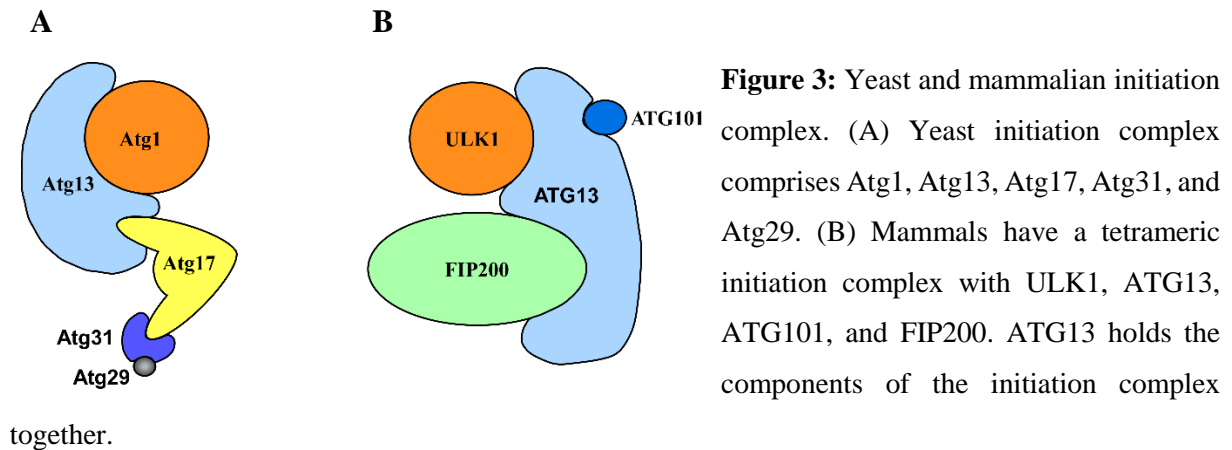
CMA involves selective delivery of substrate proteins with a specific recognition motif for lysosomal degradation, mediated by chaperone Heat shock cognate (HSC70) (**Figure 2**). The CMA recognition motif contains one or two positive residues (K or R), one or two hydrophobic residues (F, L, I or V), one negatively charged residue (E or D) and finally, this motif is flanked on one of the sides by glutamine (Tekirdag and Cuervo, 2018). About 40% of the mammalian proteome contains such a canonical KFERQ like motif. HSC70 recognizes misfolded proteins with KFERQ motifs and targets them to the lysosomal membrane via interaction with the cytosolic tail of LAMP2A (lysosome-associated membrane protein type 2A)(Kaushik and Cuervo, 2018). Subsequently, the proteins are unfolded and thereby translocated into the lysosomal lumen. The transportation of substrates through the lysosomal membrane requires multimerization of LAMP2A and formation of a complex with luminal HSC70 and HSC90 (Kaushik and Cuervo, 2018). CMA occurs at basal level, but can also be induced by different stresses such as starvation (Cuervo et al., 1995), DNA damage (Park et al., 2015), oxidative stress (Kiffin et al., 2004) and hypoxia (Dohi et al., 2012).

In contrast to CMA and microautophagy, macroautophagy (hereafter autophagy) involves sequestration of cytoplasmic cargo within double-membrane structures called autophagosomes and delivery of cargo into lysosomes for degradation. Initial genetic screening in yeast led to the identification of genes regulating the autophagy pathway (named ATG proteins). This provided mechanistic insight into the core autophagic pathway (Tsukada and Ohsumi, 1993). There are 41 autophagy-related genes identified to regulate the autophagy pathway in yeast (Wen and Klionsky, 2016).

Autophagosome biogenesis: Initiation, elongation, closure, and fusion

Autophagy initiation starts with activation of the initiation complex comprising ULK1/2 (Unc-51-like kinase), FIP200 /RB1CC1 (FAK family interacting protein of 200 kDa, RB1-inducible coiled-coil protein 1), ATG101 and ATG13 (Ganley et al., 2009; Hosokawa et al., 2009a; Jung et al., 2009). In *Saccharomyces cerevisiae*, the initiation complex is pentameric consisting of Atg1 (ULK1), Atg13, Atg17, Atg29 and Atg31 (He and Klionsky, 2009). Human has two *atg1* homologous genes encoding the ULK1 and ULK2 proteins. The functional roles of ULK1 are well characterized compared to ULK2. To initiate autophagy, ULK1 has to be switched on via phosphorylation events, recruited to the site of phagophore formation and finally scaffolding essential proteins at the site of autophagosome formation (Zachari and Ganley, 2017). Beside ULK1, also FIP200 acts as a scaffold protein for autophagosome

formation (Hara et al., 2008). ATG13 and ATG101 contain HORMA (Hop/Rev7/Mad2) domains that heterodimerize with each other (Qi et al., 2015; Suzuki et al., 2015). Such dimerization of ATG13 with ATG101 stabilizes ATG13 by preventing it from proteasomal degradation (Hosokawa et al., 2009b; Mercer et al., 2009). In addition to the ATG101 interaction, ATG13 interacts with FIP200 and ULK1 via two other motifs and thereby holds four proteins in a complex (Alers et al., 2014) (**Figure 3**).



The initiation of autophagy is regulated by two major kinases, mTORC1 and AMPK. Under nutrient-rich conditions, mTOR is activated by the small GTPase Rheb (Inoki et al., 2003a). Activation of mTOR leads to inactivation of ULK1 by mTOR mediated phosphorylation of the two serine residues S638 and S758 (Kim et al., 2011; Shang et al., 2011) (**Figure 4**). mTOR also phosphorylates ATG13 at S258 (Puente et al., 2016). This phosphorylation of ULK1 and ATG13 inhibit direct AMPK-dependent activation of autophagy, resulting in subsequent inhibition of autophagy. Under nutrient deficient conditions, AMPK senses the reduced ATP/AMP ratio in the cell and stimulates autophagy by mTOR inactivation and ULK1 activation. AMPK mediates mTOR inactivation by direct phosphorylation of RAPTOR (a subunit of the mTORC1 complex) and TSC2, an inhibitor of Rheb (Gwinn et al., 2008; Inoki et al., 2003b). Furthermore, AMPK phosphorylates both ULK1 and ATG13 at specific sites important for the initiation of autophagy (Puente et al., 2016; Shang et al., 2011) (**Figure 4**). ULK1 activity can also be regulated by ubiquitination. The AMBRA-TRAF6 dependent Lys-63-linked polyubiquitination of ULK1 leads to its stabilization, dimerization, and activation (Nazio et al., 2013).

Activation of ULK1 is followed by translocation of ULK1 initiation complexes to subdomains of the endoplasmic reticulum (ER) called omegasomes, a phosphatidylinositol 3-phosphate (PI3P) enriched membrane extension of ER. The mechanism involved in this precise

translocation of the initiation complex to the autophagosome nucleation site and the protein complexes involved is not well understood. Recently, it was shown that the nucleation site is marked by ATG9 vesicles (Karanasios et al., 2016) and that translocation of the ULK1 complex to the nucleation site is mediated by the Rab1 effector C9orf72 (Webster et al., 2016). Furthermore, the ER proteins VAPA and VAPB are shown to be recruited to the site of autophagosome nucleation and initiate autophagosome formation via direct interaction with FIP200 and ULK1 (Zhao et al., 2018). After activation and recruitment of the initiation complex, it is stabilized by membrane association of ULK1 and ATG13. The membrane interaction of ULK1 is mediated by its EAT domain in the C-terminal part (Chan et al., 2009; Hurley and Young, 2017). In the case of ATG13, the electrostatic interaction between the N-terminal basic residues of ATG13

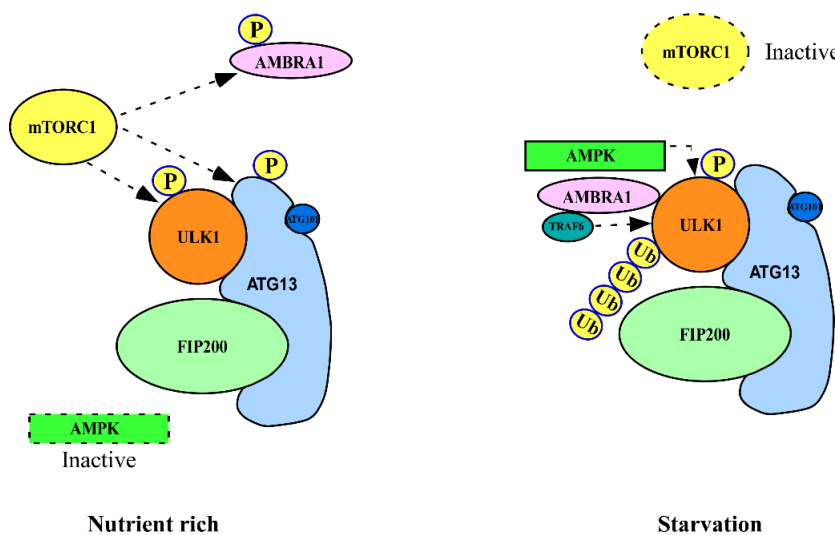
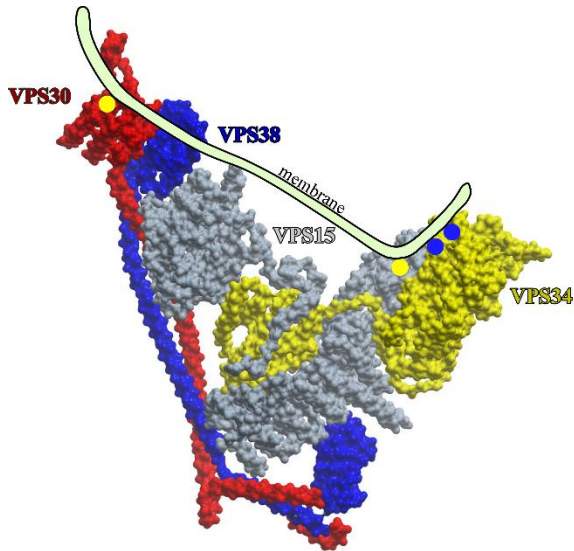


Figure 4: Regulation of initiation complex in (A) Nutrient-rich condition and (B) Starvation. Under the nutrient-rich condition, mTOR induced phosphorylation of ULK1 and ATG13 inhibits autophagy. Under starvation, AMPK induced phosphorylation of ULK1 and ATG13 leads to stimulation of autophagy. In

addition to phosphorylation-mediated activation of ULK1, polyubiquitination of ULK1 via TRAF6 also leads to activation of autophagy.

and acidic phospholipids present within the ER membrane mediates such interaction (Karanasios et al., 2013). The association of the initiation complex with omegasomes is further stabilized by LC3 interaction regions (LIR). Both ULK1 and ATG13 contain LIR motifs which mediate interactions with phosphatidylethanolamine conjugated ATG8 proteins in the omegasomes membrane, and thereby further enhances retention of the initiation complex at omegasomes (Alemu et al., 2012; Kraft et al., 2012). Following the stabilization of the initiation complex, the class III PI3K complex is recruited to the site. The class III PI3K complex forms two different complexes called PI3KC3-C1 and PI3KC3-C2. The mammalian class III PI3K

complex I (PI3KC3-C1) consists of VPS34 (Vacuolar Protein Sorting 34), VPS15 (Vacuolar Protein Sorting 15), ATG14L (Autophagy-related protein 14-Like protein (Atg14 in yeast) and Beclin-1 (BECN1) (Vps30 in yeast)(Backer, 2016). PI3KC3-C2 contains UVRAG (UV



Radiation Resistance- Associated Gene protein; Vps38 in yeast) instead of ATG14L(Backer, 2016) (**Figure 5**). The PI3K complex I is known to facilitate phagophore formation whereas PI3K complex II is involved in endosome and autophagosome maturation (Backer, 2016).

Figure 5: Complex structure of yeast Class III PI3KC3-C2 (PDB: 5DFZ)(Rostislavleva et al., 2015). The BARA domain of VPS30, N-terminal

part of VPS15, C-terminal K α 12 helix and activation loop of VPS15 is actively involved in membrane interaction at omegasomes.

Each component of the PI3KC1 complex associates with lipid membranes and contributes to the stabilization of the complex. Association of ATG14L with membrane structures and recruitment of PI3KC1 complex is mediated by its ER targeting sequence, its N-terminal cysteine-rich domain and its BATS (Barkor/ATG14L autophagosome targeting sequence) domain which interacts with both PI3P and phosphatidylinositol 3,4 bisphosphate (Fan et al., 2011; Matsunaga et al., 2010). The C-terminal BARA domain of BECN1 directly associates with lipid membranes using three aromatic residues Y359/Y360/W361 (Huang et al., 2012). VPS34 stabilizes the complex via its K α 12 helix and activation loops interacting with the membrane (Miller et al., 2010). Finally, the N-terminal part of VPS15 is involved in membrane association (Stack et al., 1995). Recently, VPS34, BECN1, and ATG14 were found to interact preferentially with GABARAP for efficient recruitment of complex to membrane structure (Birgisdottir et al., 2019). VPS34 is a protein kinase, phosphorylating phosphatidylinositol to generate PI3P. The generation of PI3P by VPS34 at omegasomes leads to recruitment of downstream PI3P effector proteins. The first effector protein to be recruited is DFCP1 (double FYVE domain-containing protein 1) which binds to PI3P through its two FYVE motifs (Axe et al., 2008). In addition to DFCP1, WIPIs (WD-repeat domain phosphoinositide-interacting proteins) are PI3P effector proteins that are essential for phagophore formation. There are four WIPI proteins in mammals. The WIPI1 and WIPI2b are shown to be recruited to the

omegasomes via their FRRG motifs interacting with PI3P (Gaugel et al., 2012; Polson et al., 2010).

The recruitment and stabilization of the PI3KC1 complex are proceeded by elongation of the phagophore. This process, in both yeasts and mammals, is achieved by two conjugation systems involving the ubiquitin-like proteins: ATG12-ATG5-ATG16 and ATG8/LC3 conjugation system (Nakatogawa, 2013; Ohsumi and Mizushima, 2004) (**Figure 6**). The ubiquitin-like protein ATG12 is covalently conjugated to ATG5 by the E1-like enzyme ATG7 (Kim et al., 1999) and E2-Like enzyme ATG10 (Shintani et al., 1999). First, ATG12 is activated by ATG7 and transferred to the E2-like enzyme ATG10 for conjugation of ATG12 to ATG5. Contrary to ubiquitin conjugation systems, the ATG12-ATG5 conjugation is irreversible and does not require an E3 ligase (Geng and Klionsky, 2008). After the conjugation of ATG12 to ATG5, ATG16L1 interacts with ATG5 and subsequently homodimerizes with itself to form a large stable ATG12-ATG5: ATG16L1 complex which later functions as an E3 Ligase for the ATG8 conjugation system (Kuma et al., 2002). The ATG8 conjugation system starts with the processing of ATG8 family proteins by the ATG4 cysteine proteases (Kirisako et al., 2000). Yeast has only one ATG4 protein and one ATG8 protein compared to mammals which have four ATG4 (ATG4A-D) and seven ATG8 proteins. The ATG8s are cleaved at the C-terminal by ATG4 leading to exposure of a glycine residue (Kirisako et al., 2000). The E1-Like ATG7 activates the processed ATG8 protein and transfers it to the E2-like enzyme ATG3 (Ichimura et al., 2000). Finally, the ATG12-ATG5-ATG16L1 E3 ligase conjugates phosphatidylethanolamine (PE) at the C-terminal glycine residue of ATG8 (Hanada et al., 2007; Ichimura et al., 2000). The PE-conjugated ATG8 leads to association with the inner and outer sides of the growing phagophore and later, outer side ATG8-PE is released to the cytoplasm by ATG4 mediated cleavage (Kirisako et al., 2000).

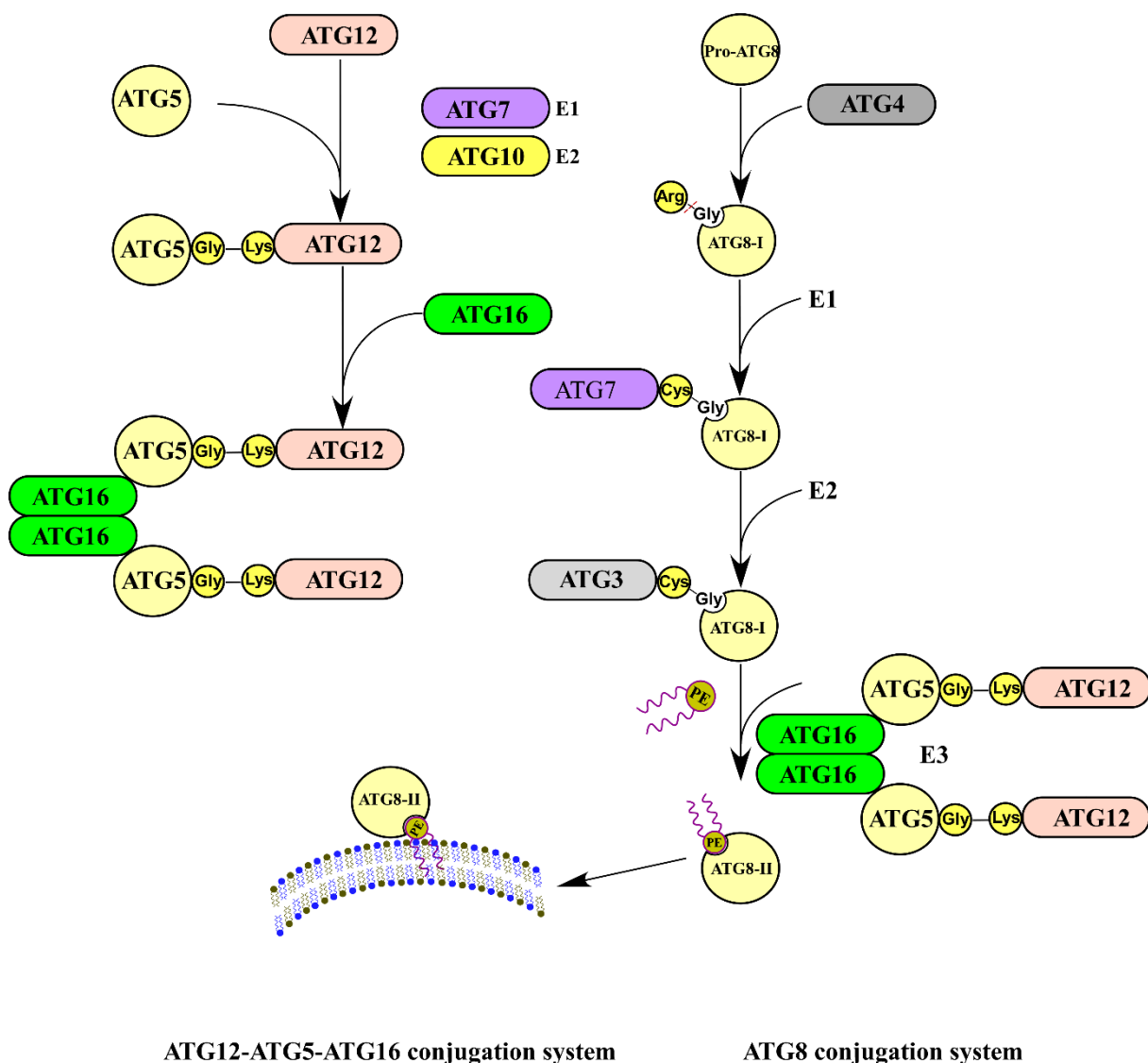


Figure 6: The two conjugation systems: The ATG12-ATG5-ATG16 conjugation system produces an E3 Ligase for the ATG8 conjugation system. In the ATG8 conjugation system, proATG8 protein is processed by ATG4 to expose C-terminal glycine residue. The processed ATG8 is transferred by ATG7 to ATG3, an E2 activating enzyme. The activated ATG8-I is conjugated to phosphatidylethanolamine (PE) at the C-terminal glycine residue by ATG12-ATG5-ATG16, E3 ligase. The PE-conjugated ATG8 is recruited to phagophore.

In addition, to the two conjugation systems, ATG9 is essential for phagophore elongation. ATG9 is a transmembrane protein containing six highly conserved transmembrane domains spanning the membrane (Noda, 2017). Under nutrient-rich conditions, ATG9 is localized within the trans-Golgi network and endosomes. Upon induction of autophagy via nutrient deprivation, ATG9 vesicles shuttle around the phagophore and transiently interact for delivery of contents necessary for phagophore elongation (Mari et al., 2010; Orsi et al., 2012;

Young et al., 2006). Such trafficking of ATG9 vesicles around the phagophore is regulated by the ULK1 kinase and depletion of it leads to inhibition of ATG9 trafficking (Orsi et al., 2012). Phosphorylation of ATG9 at S14 by ULK1 is essential for both ATG9 trafficking and autophagy induction (Zhou et al., 2017). Also, WIPI2 (WD repeat domain phosphoinositide-interacting protein 2) is shown to regulate ATG9 vesicles during autophagy initiation (Orsi et al., 2012).

The extensive studies on yeast models have helped to better understand the mechanisms involved in the activation of autophagy and the formation of autophagosomes. However, the mechanisms involved in the closure of the autophagosome and its subsequent fusion with late endosomes/lysosomes are still elusive. Its prerequisite is that only closed autophagosomes can fuse with lysosomes. Previous studies have shown that the ATG conjugation systems are essential for the closure of autophagosomes and degradation of the inner autophagy membrane (Fujita et al., 2008; Kishi-Itakura et al., 2014; Sou et al., 2008; Tsuboyama et al., 2016). In contrast, another study showed that KO of all 6 human ATG8 family proteins did not affect formation and closure of autophagosomes but affected fusion of the autophagosome with lysosomes (Nguyen et al., 2016). The closed autophagosomes are transported towards late endosomes/lysosomes present at the perinuclear region. The transport towards the perinuclear region is mediated by dynein-dynactin complexes, whereas kinesins are involved in transport towards the cell periphery (Gross et al., 2007). For efficient transport of autophagosomes towards perinuclear lysosomes, these motor proteins are essential, and their activity is facilitated by interactions with the small GTPase Rab7 (Gutierrez et al., 2004). Rab7 is a molecular switch which is activated by specific guanine nucleotide exchange factors (GEFs). Upon GTP binding, Rab7 undergoes conformational changes which lead to interaction with its downstream effector proteins (Hyttinen et al., 2013). The kinesin-driven movement towards the cell periphery is achieved by Rab7 interacting with FYCO1 (Pankiv et al., 2010), while dynein-dynactin mediated movement towards the perinuclear region is mediated by Rab7 interactions with RILP (Rab-interacting lysosomal protein) and ORPL1 (oxysterol-binding protein-related protein 1)(Jordens et al., 2001; Wijdeven et al., 2016). A complex interaction involving three major sets of protein families: Rab GTPase, membrane-tethering complex and soluble N-ethylmaleimide-sensitive factor attachment protein receptors (SNAREs) is known to be implicated in autophagosome-lysosome fusion. The Rab7 protein is essential in the recruitment of the HOPS complex (tethering factor) and SNAREs at the autophagosome lysosomes fusion site. Rab7 recruits the HOPS complex via direct interaction with its effector proteins, such as

PLEKHM1 and RILP, which bind the VPS39 and VPS41 components of the HOPS complex, respectively (Wijdeven et al., 2016). PLEKHM1 facilitates autophagosome-lysosome fusion via direct interaction with ATG8s bound to closed autophagosomes (McEwan et al., 2015). In addition, Rab7 recruits another effector protein and tethering factor called Ectopic P granules protein 5 (EPG5) which stabilizes the STX17-SNAP29-VAMP8 complex via direct interaction with each component of the complex (Wang et al., 2016b). Furthermore, EPG5 interacts directly with the ATG8s via LIR-LDS binding, which most likely promotes the autophagosome-lysosome fusion process (Wang et al., 2016b).

ATG8 and its LDS and UDS binding surfaces

The extensive studies in yeast led to the identification of at least 41 autophagy-related proteins that are found to be functionally conserved in eukaryotes. Among these proteins is the ATG8 family of proteins. In yeast there is only one ATG8 gene compared to mammals which have six functional ATG8 orthologs: microtubules associated protein 1 light chain 3 α (MAP1LC3A), β (MAP1LC3B), γ (MAP1LC3C), GABA type A receptor-associated protein (GABARAP), GABARAP-like 1 (GABARAPL1) and GABARAP like 2 (GABARAP2/GATE 16) (Schaaf et al., 2016). They share high sequence similarity and have a conserved C-terminal glycine residue for cleavage by cysteine protease ATG4 (Kirisako et al., 2000). In addition to amino acid sequence similarity, the LC3/GABARAP (Noda et al., 2009) proteins share structure similarity with two N-terminal α -helices ($\alpha 1$ and $\alpha 2$) and a C-terminal ubiquitin core (Sugawara et al., 2004) (**Figure 7**). The amino terminals of the LC3/GABARAPs show differences in their electrostatic surfaces, which is hypothesized to be a factor for determining their specific functional roles. The first $\alpha 1$ of LC3B is basic compared to $\alpha 1$ of GABARAP and GABARAPL2 which are more acidic, while $\alpha 2$ of LC3B is acidic whereas $\alpha 2$ of GABARAP and GABARAPL2 are basic and neutral, respectively (Noda et al., 2009). The C-terminal ubiquitin core contains two α helices ($\alpha 3$ and $\alpha 4$) and a four-stranded central β -sheet ($\beta 1$ - $\beta 4$). The two central β strands are parallel to each other whereas the two outer β strands are antiparallel to the central strands. Although the C-terminal ubiquitin core of the ATG8s is similar structurally to the ubiquitin protein, the amino acids sequence similarity is very low (Noda et al., 2009).

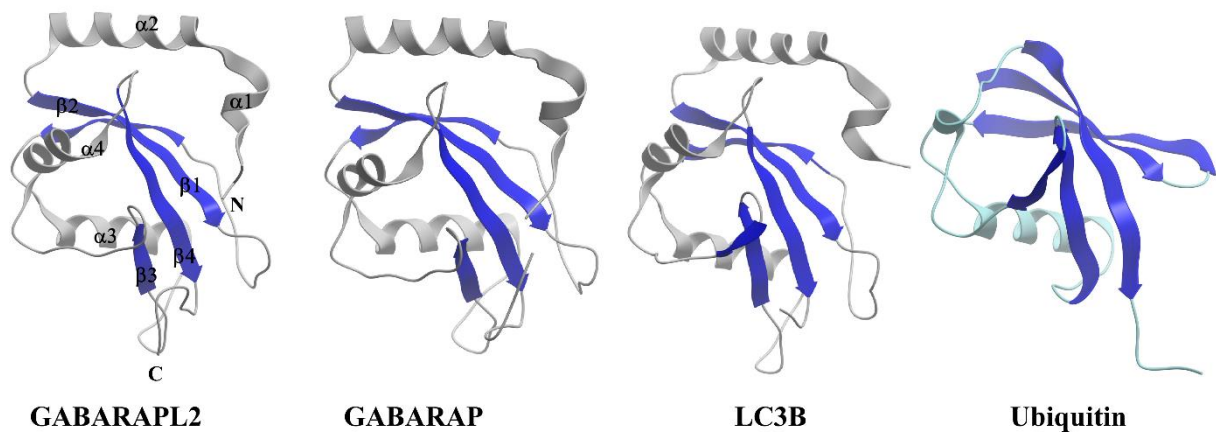


Figure 7: Structure of ATG8s homologues and Ubiquitin: Ribbon representation of GABARAPL2 (PDB code 1EO6), GABARAP (PDB code 1GNU), LC3B (PDB code 1UGM) and Ubiquitin (PDB code 1UBI).

Several proteins interact with mammalian LC3B/GABARAPs via a conserved motif called LC3 interaction region (LIR) or ATG8 interacting motif (AIM) in yeast. The canonical core LIR consensus sequences contain [W/F/Y] XX [L/I/V] residues, where X denotes any amino acid (Birgisdottir et al., 2013). The LIR motif docks into two hydrophobic pockets (HP1 and HP2) present on the ATG8s structural surfaces (**Figure 8**). The HP1 pocket accommodates hydrophobic aromatic residues whereas the HP2 pocket accommodates hydrophobic aliphatic residues. The core LIR motifs are often preceded by acidic residues (E, D, S, T), which are involved in electrostatic interactions with basic residues present in the N-terminal helices of the ATG8s (Birgisdottir et al., 2013). The binding affinity between ATG8s and their interaction partners is often regulated by phosphorylation of S or T residues flanking the core LIR motif (Birgisdottir et al., 2013; Di Rita et al., 2018; Hamacher-Brady and Brady, 2016). In contrast to the canonical LIR motif, non-canonical LIR (CLIR) motifs contain three stretches of the aliphatic residues L-V-V (in case of NDP52) and lack hydrophobic aromatic residues. These hydrophobic LVV residues interact with a complementary hydrophobic surface on the HP2 pocket of LC3C (von Muhlinen et al., 2012).

Recently, a novel binding surface was identified in *Arabidopsis thaliana* ATG8s. This binding site interacts with proteins containing a ubiquitin-interacting motif (UIM) like sequence and is called UIM docking site (UDS)(Marshall et al., 2019) (**Figure 8B**). The *Arabidopsis* RPN10 uses a UIM motif to interact with the ATG8 UDS site instead of the LDS site (Marshall et al., 2019). In addition to RPN10, several proteins belonging to the *Arabidopsis* UBX (Ubiquitin regulatory domain X) domain containing family interacts with ATG8s via UIM-UDS interfaces (Marshall et al., 2019).

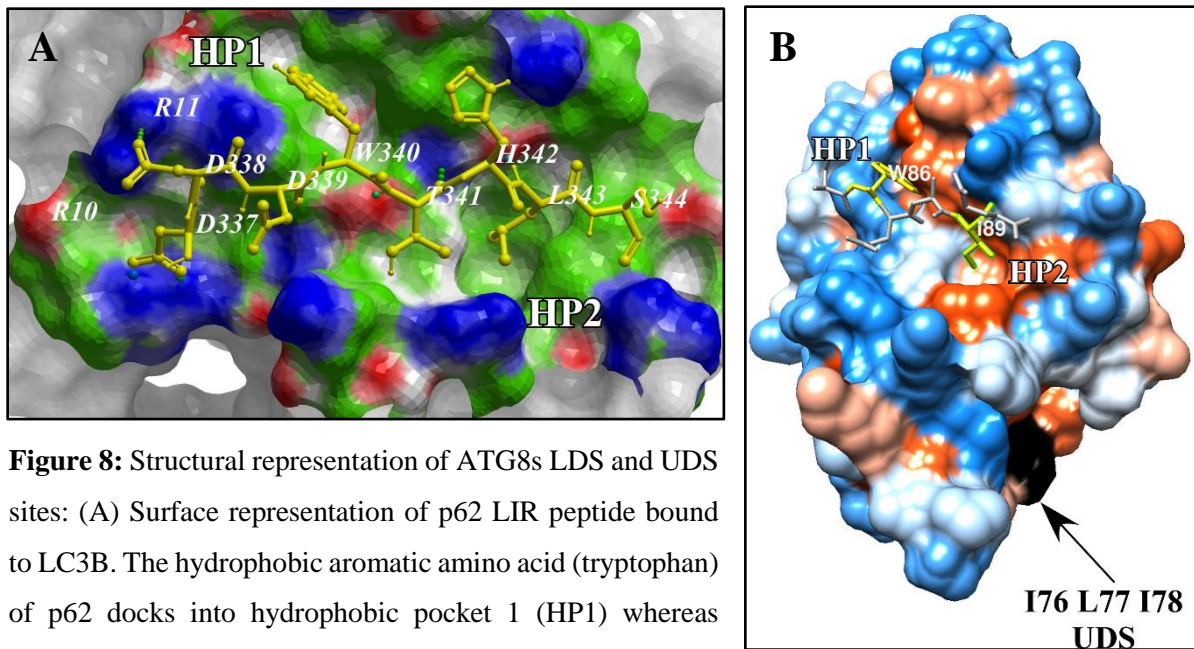


Figure 8: Structural representation of ATG8s LDS and UDS sites: (A) Surface representation of p62 LIR peptide bound to LC3B. The hydrophobic aromatic amino acid (tryptophan) of p62 docks into hydrophobic pocket 1 (HP1) whereas another hydrophobic aliphatic residue (leucine) docks into hydrophobic pocket 2 (HP2). The acidic residues preceding the LIR motif are involved in electrostatic interactions with basic residues at N-terminal helices of LC3B. (B) ATG8 interacts with proteins containing Ubiquitin interacting motif (UIM) like sequence via its non-LDS site called UDS (UIM docking site).

The structural similarity of ATG8s homologues suggests functional redundancy. However, studies have shown that the ATG8s have differential roles in the autophagy pathway. The LC3s were found to play an essential role in the early stage of autophagosome biogenesis, whereas GABARAPs are important in later stages during autophagosome maturation (Weidberg et al., 2010). In contrast to the human cell line studies, genetic analysis in *Caenorhabditis elegans* identified the GABARAP homologue LGG1 to be essential in the early stage of autophagosome formation while the LC3B homologue LGG2 was essential for autophagosome maturation (Manil-Segalen et al., 2014). LC3B and GABARAP seem to be redundant in the autophagic degradation of long-lived proteins, but LC3B is indispensable for degradation of the selective autophagy receptor p62 (Maruyama et al., 2014). Recently, it has been shown that in cell lines that are genetically KO for all ATG8s, autophagosome biogenesis still occur. The essential role of the ATG8s is restricted to mediate autophagosome-lysosome fusion (Nguyen et al., 2016). In agreement, another study showed that only GABARAPs play a role in the LDH degradation assay, indicating that the GABARAPs are the main players in autophagosome-lysosome fusion (Szalai et al., 2015). Both studies state importance for the interaction of GABARAPs with PLEKHM1 as essential for autophagosome lysosomal fusion (McEwan et al., 2015).

Additional to the autophagic roles of the ATG8s, other non-autophagic roles have been reported (Sanjuan et al., 2007). For example, LC3B is shown to be recruited to phagosome membranes and thereby enhance phagosome-lysosome fusion leading to efficient clearance of sequestered cargo in a pathway called LC3-associated phagocytosis (LAP)(Sanjuan et al., 2007).

ATG4B

The mammalian genome contains four independent genes encoding proteins homologous to the yeast ATG4 protein: ATG4A, ATG4B, ATG4C, and ATG4D. ATG4 belongs to the C54 endopeptidase family. Initially, it cleaves the ATG8s at a C-terminal glycine residue and later it delipidates ATG8s located at the outer membrane of autophagosomes. ATG4B cleaves all the ATG8s homologues, but LC3B seems to be its main substrate (Li et al., 2011; Tanida et al., 2004). Efforts are made to determine the sensitivity and specificity of the various ATG4 homologues towards the ATG8 homologues. ATG4A is shown to cleave GABARAPL2, whereas ATG4D cleavages GABARAPL1 and this cleavage is shown to be enhanced by Caspase3 cleavage at the N terminus (Betin and Lane, 2009; Scherz-Shouval et al., 2003). An *in vitro* assay showed that ATG4A cleavage activity towards GABARAPL2 was increased in the presence of the reducing agent DTT (Scherz-Shouval et al., 2003). This led to the speculations that redox potential might regulate ATG4A activity *in vivo*. Later, it was shown that starvation-induced ROS production affects cysteine residue C81 (close to active cysteine residue C74) and thereby negatively regulate ATG4A activity (Scherz-Shouval et al., 2007). The negative regulation is restricted to defined sites with high ROS, like in the vicinity of the mitochondria where autophagosome formation is initiated. At subcellular areas with lower ROS, such as at autophagosome maturation sites, ATG4A activity is facilitated and can carry out delipidation of membrane-bound ATG8s for efficient fusion with lysosomes (Scherz-Shouval et al., 2007). In addition to ROS, ATG4B activity is also regulated by an E3 ubiquitin ligase called RNF5. RNF5 mediated ubiquitination of ATG4B leads to degradation of membrane-associated ATG4B, and KO of RNF5 enhanced autophagy flux and clearance of bacterial pathogens (Kuang et al., 2012). Overexpression of catalytic deficient ATG4B inhibits lipidation of LC3B and autophagic degradation. This inhibitory effect was due to sequestration of unlipidated LC3B into stable complexes together with the ATG4B mutant, and thereby limit the availability of LC3B for phagophore elongation (Fujita et al., 2008). ATG4C is shown to be required for starvation-induced autophagy (Marino et al., 2007). However, in mice models,

KO of ATG4C seems to have minor phenotypic defects compared to KO of ATG4B (Marino et al., 2010; Marino et al., 2007).

The structure of the ATG4B-LC3B complex solved by x-ray crystallography revealed that the ATG4B interaction with the ATG8s is mediated by two mechanisms: via its N-terminal LIR motif and via its kinase domain (Satoo et al., 2009). In addition, a novel C-terminal ATG4B LIR motif plays an important role in both binding and cleavage of its ATG8 substrate (discussed in paper III). The functional role of ATG4 for cleavage and activation of the ATG8s for conjugation to lipid moieties is well understood, while the functional relevance of the de-lipidation step is unclear. It is shown that yeast Atg4 mediates Atg8 de-lipidation at the outer membrane of the autophagosome, and this has two essential functions: to provide an adequate supply of un-lipidated ATG8 for autophagosome formation and to facilitate efficient fusion of the mature autophagosomes with lysosomes (Yu et al., 2012). In addition, ATG4 de-lipidation compensates intrinsic defects in the lipidation system that constitutively and non-selectively produces ATG8-PE at different intracellular membrane structures (Nair et al., 2012). Hence, Atg4 plays an essential role in delipidating these Atg8-PEs and thereby provides a large enough pool of un-lipidated Atg8s for autophagosome formation (Nair et al., 2012).

Autophagy has an essential role in the clearance of intracellular bacteria. In response to host defense mechanisms, pathogens have developed strategies to manipulate the host cell machinery for their survival. Recently it was shown that *Legionella pneumophila* interfere with autophagy via its effector protein RavZ (Choy et al., 2012). RavZ displays preferential binding to high curvature membranes via its PI3P binding domain and functions as a cysteine protease by uncoupling lipidated ATG8 attached to autophagosome membranes. RavZ cleaves the amide bond between the C-terminal glycine and the preceding aromatic residue in ATG8, leading to the generation of ATG8s with no glycine residues for lipidation (Choy et al., 2012). Interestingly, RavZ interacts with the host ATG8s via two LIR motifs (Kwon et al., 2017).

TP53INP1 and TP53INP2

Tumor protein p53-inducible nuclear proteins 1 and 2 (TP53INP1 and TP53INP2) are described as bifunctional proteins acting as nuclear coactivators and as regulators of autophagy (Sancho et al., 2012; Seillier et al., 2012). Phylogenetic analysis shows that TP53INP1 is the ancestral gene and that TP53INP2 is a result of gene duplication (Nowak et al., 2009). TP53INP1 expression is regulated by p53 (Tomasini et al., 2002). First, it was found that

TP53INP1 interacts with a kinase that phosphorylates p53 at S46, leading to transcriptional activation of apoptotic protein p53AIP1 (Oda et al., 2000). Later two kinases, homeodomain interacting protein kinase 2 (HIPK2) and proapoptotic PKC δ were found to mediate phosphorylation of p53 S46 during genotoxic stress (Tomasini et al., 2003; Yoshida et al., 2006). Additional to its role in apoptosis, TP53INP1 is shown to interact with the ATG8 family proteins via an LIR motif and positively regulate autophagy (Seillier et al., 2012). Human TP53INP1 and TP53INP2 show 30% sequence identity and 45% similarity. TP53INP2 was first published as a transcription coactivator of the thyroid hormone receptor, thereby regulating its function (Baumgartner et al., 2007). The identification of TP53INP2 gene within chromosome 20q11.22, loci associated with human obesity leads to the nomenclature of TP53INP2 as DOR (Diabetes- and Obesity Regulated) (Baumgartner et al., 2007). Recently, TP53INP2 was found to negatively regulate adipogenesis by promoting sequestration of GSK3 β in an ESCRT dependent pathway (Romero et al., 2018). Similarly, to TP53INP1, TP53INP2 is reported to be implicated both in apoptosis and autophagy. It promotes death receptor-induced apoptosis via TRAF6 dependent ubiquitination of caspase-8 (Ivanova et al., 2019). Furthermore, TP53INP2 regulates autophagosome formation via acting as a scaffold protein recruiting ATG8s to the site of phagophore formation via interactions with VMP1 and the BECN1 complex (Nowak et al., 2009). TP53INP2 is a nuclear protein under normal conditions, but under mTOR inactivation, it translocate from the nucleus to autophagic structures in the cytoplasm (Nowak et al., 2009; Seillier et al., 2012). Moreover, TP53INP2 acts as a chaperone by translocating nuclear-deacetylated LC3B to cytoplasmic autophagosome structures (Huang et al., 2015). Here it contributes to autophagosome biogenesis by promoting LC3-ATG7 interactions (You et al., 2019). TP53INP2 is also reported to have a functional role in nutrient-rich conditions, enhancing rDNA transcription via the assembly of the rDNA transcription complex at the rDNA promoter (Xu et al., 2016). Hence, TP53INP2 has roles both when mTOR is inactive and when mTOR is active, as a facilitator of autophagy and by promoting ribosome biogenesis, respectively.

Regulation of autophagy: Posttranslational modifications

Posttranslational modifications (PTMs) regulate the stability, localization, and function of several proteins. The major types of PTMs include phosphorylation, ubiquitination, glycosylation, methylation, acetylation, SUMOylation, lipidation and proteolysis. These PTMs play essential roles in the regulation of each step of the autophagic pathway from the formation of the initiation complex to the fusion of the autophagosome with the lysosome (**Figure 9**).

Several protein kinases, E1/E2/E3 ligases, and acetyltransferases have been identified to regulate autophagy by PTMs of autophagy proteins (Wani et al., 2015; Xie et al., 2015).

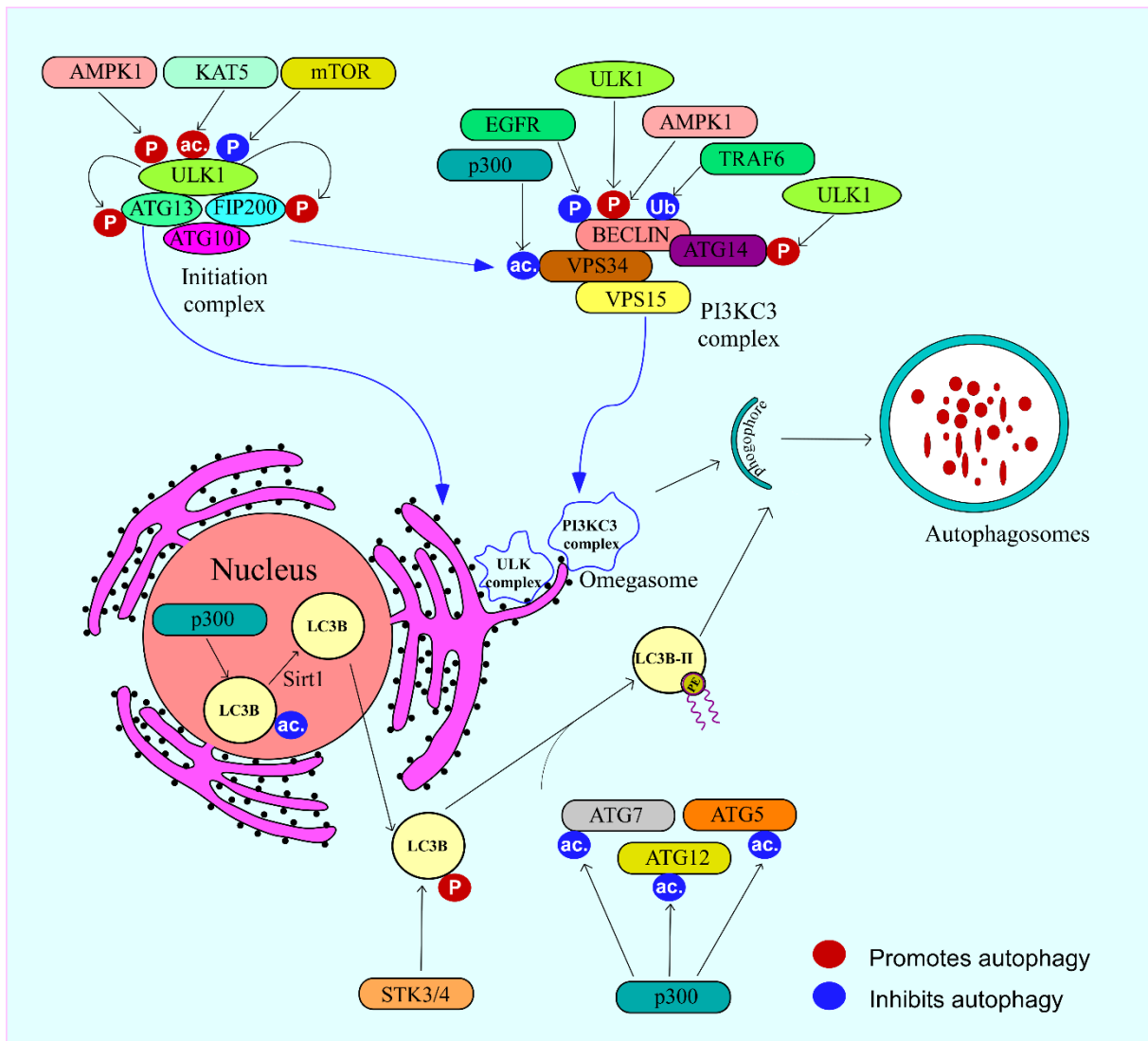


Figure 9: Overview of the regulation of autophagy by posttranslational modifications. Acetylations (ac.), phosphorylations (P) and ubiquitinations (Ub) are indicated.

ULK1, the key component of the autophagy initiation complex, is heavily regulated by PTMs. mTORC1 inhibits autophagy via phosphorylation of ULK1 at S758 and S638 (Shang et al., 2011). AMPK promotes autophagy by phosphorylation of ULK1 at S317 and S777 (Kim et al., 2011). The additional AMPK mediated phosphorylation of ULK1 (S467, S555, T574, S637) are identified to be essential in mitophagy (Egan et al., 2011). Also, PKA and AKT are implicated in phosphorylation ULK1 leading to inhibition of autophagy (Bach et al., 2011; Dorsey et al., 2009). Upon serum deprivation, acetylation of ULK1 at K162 by KAT5/TIP60 is found to be essential for the induction of autophagy (Lin et al., 2012). Moreover, K63-linked chain ubiquitination of ULK1 mediated by the AMBRA1 complex with TRAF6 promotes

ULK1 stability and its function in autophagy (Nazio et al., 2013). ULK1 itself is a kinase and is associated with regulation of autophagy via phosphorylation of FIP200 and ATG13 (Hosokawa et al., 2009a; Jung et al., 2009).

Also, the downstream PI3K3C3 complex responsible for the production of PtdIns3P is tightly regulated by PTMs. The BECN1 interaction with its negative regulator (BCL2) is increased upon epidermal growth factor receptor-mediated phosphorylation on the three residues Y229, Y233, and Y352 (Wei et al., 2013). This increases the association of BECN1 with BCL2, and thereby negatively regulates the induction of autophagy. The interaction of BECN1 with BCL2 is mediated by the BH3 domain, and phosphorylation of the T119 residue within the BH3 domain leads to dissociation of BECN1 from its negative regulator and induces autophagy (Zalckvar et al., 2009). In addition to phosphorylation, TRAF6 mediated ubiquitination of lysine residue 117 within the BH3 domain induces autophagy by affecting the interaction of BECN1 with BCL2 (Shi and Kehrl, 2010). ULK1 mediated phosphorylation of BECN1 at S14 leads to initiation of autophagy by activation of the ATG14 bound VPS34 complex (Russell et al., 2013). In mTOR dependent manner, ULK1 also directly phosphorylates ATG14 at serine 29 residues and positively regulates ATG14-VPS34 activity (Wold et al., 2016). VPS34, another component of the PI3KC3 complex, is phosphorylated by CDK1 and CDK5 which inhibits its interaction with BECN1 and thereby inhibits autophagy (Furuya et al., 2010). p300 mediated acetylation of VPS34 at K771 and K29 negatively regulates VPS34 activity. The acetylation at K771 reduces VPS34's affinity for phosphatidylinositol leading to reduced production of PI3P, while the acetylation at K29 affects the formation of the BECN1-VPS34 complex (Su et al., 2017). TRIM28, an E3 ligase, positively regulates autophagy by increasing VPS34 activity via SUMOylation of K840 (Yang et al., 2013).

The core proteins of the conjugation system, the ATG8s family proteins, are regulated by both phosphorylation and acetylation in addition to proteolysis. LC3B S12 phosphorylation mediated by protein kinase A (PKA) inhibits autophagy via reduced recruitment of LC3B to the phagophore (Cherra et al., 2010). PMA induced activation of protein kinase C leads to increased phosphorylation of LC3B at T6 and T29 (Jiang et al., 2010), but no effect on autophagy was detected. Recently, STK3/STK4 was found to phosphorylate LC3B T50, a site near the LDS. The phosphorylation of LC3B T50 enhanced autophagosome-lysosome fusion (Wilkinson et al., 2015). Two residues within the LDS site, K49, and K51 are regulated by p300 mediated acetylation. Under the nutrient-rich condition, p300 acetylates nuclear LC3B at K49 and K51, preventing its interaction with autophagy proteins such as ATG7 (Huang et al., 2015).

Upon starvation, SIRT1 deacetylates LC3B. Deacetylated LC3B is shuttled out of the nucleus by TP53INP2 to the autophagosome formation sites in the cytoplasm (Huang et al., 2015). P300 also inhibits autophagy by acetylation of proteins associated with the conjugating system such as ATG12, ATG5, and ATG7 (Lee and Finkel, 2009).

Autophagy is also regulated at the transcription level, and several transcription factors regulating autophagy have been identified. The localization and activity of many transcription factors are regulated by PTMs. For example, the FOXO family regulates the expression of several genes associated with autophagy. Starvation-induced dephosphorylation of FOXO1 and FOXO3 results in shuttling from the cytoplasm to the nucleus where they induce expression of autophagy-related genes (Sengupta et al., 2009). FOXO1 also regulate autophagy in a transcriptional independent manner by direct interaction with ATG7. Serum deprivation or oxidative stress induced acetylation of FOXO1 is required for this interaction, which promotes autophagy (Zhao et al., 2010). The transcription factor EB (TFEB) is a master regulator of lysosomal function and autophagy. Under nutrient-rich conditions, TFEB is cytoplasmic and inactive. Under nutrient deficient conditions, dephosphorylation of TFEB at S142 and S211 leads to nuclear localization, activation and subsequent transcription of its target genes (Roczniak-Ferguson et al., 2012; Settembre et al., 2011).

Regulation of autophagy by serine-threonine kinases

STK3/STK4

The mammalian sterile 20-like kinases MST1(STK4) and MST2(STK3) are closely related protein serine-threonine kinases and are orthologues of the *Drosophila* Hippo kinase. They share ~ 75% sequence identity and >95% sequence identity within their catalytic domains. They were identified in a search for protein kinases with catalytic domains related to the *Saccharomyces cerevisiae* kinase Ste20 (hence mammalian Ste20 related)(Creasy and Chernoff, 1995). STK3/STK4 contain an N-terminal kinase domain followed by an autoinhibitory domain and a C-terminal SARA domain (**Figure 10**) (Creasy et al., 1996). The coiled-coil SARA domain mediates homo- and heterodimerization. SARA domains are ~50 amino acids long and are named due to similar homologues structures within three gene families of SAV1/WW45 (*Drosophila* ortholog **Salvador**), **RASSF** 1-6, and **Hippo** (*Drosophila* orthologues)/MST1/MST2 (Khokhlatchev et al., 2002; Scheel and Hofmann, 2003).



Figure 10: Schematic diagrams of STK3 domain structure comprising N-terminal kinase domain and C-terminal SARAH domain.

Activation of STK3/STK4 requires phosphorylation of a threonine residue within the activation loop (T183 in STK4 and T180 in STK3)(Praskova et al., 2004). Deletion of the autoinhibitory domain enhances the kinase activity whereas deletion of the SARAH domain reduces its activity due to the failure of the kinase to form homodimers (Praskova et al., 2004). In the Hippo pathway, STK3 and STK4 form a complex with their regulatory protein SAV1/WW45 and phosphorylate the downstream substrate LATS1/LATS2. In addition, STK3/STK4 also phosphorylate the LATS1/2 regulatory subunits MOB1A/MOB1B. The phosphorylation of the LATS1/2-MOB1A/B complex leads to its activation, which in turn phosphorylates the transcriptional co-activators YAP and TAZ. The phosphorylations lead to inhibition of YAP and TAZ transcriptional activity by preventing their nuclear translocation and enhancing their proteasomal degradation in the cytoplasm. These transcriptional co-activators regulate transcription of target genes associated with cell proliferation and survival (Meng et al., 2016). Besides the role of STK3/STK4 in the Hippo pathway, they are shown to interact with ATG8 family proteins and negatively regulate autophagy (Behrends et al., 2010). There are several contradictory results regarding the role of STK4 in autophagy. On one hand, STK3/STK4 was identified as a kinase that phosphorylates LC3B at T50 leading to enhanced autophagosome-lysosome fusion (Wilkinson et al., 2015). Another study showed that STK4 acts as a negative regulator of autophagy by phosphorylation of BECN1 leading to increased interaction with its negative regulator BCL2 (Maejima et al., 2013).

PKC ζ

In mammals, the Protein Kinase C (PKC) superfamily consists of 10 related serine-threonine kinases. The PKC superfamily is classified into three subfamilies based on their regulatory domains and physiological activators: classical, novel and atypical. The Classical PKCs contains three members (α , β , and γ) and their activity depends on the level of intracellular calcium, diacylglycerol (DAG), and phosphatidylserine (PS). The novel PKCs comprises four members (δ , ϵ , θ , and η) and their activation depend on DAG and PS but does not require

calcium. In contrast to the classical and novel PKCs, atypical PKC does not require DAG and calcium for their activation (Spitaler and Cantrell, 2004).

The atypical PKCs consist of two members, PKC ζ and PKC $\lambda/1$. The human PKC ι and mouse PKC λ are orthologs and share 98% amino acid sequence identity and thus referred to as PKC $\lambda/1$. Moreover, amino acid sequence identity within PKC ζ and PKC $\lambda/1$ is 86%. Both PKC ζ and PKC $\lambda/1$ contain an N-terminal PB1 domain, pseudosubstrate sequence, a cysteine-rich zinc finger domain, kinase domain and hydrophobic motif at C-terminal region. (**Figure 11**) (Suzuki et al., 2003). The kinase domain of PKC ζ comprises an ATP binding region and an activation loop whereas AGC-kinase C-terminal domain contains a turn motif and a hydrophobic motif.

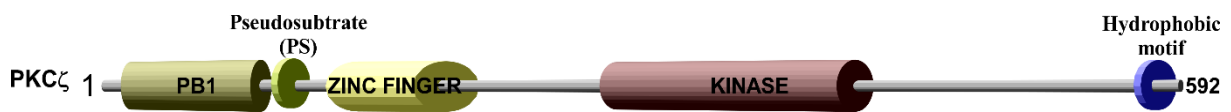


Figure 11: Schematic diagram of PKC ζ domain structure comprising N-terminal PB1 domain followed by pseudosubstrate sequence (PS), zinc finger domain, kinase domain and hydrophobic motif.

Activation of PKC ζ requires two sequential events: the first release of the pseudosubstrate from the substrate binding pocket and second phosphorylation of its kinase domain (Newton, 2001). Several lipid components such as phosphatidylinositols, phosphatidic acid, arachidonic acid, and ceramide are found to activate PKC ζ (Limatola et al., 1994; Muller et al., 1995; Nakanishi et al., 1993). Activation of PKC ζ by enzymatically synthesized phosphatidylinositol 3,4,5 triphosphate (PIP₃) suggested that it may be regulated by PI3K, a kinase which produces PIP₃ in response to several growth factors (Nakanishi et al., 1993). Pleckstrin homology domain containing proteins such as AKT and PDK1 (3'-PI-dependent protein kinase 1) are activated by direct binding to PIP₃. Activated PDK1 interacts with the C-terminal hydrophobic motif within PKC ζ and phosphorylates the T410 residues within the activation loop. This leads to exposure of its kinase active site and subsequent autophosphorylation of T560 in the turn motif, which is essential for PKC ζ catalytic activity (Le Good et al., 1998).

PKC ζ is reported to be implicated in cell polarity, p70S6-protein kinase signaling cascade, NF- κ B activation and the mitogen-activated protein kinase cascade (Reyland, 2009). Besides the canonical PKC ζ isoform, a shorter isoform lacking the N-terminal regulatory domain is found to be specific for neuron tissues and named protein kinase M zeta (PKM ζ).

PKM ζ is constitutively active and has an essential role in the maintenance of long-term memory (Sacktor, 2012).

PKC ι negatively regulates autophagy via inactivation of the PI3CA/AKT-mTOR signaling pathway (Qu et al., 2016). However, the roles of atypical PKCs in autophagy is not well understood.

NIMA-related Kinase 9 (NEK9)

Genetic screening in *Aspergillus nidulans* for cell cycle mutants lead to the identification of never-in-mitosis A (NIMA), a serine-threonine kinase (Oakley and Morris, 1983). The deletion of NIMA kinase was found to be associated with G2 cell cycle arrest, whereas overexpression leads to premature entry into mitosis (Osmani et al., 1988). Subsequently, NIMA related kinases were found in a wide range of organisms. The human genome contains 11 genes that encode NEK1-NEK11 compared to *Aspergillus nidulans* which has a single gene. All members of this kinase family contain an N-terminal kinase domain, with exception of NEK10 having a centrally located kinase domain. The kinase domain contains a His-Arg-Asp (HRD) motif which is positively regulated by phosphorylation (Johnson et al., 1996). In addition, the kinase activity is regulated by phosphorylation of serine or threonine residues within the activation loop (Roig et al., 2005). The human NEK consensus motif for substrate phosphorylation is F/L XX S/T (where xx denote any residue), with a preference for hydrophobic residues preceding the phosphorylation site (Alexander et al., 2011; Lizcano et al., 2002). The domain structure of human NEK9 is shown in (**Figure 12**).



Figure 12: Schematic diagrams of NEK9 domain structure comprising N-terminal kinase domain, 6 repeats of regulator of chromosome condensation 1(RCC1) domain and a C-terminal coiled-coil domain.

The functions of NEKs are associated with mitotic spindle assembly, centrosome separation, chromatin condensation, disassembly of the nuclear pore complex and breakdown of the nuclear envelope (Quarmby and Mahjoub, 2005). Knockdown of NEK6, NEK7, and NEK9 leads to a defect in centrosome separation and formation of a weak mitotic spindle (Sdelci et al., 2011). NEK9 acts as an upstream kinase that phosphorylates both NEK6 and NEK7 and thereby activates their kinase activity (Roig et al., 2005). The role of NEKs in autophagy is unknown. However, an autophagy interactome study showed the interaction of

NEK9 with the human ATG8 family proteins, indicating its potential as a regulator of autophagy (Behrends et al., 2010).

Aims of the study

The autophagy process is tightly regulated and induced upon various types of cellular stresses. Furthermore, the activity of many autophagy proteins is regulated by subcellular localization. For example, the most recognized autophagy marker protein LC3B is enriched in the cell nucleus under normal cellular conditions. However, when mTOR activity is impaired due to starvation conditions, LC3B is redistributed to autophagy structures in the cytoplasm. The main hypothesis of this work was that the interaction of LC3 with LIR-containing proteins is regulated by posttranslational modifications induced by cellular stress.

To test this hypothesis, the following aims of the study were defined:

- i) Identify protein kinases that have the capacity to modulate LDS-LIR interactions by phosphorylation events.
- ii) Identify the mechanisms involved in the subcellular regulation of TP53INP2 which has been reported to act as a LC3B chaperone facilitating nuclear export of LC3B upon mTOR inhibition.
- iii) Study the importance of LIR motifs for the interaction of ATG4B with LC3s and GABARAPs.

Summary of papers

Paper I

Birendra Kumar Shrestha Mads Skytte Rasmussen, Yakubu Abudu Princely, Jack-Ansgar Bruun, Kenneth Bowitz Larsen, Endalkachew A. Alemu, Eva Sjøttem, Trond Lamark & Terje Johansen (2019)

Phosphorylation of LC3B at threonine-50 inhibits selective autophagy. *Manuscript*

In this study, we showed that four serine-threonine kinases mediate phosphorylation of LC3B at the T50 residue *in vitro*. Various binding assays showed that three of these, STK3, PKC ζ and NEK9, bound to the ATG8 proteins via LIR motifs within the kinases. A phospho-mimicking T50E mutant of LC3B displayed reduced binding to various autophagy-related proteins. Furthermore, reconstitution of the phospho-mimicking LC3B T50E mutant in LC3B KO cells resulted in reduced selective autophagy compared to wild type cells. Importantly, and in contrast to STK3, ablation of NEK9 lead to enhanced autophagic flux. This indicates that NEK9 has the potential to regulate selective autophagy by mediating phosphorylation of LC3B at T50.

Paper II

Birendra Kumar Shrestha, Eva Sjøttem, Aud Øvervatn, Hanne B Brenne, Jack-Ansgar Bruun, Trond Lamark & Terje Johansen (2019)

Subcellular localization of TP53INP2 is regulated by acetylation. *Manuscript*

Here we show that the subcellular localization of TP53INP2 is regulated by acetylation events in an mTOR dependent manner. TP53INP2 is a nuclear protein under normal cellular conditions, and we mapped a nuclear localization signal (NLS) encompassing a nucleolar localization signal (NoLS) sequence within the C-terminal part of TP53INP2. Deletion of the NLS leads to cytoplasmic accumulation and degradation of TP53INP2 via the autophagy pathway. Similarly, inactivation of mTORC1 leads to cytoplasmic accumulation of TP53INP2. We found that this was due to acetylation of K187 within the NLS leading to inhibition of nuclear import of TP53INP2. Moreover, mTOR inhibition leads to ablation of nuclear TP53INP2, and we show that this is regulated by facilitated proteasomal degradation of TP53INP2. We identified that acetylation of the residues K159 and K204 within TP53INP2 is implicated in this regulation.

Paper III

Mads Skytte Rasmussen, Stéphane Mouilleron, Birendra Kumar Shrestha, Martina Wirth, Rebecca Lee, Kenneth Bowitz Larsen, Yakubu Abudu Princely, Nicola O'Reilly, Eva Sjøttem, Sharon A. Tooze, Trond Lamark & Terje Johansen (2017)

ATG4B contains a C-terminal LIR motif important for binding and efficient cleavage of mammalian orthologs of yeast Atg8. *Autophagy* 13: 834-853.

In this study, we show that human ATG4B contains an LC3 interacting region (LIR) motif in its C-terminal region. We solved the crystal structure of GABARAPL1 in complex with a peptide containing the ATG4B C-terminal LIR motif, revealing the essential residues that mediated the LIR-LDS interaction. These residues were further confirmed by mutation analysis. By *in vitro* and in cell studies we found that the ATG4B C-terminal LIR motif is important for efficient cleavage and delipidation of the ATG8 family protein. In addition, we found that the C-terminal LIR motif stabilizes unlipidated GABARAP and GABARAPL1 by preventing them from proteasomal degradation.

Discussion

In this thesis, we set out to study the regulation of the ATG8-LIR interactions by posttranslational modifications mediated by stress signaling pathways. An earlier publication showed that phosphorylation of LC3B threonine-50 (T50) by STK3/STK4 positively regulated autophagy (Wilkinson et al., 2015). We sought for kinases with potential to phosphorylate the T50 residue and identified NEK9 and PKC ζ as additional candidates (Paper I). We further investigated whether phosphorylation of T50 in LC3B, a site close to the LDS region, affected the interaction of LC3B with various autophagy proteins. The autophagic activity of LC3B is also regulated by nucleo-cytoplasmic shuttling, reported to be chaperoned by the nuclear protein TP53INP2 (Huang et al., 2015). The subcellular localization of TP53INP2 itself is regulated by cellular stresses like starvation (Nowak et al., 2009), and in Paper II we found that this is mediated by acetylation events on specific lysine residues within TP53INP2. We revealed that the subcellular redistribution of TP53INP2 involved cytoplasmic retention and nuclear degradation in an mTOR dependent pathway. This will shed more light on the regulation of LC3B localization upon autophagy induction. In Paper III, we looked into the regulation of LC3B by proteolytic cleavage mediated by the protease ATG4B. We identified a C-terminal LIR motif in ATG4B important for efficient cleavage and delipidation of LC3B.

In this chapter, the work conducted in the three papers will be discussed separately and put into context. For a more detailed discussion of the individual results, please consult the discussion sections of the respective papers.

Regulation of the LC3B by phosphorylation of threonine-50 (Paper I)

A previous work on the ATG8 interactome by Christian Behrends and colleagues identified several kinases with potential to bind ATG8 proteins. Here we set out to verify these interactions further and to determine their biological relevance (Behrends et al., 2010).

We confirmed that the STK3, PKC ζ , and NEK9 serine-threonine kinases interacted with human ATG8s. In contrast, we could not find any direct interaction of STK4 with the ATG8s. STK3 displayed very strong binding to LC3C and GABARAP but surprisingly the interaction with LC3B was weak. The strong preference for LC3C suggested that the interaction might involve a C type LIR motif. This was in line with the finding that interaction of STK3 with LC3C F58A, an LDS mutant, completely impaired binding. Furthermore, we identified a CLIR-like motif “**MVI**” in STK3 mediating the strong interaction with LC3C and GABARAP. It is previously published that LC3B is phosphorylated by STK3/STK4 at T50, which was

confirmed in our study. The functional relevance of this phosphorylation was shown to be enhanced autophagosome lysosomal fusion and elimination of pathogens (Wilkinson et al., 2015). Our finding that STK3 displays strong preference towards LC3C, combined with the knowledge on important roles of LC3C in xenophagy via NDP52 interactions, could indicate that STK3 also plays a role in xenophagy via phosphorylation of LC3C. Interestingly, we found that the phospho-mimicking LC3C T56E mutant had reduced the ability to interact with NDP52. This suggests that STK3 may be a negative regulator of xenophagy. Whether STK3 phosphorylates LC3C *in vivo* and thereby regulates xenophagy will be an important question to address in future studies.

We found the atypical serine-threonine kinase, PKC ζ , to interact with all the human ATG8s homologues, with a preference for GABARAP. Both *in vitro* and *in vivo* association assays showed that PKC ζ strongly interacts with GABARAP. Binding assays using LC3B and GABARAP LDS mutants suggested that the interaction was mediated by LIR motifs, and we identified a canonical LIR motif located within the C-terminal part of the kinase. Interestingly, the LIR motif completely overlapped with a hydrophobic motif known to mediate PKC ζ interaction with its activating kinase, PDK1 (Parekh et al., 2000). This hydrophobic motif is essential for the activation of PKC ζ by PDK1. It will be interesting to investigate whether interactions mediated by these overlapping motifs differentiate the roles of PKC ζ in autophagy and other cellular processes. The PB1 domain of PKC ζ mediates interaction with the autophagic receptor p62, which adds another dimension to its possible role in autophagy. By *in vitro* kinase assays, we found that PKC ζ has the potential to phosphorylate LC3B at T50. An important question to address in future studies will be the effect of KD/KO of PKC ζ on basal autophagy.

NEK9 is previously reported to interact with the ATG8 proteins (Behrends et al., 2010), but its role in the regulation of autophagy is not well understood. Here we found that NEK9 interacts with all human ATG8s homologues both in *in vitro* and *in vivo* binding assays. The interaction was LIR-LDS-mediated since the NEK9 interaction with a GABARAP LDS mutant was impaired. We screened all potential LIR motifs within NEK9 and identified that mutation of the residues W967 and L970 reduced its interaction with the ATG8s. This LIR motif is preceded by a stretch of acidic aspartic residues (D963 and D965) and serine residues (S964 and S966) and followed by an acidic aspartic residue (D973), threonine (D972) and serine (S974) residues. Phosphorylatable amino acid residues are often associated with the regulation of LIR-LDS-interactions (Birgisdottir et al., 2013). We observed increased ATG8 binding of a NEK9 LIR peptide, when the serine residue at S966, threonine at T972 and serine at S974 were

substituted with glutamic acids, suggesting phosphorylation-mediated regulation of the NEK9 LIR-LDS interaction. Interestingly, *in vitro* kinase assay showed that NEK9 has the ability to phosphorylate LC3B at T50, while siRNA mediated knockdown of NEK9 resulted in increased autophagic flux indicated by enhanced degradation of the autophagic receptor proteins p62 and NBR1. These results were supported by analysis of autophagic flux in a CRISPR/CAS9 NEK9 KO cell line. Hence, our results suggest that a possible mechanism for NEK9 to regulate selective autophagy implicates phosphorylation of LC3B T50.

The phospho-mimicking T50E mutant of LC3B regulates LIR-LDS interactions (Paper I)

PTMs act as switches in the regulating of protein-protein interactions and thereby regulation of protein function. LC3B interacts with several autophagy-related proteins via LIR-LDS interactions (Birgisdottir et al., 2013). Interestingly, the LC3B LDS contains two lysine residues (K49 and K51) and one threonine residue (T50) indicating possible regulation of function via PTMs. Recently, it was shown that under nutrient-rich condition, nuclear LC3B is acetylated at the K49 and K51 residues by the acetyltransferases p300 and CBP (Huang et al., 2015). These acetylations inhibit interaction with TP53INP2 and thereby prevents the nuclear export of LC3B. Upon starvation or mTOR inactivation, SIRT1 deacetylates nuclear LC3B K49 and K51 residues and restores its interaction with TP53INP2 leading to nuclear export of LC3B. In the cytoplasm, this nuclear LC3B protein pool interacts with autophagy-related proteins to initiate autophagosome formation (Huang et al., 2015). The STK3/STK4 kinases are previously reported to phosphorylate the T50 residue regulating autophagosome-lysosome fusion (Wilkinson et al., 2015). We set out to investigate the functional effects of the T50 phosphorylation using a phospho-mimicking LC3B T50E mutant. To avoid possible effects of endogenous LC3B, we used CRISPR/Cas9 to KO endogenous LC3B and later reconstitute the KO cell line with Myc tagged LC3B WT, LC3B T50A, T50E, and the LDS mutant F52A/L53A. The LC3B KO cells showed reduced autophagic flux, indicated by increased accumulation of p62 and NBR1 (Maruyama et al., 2014), which was restored by reconstitution with LC3B WT. Interestingly, reconstitutions with LC3B T50E and F52A/L53A lead to increased inhibition of autophagic flux compared to the LC3B KO cell line, suggesting negative regulation of autophagy via T50 phosphorylation. These results were supported by reconstitution of the LC3B KO cells with mCherry-EYFP-LC3B WT and T50E, showing that mCherry-EYFP-LC3B T50E formed fewer autophagosomes than WT. The drawback of using a phospho-

mimicking mutant is that it is constitutively mimicking phosphorylation. In cells, phosphorylation is a dynamic process often acting as a switch to turn on or off interaction or activities regulated by specific kinases and phosphatases. To further investigate the consequences of LC3B T50 phosphorylation, we performed various binding assays with autophagy-related proteins containing LIR motifs. Importantly, we revealed that binding of the LC3B T50E mutant with autophagic receptors such as p62 and NBR1 is significantly reduced compared to the wild type protein. Moreover, the interactions with ATG4B and with ATG7 were both severely reduced. Interestingly, the LC3B-ATG7 interaction was not affected by the LC3B F52A/L53A mutation, indicating that the interaction of LC3B with ATG7 does not involve the LDS site directly, but rather electrostatic interactions. This displays similarity with a previous study showing that Lamin B1 interacts with LC3B via electrostatic interactions with the R10 and R11 residues (Dou et al., 2015). From the predicted structure (**Paper I, Figure 6A**), phosphorylation of LC3B T50 inhibits such electrostatic interactions. Altogether, these results show that phosphorylation of LC3B T50 can affect the cleavage and lipidation steps. Furthermore, we observed reduced interaction of the LC3B T50E mutant with FYCO1, indicating that completed autophagosomes might have reduced capacity to be transported to perinuclear lysosomal compartments for lysosomal fusion. The LC3B interaction partner syntaxin 17 is associated with autophagosome-lysosome fusion (Itakura et al., 2012). It is published that the LC3B-syntaxin 17 interaction is LIR-LDS mediated (Kumar et al., 2018). We found reduced interaction of LC3B T50E with syntaxin 17 compared to wild type LC3B, indicating that the phosphorylation may negatively regulate the autophagosome lysosomal fusion process. Thus, phosphorylation of LC3B T50 seems to have a negative effect on LIR-LDS interactions in general and may be an important site for regulation of the autophagic activity of LC3B.

Acetylation regulates subcellular localization and degradation of TP53INP2 (Paper II)

TP53INP2 in a previous study showed to act as a LC3B chaperone, mediating nuclear export of LC3B upon starvation conditions (Huang et al., 2015). The study showed that nuclear export of TP53INP2 itself is regulated by 4 major factors: mTOR activity, a nuclear export signal, interactions with ATG8s via an LIR motif, and ATG5 (Nowak et al., 2009; Sancho et al., 2012). In this paper, we report several conflicting results to these studies. Instead of nuclear export, we found that upon mTOR inactivation, the relocalization of TP53INP2 is due to inhibition of nuclear import combined with rapid degradation of the nuclear pool of TP53INP2

proteins. These findings were supported by the absence of a functional NES motif in TP53INP2, failure of the CRM1 inhibitor LMB to restrict TP53INP2 inside the nucleus, reduced interaction of TP53INP2 with importin under mTOR inhibition, and finally FRAP experiments showing no export of nuclear proteins. Furthermore, analysis in ATG5 KO cells showed similar localization of TP53INP2 as the WT cells under cellular stress conditions, indicating that the redistribution of TP53INP2 is independent of autophagy. To conclude, our study does not rule out nuclear export of deacetylated LC3B upon mTOR inhibition, but our data strongly suggest that TP53INP2 does not act as a scaffolding protein for this process.

The role of TP53INP2 in autophagosome formation is well recognized, recruiting LC3B and the BECN1 complex to the forming autophagosome (Nowak et al., 2009). The recruitment of LC3B to the autophagosome structure is mediated by a direct LIR motif dependent interaction, whereas the BECN1 complex is recruited by VMP1 interactions (Nowak et al., 2009). Furthermore, TP53INP2 is reported to contribute to autophagosome formation by facilitating the interaction of LC3 with ATG7 (You et al., 2019). However, this study failed to prove the contribution of TP53INP2 in autophagosome formation, as KD of TP53INP2 did not affect the formation of autophagosomes. In line with this study, we did not detect any significant effect of TP53INP2 KO on basal autophagy or starvation-induced autophagy. However, we cannot rule out the possibility that TP53INP1 and TP53INP2 may have redundant functions in autophagosome formation. This has to be addressed by future studies in a TP53INP1/TP53INP2 double KO cell model. Furthermore, our data also suggest that the recruitment of TP53INP2 into autophagosome structures observed in previous studies might be the result of overwhelming the regulation of TP53INP2 for degradation by the proteasomal pathway - leading to cytoplasmic overexpression and degradation by a compensatory autophagy pathway. This is based on our finding that an expression level of TP53INP2 close to endogenous level (which we obtained by reconstituting TP53INP2 KO cells with EGFP-TP53INP2), failed to co-localize with LC3B positive structures in the cytoplasm. However, over-expressed EGFP-TP53INP2 colocalized with cytoplasmic LC3B positive structures. Furthermore, deletion of the NLS signal in TP53INP2 resulted in cytoplasmic over-expression and co-localization with cytoplasmic LC3B dots. Thus, according to our results, the cytoplasmic degradation of TP53INP2 is regulated by C-terminal lysine residue modification. During the overexpression of TP53INP2, such regulation is overridden. As mentioned above, we could not see any effect of KO of TP53INP2 in autophagic flux, lead to raising a question for a novel functional role of cytoplasmic TP53INP2 on mTOR inactivation. Interestingly, recently a novel role of TP53INP2

in death receptor signaling was reported (Ivanova et al., 2019). This study showed that TP53INP2 sensitizes various cell lines to death receptor-induced apoptosis by increasing the activation of caspase 8 upon TRAF6 dependent K63 ubiquitination (Ivanova et al., 2019). Hence, TP52INP2 seems to have functional roles in the cytoplasm unrelated to the regulation of the autophagy pathway. The nuclear role of TP53INP2 is well understood. Under the nutrient-rich condition, TP53INP2 is localized to both nucleus and nucleoli where it facilitates the transcription activity of the thyroid hormone receptor and of RNA polymerase I important for biogenesis of the ribosomes (Baumgartner et al., 2007). These observations are in line with our study, as TP53INP2 KO cells displayed reduced cell proliferation and transcription of rDNA.

Several transcription factor's subcellular localization is regulated by posttranslational modifications. For example, the nuclear-cytoplasmic shuttling of TFEB, a master regulator of lysosomal biogenesis, is controlled by phosphorylation of two key serine residues (S142 and S211)(Roczniak-Ferguson et al., 2012; Settembre et al., 2011). Under mTOR inactivation, these serine residues are dephosphorylated leading to nuclear import. With this in mind, we investigated the potential role of phosphorylation events in regulating nuclear-cytoplasmic shuttling of TP53INP2. However, deletion of serine/threonine residues did not display any effect on nuclear import. Instead, the mutation of lysine residue K187 completely inhibited nuclear import of TP53INP2, indicating that acetylation could be involved in the regulation of the nuclear-cytoplasmic localization. Mass spectrometry data indicated that all three-lysine residues in the C-terminal, K165, K187, and K204, undergo acetylation under starvation. Mutation of K165 and K204 resulted in accumulation of TP53INP2, suggesting that acetylation of these residues enhances degradation of nuclear TP53INP2 under starvation. This fits with its anabolic role under nutrient-rich conditions, facilitating ribosomal biogenesis. Unlike other autophagy-related proteins, such as ATG7, ATG8, and ATG12 which are deacetylated upon starvation (Lee and Finkel, 2009), TP53INP2 undergoes acetylation upon starvation. However, acetylation is observed for other proteins like tubulin, which undergoes hyperacetylation under starvation conditions (Geeraert et al., 2010). Interestingly, a study showed that AMPK mediates p300 dependent acetylation of importin α 1 and thereby regulates the nuclear import of the RNA binding protein, Hu-antigen R (Wang et al., 2004). P300 mediated acetylation of the histone deacetylase HDAC6 blocks its interaction with importin α and thereby inhibits HDAC6 nuclear import (Liu et al., 2012). In line with these studies, we found that p300/CBP can mediate

acetylation of all three-lysine residue in TP53INP2 and thereby regulate both nuclear degradation and nuclear import of TP53INP2.

In contrast to TP53INP1 which undergoes lysosomal degradation under nutrient-rich conditions (Seillier et al., 2012), our data indicate that TP53INP2 can be degraded by a nucleolar ubiquitin-independent proteasomal pathway. The nucleolar ubiquitin-independent proteasomal pathway is not well characterized. Recently, a protein interacting with carboxyl terminus 1 (PICT1), a nucleolar ribosomal protein and regulator of p53, was shown to be degraded by a nucleolar ubiquitin-independent proteasomal pathway (Maehama et al., 2014). Interestingly, under starvation, we observed increased levels of TP53INP2. This increased level was not only due to cytoplasmic retention but predominantly resulted from new protein synthesis. Inhibition of protein synthesis by cycloheximide treatment of cells exposed to starvation showed no increased accumulation of TP53INP2. Interestingly, a study has shown that the expression of p53, an inducer of TP53INP2, is increased in hepatic tissue under starvation. This was required for gluconeogenesis and amino acid catabolism, and dependent on AMPK signaling (Prokesch et al., 2017). Moreover, a study performed proteomic profiling of de novo protein synthesis under starvation-induced autophagy was recently published (Wang et al., 2016a), pointing towards increasing interest on proteins that are stabilized and hence may serve important roles in starving cells. Thus, the functional role of starvation-induced stabilization of TP53INP2 will be an important subject for future research.

ATG4B-mediated regulation of ATG8s via LIR-mediated binding (Paper III)

The functional roles of the cysteine protease ATG4B for initial cleavage of pre-ATG8s and later delipidation of ATG8s from membrane structures, are well established (Kabeya et al., 2004; Kirisako et al., 2000). The structure of the ATG4B-LC3B complex has been solved by x-ray crystallography, which has explained the mechanisms involved in LC3B processing and delipidation (Satoo et al., 2009). The ATG4B protein used in the structure analysis lacked the C-terminal region (355-393) because of high flexibility. Thus, the structure failed to provide the contribution of the C-terminal region of ATG4B for binding and cleavage activity. However, the published structure predict the LIR motif in the N-terminal part of ATG4B might mediate interaction with adjacent non-substrate LC3Bs (Satoo et al., 2009). This LIR motif, LIR^N, lacks any preceding acidic residues which are often involved in electrostatic interactions with LC3B. We identified an LIR motif in the C-terminal part of ATG4B, LIR^C, and performed

in vitro and *in vivo* binding and cleavage assays to delineate the roles of each LIR motif for LC3B binding and processing. Interestingly, we found that strong binding between ATG4B and LC3B or GABARAP is mediated by two main interaction sites: the catalytic domain interaction and the LIR^C-LDS interaction. Our modeled structure suggests that such two-surface interactions are possible by a long and flexible linker between the catalytic domain and LIR^C. The requirement of ATG4B LIR^C motif for efficient cleavage of its substrate was further supported by an independent study of ATG4B in *Xenopus Laevis* (Frey and Gorlich, 2015). In this study, the cleavage efficiency of ATG4B was significantly affected by deletion of the ATG4B C-terminal part (Δ 345-384) rather than the N-terminal part (Δ 1-14). However, they did find a reduced activity when a longer region (1-25) was deleted (Frey and Gorlich, 2015). By combining these three studies, we could interpret the ATG4B-LC3B interaction as a three-surface interaction. First, LIR^N may play a role by trans-interaction with an adjacent membrane conjugated LC3B, thereby opening the active site of ATG4B. Secondly, this change in the ATG4B conformation, allows the catalytic site to interact with the ATG8s in a non LIR-LDS manner. Thirdly, the ATG4B LIR^C motif mediates cis-interaction with its substrate LC3B for efficient binding and cleavage. This kind of cis-trans-interaction might be involved *in vivo* for efficient cleavage and delipidation of LC3B on membranous structures. In contrast to human ATG4B, yeast ATG4 displayed a unique type of interaction with ATG8. Yeast ATG4 contains four putative LIR motifs, of which three were found to be functional (Abreu et al., 2017). The yeast LIR motif ¹⁰²**FVPI**¹⁰⁵ was essential for mediating interaction with lipidated ATG8 and is called the ATG8-PE associated region (APEAR). The specific interaction with lipidated ATG8 indicated a specific role in the deconjugation step as deletion of the APEAR motif resulted in defects in cleavage and delipidation. We predict that the human ATG4B LIR^C is functional related to the yeast APEAR since mutation of LIR^C only affected the binding with the ATG8s, while cleavage and autophagic flux was unaltered (Abreu et al., 2017). In contrast, a study in human cells showed that de-lipidation by ATG4B is not a prerequisite for autophagosome formation and fusion with lysosomes. In this study, overexpression of pre-primed LC3B(LC3B with exposed C-terminal glycine) in ATG4B KO cells rescued the autophagic flux (Agrotis et al., 2019).

LIR-LDS interactions are often regulated by phosphorylation of adjacent residues (Birgisdottir et al., 2013). During our study, another research group reported the regulation of ATG4B activity by phosphorylation of two serine residues flanking each side of the ATG4B LIR^C motif (S383 and S392). The phosphorylations of the S383 and S392 residues were shown

to be increased upon mTOR inactivation mediated by Rapamycin, and thereby lead to increased ATG4B cleavage activity (Yang et al., 2015). In support, another study showed that MST4 mediated phosphorylation of ATG4B at S383 leads to enhanced ATG4B activity and autophagy flux in glioblastoma cells. Our GABARAPL1-ATG4B LIR^C structure, however, revealed that phosphorylated S392 is facing toward the solvent and phospho-mimicking mutants of these residues (S383 or S392E) did not significantly affect binding. Recently, a study showed that ULK1-mediated phosphorylation of S316 residues within the kinase domain of ATG4B negatively regulates its catalytic activity (Pengo et al., 2017).

Delipidation of ATG8-PE from the autophagosome membrane is essential for providing an unlipidated pool of ATG8s and for efficient autophagosome lysosomal fusion (Nair et al., 2012). Studies in yeast have shown that for a continuous supply of unlipidated ATG8s, ATG4 dependent delipidation of ATG8-PE from nonPAS membranous structures is required (Yu et al., 2012). Other studies have shown that overexpression of ATG4B stabilizes unlipidated GABARAP and GABARAPL1 sequestering it from delivery to ATG7 (Fujita et al., 2008). In line with these studies, we observed reduced amounts of unlipidated GABARAP and GABARAPL1 in ATG4B KO cells reconstituted with the EGFP-ATG4B LIR^C mutant or the EGFP-ATG4B Δ LIR^C. This result indicates that ATG4 LIR^C motif is required for the formation of a stable complex with GABARAP and GABARAPL1 mediating efficient delipidation. In cells lacking ATG4B, stabilization of the ATG8s was impaired due to rapid proteasomal degradation resulting in a reduced availability of unlipidated ATG8s for autophagosome formation. The strong binding to the ATG8 proteins mediated by the ATG4B LIR^C motif may sequester them from ATG7, and thereby inhibit autophagosome formation. Hence, despite enhancing binding affinity and cleavage efficiency, the ATG4B LIR^C may be associated with negative regulation of autophagy. This negative regulatory effect is probably dependent on the expression level of ATG4B, as observed in another study where overexpression of ATG4B WT had a negative effect on autophagosome formation (Fujita et al., 2008). However, at the low endogenous expression level of ATG4B, the LIR^C may have a positive effect on autophagosome formation due to increased binding affinity and cleavage efficiency.

Methodological considerations

In our study, we used CRISPR/Cas9 technology to generate various KO cell lines. For this purpose, we cloned specific guide RNA sequences targeting the gene of interest into a plasmid expressing Cas9 WT. The Cas9 WT makes double-stranded DNA cut after recognition of PAM sequence and binding of guide RNA with its specific target gene sequence. The guide RNA is normally 21 nucleotides long and can potentially bind to non-target genes leading to off-target effects (Fu et al., 2013). The specificity of CRISPR/Cas9 can be increased using a mutant form of Cas9, which makes single-stranded DNA nicks and requires binding of two guide RNA target sequences for generating a staggered double-stranded DNA cut (Ran et al., 2013). The KO cells generated in this study were made using wild type Cas9, so we cannot rule out possible off-target effects and artifacts due to clonal selection. In paper I, we observed decreased autophagic flux in the LC3B KO cells, leading to accumulation of autophagy receptors such as p62 and NBR1. However, the decreased autophagic flux was restored to normal levels when the LC3B KO cells were reconstituted with myc-tagged LC3B. This strongly indicated that the reduced autophagy flux was a phenotype due to ablation of LC3B, and not due to off-target effects.

The use of double-tagged mCherry-EYFP LC3B could affect the function of LC3B, as a study has shown that the use of EGFP tagged ATG8s failed to rescue ATG8 KO cells (Nguyen et al., 2016). Hence, we do not know to what extent double tagged LC3B punctate structures mimic endogenous LC3B.

We applied the Flp-In T-REx system for reconstitution of LC3B/TP53INP2 KO cells. This system is based on the tetracycline-inducible expression of the gene of interest. Hence, the level of gene expression can be regulated by titration of the inducing agent. However, an expression level completely similar to the endogenous expression levels is hard to obtain. Furthermore, the gene of interest is not under the control of the endogenous promoter, but instead a CMV promoter in the FlpIn system. Hence, a main drawback with the reconstituted KO cells is that the expression of the reconstituted protein is not at the same level or regulated in the same way as the endogenous protein. Thus, if the protein of interest is tightly regulated by the endogenous promoter, higher or lower expression levels could have detrimental functional effects such as in the case of ATG4B where overexpressed ATG4B inhibits autophagosome formation (Fujita et al., 2008). In our ATG4B study, we observed a clear effect of ATG4B on the stabilization of unlipidated GABARAB. Hence, we cannot rule out the possibility of adverse effects of this pool of unlipidated GABARAPs on ULK1 activation

(Joachim et al., 2015). Similar to the negative effect of higher expression of ATG4B, our study suggests that overexpression of TP53INP2 performed in many other studies can override the regulation by PTMs and turn on activation of an alternative degradation pathway.

The use of a phospho-mimicking LC3B T50E construct is not a true reflection of the phosphorylation of T50. Phosphorylation is a dynamic process which is switched on and off at a precise time point, while reconstitution with a phospho-mimicking mutant creates a constitutively active phosphorylation state. Furthermore, glutamic acid does not completely resemble the size and charge of a phosphate group covalently bound to the side chain of threonine.

References

- Abreu, S., F. Kriegenburg, R. Gomez-Sanchez, M. Mari, J. Sanchez-Wandelmer, M. Skytte Rasmussen, R. Soares Guimaraes, B. Zens, M. Schuschnig, R. Hardenberg, M. Peter, T. Johansen, C. Kraft, S. Martens, and F. Reggiori. 2017. 'Conserved Atg8 recognition sites mediate Atg4 association with autophagosomal membranes and Atg8 deconjugation', *EMBO Rep*, 18: 765-80.
- Agrotis, A., N. Pengo, J. J. Burden, and R. Ketteler. 2019. 'Redundancy of human ATG4 protease isoforms in autophagy and LC3/GABARAP processing revealed in cells', *Autophagy*, 15: 976-97.
- Alemu, E. A., T. Lamark, K. M. Torgersen, A. B. Birgisdottir, K. B. Larsen, A. Jain, H. Olsvik, A. Overvatn, V. Kirkin, and T. Johansen. 2012. 'ATG8 family proteins act as scaffolds for assembly of the ULK complex: sequence requirements for LC3-interacting region (LIR) motifs', *J Biol Chem*, 287: 39275-90.
- Alers, S., A. S. Loffler, F. Paasch, A. M. Dieterle, H. Keppeler, K. Lauber, D. G. Campbell, B. Fehrenbacher, M. Schaller, S. Wesselborg, and B. Stork. 2011. 'Atg13 and FIP200 act independently of Ulk1 and Ulk2 in autophagy induction', *Autophagy*, 7: 1423-33.
- Alers, S., S. Wesselborg, and B. Stork. 2014. 'ATG13: just a companion, or an executor of the autophagic program?', *Autophagy*, 10: 944-56.
- Alexander, J., D. Lim, B. A. Joughin, B. Hegemann, J. R. Hutchins, T. Ehrenberger, F. Ivins, F. Sessa, O. Hudecz, E. A. Nigg, A. M. Fry, A. Musacchio, P. T. Stukenberg, K. Mechtler, J. M. Peters, S. J. Smerdon, and M. B. Yaffe. 2011. 'Spatial exclusivity combined with positive and negative selection of phosphorylation motifs is the basis for context-dependent mitotic signaling', *Sci Signal*, 4: ra42.
- Arstila, A. U., and B. F. Trump. 1968. 'Studies on cellular autophagocytosis. The formation of autophagic vacuoles in the liver after glucagon administration', *Am J Pathol*, 53: 687-733.
- Asher, G., P. Tsvetkov, C. Kahana, and Y. Shaul. 2005. 'A mechanism of ubiquitin-independent proteasomal degradation of the tumor suppressors p53 and p73', *Genes Dev*, 19: 316-21.
- Axe, E. L., S. A. Walker, M. Manifava, P. Chandra, H. L. Roderick, A. Habermann, G. Griffiths, and N. T. Ktistakis. 2008. 'Autophagosome formation from membrane compartments enriched in phosphatidylinositol 3-phosphate and dynamically connected to the endoplasmic reticulum', *J Cell Biol*, 182: 685-701.
- Bach, M., M. Larance, D. E. James, and G. Ramm. 2011. 'The serine/threonine kinase ULK1 is a target of multiple phosphorylation events', *Biochem J*, 440: 283-91.
- Backer, J. M. 2016. 'The intricate regulation and complex functions of the Class III phosphoinositide 3-kinase Vps34', *Biochem J*, 473: 2251-71.
- Balch, W. E., R. I. Morimoto, A. Dillin, and J. W. Kelly. 2008. 'Adapting proteostasis for disease intervention', *Science*, 319: 916-9.
- Baumgartner, B. G., M. Orpinell, J. Duran, V. Ribas, H. E. Burghardt, D. Bach, A. V. Villar, J. C. Paz, M. Gonzalez, M. Camps, J. Oriola, F. Rivera, M. Palacin, and A. Zorzano. 2007. 'Identification of a novel modulator of thyroid hormone receptor-mediated action', *PLoS One*, 2: e1183.
- Behrends, C., M. E. Sowa, S. P. Gygi, and J. W. Harper. 2010. 'Network organization of the human autophagy system', *Nature*, 466: 68-76.
- Betin, V. M., and J. D. Lane. 2009. 'Caspase cleavage of Atg4D stimulates GABARAP-L1 processing and triggers mitochondrial targeting and apoptosis', *J Cell Sci*, 122: 2554-66.
- Birgisdottir, A. B., T. Lamark, and T. Johansen. 2013. 'The LIR motif - crucial for selective autophagy', *J Cell Sci*, 126: 3237-47.

- Birgisdottir, A. B., S. Mouilleron, Z. Bhujabal, M. Wirth, E. Sjøttem, G. Evjen, W. Zhang, R. Lee, N. O'Reilly, S. A. Tooze, T. Lamark, and T. Johansen. 2019. 'Members of the autophagy class III phosphatidylinositol 3-kinase complex I interact with GABARAP and GABARAPL1 via LIR motifs', *Autophagy*: 1-23.
- Buetow, L., and D. T. Huang. 2016. 'Structural insights into the catalysis and regulation of E3 ubiquitin ligases', *Nat Rev Mol Cell Biol*, 17: 626-42.
- Chan, E. Y., A. Longatti, N. C. McKnight, and S. A. Tooze. 2009. 'Kinase-inactivated ULK proteins inhibit autophagy via their conserved C-terminal domains using an Atg13-independent mechanism', *Mol Cell Biol*, 29: 157-71.
- Cherra, S. J., 3rd, S. M. Kulich, G. Uechi, M. Balasubramani, J. Mountzouris, B. W. Day, and C. T. Chu. 2010. 'Regulation of the autophagy protein LC3 by phosphorylation', *J Cell Biol*, 190: 533-9.
- Choy, A., J. Dancourt, B. Mugo, T. J. O'Connor, R. R. Isberg, T. J. Melia, and C. R. Roy. 2012. 'The Legionella effector RavZ inhibits host autophagy through irreversible Atg8 deconjugation', *Science*, 338: 1072-6.
- Creasy, C. L., D. M. Ambrose, and J. Chernoff. 1996. 'The Ste20-like protein kinase, Mst1, dimerizes and contains an inhibitory domain', *J Biol Chem*, 271: 21049-53.
- Creasy, C. L., and J. Chernoff. 1995. 'Cloning and characterization of a human protein kinase with homology to Ste20', *J Biol Chem*, 270: 21695-700.
- Cuervo, A. M., E. Knecht, S. R. Terlecky, and J. F. Dice. 1995. 'Activation of a selective pathway of lysosomal proteolysis in rat liver by prolonged starvation', *Am J Physiol*, 269: C1200-8.
- De Duve, C., B. C. Pressman, R. Gianetto, R. Wattiaux, and F. Appelmans. 1955. 'Tissue fractionation studies. 6. Intracellular distribution patterns of enzymes in rat-liver tissue', *Biochem J*, 60: 604-17.
- de Waal, E. J., H. Vreeling-Sindelarova, J. P. Schellens, J. M. Houtkooper, and J. James. 1986. 'Quantitative changes in the lysosomal vacuolar system of rat hepatocytes during short-term starvation. A morphometric analysis with special reference to macro- and microautophagy', *Cell Tissue Res*, 243: 641-8.
- Di Rita, A., A. Peschiaroli, D' Acunzo P, D. Strobbe, Z. Hu, J. Gruber, M. Nygaard, M. Lambrugh, G. Melino, E. Papaleo, J. Dengjel, S. El Alaoui, M. Campanella, V. Dotsch, V. V. Rogov, F. Strappazon, and F. Cecconi. 2018. 'HUWE1 E3 ligase promotes PINK1/PARKIN-independent mitophagy by regulating AMBRA1 activation via IKKalpha', *Nat Commun*, 9: 3755.
- Dohi, E., S. Tanaka, T. Seki, T. Miyagi, I. Hide, T. Takahashi, M. Matsumoto, and N. Sakai. 2012. 'Hypoxic stress activates chaperone-mediated autophagy and modulates neuronal cell survival', *Neurochem Int*, 60: 431-42.
- Dorsey, F. C., K. L. Rose, S. Coenen, S. M. Prater, V. Cavett, J. L. Cleveland, and J. Caldwell-Busby. 2009. 'Mapping the phosphorylation sites of Ulk1', *J Proteome Res*, 8: 5253-63.
- Dou, Z., C. Xu, G. Donahue, T. Shimi, J. A. Pan, J. Zhu, A. Ivanov, B. C. Capell, A. M. Drake, P. P. Shah, J. M. Catanzaro, M. D. Ricketts, T. Lamark, S. A. Adam, R. Marmorstein, W. X. Zong, T. Johansen, R. D. Goldman, P. D. Adams, and S. L. Berger. 2015. 'Autophagy mediates degradation of nuclear lamina', *Nature*, 527: 105-9.
- Dubouloz, F., O. Deloche, V. Wanke, E. Camerini, and C. De Virgilio. 2005. 'The TOR and EGO protein complexes orchestrate microautophagy in yeast', *Mol Cell*, 19: 15-26.
- Dyson, H. J., and P. E. Wright. 2005. 'Intrinsically unstructured proteins and their functions', *Nat Rev Mol Cell Biol*, 6: 197-208.
- Egan, D. F., D. B. Shackelford, M. M. Mihaylova, S. Gelino, R. A. Kohnz, W. Mair, D. S. Vasquez, A. Joshi, D. M. Gwinn, R. Taylor, J. M. Asara, J. Fitzpatrick, A. Dillin, B. Viollet, M. Kundu, M. Hansen, and R. J. Shaw. 2011. 'Phosphorylation of ULK1

- (hATG1) by AMP-activated protein kinase connects energy sensing to mitophagy', *Science*, 331: 456-61.
- Fan, W., A. Nassiri, and Q. Zhong. 2011. 'Autophagosome targeting and membrane curvature sensing by Barkor/Atg14(L)', *Proc Natl Acad Sci U S A*, 108: 7769-74.
- Finley, D. 2009. 'Recognition and processing of ubiquitin-protein conjugates by the proteasome', *Annu Rev Biochem*, 78: 477-513.
- Floyd, Z. E., J. S. Trausch-Azar, E. Reinstein, A. Ciechanover, and A. L. Schwartz. 2001. 'The nuclear ubiquitin-proteasome system degrades MyoD', *J Biol Chem*, 276: 22468-75.
- Frey, S., and D. Gorlich. 2015. 'The *Xenopus laevis* Atg4B Protease: Insights into Substrate Recognition and Application for Tag Removal from Proteins Expressed in Pro- and Eukaryotic Hosts', *PLoS One*, 10: e0125099.
- Fu, Y., J. A. Foden, C. Khayter, M. L. Maeder, D. Reyon, J. K. Joung, and J. D. Sander. 2013. 'High-frequency off-target mutagenesis induced by CRISPR-Cas nucleases in human cells', *Nat Biotechnol*, 31: 822-6.
- Fujita, N., M. Hayashi-Nishino, H. Fukumoto, H. Omori, A. Yamamoto, T. Noda, and T. Yoshimori. 2008. 'An Atg4B mutant hampers the lipidation of LC3 paralogues and causes defects in autophagosome closure', *Mol Biol Cell*, 19: 4651-9.
- Furuya, T., M. Kim, M. Lipinski, J. Li, D. Kim, T. Lu, Y. Shen, L. Rameh, B. Yankner, L. H. Tsai, and J. Yuan. 2010. 'Negative regulation of Vps34 by Cdk mediated phosphorylation', *Mol Cell*, 38: 500-11.
- Ganley, I. G., H. Lam du, J. Wang, X. Ding, S. Chen, and X. Jiang. 2009. 'ULK1.ATG13.FIP200 complex mediates mTOR signaling and is essential for autophagy', *J Biol Chem*, 284: 12297-305.
- Gaugel, A., D. Bakula, A. Hoffmann, and T. Proikas-Cezanne. 2012. 'Defining regulatory and phosphoinositide-binding sites in the human WIPI-1 beta-propeller responsible for autophagosomal membrane localization downstream of mTORC1 inhibition', *J Mol Signal*, 7: 16.
- Geeraert, C., A. Ratier, S. G. Pfisterer, D. Perdiz, I. Cantaloube, A. Rouault, S. Pattingre, T. Proikas-Cezanne, P. Codogno, and C. Pous. 2010. 'Starvation-induced hyperacetylation of tubulin is required for the stimulation of autophagy by nutrient deprivation', *J Biol Chem*, 285: 24184-94.
- Geng, J., and D. J. Klionsky. 2008. 'The Atg8 and Atg12 ubiquitin-like conjugation systems in macroautophagy. 'Protein modifications: beyond the usual suspects' review series', *EMBO Rep*, 9: 859-64.
- Gross, S. P., M. Vershinin, and G. T. Shubeita. 2007. 'Cargo transport: two motors are sometimes better than one', *Curr Biol*, 17: R478-86.
- Gutierrez, M. G., D. B. Munafò, W. Beron, and M. I. Colombo. 2004. 'Rab7 is required for the normal progression of the autophagic pathway in mammalian cells', *J Cell Sci*, 117: 2687-97.
- Gwinn, D. M., D. B. Shackelford, D. F. Egan, M. M. Mihaylova, A. Mery, D. S. Vasquez, B. E. Turk, and R. J. Shaw. 2008. 'AMPK phosphorylation of raptor mediates a metabolic checkpoint', *Mol Cell*, 30: 214-26.
- Hamacher-Brady, A., and N. R. Brady. 2016. 'Mitophagy programs: mechanisms and physiological implications of mitochondrial targeting by autophagy', *Cell Mol Life Sci*, 73: 775-95.
- Hanada, T., N. N. Noda, Y. Satomi, Y. Ichimura, Y. Fujioka, T. Takao, F. Inagaki, and Y. Ohsumi. 2007. 'The Atg12-Atg5 conjugate has a novel E3-like activity for protein lipidation in autophagy', *J Biol Chem*, 282: 37298-302.

- Hara, T., A. Takamura, C. Kishi, S. Iemura, T. Natsume, J. L. Guan, and N. Mizushima. 2008. 'FIP200, a ULK-interacting protein, is required for autophagosome formation in mammalian cells', *J Cell Biol*, 181: 497-510.
- He, C., and D. J. Klionsky. 2009. 'Regulation mechanisms and signaling pathways of autophagy', *Annu Rev Genet*, 43: 67-93.
- Hicke, L., H. L. Schubert, and C. P. Hill. 2005. 'Ubiquitin-binding domains', *Nat Rev Mol Cell Biol*, 6: 610-21.
- Hosokawa, N., T. Hara, T. Kaizuka, C. Kishi, A. Takamura, Y. Miura, S. Iemura, T. Natsume, K. Takehana, N. Yamada, J. L. Guan, N. Oshiro, and N. Mizushima. 2009. 'Nutrient-dependent mTORC1 association with the ULK1-Atg13-FIP200 complex required for autophagy', *Mol Biol Cell*, 20: 1981-91.
- Hosokawa, N., T. Sasaki, S. Iemura, T. Natsume, T. Hara, and N. Mizushima. 2009. 'Atg101, a novel mammalian autophagy protein interacting with Atg13', *Autophagy*, 5: 973-9.
- Huang, R., Y. Xu, W. Wan, X. Shou, J. Qian, Z. You, B. Liu, C. Chang, T. Zhou, J. Lippincott-Schwartz, and W. Liu. 2015. 'Deacetylation of nuclear LC3 drives autophagy initiation under starvation', *Mol Cell*, 57: 456-66.
- Huang, T., C. K. Kim, A. A. Alvarez, R. P. Pangen, X. Wan, X. Song, T. Shi, Y. Yang, N. Sastry, C. M. Horbinski, S. Lu, R. Stupp, J. A. Kessler, R. Nishikawa, I. Nakano, E. P. Sulman, X. Lu, C. D. James, X. M. Yin, B. Hu, and S. Y. Cheng. 2017. 'MST4 Phosphorylation of ATG4B Regulates Autophagic Activity, Tumorigenicity, and Radioresistance in Glioblastoma', *Cancer Cell*, 32: 840-55.e8.
- Huang, W., W. Choi, W. Hu, N. Mi, Q. Guo, M. Ma, M. Liu, Y. Tian, P. Lu, F. L. Wang, H. Deng, L. Liu, N. Gao, L. Yu, and Y. Shi. 2012. 'Crystal structure and biochemical analyses reveal Beclin 1 as a novel membrane binding protein', *Cell Res*, 22: 473-89.
- Hurley, J. H., and L. N. Young. 2017. 'Mechanisms of Autophagy Initiation', *Annu Rev Biochem*, 86: 225-44.
- Hwang, J., L. Winkler, and R. F. Kalejta. 2011. 'Ubiquitin-independent proteasomal degradation during oncogenic viral infections', *Biochim Biophys Acta*, 1816: 147-57.
- Hyttinen, J. M., M. Niittykoski, A. Salminen, and K. Kaarniranta. 2013. 'Maturation of autophagosomes and endosomes: a key role for Rab7', *Biochim Biophys Acta*, 1833: 503-10.
- Ichimura, Y., T. Kirisako, T. Takao, Y. Satomi, Y. Shimonishi, N. Ishihara, N. Mizushima, I. Tanida, E. Kominami, M. Ohsumi, T. Noda, and Y. Ohsumi. 2000. 'A ubiquitin-like system mediates protein lipidation', *Nature*, 408: 488-92.
- Inoki, K., Y. Li, T. Xu, and K. L. Guan. 2003. 'Rheb GTPase is a direct target of TSC2 GAP activity and regulates mTOR signaling', *Genes Dev*, 17: 1829-34.
- Inoki, K., T. Zhu, and K. L. Guan. 2003. 'TSC2 mediates cellular energy response to control cell growth and survival', *Cell*, 115: 577-90.
- Itakura, E., C. Kishi-Itakura, and N. Mizushima. 2012. 'The hairpin-type tail-anchored SNARE syntaxin 17 targets to autophagosomes for fusion with endosomes/lysosomes', *Cell*, 151: 1256-69.
- Ivanova, S., M. Polajnar, A. J. Narbona-Perez, M. I. Hernandez-Alvarez, P. Frager, K. Slobodnyuk, N. Plana, A. R. Nebreda, M. Palacin, R. R. Gomis, C. Behrends, and A. Zorzano. 2019. 'Regulation of death receptor signaling by the autophagy protein TP53INP2', *Embo j*.
- Jiang, H., D. Cheng, W. Liu, J. Peng, and J. Feng. 2010. 'Protein kinase C inhibits autophagy and phosphorylates LC3', *Biochem Biophys Res Commun*, 395: 471-6.
- Jin, L., A. Williamson, S. Banerjee, I. Philipp, and M. Rape. 2008. 'Mechanism of ubiquitin-chain formation by the human anaphase-promoting complex', *Cell*, 133: 653-65.

- Joachim, J., H. B. Jefferies, M. Razi, D. Frith, A. P. Snijders, P. Chakravarty, D. Judith, and S. A. Tooze. 2015. 'Activation of ULK Kinase and Autophagy by GABARAP Trafficking from the Centrosome Is Regulated by WAC and GM130', *Mol Cell*, 60: 899-913.
- Johnson, L. N., M. E. Noble, and D. J. Owen. 1996. 'Active and inactive protein kinases: structural basis for regulation', *Cell*, 85: 149-58.
- Joo, J. H., F. C. Dorsey, A. Joshi, K. M. Hennessy-Walters, K. L. Rose, K. McCastlain, J. Zhang, R. Iyengar, C. H. Jung, D. F. Suen, M. A. Steeves, C. Y. Yang, S. M. Prater, D. H. Kim, C. B. Thompson, R. J. Youle, P. A. Ney, J. L. Cleveland, and M. Kundu. 2011. 'Hsp90-Cdc37 chaperone complex regulates Ulk1- and Atg13-mediated mitophagy', *Mol Cell*, 43: 572-85.
- Jordens, I., M. Fernandez-Borja, M. Marsman, S. Dusseljee, L. Janssen, J. Calafat, H. Janssen, R. Wubbolts, and J. Neefjes. 2001. 'The Rab7 effector protein RILP controls lysosomal transport by inducing the recruitment of dynein-dynactin motors', *Curr Biol*, 11: 1680-5.
- Jung, C. H., C. B. Jun, S. H. Ro, Y. M. Kim, N. M. Otto, J. Cao, M. Kundu, and D. H. Kim. 2009. 'ULK-Atg13-FIP200 complexes mediate mTOR signaling to the autophagy machinery', *Mol Biol Cell*, 20: 1992-2003.
- Kabeya, Y., N. Mizushima, A. Yamamoto, S. Oshitani-Okamoto, Y. Ohsumi, and T. Yoshimori. 2004. 'LC3, GABARAP and GATE16 localize to autophagosomal membrane depending on form-II formation', *J Cell Sci*, 117: 2805-12.
- Karanasios, E., E. Stapleton, M. Manifava, T. Kaizuka, N. Mizushima, S. A. Walker, and N. T. Ktistakis. 2013. 'Dynamic association of the ULK1 complex with omegasomes during autophagy induction', *J Cell Sci*, 126: 5224-38.
- Karanasios, E., S. A. Walker, H. Okkenhaug, M. Manifava, E. Hummel, H. Zimmermann, Q. Ahmed, M. C. Domart, L. Collinson, and N. T. Ktistakis. 2016. 'Autophagy initiation by ULK complex assembly on ER tubulovesicular regions marked by ATG9 vesicles', *Nat Commun*, 7: 12420.
- Kaushik, S., and A. M. Cuervo. 2018. 'The coming of age of chaperone-mediated autophagy', *Nat Rev Mol Cell Biol*, 19: 365-81.
- Khokhlatchev, A., S. Rabizadeh, R. Xavier, M. Nedwidek, T. Chen, X. F. Zhang, B. Seed, and J. Avruch. 2002. 'Identification of a novel Ras-regulated proapoptotic pathway', *Curr Biol*, 12: 253-65.
- Kiffin, R., C. Christian, E. Knecht, and A. M. Cuervo. 2004. 'Activation of chaperone-mediated autophagy during oxidative stress', *Mol Biol Cell*, 15: 4829-40.
- Kim, J., V. M. Dalton, K. P. Eggerton, S. V. Scott, and D. J. Klionsky. 1999. 'Apg7p/Cvt2p is required for the cytoplasm-to-vacuole targeting, macroautophagy, and peroxisome degradation pathways', *Mol Biol Cell*, 10: 1337-51.
- Kim, J., M. Kundu, B. Viollet, and K. L. Guan. 2011. 'AMPK and mTOR regulate autophagy through direct phosphorylation of Ulk1', *Nat Cell Biol*, 13: 132-41.
- Kirisako, T., Y. Ichimura, H. Okada, Y. Kabeya, N. Mizushima, T. Yoshimori, M. Ohsumi, T. Takao, T. Noda, and Y. Ohsumi. 2000. 'The reversible modification regulates the membrane-binding state of Apg8/Aut7 essential for autophagy and the cytoplasm to vacuole targeting pathway', *J Cell Biol*, 151: 263-76.
- Kishi-Itakura, C., I. Koyama-Honda, E. Itakura, and N. Mizushima. 2014. 'Ultrastructural analysis of autophagosome organization using mammalian autophagy-deficient cells', *J Cell Sci*, 127: 4089-102.
- Kissova, I., B. Salin, J. Schaeffer, S. Bhatia, S. Manon, and N. Camougrand. 2007. 'Selective and non-selective autophagic degradation of mitochondria in yeast', *Autophagy*, 3: 329-36.

- Kleinschmidt, J. A., B. Hugel, C. Grund, and W. W. Franke. 1983. 'The 22 S cylinder particles of *Xenopus laevis*. I. Biochemical and electron microscopic characterization', *Eur J Cell Biol*, 32: 143-56.
- Kraft, C., M. Kijanska, E. Kalie, E. Siergiejuk, S. S. Lee, G. Semplicio, I. Stoffel, A. Brezovich, M. Verma, I. Hansmann, G. Ammerer, K. Hofmann, S. Tooze, and M. Peter. 2012. 'Binding of the Atg1/ULK1 kinase to the ubiquitin-like protein Atg8 regulates autophagy', *Embo j*, 31: 3691-703.
- Krick, R., Y. Muhe, T. Prick, M. Bredschneider, S. Bremer, D. Wenzel, E. L. Eskelinen, and M. Thumm. 2009. 'Piecemeal microautophagy of the nucleus: genetic and morphological traits', *Autophagy*, 5: 270-2.
- Krogan, N. J., M. H. Lam, J. Fillingham, M. C. Keogh, M. Gebbia, J. Li, N. Datta, G. Cagney, S. Buratowski, A. Emili, and J. F. Greenblatt. 2004. 'Proteasome involvement in the repair of DNA double-strand breaks', *Mol Cell*, 16: 1027-34.
- Kuang, E., C. Y. Okumura, S. Sheffy-Levin, T. Varsano, V. C. Shu, J. Qi, I. R. Niesman, H. J. Yang, C. Lopez-Otin, W. Y. Yang, J. C. Reed, L. Broday, V. Nizet, and Z. A. Ronai. 2012. 'Regulation of ATG4B stability by RNF5 limits basal levels of autophagy and influences susceptibility to bacterial infection', *PLoS Genet*, 8: e1003007.
- Kuma, A., N. Mizushima, N. Ishihara, and Y. Ohsumi. 2002. 'Formation of the approximately 350-kDa Apg12-Apg5-Apg16 multimeric complex, mediated by Apg16 oligomerization, is essential for autophagy in yeast', *J Biol Chem*, 277: 18619-25.
- Kumar, S., A. Jain, F. Farzam, J. Jia, Y. Gu, S. W. Choi, M. H. Mudd, A. Claude-Taupin, M. J. Wester, K. A. Lidke, T. E. Rusten, and V. Deretic. 2018. 'Mechanism of Stx17 recruitment to autophagosomes via IRGM and mammalian Atg8 proteins', *J Cell Biol*, 217: 997-1013.
- Kwon, D. H., S. Kim, Y. O. Jung, K. H. Roh, L. Kim, B. W. Kim, S. B. Hong, I. Y. Lee, J. H. Song, W. C. Lee, E. J. Choi, K. Y. Hwang, and H. K. Song. 2017. 'The 1:2 complex between RavZ and LC3 reveals a mechanism for deconjugation of LC3 on the phagophore membrane', *Autophagy*, 13: 70-81.
- Le Good, J. A., W. H. Ziegler, D. B. Parekh, D. R. Alessi, P. Cohen, and P. J. Parker. 1998. 'Protein kinase C isotypes controlled by phosphoinositide 3-kinase through the protein kinase PDK1', *Science*, 281: 2042-5.
- Lee, I. H., and T. Finkel. 2009. 'Regulation of autophagy by the p300 acetyltransferase', *J Biol Chem*, 284: 6322-8.
- Li, M., Y. Hou, J. Wang, X. Chen, Z. M. Shao, and X. M. Yin. 2011. 'Kinetics comparisons of mammalian Atg4 homologues indicate selective preferences toward diverse Atg8 substrates', *J Biol Chem*, 286: 7327-38.
- Li, W. W., J. Li, and J. K. Bao. 2012. 'Microautophagy: lesser-known self-eating', *Cell Mol Life Sci*, 69: 1125-36.
- Limatola, C., D. Schaap, W. H. Moolenaar, and W. J. van Blitterswijk. 1994. 'Phosphatidic acid activation of protein kinase C-zeta overexpressed in COS cells: comparison with other protein kinase C isotypes and other acidic lipids', *Biochem J*, 304 (Pt 3): 1001-8.
- Lin, S. Y., T. Y. Li, Q. Liu, C. Zhang, X. Li, Y. Chen, S. M. Zhang, G. Lian, Q. Liu, K. Ruan, Z. Wang, C. S. Zhang, K. Y. Chien, J. Wu, Q. Li, J. Han, and S. C. Lin. 2012. 'GSK3-TIP60-ULK1 signaling pathway links growth factor deprivation to autophagy', *Science*, 336: 477-81.
- Liu, Y., L. Peng, E. Seto, S. Huang, and Y. Qiu. 2012. 'Modulation of histone deacetylase 6 (HDAC6) nuclear import and tubulin deacetylase activity through acetylation', *J Biol Chem*, 287: 29168-74.
- Lizcano, J. M., M. Deak, N. Morrice, A. Kieloch, C. J. Hastie, L. Dong, M. Schutkowski, U. Reimer, and D. R. Alessi. 2002. 'Molecular basis for the substrate specificity of NIMA-

- related kinase-6 (NEK6). Evidence that NEK6 does not phosphorylate the hydrophobic motif of ribosomal S6 protein kinase and serum- and glucocorticoid-induced protein kinase in vivo', *J Biol Chem*, 277: 27839-49.
- Maehama, T., K. Kawahara, M. Nishio, A. Suzuki, and K. Hanada. 2014. 'Nucleolar stress induces ubiquitination-independent proteasomal degradation of PICT1 protein', *J Biol Chem*, 289: 20802-12.
- Maejima, Y., S. Kyoi, P. Zhai, T. Liu, H. Li, A. Ivessa, S. Sciarretta, D. P. Del Re, D. K. Zablocki, C. P. Hsu, D. S. Lim, M. Isobe, and J. Sadoshima. 2013. 'Mst1 inhibits autophagy by promoting the interaction between Beclin1 and Bcl-2', *Nat Med*, 19: 1478-88.
- Manil-Segalen, M., C. Lefebvre, C. Jenzer, M. Trichet, C. Boulogne, B. Satiat-Jeunemaitre, and R. Legouis. 2014. 'The C. elegans LC3 acts downstream of GABARAP to degrade autophagosomes by interacting with the HOPS subunit VPS39', *Dev Cell*, 28: 43-55.
- Mari, M., J. Griffith, E. Rieter, L. Krishnappa, D. J. Klionsky, and F. Reggiori. 2010. 'An Atg9-containing compartment that functions in the early steps of autophagosome biogenesis', *J Cell Biol*, 190: 1005-22.
- Marino, G., A. F. Fernandez, S. Cabrera, Y. W. Lundberg, R. Cabanillas, F. Rodriguez, N. Salvador-Montoliu, J. A. Vega, A. Germana, A. Fueyo, J. M. Freije, and C. Lopez-Otin. 2010. 'Autophagy is essential for mouse sense of balance', *J Clin Invest*, 120: 2331-44.
- Marino, G., N. Salvador-Montoliu, A. Fueyo, E. Knecht, N. Mizushima, and C. Lopez-Otin. 2007. 'Tissue-specific autophagy alterations and increased tumorigenesis in mice deficient in Atg4C/autophagin-3', *J Biol Chem*, 282: 18573-83.
- Marshall, R. S., Z. Hua, S. Mali, F. McLoughlin, and R. D. Vierstra. 2019. 'ATG8-Binding UIM Proteins Define a New Class of Autophagy Adaptors and Receptors', *Cell*, 177: 766-81.e24.
- Maruyama, Y., Y. S. Sou, S. Kageyama, T. Takahashi, T. Ueno, K. Tanaka, M. Komatsu, and Y. Ichimura. 2014. 'LC3B is indispensable for selective autophagy of p62 but not basal autophagy', *Biochem Biophys Res Commun*, 446: 309-15.
- Matsunaga, K., E. Morita, T. Saitoh, S. Akira, N. T. Ktistakis, T. Izumi, T. Noda, and T. Yoshimori. 2010. 'Autophagy requires endoplasmic reticulum targeting of the PI3-kinase complex via Atg14L', *J Cell Biol*, 190: 511-21.
- McClellan, A. J., S. Tam, D. Kaganovich, and J. Frydman. 2005. 'Protein quality control: chaperones culling corrupt conformations', *Nat Cell Biol*, 7: 736-41.
- McEwan, D. G., D. Popovic, A. Gubas, S. Terawaki, H. Suzuki, D. Stadel, F. P. Coxon, D. Miranda de Stegmann, S. Bhogaraju, K. Maddi, A. Kirchof, E. Gatti, M. H. Helfrich, S. Wakatsuki, C. Behrends, P. Pierre, and I. Dikic. 2015. 'PLEKHM1 regulates autophagosome-lysosome fusion through HOPS complex and LC3/GABARAP proteins', *Mol Cell*, 57: 39-54.
- Mejlvang, J., H. Olsvik, S. Svenning, J. A. Bruun, Y. P. Abudu, K. B. Larsen, A. Brech, T. E. Hansen, H. Brenne, T. Hansen, H. Stenmark, and T. Johansen. 2018. 'Starvation induces rapid degradation of selective autophagy receptors by endosomal microautophagy', *J Cell Biol*, 217: 3640-55.
- Mendez, J., X. H. Zou-Yang, S. Y. Kim, M. Hidaka, W. P. Tansey, and B. Stillman. 2002. 'Human origin recognition complex large subunit is degraded by ubiquitin-mediated proteolysis after initiation of DNA replication', *Mol Cell*, 9: 481-91.
- Meng, Z., T. Moroishi, and K. L. Guan. 2016. 'Mechanisms of Hippo pathway regulation', *Genes Dev*, 30: 1-17.
- Mercer, C. A., A. Kaliappan, and P. B. Dennis. 2009. 'A novel, human Atg13 binding protein, Atg101, interacts with ULK1 and is essential for macroautophagy', *Autophagy*, 5: 649-62.

- Miller, S., B. Tavshanjian, A. Oleksy, O. Perisic, B. T. Houseman, K. M. Shokat, and R. L. Williams. 2010. 'Shaping development of autophagy inhibitors with the structure of the lipid kinase Vps34', *Science*, 327: 1638-42.
- Mortimore, G. E., B. R. Lardeux, and C. E. Adams. 1988. 'Regulation of microautophagy and basal protein turnover in rat liver. Effects of short-term starvation', *J Biol Chem*, 263: 2506-12.
- Muller, G., M. Ayoub, P. Storz, J. Rennecke, D. Fabbro, and K. Pfizenmaier. 1995. 'PKC zeta is a molecular switch in signal transduction of TNF-alpha, bifunctionally regulated by ceramide and arachidonic acid', *Embo j*, 14: 1961-9.
- Murai, Noriyuki, Yasuko Murakami, Ayasa Tajima, and Senya Matsufuji. 2018. 'Novel ubiquitin-independent nucleolar c-Myc degradation pathway mediated by antizyme 2', *Scientific Reports*, 8: 3005.
- Murata, S., Y. Minami, M. Minami, T. Chiba, and K. Tanaka. 2001. 'CHIP is a chaperone-dependent E3 ligase that ubiquitylates unfolded protein', *EMBO Rep*, 2: 1133-8.
- Nair, U., W. L. Yen, M. Mari, Y. Cao, Z. Xie, M. Baba, F. Reggiori, and D. J. Klionsky. 2012. 'A role for Atg8-PE deconjugation in autophagosome biogenesis', *Autophagy*, 8: 780-93.
- Nakanishi, H., K. A. Brewer, and J. H. Exton. 1993. 'Activation of the zeta isozyme of protein kinase C by phosphatidylinositol 3,4,5-trisphosphate', *J Biol Chem*, 268: 13-6.
- Nakatogawa, H. 2013. 'Two ubiquitin-like conjugation systems that mediate membrane formation during autophagy', *Essays Biochem*, 55: 39-50.
- Nazio, F., F. Strappazon, M. Antonioli, P. Bielli, V. Cianfanelli, M. Bordi, C. Gretzmeier, J. Dengjel, M. Piacentini, G. M. Fimia, and F. Cecconi. 2013. 'mTOR inhibits autophagy by controlling ULK1 ubiquitylation, self-association and function through AMBRA1 and TRAF6', *Nat Cell Biol*, 15: 406-16.
- Newton, A. C. 2001. 'Protein kinase C: structural and spatial regulation by phosphorylation, cofactors, and macromolecular interactions', *Chem Rev*, 101: 2353-64.
- Nguyen, T. N., B. S. Padman, J. Usher, V. Oorschot, G. Ramm, and M. Lazarou. 2016. 'Atg8 family LC3/GABARAP proteins are crucial for autophagosome-lysosome fusion but not autophagosome formation during PINK1/Parkin mitophagy and starvation', *J Cell Biol*, 215: 857-74.
- Noda, N. N., Y. Ohsumi, and F. Inagaki. 2009. 'ATG systems from the protein structural point of view', *Chem Rev*, 109: 1587-98.
- Noda, T. 2017. 'Autophagy in the context of the cellular membrane-trafficking system: the enigma of Atg9 vesicles', *Biochem Soc Trans*, 45: 1323-31.
- Novikoff, A. B., H. Beaufay, and C. De Duve. 1956. 'Electron microscopy of lysosomeric fractions from rat liver', *J Biophys Biochem Cytol*, 2: 179-84.
- Nowak, J., C. Archange, J. Tardivel-Lacombe, P. Pontarotti, M. J. Pebusque, M. I. Vaccaro, G. Velasco, J. C. Dagorn, and J. L. Iovanna. 2009. 'The TP53INP2 protein is required for autophagy in mammalian cells', *Mol Biol Cell*, 20: 870-81.
- Oakley, B. R., and N. R. Morris. 1983. 'A mutation in *Aspergillus nidulans* that blocks the transition from interphase to prophase', *J Cell Biol*, 96: 1155-8.
- Oda, K., H. Arakawa, T. Tanaka, K. Matsuda, C. Tanikawa, T. Mori, H. Nishimori, K. Tamai, T. Tokino, Y. Nakamura, and Y. Taya. 2000. 'p53AIP1, a potential mediator of p53-dependent apoptosis, and its regulation by Ser-46-phosphorylated p53', *Cell*, 102: 849-62.
- Ohsumi, Y., and N. Mizushima. 2004. 'Two ubiquitin-like conjugation systems essential for autophagy', *Semin Cell Dev Biol*, 15: 231-6.

- Orsi, A., M. Razi, H. C. Dooley, D. Robinson, A. E. Weston, L. M. Collinson, and S. A. Tooze. 2012. 'Dynamic and transient interactions of Atg9 with autophagosomes, but not membrane integration, are required for autophagy', *Mol Biol Cell*, 23: 1860-73.
- Osmani, S. A., R. T. Pu, and N. R. Morris. 1988. 'Mitotic induction and maintenance by overexpression of a G2-specific gene that encodes a potential protein kinase', *Cell*, 53: 237-44.
- Pankiv, S., E. A. Alemu, A. Brech, J. A. Bruun, T. Lamark, A. Overvatn, G. Bjorkoy, and T. Johansen. 2010. 'FYCO1 is a Rab7 effector that binds to LC3 and PI3P to mediate microtubule plus end-directed vesicle transport', *J Cell Biol*, 188: 253-69.
- Parekh, D. B., W. Ziegler, and P. J. Parker. 2000. 'Multiple pathways control protein kinase C phosphorylation', *Embo j*, 19: 496-503.
- Park, C., Y. Suh, and A. M. Cuervo. 2015. 'Regulated degradation of Chk1 by chaperone-mediated autophagy in response to DNA damage', *Nat Commun*, 6: 6823.
- Pengo, N., A. Agrotis, K. Prak, J. Jones, and R. Ketteler. 2017. 'A reversible phospho-switch mediated by ULK1 regulates the activity of autophagy protease ATG4B', *Nat Commun*, 8: 294.
- Polson, H. E., J. de Lartigue, D. J. Rigden, M. Reedijk, S. Urbe, M. J. Clague, and S. A. Tooze. 2010. 'Mammalian Atg18 (WIPI2) localizes to omegasome-anchored phagophores and positively regulates LC3 lipidation', *Autophagy*, 6: 506-22.
- Praskova, M., A. Khoklatchev, S. Ortiz-Vega, and J. Avruch. 2004. 'Regulation of the MST1 kinase by autophosphorylation, by the growth inhibitory proteins, RASSF1 and NORE1, and by Ras', *Biochem J*, 381: 453-62.
- Prokesch, A., F. A. Graef, T. Madl, J. Kahlhofer, S. Heidenreich, A. Schumann, E. Moyschewitz, P. Pristoynik, A. Blaschitz, M. Knauer, M. Muenzner, J. G. Bogner-Strauss, G. Dohr, T. J. Schulz, and M. Schupp. 2017. 'Liver p53 is stabilized upon starvation and required for amino acid catabolism and gluconeogenesis', *Faseb j*, 31: 732-42.
- Puente, C., R. C. Hendrickson, and X. Jiang. 2016. 'Nutrient-regulated Phosphorylation of ATG13 Inhibits Starvation-induced Autophagy', *J Biol Chem*, 291: 6026-35.
- Qi, S., D. J. Kim, G. Stjepanovic, and J. H. Hurley. 2015. 'Structure of the Human Atg13-Atg101 HORMA Heterodimer: an Interaction Hub within the ULK1 Complex', *Structure*, 23: 1848-57.
- Qu, L., G. Li, D. Xia, B. Hongdu, C. Xu, X. Lin, and Y. Chen. 2016. 'PRKCI negatively regulates autophagy via PIK3CA/AKT-MTOR signaling', *Biochem Biophys Res Commun*, 470: 306-12.
- Quarmany, L. M., and M. R. Mahjoub. 2005. 'Caught Nek-ing: cilia and centrioles', *J Cell Sci*, 118: 5161-9.
- Ran, F. A., P. D. Hsu, C. Y. Lin, J. S. Gootenberg, S. Konermann, A. E. Trevino, D. A. Scott, A. Inoue, S. Matoba, Y. Zhang, and F. Zhang. 2013. 'Double nicking by RNA-guided CRISPR Cas9 for enhanced genome editing specificity', *Cell*, 154: 1380-9.
- Ravid, T., and M. Hochstrasser. 2008. 'Diversity of degradation signals in the ubiquitin-proteasome system', *Nat Rev Mol Cell Biol*, 9: 679-90.
- Raynes, R., L. C. Pomatto, and K. J. Davies. 2016. 'Degradation of oxidized proteins by the proteasome: Distinguishing between the 20S, 26S, and immunoproteasome proteolytic pathways', *Mol Aspects Med*, 50: 41-55.
- Reyland, M. E. 2009. 'Protein kinase C isoforms: Multi-functional regulators of cell life and death', *Front Biosci (Landmark Ed)*, 14: 2386-99.
- Roczniak-Ferguson, A., C. S. Petit, F. Froehlich, S. Qian, J. Ky, B. Angarola, T. C. Walther, and S. M. Ferguson. 2012. 'The transcription factor TFEB links mTORC1 signaling to transcriptional control of lysosome homeostasis', *Sci Signal*, 5: ra42.

- Roig, J., A. Groen, J. Caldwell, and J. Avruch. 2005. 'Active Nerccl1 protein kinase concentrates at centrosomes early in mitosis and is necessary for proper spindle assembly', *Mol Biol Cell*, 16: 4827-40.
- Romero, M., A. Sabate-Perez, V. A. Francis, I. Castrillon-Rodriguez, A. Diaz-Ramos, M. Sanchez-Feutrie, X. Duran, M. Palacin, J. M. Moreno-Navarrete, B. Gustafson, A. Hammarstedt, J. M. Fernandez-Real, J. Vendrell, U. Smith, and A. Zorzano. 2018. 'TP53INP2 regulates adiposity by activating beta-catenin through autophagy-dependent sequestration of GSK3beta', *Nat Cell Biol*, 20: 443-54.
- Rostislavleva, K., N. Soler, Y. Ohashi, L. Zhang, E. Pardon, J. E. Burke, G. R. Masson, C. Johnson, J. Steyaert, N. T. Ktistakis, and R. L. Williams. 2015. 'Structure and flexibility of the endosomal Vps34 complex reveals the basis of its function on membranes', *Science*, 350: aac7365.
- Russell, R. C., Y. Tian, H. Yuan, H. W. Park, Y. Y. Chang, J. Kim, H. Kim, T. P. Neufeld, A. Dillin, and K. L. Guan. 2013. 'ULK1 induces autophagy by phosphorylating Beclin-1 and activating VPS34 lipid kinase', *Nat Cell Biol*, 15: 741-50.
- Sacktor, T. C. 2012. 'Memory maintenance by PKMzeta--an evolutionary perspective', *Mol Brain*, 5: 31.
- Sahu, R., S. Kaushik, C. C. Clement, E. S. Cannizzo, B. Scharf, A. Follenzi, I. Potolicchio, E. Nieves, A. M. Cuervo, and L. Santambrogio. 2011. 'Microautophagy of cytosolic proteins by late endosomes', *Dev Cell*, 20: 131-9.
- Sakai, Y., A. Koller, L. K. Rangell, G. A. Keller, and S. Subramani. 1998. 'Peroxisome degradation by microautophagy in *Pichia pastoris*: identification of specific steps and morphological intermediates', *J Cell Biol*, 141: 625-36.
- Sancho, A., J. Duran, A. Garcia-Espana, C. Mauvezin, E. A. Alemu, T. Lamark, M. J. Macias, R. DeSalle, M. Royo, D. Sala, J. U. Chicote, M. Palacin, T. Johansen, and A. Zorzano. 2012. 'DOR/Tp53inp2 and Tp53inp1 constitute a metazoan gene family encoding dual regulators of autophagy and transcription', *PLoS One*, 7: e34034.
- Sanjuan, M. A., C. P. Dillon, S. W. Tait, S. Moshiah, F. Dorsey, S. Connell, M. Komatsu, K. Tanaka, J. L. Cleveland, S. Withoff, and D. R. Green. 2007. 'Toll-like receptor signalling in macrophages links the autophagy pathway to phagocytosis', *Nature*, 450: 1253-7.
- Satoo, K., N. N. Noda, H. Kumeta, Y. Fujioka, N. Mizushima, Y. Ohsumi, and F. Inagaki. 2009. 'The structure of Atg4B-LC3 complex reveals the mechanism of LC3 processing and delipidation during autophagy', *Embo j*, 28: 1341-50.
- Schaaf, M. B., T. G. Keulers, M. A. Vooijs, and K. M. Rouschop. 2016. 'LC3/GABARAP family proteins: autophagy-(un)related functions', *Faseb j*, 30: 3961-78.
- Scheel, H., and K. Hofmann. 2003. 'A novel interaction motif, SARA, connects three classes of tumor suppressor', *Curr Biol*, 13: R899-900.
- Scherz-Shouval, R., Y. Sagiv, H. Shorer, and Z. Elazar. 2003. 'The COOH terminus of GATE-16, an intra-Golgi transport modulator, is cleaved by the human cysteine protease HsApg4A', *J Biol Chem*, 278: 14053-8.
- Scherz-Shouval, R., E. Shvets, E. Fass, H. Shorer, L. Gil, and Z. Elazar. 2007. 'Reactive oxygen species are essential for autophagy and specifically regulate the activity of Atg4', *Embo j*, 26: 1749-60.
- Schubert, U., L. C. Anton, J. Gibbs, C. C. Norbury, J. W. Yewdell, and J. R. Bennink. 2000. 'Rapid degradation of a large fraction of newly synthesized proteins by proteasomes', *Nature*, 404: 770-4.
- Sdelci, S., M. T. Bertran, and J. Roig. 2011. 'Nek9, Nek6, Nek7 and the separation of centrosomes', *Cell Cycle*, 10: 3816-7.

- Seillier, M., S. Peugot, O. Gayet, C. Gauthier, P. N'Guessan, M. Monte, A. Carrier, J. L. Iovanna, and N. J. Dusetti. 2012. 'TP53INP1, a tumor suppressor, interacts with LC3 and ATG8-family proteins through the LC3-interacting region (LIR) and promotes autophagy-dependent cell death', *Cell Death Differ*, 19: 1525-35.
- Sengupta, A., J. D. Molkentin, and K. E. Yutzey. 2009. 'FoxO transcription factors promote autophagy in cardiomyocytes', *J Biol Chem*, 284: 28319-31.
- Settembre, C., C. Di Malta, V. A. Polito, M. Garcia Arencibia, F. Vetrini, S. Erdin, S. U. Erdin, T. Huynh, D. Medina, P. Colella, M. Sardiello, D. C. Rubinsztein, and A. Ballabio. 2011. 'TFEB links autophagy to lysosomal biogenesis', *Science*, 332: 1429-33.
- Shang, L., S. Chen, F. Du, S. Li, L. Zhao, and X. Wang. 2011. 'Nutrient starvation elicits an acute autophagic response mediated by Ulk1 dephosphorylation and its subsequent dissociation from AMPK', *Proc Natl Acad Sci U S A*, 108: 4788-93.
- Shi, C. S., and J. H. Kehrl. 2010. 'TRAF6 and A20 regulate lysine 63-linked ubiquitination of Beclin-1 to control TLR4-induced autophagy', *Sci Signal*, 3: ra42.
- Shintani, T., N. Mizushima, Y. Ogawa, A. Matsuura, T. Noda, and Y. Ohsumi. 1999. 'Apg10p, a novel protein-conjugating enzyme essential for autophagy in yeast', *Embo j*, 18: 5234-41.
- Skytte Rasmussen, M., S. Mouilleron, B. Kumar Shrestha, M. Wirth, R. Lee, K. Bowitz Larsen, Y. Abudu Princely, N. O'Reilly, E. Sjøttem, S. A. Tooze, T. Lamark, and T. Johansen. 2017. 'ATG4B contains a C-terminal LIR motif important for binding and efficient cleavage of mammalian orthologs of yeast Atg8', *Autophagy*, 13: 834-53.
- Smith, D. M., S. C. Chang, S. Park, D. Finley, Y. Cheng, and A. L. Goldberg. 2007. 'Docking of the proteasomal ATPases' carboxyl termini in the 20S proteasome's alpha ring opens the gate for substrate entry', *Mol Cell*, 27: 731-44.
- Sou, Y. S., S. Waguri, J. Iwata, T. Ueno, T. Fujimura, T. Hara, N. Sawada, A. Yamada, N. Mizushima, Y. Uchiyama, E. Kominami, K. Tanaka, and M. Komatsu. 2008. 'The Atg8 conjugation system is indispensable for proper development of autophagic isolation membranes in mice', *Mol Biol Cell*, 19: 4762-75.
- Spitaler, M., and D. A. Cantrell. 2004. 'Protein kinase C and beyond', *Nat Immunol*, 5: 785-90.
- Stack, J. H., D. B. DeWald, K. Takegawa, and S. D. Emr. 1995. 'Vesicle-mediated protein transport: regulatory interactions between the Vps15 protein kinase and the Vps34 PtdIns 3-kinase essential for protein sorting to the vacuole in yeast', *J Cell Biol*, 129: 321-34.
- Su, H., F. Yang, Q. Wang, Q. Shen, J. Huang, C. Peng, Y. Zhang, W. Wan, C. C. L. Wong, Q. Sun, F. Wang, T. Zhou, and W. Liu. 2017. 'VPS34 Acetylation Controls Its Lipid Kinase Activity and the Initiation of Canonical and Non-canonical Autophagy', *Mol Cell*, 67: 907-21.e7.
- Sugawara, K., N. N. Suzuki, Y. Fujioka, N. Mizushima, Y. Ohsumi, and F. Inagaki. 2004. 'The crystal structure of microtubule-associated protein light chain 3, a mammalian homologue of *Saccharomyces cerevisiae* Atg8', *Genes Cells*, 9: 611-8.
- Suzuki, A., K. Akimoto, and S. Ohno. 2003. 'Protein kinase C lambda/iota (PKClambda/iota): a PKC isotype essential for the development of multicellular organisms', *J Biochem*, 133: 9-16.
- Suzuki, H., T. Kaizuka, N. Mizushima, and N. N. Noda. 2015. 'Structure of the Atg101-Atg13 complex reveals essential roles of Atg101 in autophagy initiation', *Nat Struct Mol Biol*, 22: 572-80.
- Swatek, K. N., and D. Komander. 2016. 'Ubiquitin modifications', *Cell Res*, 26: 399-422.
- Szalai, P., L. K. Hagen, F. Saetre, M. Luhr, M. Sponheim, A. Overbye, I. G. Mills, P. O. Seglen, and N. Engedal. 2015. 'Autophagic bulk sequestration of cytosolic cargo is independent of LC3, but requires GABARAPs', *Exp Cell Res*, 333: 21-38.

- Tanida, I., Y. S. Sou, J. Ezaki, N. Minematsu-Ikeguchi, T. Ueno, and E. Kominami. 2004. 'HsAtg4B/HsApg4B/autophagin-1 cleaves the carboxyl termini of three human Atg8 homologues and delipidates microtubule-associated protein light chain 3- and GABAA receptor-associated protein-phospholipid conjugates', *J Biol Chem*, 279: 36268-76.
- Tekirdag, K., and A. M. Cuervo. 2018. 'Chaperone-mediated autophagy and endosomal microautophagy: Joint by a chaperone', *J Biol Chem*, 293: 5414-24.
- Tomasini, R., A. A. Samir, A. Carrier, D. Isnardon, B. Cecchinelli, S. Soddu, B. Malissen, J. C. Dagorn, J. L. Iovanna, and N. J. Dusetti. 2003. 'TP53INP1s and homeodomain-interacting protein kinase-2 (HIPK2) are partners in regulating p53 activity', *J Biol Chem*, 278: 37722-9.
- Tomasini, R., A. A. Samir, M. J. Pebusque, E. L. Calvo, S. Totaro, J. C. Dagorn, N. J. Dusetti, and J. L. Iovanna. 2002. 'P53-dependent expression of the stress-induced protein (SIP)', *Eur J Cell Biol*, 81: 294-301.
- Tsuboyama, K., I. Koyama-Honda, Y. Sakamaki, M. Koike, H. Morishita, and N. Mizushima. 2016. 'The ATG conjugation systems are important for degradation of the inner autophagosomal membrane', *Science*, 354: 1036-41.
- Tsukada, M., and Y. Ohsumi. 1993. 'Isolation and characterization of autophagy-defective mutants of *Saccharomyces cerevisiae*', *FEBS Lett*, 333: 169-74.
- van der Lee, R., M. Buljan, B. Lang, R. J. Weatheritt, G. W. Daughdrill, A. K. Dunker, M. Fuxreiter, J. Gough, J. Gsponer, D. T. Jones, P. M. Kim, R. W. Kriwacki, C. J. Oldfield, R. V. Pappu, P. Tompa, V. N. Uversky, P. E. Wright, and M. M. Babu. 2014. 'Classification of intrinsically disordered regions and proteins', *Chem Rev*, 114: 6589-631.
- Voges, D., P. Zwickl, and W. Baumeister. 1999. 'The 26S proteasome: a molecular machine designed for controlled proteolysis', *Annu Rev Biochem*, 68: 1015-68.
- von Muhlinen, N., M. Akutsu, B. J. Ravenhill, A. Foeglein, S. Bloor, T. J. Rutherford, S. M. Freund, D. Komander, and F. Randow. 2012. 'LC3C, bound selectively by a noncanonical LIR motif in NDP52, is required for antibacterial autophagy', *Mol Cell*, 48: 329-42.
- Wang, J., J. Zhang, Y. M. Lee, P. L. Koh, S. Ng, F. Bao, Q. Lin, and H. M. Shen. 2016. 'Quantitative chemical proteomics profiling of de novo protein synthesis during starvation-mediated autophagy', *Autophagy*, 12: 1931-44.
- Wang, W., X. Yang, T. Kawai, I. Lopez de Silanes, K. Mazan-Mamczarz, P. Chen, Y. M. Chook, C. Quensel, M. Kohler, and M. Gorospe. 2004. 'AMP-activated protein kinase-regulated phosphorylation and acetylation of importin alpha1: involvement in the nuclear import of RNA-binding protein HuR', *J Biol Chem*, 279: 48376-88.
- Wang, Z., G. Miao, X. Xue, X. Guo, C. Yuan, Z. Wang, G. Zhang, Y. Chen, D. Feng, J. Hu, and H. Zhang. 2016. 'The Vici Syndrome Protein EPG5 Is a Rab7 Effector that Determines the Fusion Specificity of Autophagosomes with Late Endosomes/Lysosomes', *Mol Cell*, 63: 781-95.
- Wani, W. Y., M. Boyer-Guittaut, M. Dodson, J. Chatham, V. Darley-Usmar, and J. Zhang. 2015. 'Regulation of autophagy by protein post-translational modification', *Lab Invest*, 95: 14-25.
- Webster, C. P., E. F. Smith, C. S. Bauer, A. Moller, G. M. Hautbergue, L. Ferraiuolo, M. A. Myszczyńska, A. Higginbottom, M. J. Walsh, A. J. Whitworth, B. K. Kaspar, K. Meyer, P. J. Shaw, A. J. Grierson, and K. J. De Vos. 2016. 'The C9orf72 protein interacts with Rab1a and the ULK1 complex to regulate initiation of autophagy', *Embo j*, 35: 1656-76.
- Wei, Y., Z. Zou, N. Becker, M. Anderson, R. Sumpter, G. Xiao, L. Kinch, P. Koduru, C. S. Christudass, R. W. Veltri, N. V. Grishin, M. Peyton, J. Minna, G. Bhagat, and B. Levine.

2013. 'EGFR-mediated Beclin 1 phosphorylation in autophagy suppression, tumor progression, and tumor chemoresistance', *Cell*, 154: 1269-84.
- Weidberg, H., E. Shvets, T. Shpilka, F. Shimron, V. Shinder, and Z. Elazar. 2010. 'LC3 and GATE-16/GABARAP subfamilies are both essential yet act differently in autophagosome biogenesis', *Embo j*, 29: 1792-802.
- Wen, X., and D. J. Klionsky. 2016. 'An overview of macroautophagy in yeast', *J Mol Biol*, 428: 1681-99.
- Wijdeven, R. H., H. Janssen, L. Nahidiazar, L. Janssen, K. Jalink, I. Berlin, and J. Neefjes. 2016. 'Cholesterol and ORP1L-mediated ER contact sites control autophagosome transport and fusion with the endocytic pathway', *Nat Commun*, 7: 11808.
- Wilkinson, D. S., J. S. Jariwala, E. Anderson, K. Mitra, J. Meisenhelder, J. T. Chang, T. Ideker, T. Hunter, V. Nizet, A. Dillin, and M. Hansen. 2015. 'Phosphorylation of LC3 by the Hippo kinases STK3/STK4 is essential for autophagy', *Mol Cell*, 57: 55-68.
- Xie, Y., R. Kang, X. Sun, M. Zhong, J. Huang, D. J. Klionsky, and D. Tang. 2015. 'Posttranslational modification of autophagy-related proteins in macroautophagy', *Autophagy*, 11: 28-45.
- Xu, P., D. M. Duong, N. T. Seyfried, D. Cheng, Y. Xie, J. Robert, J. Rush, M. Hochstrasser, D. Finley, and J. Peng. 2009. 'Quantitative proteomics reveals the function of unconventional ubiquitin chains in proteasomal degradation', *Cell*, 137: 133-45.
- Xu, Y., W. Wan, X. Shou, R. Huang, Z. You, Y. Shou, L. Wang, T. Zhou, and W. Liu. 2016. 'TP53INP2/DOR, a mediator of cell autophagy, promotes rDNA transcription via facilitating the assembly of the POLR1/RNA polymerase I preinitiation complex at rDNA promoters', *Autophagy*, 12: 1118-28.
- Yang, Y., W. Fiskus, B. Yong, P. Atadja, Y. Takahashi, T. K. Pandita, H. G. Wang, and K. N. Bhalla. 2013. 'Acetylated hsp70 and KAP1-mediated Vps34 SUMOylation is required for autophagosome creation in autophagy', *Proc Natl Acad Sci U S A*, 110: 6841-6.
- Yang, Z., R. P. Wilkie-Grantham, T. Yanagi, C. W. Shu, S. Matsuzawa, and J. C. Reed. 2015. 'ATG4B (Autophagin-1) phosphorylation modulates autophagy', *J Biol Chem*, 290: 26549-61.
- Yoshida, K., H. Liu, and Y. Miki. 2006. 'Protein kinase C delta regulates Ser46 phosphorylation of p53 tumor suppressor in the apoptotic response to DNA damage', *J Biol Chem*, 281: 5734-40.
- You, Z., Y. Xu, W. Wan, L. Zhou, J. Li, T. Zhou, Y. Shi, and W. Liu. 2019. 'TP53INP2 contributes to autophagosome formation by promoting LC3-ATG7 interaction', *Autophagy*: 1-13.
- Young, A. R., E. Y. Chan, X. W. Hu, R. Kochl, S. G. Crawshaw, S. High, D. W. Hailey, J. Lippincott-Schwartz, and S. A. Tooze. 2006. 'Starvation and ULK1-dependent cycling of mammalian Atg9 between the TGN and endosomes', *J Cell Sci*, 119: 3888-900.
- Yu, Z. Q., T. Ni, B. Hong, H. Y. Wang, F. J. Jiang, S. Zou, Y. Chen, X. L. Zheng, D. J. Klionsky, Y. Liang, and Z. Xie. 2012. 'Dual roles of Atg8-PE deconjugation by Atg4 in autophagy', *Autophagy*, 8: 883-92.
- Zachari, M., and I. G. Ganley. 2017. 'The mammalian ULK1 complex and autophagy initiation', *Essays Biochem*, 61: 585-96.
- Zalckvar, E., H. Berissi, L. Mizrachy, Y. Idelchuk, I. Koren, M. Eisenstein, H. Sabanay, R. Pinkas-Kramarski, and A. Kimchi. 2009. 'DAP-kinase-mediated phosphorylation on the BH3 domain of beclin 1 promotes dissociation of beclin 1 from Bcl-XL and induction of autophagy', *EMBO Rep*, 10: 285-92.
- Zhao, Y. G., N. Liu, G. Miao, Y. Chen, H. Zhao, and H. Zhang. 2018. 'The ER Contact Proteins VAPA/B Interact with Multiple Autophagy Proteins to Modulate Autophagosome Biogenesis', *Curr Biol*, 28: 1234-45.e4.

- Zhao, Y., J. Yang, W. Liao, X. Liu, H. Zhang, S. Wang, D. Wang, J. Feng, L. Yu, and W. G. Zhu. 2010. 'Cytosolic FoxO1 is essential for the induction of autophagy and tumour suppressor activity', *Nat Cell Biol*, 12: 665-75.
- Zhou, C., K. Ma, R. Gao, C. Mu, L. Chen, Q. Liu, Q. Luo, D. Feng, Y. Zhu, and Q. Chen. 2017. 'Regulation of mATG9 trafficking by Src- and ULK1-mediated phosphorylation in basal and starvation-induced autophagy', *Cell Res*, 27: 184-201.

Phosphorylation of LC3B at threonine-50 inhibits selective autophagy

Birendra Kumar Shrestha^{1*}, Mads Skytte Rasmussen^{1*}, Yakubu Abudu Princely¹, Jack-Ansgar Bruun¹, Kenneth Bowitz Larsen¹, Endalkachew A. Alemu¹, Eva Sjøttem¹, Trond Lamark¹, and Terje Johansen¹

¹Molecular Cancer Research Group, Department of Medical Biology, University of Tromsø – The Arctic University of Norway, 9037 Tromsø, Norway.

*These authors contributed equally to this work

Corresponding author: terje.johansen@uit.no

Running title: LC3B T50E mutant inhibits selective autophagy

Keywords: Autophagy, LC3B, NEK9, PKC ζ , STK3

Abstract

Human Atg8 orthologues are involved in all steps of the autophagy pathway, and their lipidation is essential for autophagosome formation. Lipidated Atg8 orthologues anchored to the outer surface of the phagophore serve as scaffolds for the binding of other core autophagy proteins and various effector proteins involved in trafficking or fusion events, while those at the inner surface are needed for the assembly of selective autophagy substrates. The scaffolding role of Atg8 orthologues depends on specific interactions formed between the LC3 interacting region (LIR) docking site (LDS) of the Atg8 orthologues and LIR motifs in various interaction partners. LC3B was recently reported to be phosphorylated at threonine 50 (T50) within the LDS by serine/threonine-protein kinases STK3 and STK4. Here we identify LIR motifs in STK3 and in the serine/threonine kinases atypical protein kinase C ζ (PKC ζ) and never in mitosis A (NIMA)-related kinase NEK9. All three kinases mediate phosphorylation of LC3B T50 *in vitro*. Knock-down and knock out of NEK9 resulted in enhanced degradation of the autophagic substrate p62. Introduction of a phospho-mimicking mutation at the T50 position in LC3B caused impaired binding of several LIR-containing proteins, such as ATG4B, p62, NBR1, and FYCO1. Reconstitution of LC3B KO cells with the phospho-mimicking mutant LC3B T50E lead to inhibition of autophagic degradation of the selective autophagy receptors p62/SQSTM1 and NBR1.

Introduction

Macroautophagy (hereafter referred to as autophagy) is an evolutionarily conserved pathway for degradation of cytosolic components (1). Autophagy begins with the formation of a double membrane structure termed the phagophore. The phagophore grows to envelope cytosolic content resulting in the formation of a closed double membrane structure surrounding the content, the autophagosome. The autophagosome might fuse with late endosomes before ultimately fusing with lysosomes forming an autolysosome, in which the content is degraded (2). Autophagy can either be nonspecific i.e. degradation of long-lived cytosolic proteins, termed bulk autophagy or selective, i.e. targeted the degradation of specific proteins and organelles (3). Selective autophagy is involved in the degradation of a diverse range of cytosolic components including mitochondria (mitophagy), peroxisomes (pexophagy), protein aggregates (aggrephagy), bacteria (xenophagy) and the ER (reticulophagy)(4). Selective autophagy relies on a number of cargo receptors of which the most well studied is p62/SQSTM1 (sequestosome-1) (5,6). These cargo receptors interact with ATG8 proteins through the LC3-interacting-region (LIR) motif, which tethers the cargo receptors, along with their cargo, to the phagophore (7).

| Core to the autophagic pathway is the ATG8 family of proteins that, except for an N-terminal arm, structurally resemble the ubiquitin family of proteins (8). The mammalian ATG8 family consists of 7 members subdivided into 2 families: MAP1LC3/LC3 (microtubule-associated protein 1 light chain 3) -A, -B, -B2 and -C and GABARAP (gamma-aminobutyric acid receptor-associated protein), GABARAPL1 (gamma-aminobutyric acid A receptor-associated protein-like 1) and GABARAPL2. The ATG8s are first cleaved by the cysteine protease family ATG4 exposing a C-terminal glycine (9). In a manner analogous to the ubiquitin system, ATG8s are first activated by ATG7 (E1-like), transferred to ATG3 (E2-like), before finally becoming covalently attached to phosphatidylethanolamine (PE) by the action of the ATG12-ATG5-ATG16 complex (E3-like), enabling membrane attachment (10). ATG8s are released from the phagophore, and from the outer membrane of the autophagosome, by ATG4-mediated cleavage of the ATG8-PE bond thereby restoring free ATG8 (11). The ATG8s have been shown to be involved in the nucleation, expansion (12), and closure of the phagophore (13).

The ATG8s coat the inner and outer membrane of the phagophore (14), and function as anchoring points for the autophagic machinery as well as recruitment of cargo receptors to the

phagophore (7). A growing number of protein interactions involving ATG8s have been shown to be mediated through a LIR motif on the binding partner of ATG8, which interacts with the LIR-docking-site (LDS) on ATG8 (15). The LDS consists of two hydrophobic pockets (HP1 and -2) capable of encompassing the core residues of the consensus LIR sequence separated by two variable amino acids ([W/F/Y]-X-X-[L/I/V])(16). Another type of LIR motif termed C-type LIR (CLIR) has also been shown to bind LC3C through interaction with HP2 (17). LIR motifs are very often flanked N-terminally by acidic residues that interact with basic residues in the N-terminal alpha helix of ATG8s (15). The variation within the LIR motif sequence determine preferential binding to individual ATG8 family members and determine binding affinity and thereby competitive interaction with other LIR motif-containing autophagic proteins. Such binding specificity might regulate the autophagy pathway (15). The autophagy pathway is tightly regulated by several autophagy-related proteins. Among such regulatory proteins are kinases such as ULK1 (unc-51 like autophagy activating kinase 1) and -2 and mTOR (mechanistic target of rapamycin) (18). Several other serine-threonine kinases were identified as interactors of ATG8 family proteins in a human autophagy interactomics study (19). NEK9 belongs to the NIMA (Never in Mitosis A)-related kinase family. Members of the NIMA family are associated with cell cycle-related function during mitosis. Specifically, NEK9 plays an essential role in the assembly of spindle fibers early in mitosis (20). STK3 (Serine/threonine-protein kinase 3) and STK4 play an essential role in the Hippo signaling pathway. STK3 and STK4 act as negative regulators of transcription co-activators YAP1 (Yes-associated protein 1) and WWTR1 (WW domain containing transcription regulator 1 (WWTR1)). YAP1 and WWTR1 are associated with genes that regulate cell proliferation, survival, and differentiation (21). Besides its role as a tumor suppressor, loss of STK4 leads to high susceptibility toward infection likely due to loss of immune cells (B and T lymphocytes) (22,23). STK4 was first reported as a negative regulator of autophagy. STK3 was shown to negatively regulate autophagy via phosphorylation of Beclin 1 at T108, thereby promoting interaction between Beclin 1 and Bcl-2 (24). The role of atypical protein kinase C in autophagy is less understood. Recently, protein kinase C iota (PKC_ι) was shown to negatively regulate autophagy via direct phosphorylation-mediated activation of PI3 kinase-AKT-mTOR signaling pathway (25).

Several post-translational modifications (PTMs) have been reported in LC3B both surrounding the core LDS as well as in the N-terminal arm (26). Phosphorylation of threonine-6 (T6) and T29 in the N-terminal arm of LC3B by PKC has been reported but was found to

have no effect on overall autophagy or LC3B processing (27). Several other studies have reported PTMs near the LDS including phosphorylation of T50 (28), as well as acetylation of lysine-49 (K49) and K51(29). Phosphorylation of T50 by STK3 and -4 is reported to be required for proper autophagosome-lysosome fusion (28). Furthermore, STK3^{+/-}/STK4^{-/-} knockout cells display deficient xenophagy, as these cells are unable to efficiently clear intracellular bacteria (28). Acetylation of K49 and K51 is reported to cause nuclear retention of LC3B in full medium. Upon starvation, LC3B is deacetylated by SIRT1 and transported out of the nucleus by DOR/TP53INP1. This shuttling was found to be crucial for the ability of LC3B to form puncta, most likely representing autophagosomes, in the cytosol (29).

Given the proximity to the LDS, we hypothesized that phosphorylation of T50 could regulate, the interaction between LC3B and LIR-containing proteins. To this end, we used CRISPR/Cas9 technology to establish a Flp-In T-Rex HEK293 LC3B knockout (KO) cell line. By stably reconstituting the LC3B KO cell line with LC3B WT, -T50A, -T50E and LC3B F52A/L53A (LDS mutants) we found that selective autophagic flux was strongly inhibited by both T50E and F52A/L53A mutations. Furthermore, the phospho-mimicking LC3B T50E mutant displayed significantly reduced interaction with several essential autophagy-related proteins such as p62/SQSTM1(sequestosome-1), ATG7, ATG4B, FYCO1, and Syntaxin-17. By *in vitro* phosphorylation assays, we identified NEK9 as a potential kinase that mediates phosphorylation of LC3B T50. Interestingly, the KO of NEK9 led to enhanced autophagic flux. This suggests that NEK9 may regulate autophagy involving LC3B by phosphorylation of T50 within the LDS.

Materials and methods

Plasmids

The Gateway entry clones used in this study are listed in the table below. QuickChange site-directed mutagenesis kit (Stratagene) was used to create desired point mutation which was verified by DNA sequencing (BigDye sequencing kits, Applied Biosystems). For a generation of Gateway destination plasmid, Gateway LR and BP recombination kit from Invitrogen was used.

Gateway cloning vectors

| Plasmid | Description | Source |
|-----------------|--|------------|
| pENTR1A, 2B,3C | Gateway entry vectors | Invitrogen |
| pDest 3XFlag | mammalian triple flag tagged expression vector, CMV | (30) |
| pDestEGFP-C1 | mammalian EGFP tagged expression vector, CMV | (31) |
| pDest15 | Bacterial GST tagged expression vector, T7 promoter | Invitrogen |
| pDestYFP-Flp-In | Mammalian Flp-In expression vector, Tet-inducible, CMV | (32) |

Gateway entry vectors

| Plasmid | Source |
|------------------------------|--------------------------|
| pENTR -STK3 | This study |
| pENTR -STK4 | This study |
| pDONOR223-NEK9 | Addgene (Plasmid #23459) |
| pENTR-FYCO1 | (33) |
| pENTR-NBR1 | (31) |
| pENTR-p62 | (31) |
| pENTR-ATG4B | (34) |
| pENTR-GABARAP | (35) |
| pENTR-GABARAPL1 | (35) |
| pENTR-GABARAPL2 | (35) |
| pENTR-LC3A | (35) |
| pENTR-LC3B | (35) |
| pENTR-LC3C | (35) |
| pENTR -STK3 (1-357) | This study |
| pENTR -STK3 (1-411) | This study |
| pENTR -STK3 (1-404) | This study |
| pENTR -STK3 (F402A/K405A) | This study |
| pENTR -STK3 (323-491) | This study |
| pENTR -STK3 Δ 405-411 | This study |
| pENTR -STK3 D146N | This study |
| pENTR -STK3 MVI365-367AAA | This study |
| pENTR -STK4 D149N | This study |
| pDONOR223-NEK9 D179N | This study |
| pENTR -GABARAP Y49A | (35) |
| pENTR -LC3C F58A | This study |
| pENTR-LC3B T50A | This study |
| pENTR-LC3B T50E | This study |

| | |
|----------------------------|------------|
| pENTR-LC3B F52A/L53A | This study |
| pENTR-NBR1 D50R ΔCC | (31) |
| pDONOR223-NEK9 W718A/I721A | This study |
| pDONOR223-NEK9 Y845A/L848A | This study |
| pDONOR223-NEK9 W967A/L970A | This study |
| pENTR-ATG7 | This study |
| pENTR- PKCζ | This study |
| pENTR- PKCζ F37A/L40A | This study |
| pENTR- PKCζ F252A/I255A | This study |
| pENTR- PKCζ W434A_L454A | This study |
| pENTR- PKCζ W575A/I578A | This study |
| pENTR-LC3C T56A | This study |
| pENTR-LC3C T56E | This study |

Gateway expression clones

| Plasmid | Source |
|--|------------|
| pDestmcherry YFP-Flp-In-LC3B | This study |
| pDestmcherry YFP-Flp-In-LC3B T50A | This study |
| pDestmcherry YFP-Flp-In-LC3B T50E | This study |
| pDestmcherry YFP-Flp-In-LC3B F52A/L53A | This study |
| pDestmyc-Flp-In-LC3B | This study |
| pDestmyc-Flp-In-LC3B T50A | This study |
| pDestmyc-Flp-In-LC3B T50E | This study |
| pDestmyc-Flp-In-LC3B F52A/L53A | This study |
| pDestMyc ATG4B | (36) |
| pDestMyc ATG7 | This study |
| pDestMyc NBR1 D50R ΔCC1 | (37) |
| pDestMyc NEK9 | This study |
| pDestMyc NEK9 W718A/I721A | This study |
| pDestMyc NEK9 Y845A/L848A | This study |
| pDestMyc NEK9 W967A/L970A | This study |
| pDest3XFlag-NEK9 D179N | This study |
| pDestMyc-STK3 1-357 | This study |
| pDestMyc -STK3 1-411 | This study |
| pDestMyc -STK3 1-404 | This study |
| pDestMyc -STK3 F402A/K405A | This study |
| pDestMyc -STK3 323-491 | This study |
| pDestMyc -STK3 Δ405-411 | This study |

| | |
|----------------------------------|------------|
| pDestMyc -STK3 D146N | This study |
| pDestMyc -STK3 MVI365-367AAA | This study |
| pENTR-STK4 D149N | This study |
| pENTR-STK3 D146N | This study |
| pDest15-GABARAP | (35) |
| pDest15-GABARAPL1 | (35) |
| pDest15-GABARAPL2 | (35) |
| pDest15-LC3A | (35) |
| pDest15-LC3B | (35) |
| pDest15-LC3C | (35) |
| pDestMyc-PKC ζ | This study |
| pDestMyc-PKC ζ F37A/L40A | This study |
| pDestMyc-PKC ζ F252A/I255A | This study |
| pDestMyc-PKC ζ W434A_L454A | This study |
| pDestMyc-PKC ζ W575A/I578A | This study |
| pDestMyc-LC3C T56A | This study |
| pDestMyc-LC3C T56E | This study |

Cell culture

HEK-293 cells were cultured in DMEM (Sigma-Aldrich, D6046) supplemented with 10% fetal bovine serum (Biochrom, S 0615) and 1% streptomycin-penicillin (Sigma-Aldrich, P4333). HEK-293 FlpIn T-Rex cell lines were cultured as above but with cultured in high glucose DMEM (Sigma-Aldrich, D5671). For amino acid and serum starvation, Hanks' Balanced Salt solution was used (Sigma-Aldrich, H9269).

Generation of stable cell lines

LC3B KO HEK293 FlpIn T-Rex cells were used to make stable LC3 mutant cell lines. The mCherry-YFP or myc-tagged LC3B WT, LC3B phospho-mimicking mutant (T50E), T50A and LC3B LDS mutant (F52A-L53) were cloned into pcDNA 3.1 FRT/TO plasmid. The generation of a stable cell line was made in accordance with the manufacturer's instructions (Invitrogen, V6520-20). Briefly, transfection of different mutants of LC3B expressing pcDNA 3.1 FRT/TO plasmids was transfected into LC3B KO cells. Following 48 hours of transfection, colonies of cells with the gene of interest integrated into the FRT site were selected with 150ng/ml of hygromycin (Calbiochem, 400051). The expression of the gene was induced with 1 μ g/ml of tetracycline for 24 hours.

CRISPR/Cas9

To construct the LC3B/NEK9 guide RNA the CRISPR/Cas9 plasmid, sense and antisense oligonucleotide encoding the selection guide sequence were annealed and then inserted into plasmid pSpCas9(BB)-2A-Puro (PX459). For a generation of CRISPR/Cas9 KO cells, approximately 30,000 of HEK293 Flp-In T-Rex cells were seeded into 24 well plates and then 500 ng of plasmid PX459 per well were transfected using Metafectene Pro (Biontexas, T040). The clonal selection was achieved by puromycin treatment 24 hours after transfection for 48-72 hours. Later, single cells were sorted into 96 well plate via FACS sorting. The clones were allowed to grow for 7-10 days and each clones were screened for KO by both western blot and DNA sequencing of PCR products amplified from the targeted region in the genome.

Peptide arrays

Peptides were synthesized on cellulose membranes using a MultiPep automated peptide synthesizer (INTAVIS Bioanalytical Instruments AG, Cologne, Germany), as described previously. Membranes were blocked using 5% nonfat dry milk in Tris-buffered saline containing 0.1% Tween 20. The membrane was probed by overlaying with 1 µg/ml of either GST-GABARAP for 2 hours at RT. Membranes were washed three times in Tris-buffered saline containing 0.1% Tween 20. Bound protein was detected with HRP-conjugated anti-GST antibody (GE Healthcare, RPN1236)

Antibodies and reagents

The following antibodies were used: Rabbit anti-LC3B (Novus, NB100-2220), mouse anti-p62 (BD Bioscience ,610833), rabbit anti-CALCOCO2 (Abcam, AB68588), mouse anti-NBR1 (Santa Cruz Biotechnology, sc-130380), rabbit anti-GFP (Abcam, AB290), rabbit anti-ACTIN (Sigma-Aldrich, A2066), mouse anti-FLAG (Sigma-Aldrich, F3165), rabbit anti-ATG7 (Cell signalling, 8558), rabbit anti-ATG4B (Santa Cruz Biotechnology, sc-130968) mouse anti-Myc (Cell signalling, 2276), NEK9 (Abcam,ab138488), rabbit anti-FYCO1 (Sigma-Aldrich, HPA0355526), horseradish peroxidase-conjugated goat anti-mouse (BD Biosciences, 554002) and anti-rabbit (BD Biosciences, 554021) secondary antibodies. Other reagents used were

Bafilomycin A1 (BafA1; (Santa Cruz Biotechnology, sc-201550) and [³⁵S] methionine (PerkinElmer, NEG709A500UC).

Protein purification and GST affinity isolation experiments

GST-tagged proteins were expressed in *Escherichia coli* BL21 (DE3). GST-(Atg8-family proteins) fusion proteins were purified on glutathione-Sepharose 4 Fast Flow beads (GE Healthcare, 17513201) followed by washing with NET-N buffer (100 mM NaCl, 1 mM EDTA, 0.5% Nonidet P-40 (Sigma-Aldrich, 74385), 50 mM Tris-HCl, pH 8) supplemented with cOmplete Mini EDTA-free protease inhibitor mixture tablets (Roche Applied Science, 11836170001). GST-tagged proteins were eluted with 50 mM Tris, pH 8, 200 mM NaCl, 5 mM L-glutathione reduced (Sigma-Aldrich, G425). GST affinity isolation assays were performed with ³⁵S-labeled proteins cotranscribed and translated using the TNT Coupled Reticulocyte Lysate System (Promega, L4610) as described previously. For quantifications, gels were vacuum dried and ³⁵S-labeled proteins detected on a Fujifilm bioimaging analyzer BAS-5000 (Fujifilm, Tokyo, Japan).

Kinase assay

Kinase assays were performed in 25 µl final volume, containing 50 ng recombinant active kinases, 1-2 µg substrate proteins, 60 µM ATP, 2 µCi/sample [³²P]ATP in 35.5 mM Tris-HCl (pH 7.5), 10 mM MgCl₂, 0.5 mM EGTA (pH 8.0), 0.1 mM CaCl₂. The kinase reaction was stopped by addition of 5X SDS-loading buffer followed by boiling for 5 min. Commercially available his-tagged kinases were used unless otherwise stated (PKCζ: Millipore, 14-525M. STK3: Millipore, 14-524. STK4: Millipore, 14-624). FLAG-tagged kinases were obtained by transient expression of HEK cells with WT or KD kinases, after immunoprecipitation of the FLAG-tag different amount of eluted kinase were run in the kinase assay as above. Expression of kinases from cells was verified with western blot. Proteins were resolved by SDS-page and stained with Coomassie blue and gels were vacuum dried and ³²P-labeled proteins detected on a Fujifilm bioimaging analyzer BAS-5000 (Fujifilm, Tokyo, Japan).

Mass Spectrometry

Gel bands containing GST-LC3 were excised and subjected to in-gel reduction, alkylation, and tryptic digestion using 2–10 ng/μl trypsin (V511A; Promega). Peptide mixtures containing 0.1% formic acid were loaded onto a nanoACQUITY UltraPerformance LC (Waters), containing a 3-μm Symmetry C18 Trap column (180 μm × 22mm; Waters) in front of a 3-μm Atlantis C18 analytical column (100 μm × 100 mm; meters). Peptides were separated with a gradient of 5–95% acetonitrile, 0.1% formic acid, with a flow of 0.4 μl/min eluted to a Q-TOF Ultima Global mass spectrometer (Micromass/Waters). Each sample was run in MS and data dependent tandem MS mode. Peak lists were generated from MS/MS by the ProteinLynx Global server software (version 2.1; Waters). The resulting pkl files were searched against the Swiss-Prot 51.6 protein sequence databases using an in-house Mascot server (Matrix Sciences). Peptide mass tolerances used in the search were 100 ppm, and fragment mass tolerance was 0.1 Da. Mascot analysis confirmed that the sample contained GST-LC3. Data from MS mode was manually inspected to find potential phosphorylated peptides.

Western blot and immunoprecipitation experiments

For western blotting experiments, cells were washed in PBS (137 mM NaCl, 2.7 mM KCl, 4.3 mM Na₂HPO₄, 1.47 mM KH₂PO₄, pH 7.4.) followed by lysis directly in SDS-PAGE loading buffer (2% SDS, 10% glycerol 50 mM Tris-HCl, pH 6.8) and boiled for 10 min. Protein concentration was measured followed by addition of bromophenol blue (0.1%) and DTT (100 mM). Samples (20 μg) were run on 10-16% gradient- or 10%- SDS-polyacrylamide gels and blotted on Hybond nitrocellulose membranes (GE Healthcare, 10600003) followed by Ponceau S staining. Blocking was performed in 5% nonfat dry milk in PBS-Tween 20 (0.1%). Primary antibody was diluted in PBS-Tween 20 containing 5% nonfat dry milk and incubation was performed overnight at 4°C. Secondary antibody incubation was performed at room temperature for 1 h in PBS-Tween 20 containing 5% nonfat dry milk. Membranes were washed 3 times prior to the addition of secondary antibody and development using LAS-300 (Fujifilm, Tokyo, Japan). Immunoprecipitations were performed by use of either GFP-trap_A system in accordance with the manufacturer's instructions (Chromotek, gta-20) or anti-FLAG Affinity Gel (Sigma-Aldrich, A2220). For immunoprecipitations of FLAG-tagged proteins, cells were grown and transfected with 2 μg of the plasmid in 6 cm dishes, after 24 hours cells were washed and lysed in RIPA buffer followed by centrifugation to remove cell debris. After removal of

input control, the lysate was incubated with FLAG affinity gel overnight. The gel was washed five times in RIPA buffer and analyzed by western blotting. For GST pulldowns using cell extracts FLAG-tagged kinases were eluted by addition of FLAG-peptide (100 µg/ml) (Sigma-Aldrich, F3290) and the eluate evenly divided to tubes containing GST-tagged ATG8s prepared as described above.

Bioinformatics and statistics

Data in all figures are shown as mean \pm SEM from at least 3 independent experiments unless otherwise stated. Statistical significance was evaluated with one-way ANOVA followed by the Tukey multiple comparison test performed in PRISM (Graphpad) (ns $P > 0.05$, * $P \leq 0.05$, ** $P \leq 0.01$, *** $P \leq 0.001$).

Results

LC3B is phosphorylated *in vitro* by STK3, STK4, NEK9, and PKC ζ

The pioneering proteomic analysis of the autophagy interaction network in human cells by Behrends et al. revealed several kinases interacting with ATG8s including STK3, STK4, NEK9 and PKC ζ (19). Recently, the hippo kinases STK3 and STK4 were shown to phosphorylate LC3B on T50 leading to enhanced autophagosome-lysosome fusion (28). Previously only STK3 and -4 have been reported to phosphorylate LC3B on T50 and this phosphorylation was found to be important for the fusion of autophagosomes with lysosomes (28). However, several other protein kinases have been reported to bind to ATG8s (19). Besides STK3 and -4, these include ULK1 and -2 (32), the yeast orthologue Atg1 (38), and the atypical PKC ι (19). NEK9 has also been reported to bind ATG8s and positively regulate autophagy (19). Thus, we asked if other kinases binding to LC3B are similarly able to phosphorylate LC3B at T50. We chose to focus on NEK9 and PKC ζ . PKC ζ is the homolog of PKC ι and has not previously been tested for binding to ATG8s. Neither of these three kinases have been reported to mediate phosphorylation of LC3B. First, we validated that NEK9 and PKC ζ bound to LC3B *in vivo*. NEK9, PKC ζ and STK3 and -4 were transiently co-expressed with GABARAP or LC3B in HEK293 cells. The kinases were immunoprecipitated and co-precipitated ATG8s detected by western blotting (Fig. 1A). For this purpose, we used both a functional kinase (WT) and a kinase-deficient mutant (KD). Previously, mutations in the Mg²⁺ binding motif (DFG) or the

ATP binding motif (VAIK) of PKCs, which both abolish ATP binding, have been shown to cause apoptotic effects *in vivo* (39). We, therefore, choose to mutate the aspartic acid (D) of the His-Arg-Asp (HRD) motif necessary for proton transfer from the serine/threonine residue (Fig. 1B). The ATG8s co-immunoprecipitated with all the tested kinases independent of their kinase activity. Albeit the kinase-dead variants of STK3 and NEK9 bound slightly less to both GABARAP and LC3B in the experiments shown (Fig. 1A and B), this was not consistently observed. Of note, co-expression of the GFP tag alone with the kinases caused apoptosis leading to a low yield of STK-3 and -4, PKC ζ and NEK9, as previously reported (40). Next we asked if PKC ζ and NEK9 were able to phosphorylate LC3B *in vitro*, and furthermore, if PKC ζ and NEK9 also phosphorylated LC3B at position T50. STK3 and -4 were included as positive controls. We constructed a GST-LC3B T50A non-phosphorylatable mutant and conducted an *in vitro* kinase assay. PKC ζ as well as NEK9 were able to phosphorylate LC3B and interestingly exhibited less phosphorylation when probed against LC3B T50A (Fig. 1C and D). As previously reported (28), both hippo kinases were able to phosphorylate LC3B and displayed reduced phosphorylation of LC3B T50A (Fig. 1C and D). To validate that PKC ζ phosphorylates LC3B at T50 and that the reduced phosphorylation of LC3B T50A is not a result of interference with the structural integrity of LC3B we choose to employ mass spectroscopy. We performed an *in vitro* kinase assay on GST-tagged LC3B and analyzed the phosphorylated product by MS/MS (Fig. 1E). We detected a peptide of 985.6 m/z (1969.2 Da) in the phosphorylated LC3B sample but not in the unphosphorylated control LC3B. A peptide of 1889.2 Da was detected in both samples, corresponding to a difference of 80 Da between the two, indicating a phosphate group. The 1889.2 Da peptide corresponds to a peptide encompassing residues 50 to 65 (50-TKFLVPDRVNMSELIK-65). Notably, both T50 and S61 are phosphorylatable residues in this peptide and therefore the MS/MS did not exclude the possibility of phosphorylation on S61. However together with the LC3B T50A kinase assay, this strongly suggests phosphorylation of LC3B at T50 by PKC ζ *in vitro*.

STK3 interacts with LC3C and GABARAP via a C-type LIR (CLIR)

To further characterize the interaction between the kinases and ATG8 family proteins we first addressed the interactions between the hippo kinases and ATG8 family proteins. To this end, GST-pulldown assays using *in vitro* translated STK3 showed that STK3 interacted directly with several of the ATG8s, but most strongly with LC3C and GABARAP and more weakly with

GABARAPL1 (Fig. 2A and B). However, STK4 interacted very weakly with the ATG8s (Fig. 2C). STK3 contains an N-terminal kinase domain followed by an unstructured region important for inhibition of the kinase activity by covering the active site. In the far C-terminal region resides the SARA domain, which is important for dimerization(41) (Fig. 2D). A caspase-3 cleavage site (D322) is located at position D322 which, if cleaved, produces a C-terminally truncated, activated version of STK3 (42). To map the binding site for ATG8 on STK3 we established expression constructs corresponding to the fragment produced by caspase cleavage *in vivo* as well as various C-terminally deleted constructs (Fig. 2D). GST pulldown assays using the various deletion constructs of STK3 identified the interaction to be mediated by the fragment encompassing the C-terminal region from amino acid position 323, and not the N-terminal part (from position 1 to 357) (Fig. 2E). GABARAP was used as interaction partner in these LIR mapping experiments since it bound strongly to STK3. However, because STK3 also bound strongly to LC3C, we searched the C-terminal part of STK3 for C-type LIRs (CLIR) with the consensus $\Phi\Phi\Phi$ where Φ is an aliphatic amino acid. A candidate CLIR, 'MVI' was located at positions 365-367, reminiscent of the CLIR previously described for the interaction between CALCOCO2/NDP52 AND LC3C(43). Strikingly, mutation of this CLIR motif to AAA abolished binding between STK3 and LC3C (Fig. 2F). Consistently, the mutation of the LDS in LC3C F58A resulted in strongly decreased binding to STK3 (Fig. 2G). GST-pulldown assays using extracts from HeLa cells expressing FLAG-STK3 or FLAG-STK3 MVI/AAA CLIR mutant verified the strong binding of FLAG-STK3 to GABARAP and LC3C whereas the CLIR mutant FLAG-STK3 MVI/AAA did not show significant binding. The GABARAP Y49A LDS mutant lost almost all binding to FLAG-STK3 (Fig. 2H). Taken together, the results show that the CLIR motif in STK3 mediated LDS-dependent binding to both LC3C and GABARAP.

PKC ζ binds to GABARAP and GABARAPL1 via a LIR motif overlapping with the AGC kinase docking motif

GST-pulldown assays with *in vitro* translated PKC ζ (Fig. 3A), or lysates from HEK293 cells transfected with FLAG-PKC ζ (Fig. 3B), showed that PKC ζ has a binding preference for GABARAP and GABARAPL1. PKC ζ does not interact with LC3C, indicating that the binding is not mediated by a CLIR-like motif. The interaction with LC3B *in vitro* is very weak (Fig. 3A), although LC3B is efficiently immunoprecipitated with PKC ζ from cell extracts (Fig. 1A).

This suggests that either PTMs of LC3B or PKC ζ are required for efficient binding, or the association is not direct i.e. they are part of a larger complex. To study the regions or motifs in PKC ζ required for binding the ATG8s *in vitro*, we chose to use the high-affinity binder GABARAP for *in vitro* interaction assays. The atypical PKCs contain a C-terminal kinase domain whose activity is regulated by the N-terminal region composed of an N-terminal Phox and Bem1p (PB1) domain, followed by a C1-like zinc finger domain which is preceded by a pseudosubstrate peptide (Fig. 3C). We conducted a peptide array screen to probe the entire PKC ζ for any LIR-like motifs (44). Three candidate motifs were identified (Fig. 3D). Since there are no 3D structures available for PKC ζ we used the structure of PKC ι (PDB:3A8W) to assess whether the motifs that were positive hits from the peptide array were likely to be exposed on the surface of PKC ζ . The motif “DIDWVQ” is located in a solvent-exposed part of the kinase domain of PKC ζ/ι , in an α -helical structure with the aromatic tryptophan pointing inwards towards the ATP binding pocket. “WDLL” (WDMM in PKC ι) is located just C-terminal to the kinase domain and is solvent exposed in the structure, however tryptophan is facing inwards between two α -helices. The motif showing the strongest binding in the peptide array “FEYI” overlaps with the AGC Kinase docking motif (FEGFEYI), important for the binding and activation of PKC ζ/ι by PDK1(45), and is located in a solvent-exposed region in the far C-terminal part of PKC ζ/ι . However, again the aromatic phenylalanine is pointing inward in the structure. Mutation of the aromatic F residue in the FEYI core sequence in a peptide covering the C-terminal part of PKC ζ prevented the interaction with GABARAP and mutation of the hydrophobic I residue strongly reduced binding (Fig. 3E). This supports that FEYI might be a functional LIR motif. This was confirmed by GST-pulldown assays with full-length PKC ζ with both the aromatic and hydrophobic residues in the core LIR mutated to alanines which strongly inhibited binding to the ATG8s (Fig. 3F).

NEK9 interacts with ATG8s via a C-terminal LIR motif

NEK9 comprises an N-terminal kinase domain, a RCC1 (regulator of chromatin condensation)-like β -propeller domain with 6 RCC repeats followed by a C terminal domain with an unstructured region that binds to NEK6 and a coiled-coil region (Fig. 4A). To identify putative LIR motifs within NEK9, we employed the iLIR prediction server (46) and peptide array screening methods (44). The iLIR server predicted 3 putative C terminal LIR motifs; ⁷¹⁸WHTI⁷⁵¹, ⁸⁴⁵YEEL⁸⁴⁸, and ⁹⁶⁷WCLL⁹⁷⁰, while the peptide array revealed only the most C

terminal LIR motif as a candidate ATG8 binding domain (Fig. 4B). To determine if any of the predicted LIR motifs mediated the ATG8s interaction, the aromatic and hydrophobic residues of the putative core LIRs were mutated to alanine in the three predicted LIRs. NEK9 WT and the three mutants were assayed for GABARAP binding in a GST-pulldown assay. The NEK9 W967A/L970A mutant displayed strongly reduced binding with GST GABARAP while the other mutations did not affect binding at all (Fig. 4C). The strong NEK9 mediated phosphorylation of LC3B (Fig. 1C and D) could suggest a strong binding of NEK9 to this ATG8 family protein contrary to what we found for STK3 and PKC ζ . Indeed, GST-pulldown assay with *in vitro* translated NEK9 showed that NEK9 interacted very well with all ATG8s. The LIR mutant almost completely lost all binding to the ATG8s (Fig. 4D). A similar binding pattern was seen in GST-pulldown assays, where whole cell lysate from HeLa cells transiently transfected with myc-tagged NEK9 WT and NEK9 LIR mutant constructs were incubated with recombinant GST or GST-ATG8s beads and NEK9 detected with immunoblotting using NEK9 antibody. All ATG8 proteins bound well while the LIR mutation abolished binding (Fig. 4E). Co-immunoprecipitation of GFP-LC3B or GFP-GABARAP from cells co-transfected with FLAG-NEK9 wild-type or kinase-dead showed that NEK9 interaction with the ATG8s is not dependent on an active kinase (Fig. 1A). In conclusion, NEK9 contains a C-terminal LIR motif with the core LIR sequence ⁹⁶⁷WCLL⁹⁷⁰.

To further analyze the sequence requirements for binding to GABARAP of the C terminal LIR of NEK9, a two-dimensional peptide array mutation analysis was performed. Each position of an 18-mer NEK9 peptide encompassing amino acids 960-977 was substituted with all 19 alternative amino acids and the array was probed with GST-GABARAP (Fig. 4F). The results confirm the absolute requirements of an aromatic residue at position 0 and either Leu (L), Ile (I) or Val (V) at the hydrophobic position +3. Tyr is not as efficient in replacing Trp (W) as Phe (F) at position 0. Apart from the invariant aromatic and hydrophobic positions of the core LIR, the intermediate +1 and +2 position also show clear preferences for allowed substitutions. The rather unusual Cys (C) in position +1 is most effectively replaced by E (Glu), V or T (Thr) while the Leu (L) in +2 is only productively substituted by the hydrophobic I or V and the aromatic residues (W, F, Y). As almost always seen (15,32), basic residues (R, K) and proline (P) and glycine (G) are selected against in the core LIR. Interestingly, there are serines at the -1 and -3 positions suggesting that LIR binding can be positively regulated by phosphorylation. There are also acidic residues at position -2 and -4 which are often involved in electrostatic interactions with N terminal residues of the ATG8s (15). Position -1 shows a

preference for either acidic, S, T, P or G residues. These residues are most often found at this position (15,47). Position -2 also shows a strong preference for acidic (D, E) or Ser residues. At position +4 C-terminal to the core LIR, Cys, aromatic and hydrophobic residues (L, I, V) are detrimental to the binding. There is a tendency for counterselection of these residues in the following +5 to +7 positions as well. A recent study of determinants regulating the selective binding of autophagy adapters and receptors to ATG8 proteins allow us to speculate that the fact that NEK9 binds so well to LC3B may perhaps be explained by favorable residues for LC3B binding located at +2 and -1 and -2 of the NEK9 LIR (47).

NEK9 inhibits the selective autophagic degradation of p62 and NBR1

The efficient NEK9-mediated phosphorylation of LC3B *in vitro* raised the question of whether NEK9 could impact selective autophagy. To address this, we knocked down NEK9 and observed an increased turnover of p62 in full medium (Fig. 5A-C). To further validate the NEK9 knockdown data, we generated HeLa NEK9 KO cells (Suppl. Fig. S1A and B). In HeLa NEK9 KO cells we also observed increased autophagic degradation of p62 and NBR1 (Fig. 5D). Hence, our results suggest that NEK9 inhibits autophagic degradation of p62 and NBR1. This inhibition may be mediated by phosphorylation of LC3B at T50E.

A phospho-mimicking T50 mutant of LC3B inhibits LIR-LDS binding

Phosphorylation of LC3B at Thr⁵⁰ (T50) has been reported to be crucial for the fusion of the autophagosome with the lysosome (28). T50 is located close to Arg¹⁰ (R10) in the N-terminal arm of LC3B which forms part of the LDS (Fig. 6A). The R10 residue is involved in electrostatic interactions with several LIR containing proteins, including the Asp³³⁶ (D336) residue at position -2 of the p62 LIR (48)(Fig. 6A). Phosphorylation of T50 can be suspected to impose a steric hindrance for LIR-LDS interactions where R10 of LC3B is engaged in binding an acidic residue N-terminal to the core LIR, such as in p62. We tested this first for the p62-LC3B LIR-LDS interaction. We employed myc-p62 with a mutated PB1 domain, unable to form polymers (31). The phospho-mimicking T50E mutant of LC3B exhibited a 60% reduced binding to p62 compared to WT in an *in vitro* GST-pulldown assay. The LC3B F52A/L53A double mutant affecting both hydrophobic pockets (HP1 and -2) of the LDS completely lost binding to p62. (Fig. 6B and C). Furthermore, endogenous p62 co-precipitated with GFP-LC3B from HeLa cell

extracts bound with less affinity to LC3B T50E compared to WT LC3B (Fig. 6D). Similar results were obtained for endogenous p62 from HeLa cell lysates when bound to GST-LC3B WT, GST-LC3B T50A, GST-LC3B T50E and GST-LC3B F52A/L53A (Fig. 6E). These results clearly show that introducing a phospho-mimicking T50E mutation in LC3B reduces its affinity for the cargo receptor p62. Next, the binding of LC3B T50E to the autophagy receptor NBR1 was analyzed. Whole cells extract from HeLa cells was subjected to pulldown assays with WT, T50A, T50E or F52A/L53A mutants of GST-LC3B and bound endogenous NBR1 detected by immunoblotting with NBR1 antibody. The phospho-mimicking mutant T50E mutant showed a 45% reduction in binding with endogenous NBR1 compared to WT LC3B (Fig. 6F).

T50 is conserved in the LC3 subfamily of ATG8s, but not present in the GABARAP subfamily. The kinesin adaptor and Rab7 effector FYCO1 transports autophagosomes along microtubules in the plus end direction and has a clear preference for binding to LC3A and -B (49). The LC3B T50E mutation strongly reduced binding to endogenous FYCO1 in GST-pulldown assays and also when co-immunoprecipitated with myc FYCO1 (Fig. 6G, H and I). It is important to note that both NBR1 and FYCO1 also displayed a slight reduction in binding with LC3B T50A, indicating that this substitution also affects LIR-LDS binding, albeit slightly.

The cysteine protease ATG4B is required for processing of LC3B before conjugation to phosphatidylethanolamine (PE) and for delipidation and recycling of LC3B(50). To test if T50E would compromise efficient binding of ATG4B, we conducted a GST pulldown assay with *in vitro* translated ATG4B probed against GST-LC3B WT, T50A, T50E, and the LDS double mutant F52A/L53A. Importantly, ATG4B displayed less affinity for LC3B T50E than for WT LC3B (Fig. 7A). In GST-pulldown assays with endogenous ATG4B from HeLa cell lysates LC3B T50E showed 74% reduction in binding with ATG4B compared to LC3B WT and very little binding to the LDS mutant (Fig. 7B and C).

Efficient conjugation of LC3 to PE requires sequential interaction of LC3 with ATG3 and ATG7 (51,52). To investigate whether the interaction of LC3B with ATG7 was affected by the T50E mutant GST pulldown with endogenous ATG7 was done. The phospho-mimicking mutant LC3B T50E almost lost all binding to ATG7 while LC3B T50A and LC3B F52A/L53A (LDS) bound similarly to WT (Fig. 7D and E).

ATG8s family protein is essential both for efficient autophagosome biogenesis and fusion with lysosomes (13). The role of ATG8s in the fusion of autophagosomes with lysosomes has been shown via its interaction with syntaxin 17 (STX17)(53) and

PLEKHM1(54). Both STX17 and PLEKHM1 are known to interact with ATG8s via LIR motifs (53,54). Consistent with the results obtained for interaction with the other LIR-containing ATG8 interactors tested here LC3B T50E showed strongly reduced binding affinity for STX17. Almost no binding of STX17 was seen for the LDS mutant LC3B F52A/L53A, and there was also reduced binding to LC3B T50A (Fig. 7F and G).

Taken together all these results show that binding of LIR-containing protein to LC3B T50E is compromised. This can be explained by steric hindrance and charge repulsions occurring due to the close proximity of T50 to the LDS. Phosphorylation of T50 will most likely exaggerate the effects observed with T50E, having an even stronger impact on LIR-LDS interactions.

The LC3B T50E phospho-mimicking mutant impairs selective autophagic flux

To investigate the importance of the phosphorylation of LC3B on T50 we established a LC3B knockout (KO) cell line to avoid the influence of endogenous LC3B. We employed the CRISPR/Cas9 system targeting exon 2 of the human LC3B gene on chromosome 16 to generate a Flp-In T-Rex HEK293 cell line lacking expression of LC3B (Suppl. Fig. 1C and D). The LC3B KO cells showed accumulation of the selective autophagy receptors p62/SQSTM1 and NBR1 compared to wild type cells (Fig. 8A and B). To avoid any overexpression artefacts, we employed stable reconstitution of the LC3B KO cells by use of the Flp-In system under the control of a tetracycline-inducible promoter. LC3B KO cell lines with reintroduced Myc-LC3B WT, Myc-LC3B T50A, Myc-LC3B T50E, and the LDS mutant F52A/L53A were established (Fig. 8C). Reduced lipidation was observed for T50E and no lipidation was seen for the LDS mutant (Fig. 8C). The reconstitution of LC3B KO cells with Myc-LC3B WT restored the autophagic flux as indicated by a reduced level of p62 and NBR1. Interestingly, reconstitution of Myc-LC3B T50E and Myc-LC3B F52A/L53A led to strongly reduced autophagic degradation of p62 and NBR1 (Fig. 8D). To further investigate the autophagic turnover of the LC3B T50 mutations in the KO cells, we reintroduced mCherry-YFP-LC3B wild type and mutants. The mCherry-YFP tag allows for monitoring entry into acidic structures such as the lysosome since YFP fluorescence is rapidly lost in acidic structures, leaving only mCherry as a functioning fluorophore (35). First, we quantitated the amount of LC3B-containing puncta (indicative of autophagosomes) per cell. We scored the ability of the different cell lines to produce LC3B puncta during starvation. While more than 90% of LC3B WT (n=550) and T50A

cells (n=710) contained LC3B puncta, the T50E cell line (n=680) exhibited puncta in 75% of the cells. We had to exclude the LC3B F52A/L53A cell line since, as expected, only a few cells produced LC3B puncta. Only by actively searching for LC3B puncta containing cells were we able to identify cells with LC3B puncta (less than 15%; n=220) (Fig. 8E). Next, we focused on the cells containing LC3B puncta in WT, T50A, and T50E cell lines. Looking at the number of puncta per cell volume, we found slightly fewer LC3B puncta in the T50A cell line when compared with LC3B WT (Fig. 8F) and more so during starvation (Fig. 8G). LC3B T50E expressing cells displayed a strongly reduced amount of LC3B-containing puncta, both when grown in full medium and when starved in Hanks medium (Fig. 8F and G). Hence, either fewer LC3B-containing puncta are produced when LC3B T50E is expressed, or LC3B T50E puncta are more readily removed thus having a higher turnover-rate. To discriminate between these two possibilities we determined the ratio of red-only to yellow puncta. When grown in full medium LC3B T50E displayed a slightly reduced fraction of red only puncta compared to LC3B WT and T50A, strongly indicating that T50E positive puncta do not have a higher turnover rate (Fig. 8H). In conclusion, the lower total amount of puncta in the T50E cell line is caused by a reduced ability of LC3B T50E to become lipidated. Notably, the lower fraction of red-only puncta under basal conditions may indicate that not only formation but also maturation of LC3B positive puncta is affected by the T50E mutation (Fig. 8H). However, when starved, there was no statistically significant difference in the fraction of red-only puncta between the cells (Fig. 8H).

Discussion

The hippo kinases have previously been reported to phosphorylate LC3B at T50 (28). Here we show that *in vitro* PKC ζ and NEK9 are also able to phosphorylate this residue. Furthermore, we mapped an atypical C-type LIR motif mediating binding to LC3C and GABARAP in STK3, a GABARAP-preferring LIR motif overlapping with the AGC kinase docking motif in PKC ζ , and a C-terminal LIR motif in NEK9 mediating efficient binding to both LC3 and GABARAP subfamily members of the ATG8 family proteins. Knock down and KO experiments showed that NEK9 may be acting to inhibit the selective autophagic degradation of p62 and NBR1. It is likely that this inhibition can be mediated via phosphorylation of T50 in LC3B. This reasoning is based on our findings that the LC3B T50E phospho-mimicking mutant impaired selective autophagic flux by inhibiting LIR-LDS binding to a number of autophagy-related

proteins. These include the selective autophagy receptors p62 and NBR1, the basal autophagy proteins important for conjugation and delipidation of LC3B ATG7 and ATG4B, FYCO1 involved in microtubule-dependent transport of autophagosomes and lysosomes, and the SNARE STX17 implicated both early and late in the process of autophagosome formation and maturation.

We were unable to detect *in vitro* binding of STK4 to ATG8s. STK3 therefore clearly seems to have the strongest affinity for ATG8s of the two hippo kinases. STK4 has previously been shown to bind to ATG8s *in vitro*. However, the binding appeared weaker than the binding of STK3 to the ATG8s (19). It is entirely likely that STK4 binds ATG8s *in vivo*. However, this binding is apparently not strong enough to be detected by the *in vitro* methods employed in this study. Interestingly, knockdown of STK3 was recently shown to have the most dramatic effect on autophagy measured as an increased basal level of p62 and increased LC3B lipidation (28). In addition to influencing basal autophagy, STK3 was also shown to stimulate xenophagy by enhancing the clearance of bacteria via phosphorylation of the LC3B T50 site (28). The xenophagy receptor NDP52 has been shown to rely on binding to LC3C (17,43). Here we show that STK3 has a preference for binding to GABARAP and LC3C and we identified a C-type LIR (MVI) in STK3. Consistent with our finding that the phospho-mimicking mutant T50E negatively affects its LIR-LDS-mediated interactions the LC3C T56A/E mutants significantly reduced its interaction with NDP52 (Suppl. Fig. 1E and F). Clearly, this link to the regulation of xenophagy warrants further studies.

Interestingly, the CLIR of STK3 and surrounding residues have been identified as a nuclear export signal (55). Furthermore, the STK3 substrate MOB1 has been shown to bind to STK3 dependent on several phosphorylated threonines, with T364 (next to the LIR) being the most crucial for this binding (56), indicating a possible competition for this site in STK3.

Previously, PKC ζ has only been indirectly implicated in the phosphorylation of LC3B (27). However, it has long been known that PKC ζ / ι bind p62 (31), and thereby might co-localize with LC3B *in vivo*. The atypical PKC ι , which is very similar to PKC ζ , has been shown to negatively regulate autophagy via PIK3CA/AKT-MTOR signaling (25). The LIR motif we mapped in PKC ζ overlaps completely with AGC kinase docking motif, a hydrophobic motif known to mediate PKC ζ interaction with its activating kinase, PDK1 (57). This hydrophobic motif is essential for the activation of PKC ζ by PDK1. In future studies, it will be interesting to

investigate whether interactions mediated by these overlapping motifs may affect the roles played by PKC ζ , or PKC ι , in autophagy and other cellular processes.

Except for the pioneering study of Behrends et al. (19), NEK9 has not been implicated in autophagy processes or the regulation of autophagy before. In the Behrends et al. paper NEK9 was scored among the positive regulators of autophagosome formation based on a reduced amount of LC3-positive puncta formed upon siRNA-mediated KD of NEK9. We also see reduced lipidated LC3B upon KO of NEK9, but this can also be interpreted as increased turnover (Fig. 5D). This would then be consistent with our findings of an inhibitory role of NEK9 on selective autophagy. We found that NEK9 interacts strongly with all ATG8s compared to PKC ζ which showed preferential binding towards GABARAPs.

We show that the T50 phospho-mimicking mutant displays a strongly reduced binding to several autophagic related proteins. A phosphorylatable residue in the LDS of LC3B is intriguing as it might function as a dynamic “switch” governing which proteins bind to LC3B. Regulation of LDS binding by phosphorylation/dephosphorylation might be executed at a certain stage(s) of autophagosome formation and maturation adding another regulatory layer. An intriguing idea is that LC3B on a fully matured autophagosome becomes phosphorylated at T50. This causes canonical LIR-binding proteins to dissociate, leaving ATG4B to delipidate LC3B from the autophagosome. Such a model might also explain why we observed less II-form of LC3B T50E. If LC3B T50E is unable to bind effectively to cargo receptors such as p62 on the inside of the phagophore, LC3B might be exposed for ATG4B-mediated delipidation. This way LC3B T50E is delipidated, removed from the autophagosome before maturation, and thus no longer sequestered inside the autophagosome, hence the lower amount of LC3B-II. Importantly, phosphorylation is assumed to have a greater effect on all the interactions and functions of LC3B, due to the more negatively charged and bulky phosphate compared to our phospho-mimicking glutamic acid. One of the limitations of using a phospho-mimicking T50E mutant is that it is mimicking a constitutively phosphorylated state. So, the phospho-mimicking T50E mutant behaves as a constitutively dominant negative on LIR-LDS interactions which might affect both autophagosome formation and autophagosome-lysosomal fusion. Such an effect is supported by our results where the selective autophagic flux is reduced as well as the formation of autophagosomes (fewer puncta).

Interestingly, during starvation, the LC3B T50A cell line was also less able to make puncta than LC3B WT (Fig. 8E and G). This may indicate that phosphorylation of T50 is

important for autophagosome formation. However, as previously noted, LC3B T50A displayed slightly reduced binding to several LIR-containing proteins (**Fig. 1**). Hence, puncta formation might be inhibited and this might be more evident during the fast protein turnover occurring during starvation. We saw no consistent difference between the myc-tagged versions of LC3B WT and T50A neither in the amount of p62 nor the band pattern of LC3B. Furthermore, there was no difference between LC3B WT and T50A in the fraction of red-only puncta between full medium and starvation. This indicates that the slightly negative effect of T50A is occurring during autophagosome formation.

The reduced ability of LC3B T50E to become lipidated may seem surprising when considering the reported positive effect on the fusion of autophagosomes and lysosomes (28). However, neither our *in vitro* binding data nor *in vivo* data support a pro-autophagic role of the phosphorylation of T50. There are, however, important differences between the studies. First, the study by Wilkinson et al. (28) is based on the transient overexpression of LC3B harboring T50 mutations. Second, they did not use a LC3B knockout cell line. Our cell lines mimic global phosphorylation, which might retard a dynamic process depending on only a fractional pool of phosphorylated LC3B at any one time. Our data support that LC3B lipidation is impaired and that interactions of LC3B with effector proteins on the inner or outer surface of the phagophore/autophagosome is strongly reduced. Furthermore, roles not directly related to autophagy have been reported for LC3B (58), such as the regulation of endocytic pathways (59), and the Rho signaling pathway (60). How the phosphorylation of T50 affects these pathways *in vivo* was not addressed. Since these interactions are reported to be LIR-mediated it is likely that the phosphorylation also affects these interactors. Recently, acetylation of residues in the LDS was shown to have a drastic effect on LC3B causing LC3B to be unable to produce puncta (29). We show that the phospho-mimicking T50E mutant also strongly affects LC3B function strengthening the notion of a potent regulator of the LDS by PTMs. Both acetylation and phosphorylation sites in the LDS region are conserved within the LC3 subfamily of ATG8 proteins.

Recent KD and KO studies of ATG8 family members show that GABARAPs are critical facilitators of autophagic flux (61-63). LC3 family proteins are not required for non-selective, bulk degradation of cytosolic proteins whereas GABARAPs are required (62). A similar conclusion was reached for some forms of selective autophagy based on triple KOs of LC3 or GABARAP subfamily members (61,63). However, studying cells only KO for LC3B we did see an effect on the turnover of p62 and NBR1, although it was not very strong. The T50E

mutant had a stronger effect, most likely because it also has a dominant negative effect. More studies will be required to determine the relative contributions of the different ATG8 family members to different forms of selective autophagy. We have also just begun to elucidate how PTMs may regulate LIR-LDS interactions and the effects mediated on different steps of the autophagy pathway.

Acknowledgments

We are grateful to the proteomics and imaging core facilities at UiT, Faculty of Health Sciences for valuable assistance. This work was funded by grants from the FRIBIOMED (grant number 214448) and the TOPPFORSK (grant number 249884) programs of the Research Council of Norway, and the Norwegian Cancer Society (grant number 71043-PR-2006-0320) to T.J.

References

1. Mizushima, N., and Komatsu, M. (2011) Autophagy: renovation of cells and tissues. *Cell* **147**, 728-741
2. Wen, X., and Klionsky, D. J. (2016) An overview of macroautophagy in yeast. *J Mol Biol* **428**, 1681-1699
3. Parzych, K. R., and Klionsky, D. J. (2014) An overview of autophagy: morphology, mechanism, and regulation. *Antioxidants & redox signaling* **20**, 460-473
4. Rogov, V., Dotsch, V., Johansen, T., and Kirkin, V. (2014) Interactions between autophagy receptors and ubiquitin-like proteins form the molecular basis for selective autophagy. *Molecular cell* **53**, 167-178
5. Lamark, T., Svenning, S., and Johansen, T. (2017) Regulation of selective autophagy: the p62/SQSTM1 paradigm. *Essays Biochem* **61**, 609-624
6. Katsuragi, Y., Ichimura, Y., and Komatsu, M. (2015) p62/SQSTM1 functions as a signaling hub and an autophagy adaptor. *The FEBS journal* **282**, 4672-4678
7. Johansen, T., and Lamark, T. (2011) Selective autophagy mediated by autophagic adapter proteins. *Autophagy* **7**, 279-296
8. Shpilka, T., Weidberg, H., Pietrokovski, S., and Elazar, Z. (2011) Atg8: an autophagy-related ubiquitin-like protein family. *Genome biology* **12**, 226
9. Tanida, I., Sou, Y. S., Ezaki, J., Minematsu-Ikeguchi, N., Ueno, T., and Kominami, E. (2004) HsAtg4B/HsApg4B/autophagin-1 cleaves the carboxyl termini of three human Atg8 homologues and delipidates microtubule-associated protein light chain 3- and GABAA receptor-associated protein-phospholipid conjugates. *J Biol Chem* **279**, 36268-36276
10. Taherbhoy, A. M., Tait, S. W., Kaiser, S. E., Williams, A. H., Deng, A., Nourse, A., Hammel, M., Kurinov, I., Rock, C. O., Green, D. R., and Schulman, B. A. (2011) Atg8 transfer from Atg7 to Atg3: a distinctive E1-E2 architecture and mechanism in the autophagy pathway. *Molecular cell* **44**, 451-461
11. Yang, Z., and Klionsky, D. J. (2009) An overview of the molecular mechanism of autophagy. *Current topics in microbiology and immunology* **335**, 1-32

12. Xie, Z., Nair, U., and Klionsky, D. J. (2008) Atg8 controls phagophore expansion during autophagosome formation. *Molecular biology of the cell* **19**, 3290-3298
13. Weidberg, H., Shvets, E., Shpilka, T., Shimron, F., Shinder, V., and Elazar, Z. (2010) LC3 and GATE-16/GABARAP subfamilies are both essential yet act differently in autophagosome biogenesis. *EMBO J* **29**, 1792-1802
14. Kabeya, Y., Mizushima, N., Ueno, T., Yamamoto, A., Kirisako, T., Noda, T., Kominami, E., Ohsumi, Y., and Yoshimori, T. (2000) LC3, a mammalian homologue of yeast Apg8p, is localized in autophagosome membranes after processing. *The EMBO journal* **19**, 5720-5728
15. Birgisdottir, A. B., Lamark, T., and Johansen, T. (2013) The LIR motif - crucial for selective autophagy. *J. Cell. Sci.* **126**, 3237-3247
16. Noda, N. N., Kumeta, H., Nakatogawa, H., Satoo, K., Adachi, W., Ishii, J., Fujioka, Y., Ohsumi, Y., and Inagaki, F. (2008) Structural basis of target recognition by Atg8/LC3 during selective autophagy. *Genes to cells : devoted to molecular & cellular mechanisms* **13**, 1211-1218
17. von Muhlinen, N., Akutsu, M., Ravenhill, B. J., Foeglein, A., Bloor, S., Rutherford, T. J., Freund, S. M., Komander, D., and Randow, F. (2013) An essential role for the ATG8 ortholog LC3C in antibacterial autophagy. *Autophagy* **9**, 784-786
18. Jung, C. H., Ro, S. H., Cao, J., Otto, N. M., and Kim, D. H. (2010) mTOR regulation of autophagy. *FEBS letters* **584**, 1287-1295
19. Behrends, C., Sowa, M. E., Gygi, S. P., and Harper, J. W. (2010) Network organization of the human autophagy system. *Nature* **466**, 68-76
20. Fry, A. M., O'Regan, L., Sabir, S. R., and Bayliss, R. (2012) Cell cycle regulation by the NEK family of protein kinases. *Journal of cell science* **125**, 4423-4433
21. Piccolo, S., Dupont, S., and Cordenonsi, M. (2014) The biology of YAP/TAZ: hippo signaling and beyond. *Physiological reviews* **94**, 1287-1312
22. Nehme, N. T., Schmid, J. P., Debeurme, F., Andre-Schmutz, I., Lim, A., Nitschke, P., Rieux-Laucat, F., Lutz, P., Picard, C., Mahlaoui, N., Fischer, A., and de Saint Basile, G. (2012) MST1 mutations in autosomal recessive primary immunodeficiency characterized by defective naive T-cell survival. *Blood* **119**, 3458-3468
23. Abdollahpour, H., Appaswamy, G., Kotlarz, D., Diestelhorst, J., Beier, R., Schaffer, A. A., Gertz, E. M., Schambach, A., Kreipe, H. H., Pfeifer, D., Engelhardt, K. R., Rezaei, N., Grimbacher, B., Lohrmann, S., Sherkat, R., and Klein, C. (2012) The phenotype of human STK4 deficiency. *Blood* **119**, 3450-3457
24. Maejima, Y., Kyoji, S., Zhai, P., Liu, T., Li, H., Ivessa, A., Sciarretta, S., Del Re, D. P., Zablocki, D. K., Hsu, C. P., Lim, D. S., Isobe, M., and Sadoshima, J. (2013) Mst1 inhibits autophagy by promoting the interaction between Beclin1 and Bcl-2. *Nat Med* **19**, 1478-1488
25. Qu, L., Li, G., Xia, D., Hongdu, B., Xu, C., Lin, X., and Chen, Y. (2016) PRKCI negatively regulates autophagy via PIK3CA/AKT-MTOR signaling. *Biochem Biophys Res Commun* **470**, 306-312
26. Xie, Y., Kang, R., Sun, X., Zhong, M., Huang, J., Klionsky, D. J., and Tang, D. (2015) Posttranslational modification of autophagy-related proteins in macroautophagy. *Autophagy* **11**, 28-45
27. Jiang, H., Cheng, D., Liu, W., Peng, J., and Feng, J. (2010) Protein kinase C inhibits autophagy and phosphorylates LC3. *Biochem Biophys Res Commun* **395**, 471-476
28. Wilkinson, D. S., Jariwala, J. S., Anderson, E., Mitra, K., Meisenhelder, J., Chang, J. T., Ideker, T., Hunter, T., Nizet, V., Dillin, A., and Hansen, M. (2015) Phosphorylation of LC3 by the Hippo kinases STK3/STK4 is essential for autophagy. *Mol Cell* **57**, 55-68
29. Huang, R., Xu, Y., Wan, W., Shou, X., Qian, J., You, Z., Liu, B., Chang, C., Zhou, T., Lippincott-Schwartz, J., and Liu, W. (2015) Deacetylation of nuclear LC3 drives autophagy initiation under starvation. *Mol Cell* **57**, 456-466
30. Jain, A., Lamark, T., Sjøttem, E., Bowitz Larsen, K., Awuh, J. A., Øvervatn, A., McMahon, M., Hayes, J. D., and Johansen, T. (2010) p62/SQSTM1 is a target gene for transcription factor NRF2 and creates a positive feedback loop by inducing antioxidant response element-driven gene transcription. *J Biol Chem* **285**, 22576-22591

31. Lamark, T., Perander, M., Outzen, H., Kristiansen, K., Øvervatn, A., Michaelsen, E., Bjørkøy, G., and Johansen, T. (2003) Interaction codes within the family of mammalian Phox and Bem1p domain-containing proteins. *J Biol Chem* **278**, 34568-34581
32. Alemu, E. A., Lamark, T., Torgersen, K. M., Birgisdottir, A. B., Larsen, K. B., Jain, A., Olsvik, H., Overvatn, A., Kirkin, V., and Johansen, T. (2012) ATG8 Family Proteins Act as Scaffolds for Assembly of the ULK Complex: SEQUENCE REQUIREMENTS FOR LC3-INTERACTING REGION (LIR) MOTIFS. *J Biol Chem* **287**, 39275-39290
33. Pankiv, S., Alemu, E. A., Brech, A., Bruun, J. A., Lamark, T., Overvatn, A., Bjorkoy, G., and Johansen, T. (2010) FYCO1 is a Rab7 effector that binds to LC3 and PI3P to mediate microtubule plus end-directed vesicle transport. *The Journal of cell biology* **188**, 253-269
34. Skytte Rasmussen, M., Mouilleron, S., Kumar Shrestha, B., Wirth, M., Lee, R., Bowitz Larsen, K., Abudu Princely, Y., O'Reilly, N., Sjøttem, E., Tooze, S. A., Lamark, T., and Johansen, T. (2017) ATG4B contains a C-terminal LIR motif important for binding and efficient cleavage of mammalian orthologs of yeast Atg8. *Autophagy* **13**, 834-853
35. Pankiv, S., Clausen, T. H., Lamark, T., Brech, A., Bruun, J. A., Outzen, H., Overvatn, A., Bjorkoy, G., and Johansen, T. (2007) p62/SQSTM1 binds directly to Atg8/LC3 to facilitate degradation of ubiquitinated protein aggregates by autophagy. *The Journal of biological chemistry* **282**, 24131-24145
36. Skytte Rasmussen, M., Mouilleron, S., Kumar Shrestha, B., Wirth, M., Lee, R., Bowitz Larsen, K., Abudu Princely, Y., O'Reilly, N., Sjøttem, E., Tooze, S. A., Lamark, T., and Johansen, T. (2017) ATG4B contains a C-terminal LIR motif important for binding and efficient cleavage of mammalian orthologs of yeast Atg8. *Autophagy*, 1-20
37. Kirkin, V., Lamark, T., Sou, Y. S., Bjorkoy, G., Nunn, J. L., Bruun, J. A., Shvets, E., McEwan, D. G., Clausen, T. H., Wild, P., Bilusic, I., Theurillat, J. P., Overvatn, A., Ishii, T., Elazar, Z., Komatsu, M., Dikic, I., and Johansen, T. (2009) A role for NBR1 in autophagosomal degradation of ubiquitinated substrates. *Molecular cell* **33**, 505-516
38. Kraft, C., Kijanska, M., Kalie, E., Siergiejuk, E., Lee, S. S., Semplicio, G., Stoffel, I., Brezovich, A., Verma, M., Hansmann, I., Ammerer, G., Hofmann, K., Tooze, S., and Peter, M. (2012) Binding of the Atg1/ULK1 kinase to the ubiquitin-like protein Atg8 regulates autophagy. *EMBO J* **31**, 3691-3703
39. Cameron, A. J., Escribano, C., Saurin, A. T., Kostelecky, B., and Parker, P. J. (2009) PKC maturation is promoted by nucleotide pocket occupation independently of intrinsic kinase activity. *Nature structural & molecular biology* **16**, 624-630
40. Liu, H. S., Jan, M. S., Chou, C. K., Chen, P. H., and Ke, N. J. (1999) Is green fluorescent protein toxic to the living cells? *Biochemical and biophysical research communications* **260**, 712-717
41. Ni, L., Li, S., Yu, J., Min, J., Brautigam, C. A., Tomchick, D. R., Pan, D., and Luo, X. (2013) Structural basis for autoactivation of human Mst2 kinase and its regulation by RASSF5. *Structure* **21**, 1757-1768
42. Avruch, J., Zhou, D., Fitamant, J., Bardeesy, N., Mou, F., and Barrufet, L. R. (2012) Protein kinases of the Hippo pathway: regulation and substrates. *Seminars in cell & developmental biology* **23**, 770-784
43. von Muhlinen, N., Akutsu, M., Ravenhill, B. J., Foeglein, A., Bloor, S., Rutherford, T. J., Freund, S. M., Komander, D., and Randow, F. (2012) LC3C, bound selectively by a noncanonical LIR motif in NDP52, is required for antibacterial autophagy. *Mol Cell* **48**, 329-342
44. Johansen, T., Birgisdottir, A. B., Huber, J., Kniss, A., Dotsch, V., Kirkin, V., and Rogov, V. V. (2017) Methods for Studying Interactions Between Atg8/LC3/GABARAP and LIR-Containing Proteins. *Methods in enzymology* **587**, 143-169
45. Balendran, A., Biondi, R. M., Cheung, P. C., Casamayor, A., Deak, M., and Alessi, D. R. (2000) A 3-phosphoinositide-dependent protein kinase-1 (PDK1) docking site is required for the phosphorylation of protein kinase C ζ (PKC ζ) and PKC-related kinase 2 by PDK1. *The Journal of biological chemistry* **275**, 20806-20813

46. Kalvari, I., Tsompanis, S., Mulakkal, N. C., Osgood, R., Johansen, T., Nezis, I. P., and Promponas, V. J. (2014) iLIR: A web resource for prediction of Atg8-family interacting proteins. *Autophagy* **10**, 913-925
47. Wirth, M., Zhang, W., Razi, M., Nyoni, L., Joshi, D., O'Reilly, N., Johansen, T., Tooze, S. A., and Mouilleron, S. (2019) Molecular determinants regulating selective binding of autophagy adaptors and receptors to ATG8 proteins. *Nat Commun* **10**, 2055
48. Ichimura, Y., Kumanomidou, T., Sou, Y. S., Mizushima, T., Ezaki, J., Ueno, T., Kominami, E., Yamane, T., Tanaka, K., and Komatsu, M. (2008) Structural basis for sorting mechanism of p62 in selective autophagy. *The Journal of biological chemistry* **283**, 22847-22857
49. Olsvik, H. L., Lamark, T., Takagi, K., Larsen, K. B., Evjen, G., Overvatn, A., Mizushima, T., and Johansen, T. (2015) FYCO1 Contains a C-terminally Extended, LC3A/B-preferring LC3-interacting Region (LIR) Motif Required for Efficient Maturation of Autophagosomes during Basal Autophagy. *The Journal of biological chemistry* **290**, 29361-29374
50. Nair, U., Yen, W. L., Mari, M., Cao, Y., Xie, Z., Baba, M., Reggiori, F., and Klionsky, D. J. (2012) A role for Atg8-PE deconjugation in autophagosome biogenesis. *Autophagy* **8**, 780-793
51. Ichimura, Y., Kirisako, T., Takao, T., Satomi, Y., Shimonishi, Y., Ishihara, N., Mizushima, N., Tanida, I., Kominami, E., Ohsumi, M., Noda, T., and Ohsumi, Y. (2000) A ubiquitin-like system mediates protein lipidation. *Nature* **408**, 488-492
52. Nakatogawa, H., Ichimura, Y., and Ohsumi, Y. (2007) Atg8, a ubiquitin-like protein required for autophagosome formation, mediates membrane tethering and hemifusion. *Cell* **130**, 165-178
53. Kumar, S., Jain, A., Farzam, F., Jia, J., Gu, Y., Choi, S. W., Mudd, M. H., Claude-Taupin, A., Wester, M. J., Lidke, K. A., Rusten, T. E., and Deretic, V. (2018) Mechanism of Stx17 recruitment to autophagosomes via IRGM and mammalian Atg8 proteins. *J Cell Biol* **217**, 997-1013
54. McEwan, D. G., Popovic, D., Gubas, A., Terawaki, S., Suzuki, H., Stadel, D., Coxon, F. P., Miranda de Stegmann, D., Bhogaraju, S., Maddi, K., Kirchof, A., Gatti, E., Helfrich, M. H., Wakatsuki, S., Behrends, C., Pierre, P., and Dikic, I. (2015) PLEKHM1 Regulates Autophagosome-Lysosome Fusion through HOPS Complex and LC3/GABARAP Proteins. *Mol Cell* **57**, 39-54
55. Lee, K. K., and Yonehara, S. (2002) Phosphorylation and dimerization regulate nucleocytoplasmic shuttling of mammalian STE20-like kinase (MST). *The Journal of biological chemistry* **277**, 12351-12358
56. Ni, L., Zheng, Y., Hara, M., Pan, D., and Luo, X. (2015) Structural basis for Mob1-dependent activation of the core Mst-Lats kinase cascade in Hippo signaling. *Genes & development* **29**, 1416-1431
57. Parekh, D. B., Ziegler, W., and Parker, P. J. (2000) Multiple pathways control protein kinase C phosphorylation. *The EMBO journal* **19**, 496-503
58. Subramani, S., and Malhotra, V. (2013) Non-autophagic roles of autophagy-related proteins. *EMBO reports* **14**, 143-151
59. Popovic, D., Akutsu, M., Novak, I., Harper, J. W., Behrends, C., and Dikic, I. (2012) Rab GTPase-activating proteins in autophagy: regulation of endocytic and autophagy pathways by direct binding to human ATG8 modifiers. *Molecular and cellular biology* **32**, 1733-1744
60. Baisamy, L., Cavin, S., Jurisch, N., and Diviani, D. (2009) The ubiquitin-like protein LC3 regulates the Rho-GEF activity of AKAP-Lbc. *The Journal of biological chemistry* **284**, 28232-28242
61. Nguyen, T. N., Padman, B. S., Usher, J., Oorschot, V., Ramm, G., and Lazarou, M. (2016) Atg8 family LC3/GABARAP proteins are crucial for autophagosome-lysosome fusion but not autophagosome formation during PINK1/Parkin mitophagy and starvation. *J Cell Biol* **215**, 857-874

62. Szalai, P., Hagen, L. K., Saetre, F., Luhr, M., Sponheim, M., Overbye, A., Mills, I. G., Seglen, P. O., and Engedal, N. (2015) Autophagic bulk sequestration of cytosolic cargo is independent of LC3, but requires GABARAPs. *Experimental cell research* **333**, 21-38
63. Vaites, L. P., Paulo, J. A., Huttlin, E. L., and Harper, J. W. (2018) Systematic Analysis of Human Cells Lacking ATG8 Proteins Uncovers Roles for GABARAPs and the CCZ1/MON1 Regulator C18orf8/RMC1 in Macroautophagic and Selective Autophagic Flux. *Mol Cell Biol* **38**

FIGURE LEGENDS

Figure 1. NEK9, PKC ζ and STK3/4 associate with ATG8s *in vivo* and phosphorylate LC3B *in vitro*. **(A)** HEK293 cells were transiently co-transfected with the indicated FLAG-tagged kinases, wild type (WT) or kinase dead (KD), and either GFP-LC3B or GFP-GABARAP. Cell lysates were immunoprecipitated with FLAG antibodies and analyzed by western blotting. **(B)** GST-STK3 and FLAG-tagged PKC ζ or NEK9 were expressed and purified from HEK293 cells and analyzed for kinase activity when incubated with myelin basic protein (MBP) and [γ -³²P]ATP. **(C)** GST-tagged LC3B or LC3B T50A were incubated with the indicated kinases in the presence of [γ -³²P]ATP. Of note, FLAG-NEK9 was purified from HEK293 cells while the other kinases were obtained from commercial vendors. Incorporation of radioactive labeled phosphate was detected by autoradiography (AR), and immobilized GST or GST-tagged proteins visualized by Coomassie Brilliant Blue staining (CBB). **(D)** Quantifications of STK4/NEK9 (n=2) and STK3/PKC ζ (n=5). Relative phosphorylation of LC3B WT/T50A normalized to the autophosphorylation of the kinase. **(E)** GST-tagged LC3B was incubated or not with PKC ζ in the presence of ATP and the product was resolved by SDS-PAGE. The GST-LC3B band was excised and analysed by LC-MS/MS. Shown are the MS spectra from LC-MS without PKC ζ (top) and with PKC ζ (bottom). Peptides are shown above the spectra. Note that this LC3B construct contained a mutation in residue H57 to R57.

Figure 2. STK3 interacts with LC3C and GABARAP via a C-type atypical LIR motif. **(A)** Myc-tagged STK3 kinase constructs were *in vitro* translated in the presence of [³⁵S]methionine, and analyzed in GST affinity isolation experiments for binding to the indicated ATG8s fused to GST. Bound proteins were detected by autoradiography, and immobilized GST or GST-tagged proteins visualized by Coomassie Brilliant Blue staining. **(B)** Quantification of STK3 binding shown in **(A)**, based on three independent experiments. **(C)** Myc-tagged STK4 kinase construct was *in vitro* translated in the presence of [³⁵S]methionine, and analyzed in GST affinity isolation experiments for binding to the indicated ATG8s fused to GST. **(D)** Schematic drawing of the domain organization of STK3 with the kinase domain, the LIR motif and the SARAH domain indicated. The extent of deletion mutants and the location of MVI/AAA LIR mutation are shown below the domain cartoon. **(E)** GST pulldown analyses of binding of the myc-tagged STK3 deletion constructs shown in **(D)** to GST-GABARAP. The deletion constructs were *in vitro* translated in the presence of [³⁵S]methionine. **(F and G)** GST pulldown

analyses of binding of myc-tagged STK3 WT and LIR mutant *in vitro* translated in the presence of [³⁵S]methionine to GST-LC3C (F) or myc-tagged STK3 WT *in vitro* translated in the presence of [³⁵S]methionine to GST-LC3C or GST-LC3C F58A (G). The F58A mutant inhibits binding to the LDS of LC3C. (H) HEK293 cells were transiently transfected with FLAG-tagged constructs of STK3 WT and LIR mutant (MVI/AAA) and whole cell lysates were incubated with recombinant GST or GST-ATG8s family proteins. The bound FLAG-tagged STK3 protein was detected by western blot using anti-FLAG antibodies and immobilized GST or GST-tagged proteins visualized by Ponceau S staining. AR, autoradiography; CBB, Coomassie Brilliant Blue.

Figure 3. PKC ζ binds to GABARAP and GABARAPL1 via a LIR motif overlapping with the AGC kinase docking motif. (A) Myc-tagged PKC ζ was *in vitro* translated in the presence of [³⁵S]methionine, and tested in GST affinity isolation experiments for binding to human ATG8 family proteins. Bound proteins were detected by autoradiography (AR), and immobilized GST or GST-tagged proteins by Coomassie Brilliant Blue staining (CBB). (B) HEK293 cells were transiently transfected with FLAG-tagged PKC ζ expression construct and whole cell lysate was incubated with recombinant GST or GST-ATG8 family proteins including the LDS mutants GABARAP Y49A and LC3B F52A/L53A. The bound FLAG-tagged PKC ζ protein was detected by western blot using anti-FLAG antibodies and immobilized GST or GST-tagged proteins visualized by Ponceau S staining. (C) Schematic diagram of the domain organization of PKC ζ with the N-terminal PB1 domain involved in heterodimerization, the pseudosubstrate sequence (PS), the zinc finger domain (ZnF), the kinase domain and the overlapping AGC kinase docking- and LIR motifs. (D) Identification of GABARAP-binding putative LIR motifs in PKC ζ . An array of 20-mer peptides covering full-length PKC ζ (each peptide shifted three amino acids relative to the previous) was mixed with GST-GABARAP (1 μ g/ml) and binding detected using anti-GST antibodies. The extension of the most strongly interacting peptides are indicated of which the overlapping peptides harboring the FEYI core LIR motif clearly bound most strongly. (E) Peptide array of FEYI where the core F (phenylalanine) and/or I (isoleucine) residues are mutated to alanine. Peptide array performed as in (D) but with the 20-mer harboring the FEYI motif with or without mutations. (F) GST pulldown assay performed as in (A) with Myc-tagged PKC ζ WT and LIR mutant F575A/I578A *in vitro* translated in the presence of [³⁵S]methionine, and tested in GST affinity isolation experiments for binding to human ATG8

family proteins. Bound proteins were detected by autoradiography (AR), and immobilized GST or GST-tagged proteins by Coomassie Brilliant Blue staining (CBB).

Figure 4. NEK9 interacts with ATG8s via a C-terminal LIR motif. **(A)** Schematic diagram of NEK9 domain structure comprising the N-terminal kinase domain, regulator of chromosome condensation 1(RCC1) repeats, a NEK6-binding region, a coiled coil domain (CC) and the C-terminal LIR motif. **(B)** Identification of a GABARAP-binding LIR motifs in the C terminus of NEK9. An array of 20-mer peptides, moved increments of 3 amino acids, covering the entire 979 amino acid long sequence of NEK9 was probed with GST-GABARAP (1 μ g/ml) and binding detected using anti-GST antibodies. The sequences of the overlapping peptides giving a positive signal are shown below the array with the core LIR motif WCLL indicated. **(C)** Myc-tagged NEK9 LIR mutant constructs were *in vitro* translated, labelled with [³⁵S]methionine and analyzed for binding to GST-GABARAP. **(D)** GST pulldown assays with *in vitro* translated and [³⁵S]methionine-labelled Myc-tagged NEK9 WT and LIR mutant W967A/L970A and GST-ATG8 proteins. Bound proteins were detected by autoradiography (AR), and immobilized GST or GST-tagged proteins by Coomassie Brilliant Blue staining (CBB). **(E)** GST pull down assay, where Myc-tagged NEK9 WT and NEK9 LIR mutant constructs were transiently transfected into HeLa cells. The whole cell lysates were incubated with recombinant GST or GST-ATG8s beads and bound NEK9 was detected by immunoblotting using anti-NEK9 antibody. The GST and GST-ATG8 proteins were visualized by Ponceau S staining. **(F)** Two dimensional peptide array to investigate effects of single amino acid substitution at all position of an 18-mer peptide from NEK9 (960-977) harboring the LIR motif. The array was probed with GST-GABARAP (1 μ g/ml) and binding detected using anti-GST antibodies.

Figure 5. NEK9 inhibits the selective autophagic degradation of p62 and NBR1. **(A and B)** Western blot analysis of p62 in HeLa cells with control siRNA and NEK9 smartpool siRNA. Actin was used as loading control. **(C)** Quantification of p62 levels following siRNA-mediated knockdown of NEK9 in full medium based on three biological replicates. **(D)** Western blots of cell extracts from HeLa WT and HeLa NEK9 KO cells with antibodies against NEK9, NBR1, p62 and LC3B with β -actin as loading control.

Figure 6. The phospho-mimicking T50E mutant of LC3B inhibits LIR-LDS interactions. **(A)** Structure of LC3B and p62 (PDB: 2ZJD) in which T50 is substituted by a glutamic acid (E). The p62-LIR peptide is shown with a black backbone. The core p62 LIR residues W338 and L341 (both purple) are shown docking into HP1 and HP2, respectively. The structure shows the side-chain of R10 (green) of LC3B interacting with D336 (yellow) of p62. T50E (red) is very close to R10. **(B)** Myc-tagged p62 R21A/D69A (monomeric mutant) was *in vitro* translated and tested for binding to LC3B fused to GST with or without mutations at T50 or the LDS of LC3B. Bound proteins were detected by autoradiography (AR), and immobilized GST or GST-tagged proteins by Coomassie Brilliant Blue staining (CBB). **(C)** Quantification of p62 binding shown in (B), based on three independent experiments. **(D)** HEK293 cells were transiently transfected with the indicated GFP-tagged LC3B constructs. Cell lysates were immunoprecipitated with GFP antibodies and endogenous p62 was analyzed by western blotting. **(E)** Recombinant GST or GST LC3B with or without mutation of T50 and LDS mutation were incubated with RIPA buffer cell lysate from HeLa cells. The bound endogenous NBR1 was detected by immunoblotting with NBR1 antibodies. **(F)** Quantification of NBR1 binding shown in (E), based on three independent experiments. **(G)** Recombinant GST or GST LC3B with or without mutation of T50 and LDS mutation were incubated with RIPA buffer cell lysate from HeLa cells and bound endogenous FYCO1 detected by immunoblotting. **(H)** Quantification of binding affinity of endogenous FYCO1 based on three independent replicates. **(I)** HEK293 cells were transiently transfected with myc-FYCO1 and FLAG-LC3B. Cell lysates were immunoprecipitated with anti-FLAG antibodies and analyzed by western blotting.

Figure 7. The T50E mutant of LC3B inhibits LIR-LDS interactions with ATG4B, ATG7 and syntaxin-17 (STX17). **(A)** Myc-tagged ATG4B was *in vitro* translated in the presence of [³⁵S]methionine and subjected to GST pulldown assays with recombinant GST-LC3B WT, T50A, T50E, and the LDS double mutant F52A/L53A. Bound proteins were detected by autoradiography (AR), and immobilized GST or GST-tagged proteins by Coomassie Brilliant Blue staining (CBB). **(B)** GST pulldown assays using RIPA buffer cell lysate from HeLa cells with recombinant GST-LC3B WT, T50A, T50E, and the LDS double mutant F52A/L53A. The bound endogenous ATG4B was detected by immunoblotting. **(C)** Quantification of binding affinity of endogenous ATG4B based on three biological replicates. **(D)** HeLa cell lysates were used in GST pulldown assays as in (B) except that ATG7 binding was analyzed by immunoblotting of the bound fraction. **(E)** Quantification of ATG7 binding affinity from three

independent experiments. **(F)** HeLa cells were transfected with EGFP-Syntaxin 17 (GFP-STX17) and cells were lysed with RIPA buffer. The cell lysate was incubated with recombinant GST or GST LC3B with or without the indicated mutations. Bound GFP-STX17 was detected by western blot with EGFP antibody. **(G)** Quantification of binding affinity of GFP-STX17 based on three biological replicates.

Figure 8. The phospho-mimicking T50E mutation inhibits autophagic flux of the selective autophagy receptors p62 and NBR1. **(A)** Western blot analysis of p62 and NBR1 levels in HEK293 WT and HEK293 LC3B KO cells. Actin was probed as a loading control. **(B)** Quantification of p62 and NBR1 levels in WT and LC3B KO cells from three biological replicates. **(C)** Western blots of Myc-LC3B in cell lysates from HEK293 LC3B KO cells reconstituted with Myc-LC3B -WT, -LC3B T50A, -LC3B T50E, and Myc-LC3B F52A/L53A and grown in full medium only, or in full media first and then incubated for 4 hours in Hanks balanced salt solution (HBSS), or for 4 hours in HBSS with Bafilomycin A1 (HBSS+BAF). The blot was developed using anti-Myc antibodies and PCNA was used as loading control. **(D)** Western blots of p62 and NBR1 in cell lysates from HEK293 WT and LC3B KO cells reconstituted with Myc-LC3B -WT, -LC3B T50A, -LC3B T50E, and Myc-LC3B F52A/L53A and grown in full medium. Actin was used as a loading control. **(E-H)** Under basal conditions (full medium) both formation and maturation of LC3B positive puncta (autophagosomes) are negatively affected by the T50E mutation. **(E)** Representative confocal fluorescence microscopy images of starving cells expressing the different mCherry-YFP-LC3B constructs used in (F-H). The indicated LC3B cell lines expressing mCherry-YFP-LC3B WT, -LC3B T50A, -LC3B T50E, and mCherry-YFP-LC3B F52A/L53A were induced with tetracycline (1 μ g/ml) for 24 hours and grown in full medium or buffered Hanks balanced salt solution for 2 hours after which the cells were fixed and analyzed by confocal microscopy. Individual cells were marked and LC3B-containing puncta were plotted as a function of cell volume for cells grown in full medium **(F)** or in Hanks balanced salt solution for the final 2 hours **(G)**. Total number of cells scored is indicated above the plots. Note only cells positive for LC3B puncta are included. Results represent three independent experiments **(H)** The ratio of red-only to yellow puncta from the experiment shown in (F and G) was analyzed for the different cell lines. Mean \pm SEM of 3 independent experiments, NS $P > 0.05$, * $P \leq 0.05$, ** $P \leq 0.01$, *** $P \leq 0.001$. One-way ANNOVA followed by the Tukey multiple comparison test.

Figure 1

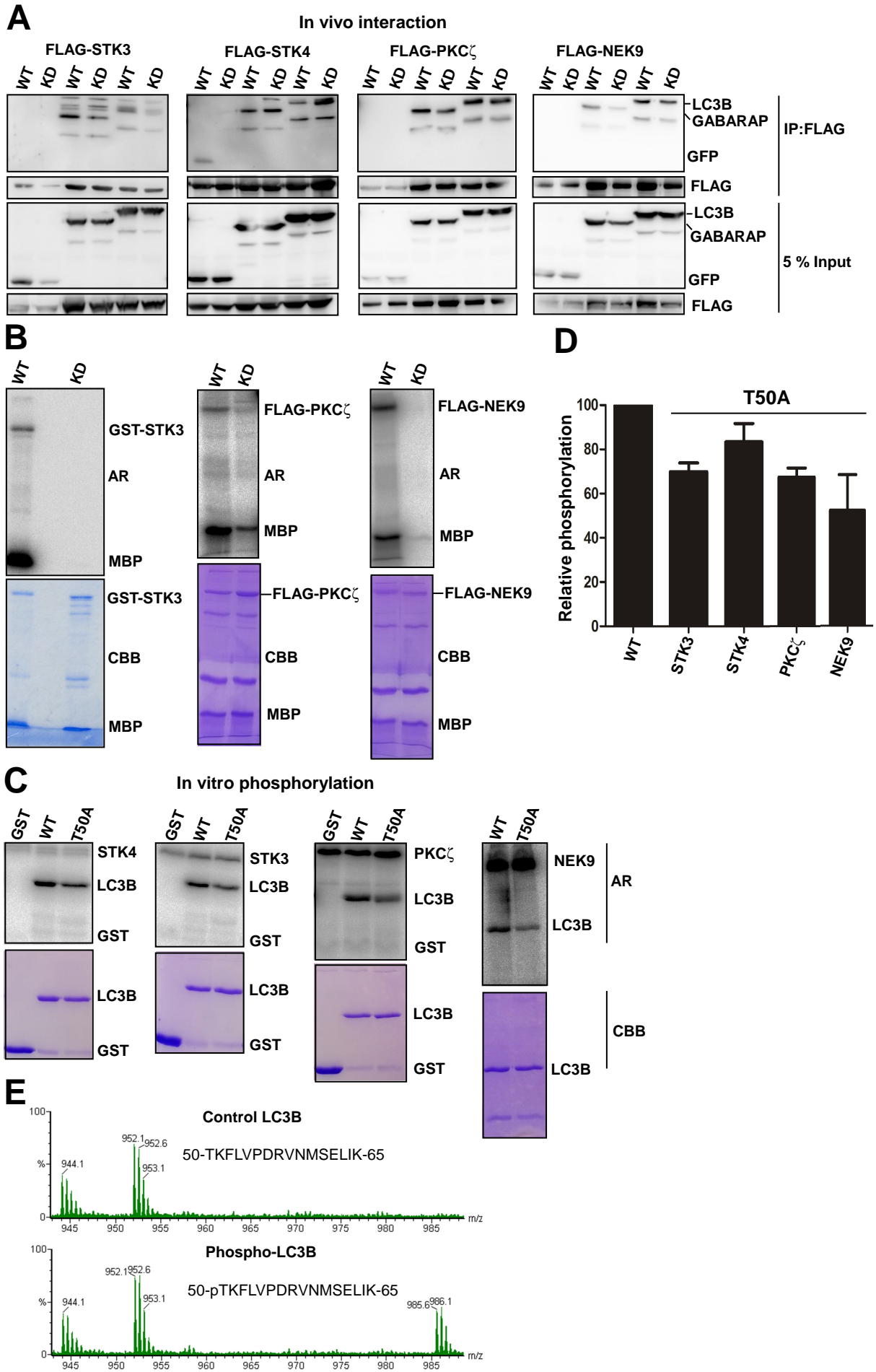


Figure 2

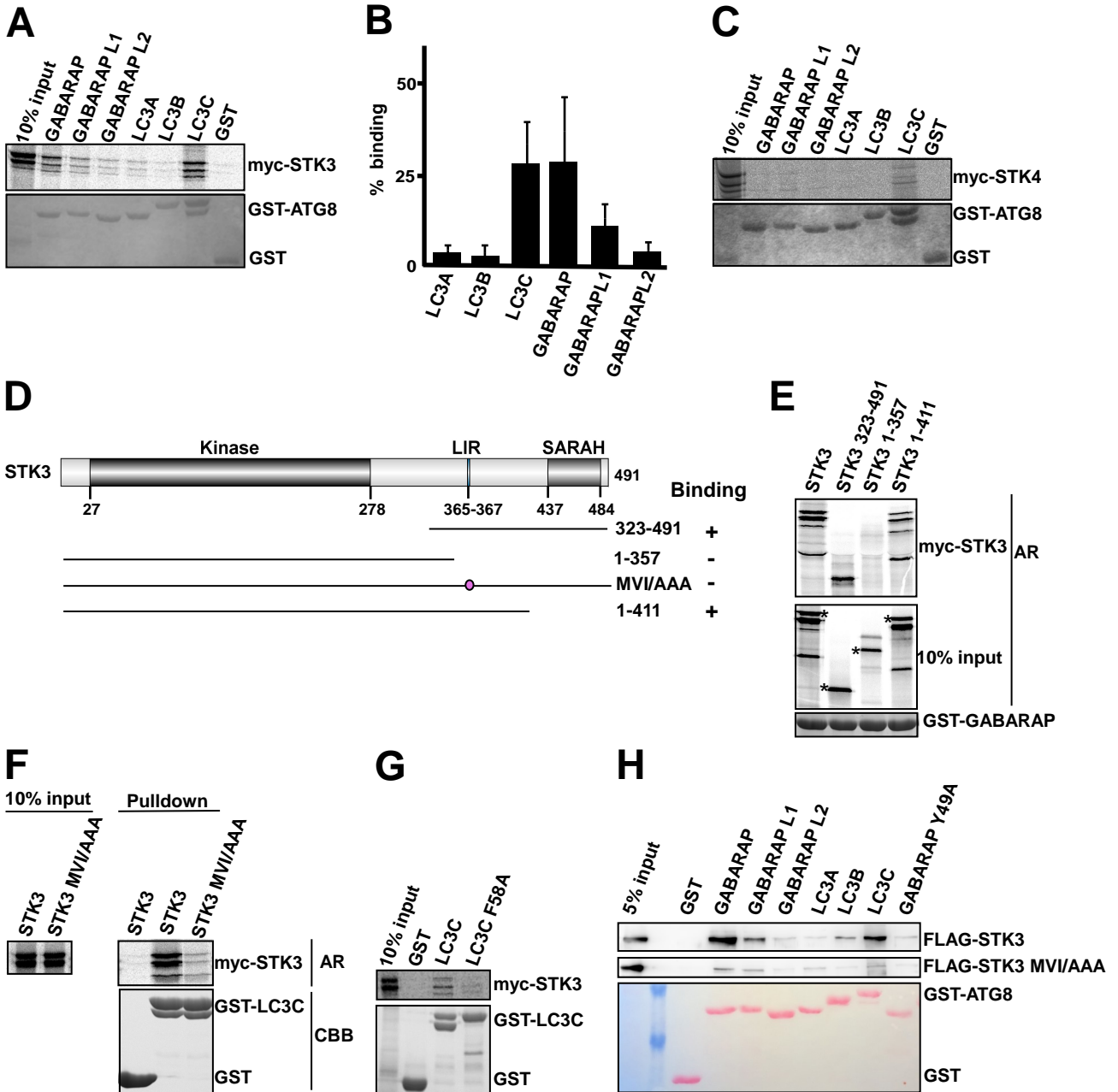
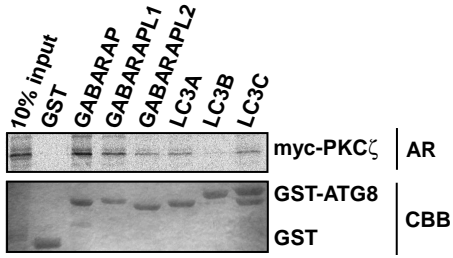
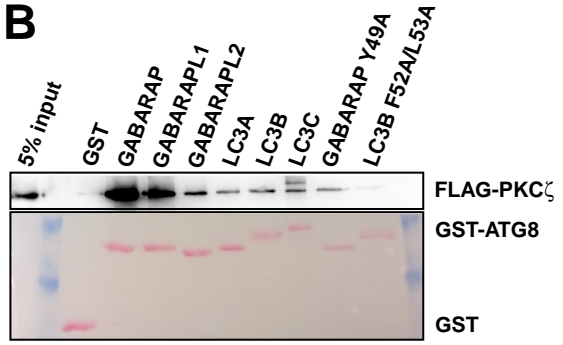


Figure 3

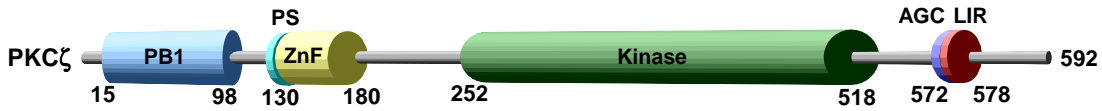
A



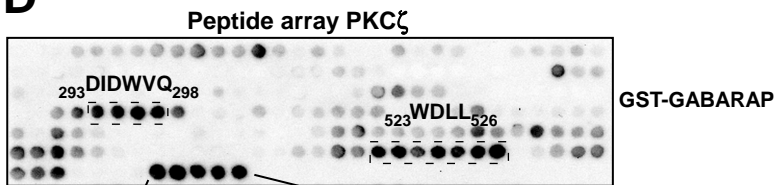
B



C

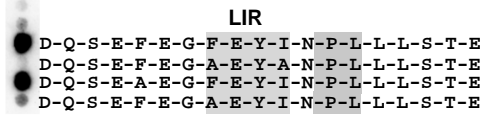


D



PKC ζ 562 D-D-E-D-A-I-K-R-I-D-Q-S-E-F-E-G-F-E-Y-I-N-P-L-L-L-S-T-E-E-S-V 592

E



F

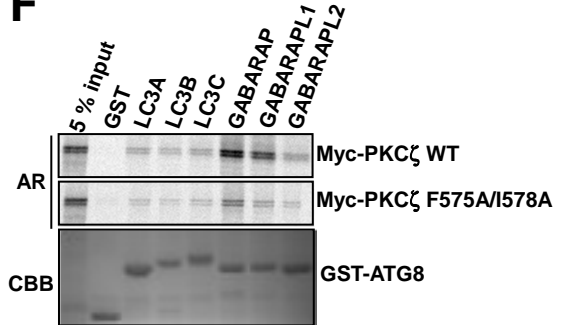


Figure 4

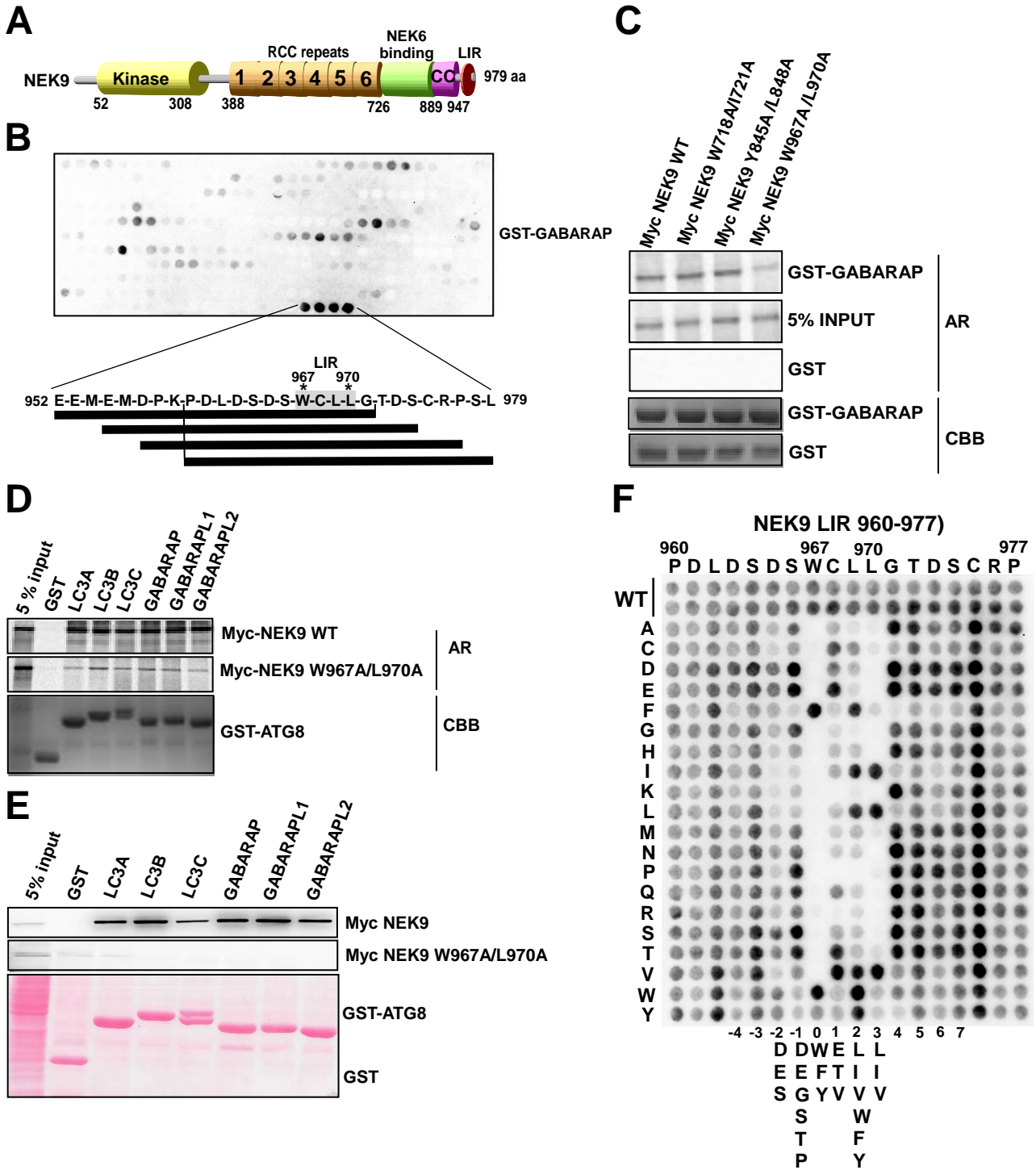


Figure 5

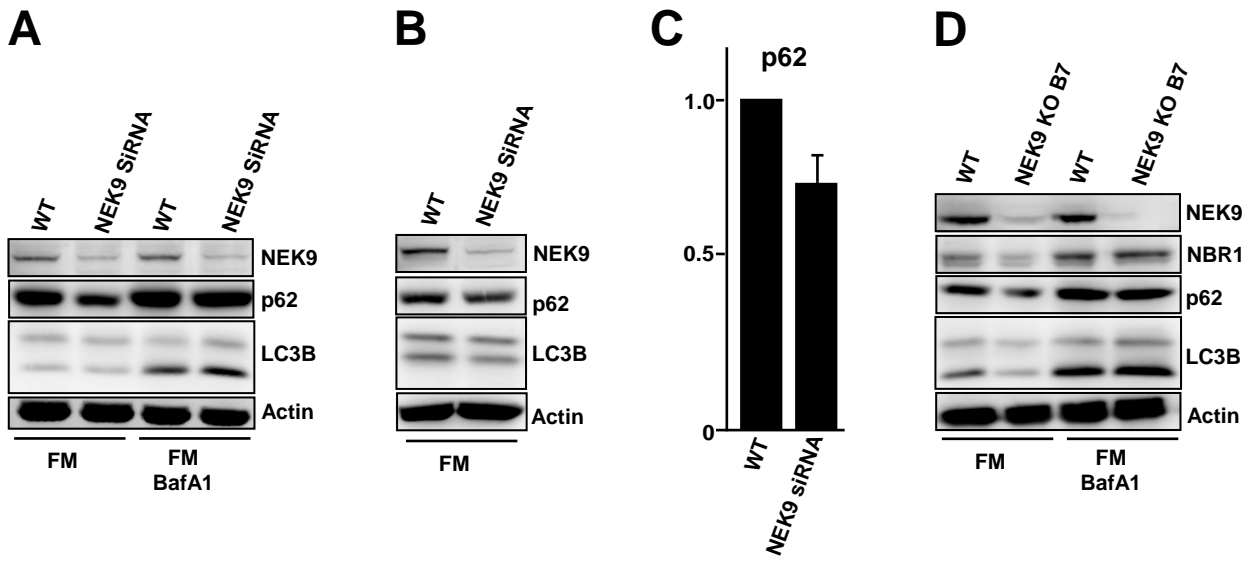
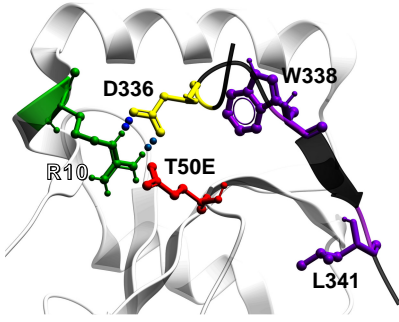
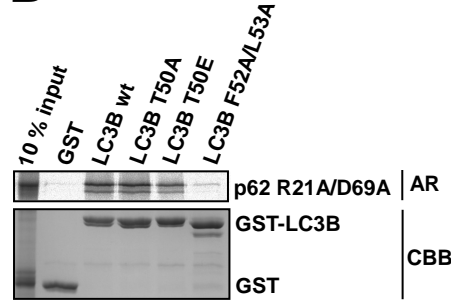


Figure 6

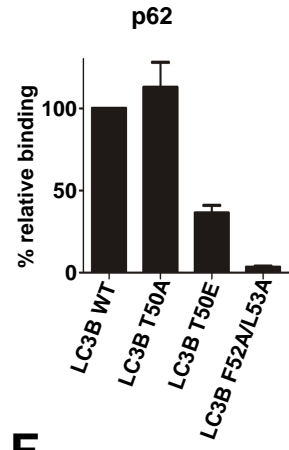
A



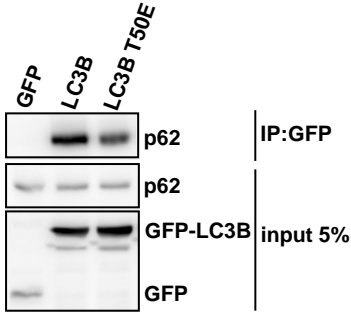
B



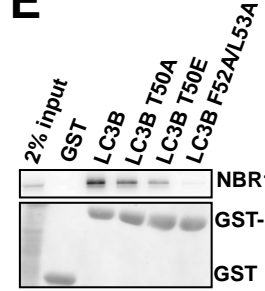
C



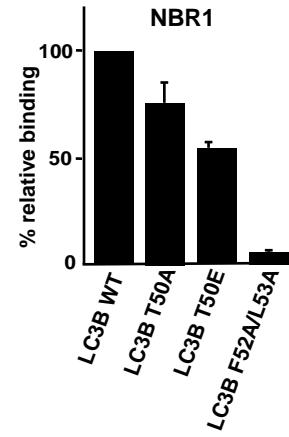
D



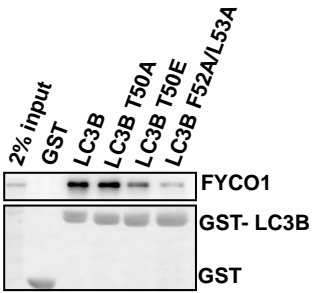
E



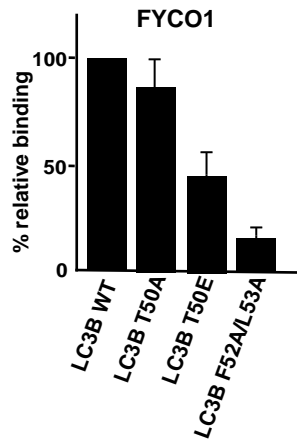
F



G



H



I

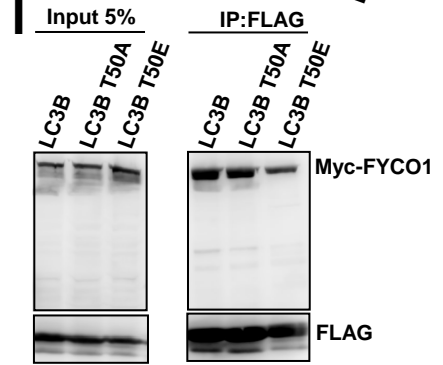
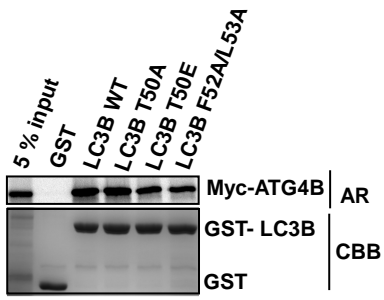
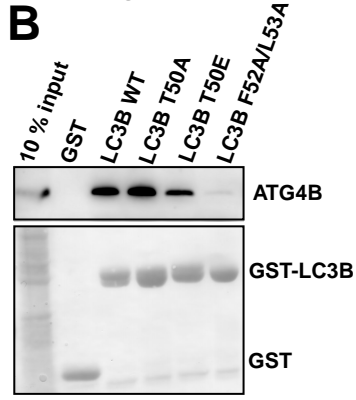


Figure 7

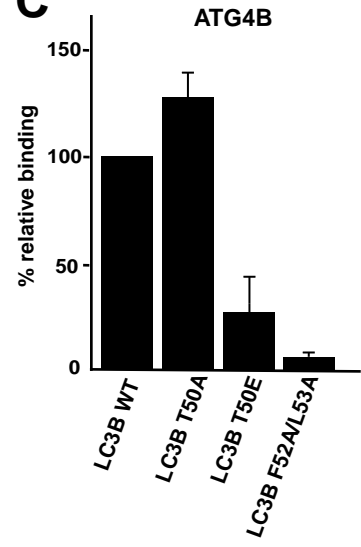
A



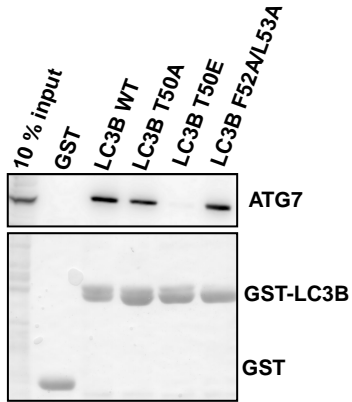
B



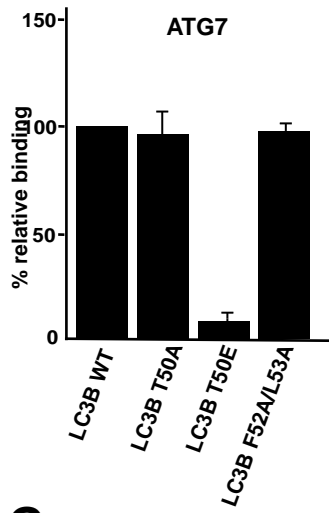
C



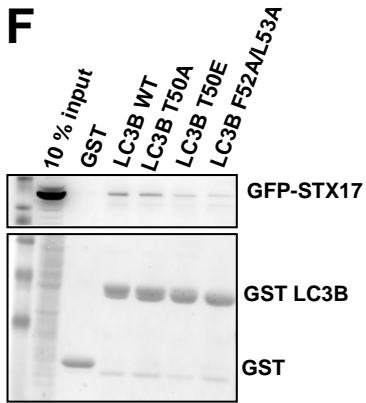
D



E



F



G

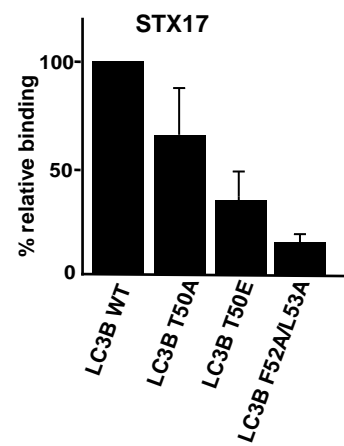
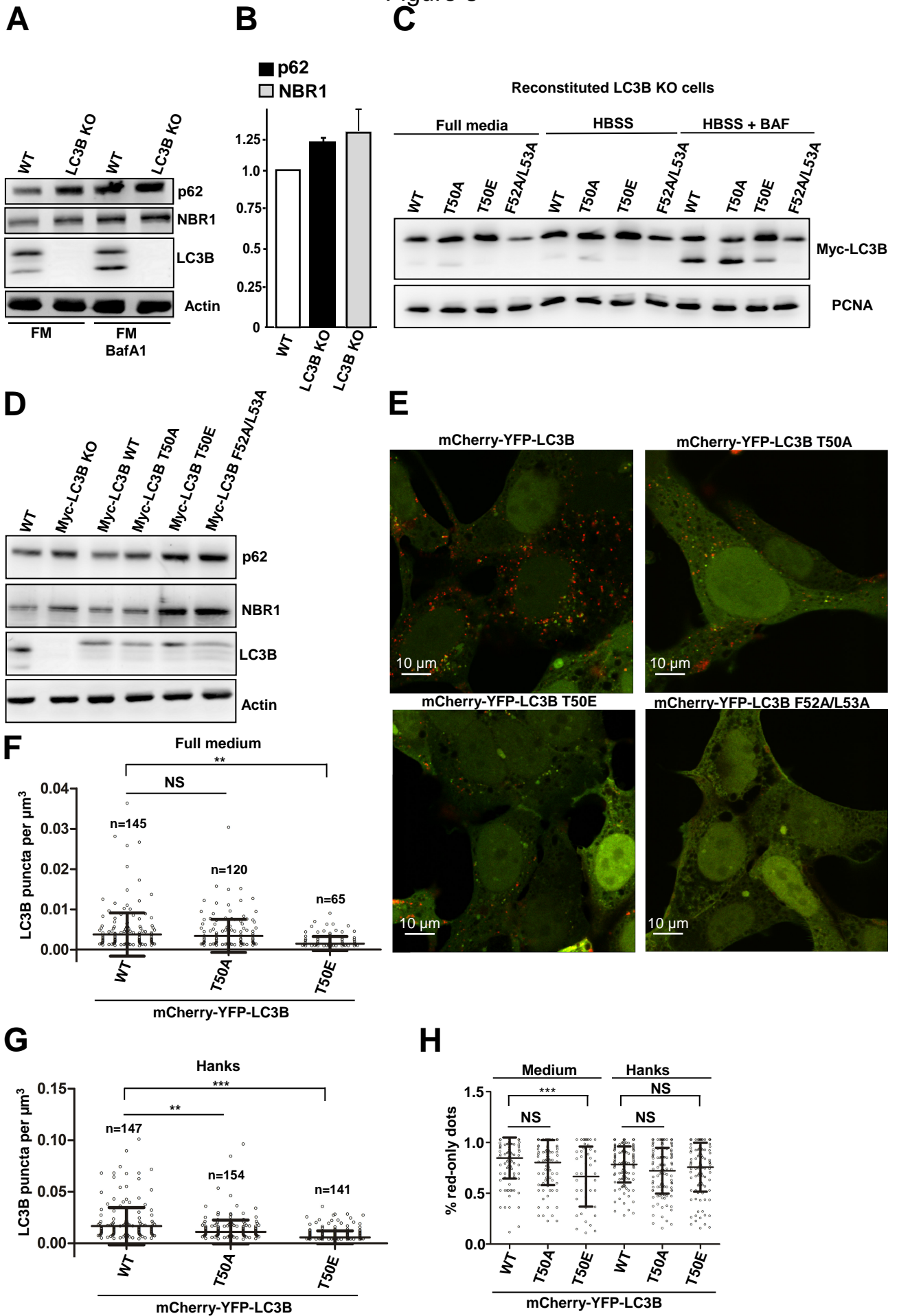


Figure 8



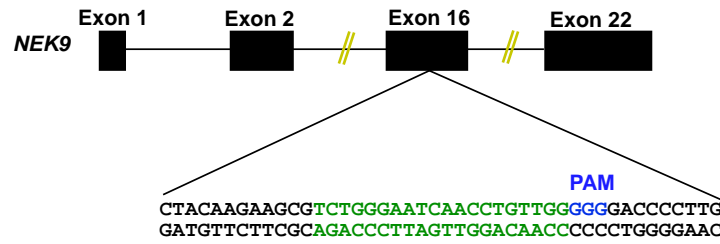
SUPPLEMENTARY FIGURE LEGENDS

Supplementary Figure S1. Generation of CRISPR/CAS9-mediated HEK293 FlpIn LC3B KO cells and HeLa NEK9 KO cells and GST pulldown analyses of NDP52 binding to T50 mutants of LC3C. **(A)** The genomic sequence from exon 16 of NEK9 targeted by gRNA. **(B)** Western blot of various clones from the KO experiments probed with antiNEK9 antibodies. Clone B7 was used for our studies. **(C)** The genomic sequence from exon 2 of *MAP1BLC3B* targeted by guide RNA. **(D)** Western blot analysis of various clones from the KO experiments. Clone 7 was used for our studies. **(E)** Whole cell lysates from HeLa cells were subjected to GST pulldown assays to analyze binding of endogenous NDP52 to recombinant GST or GST-LC3C with or without mutations. The bound endogenous NDP52 was detected by immunoblotting with anti-NDP52 antibodies and GST and GST-ATG8 proteins were visualized by coomassie blue staining. **(F)** Quantification of NDP52 binding affinity from three biological replicates.

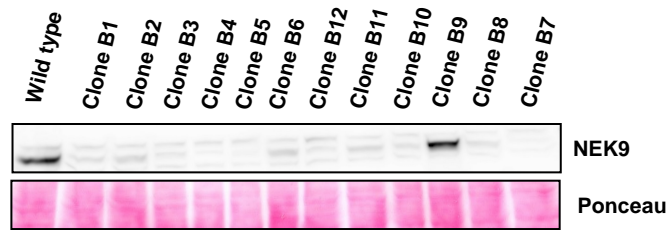
Supplementary Figure S1

A

CRISPR/CAS9 KO of *NEK9* in HeLa cells

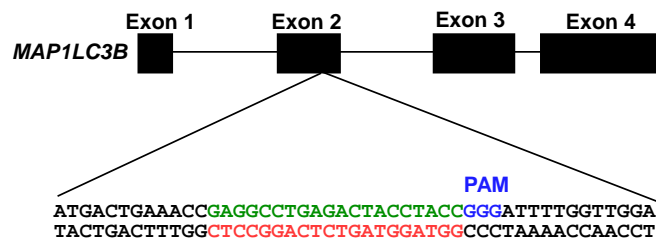


B

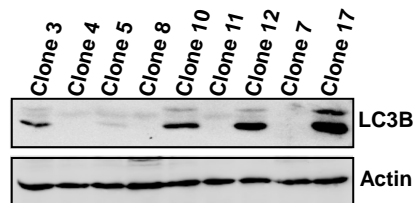


C

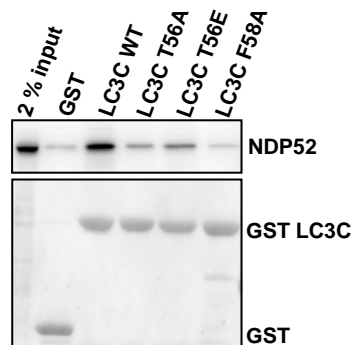
CRISPR/CAS9 KO of *MAP1LC3B* in HEK293 FlpIn cells



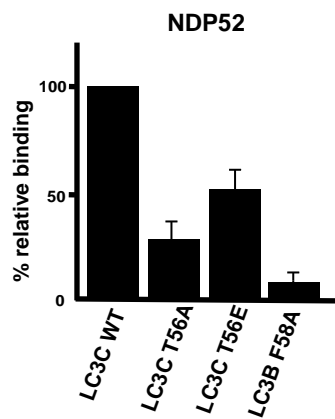
D



E



F



Subcellular localization of TP53INP2 is regulated by acetylation

Birendra Kumar Shrestha, Eva Sjøttem, Aud Øvervatn, Jack-Ansgar Bruun, Trond Lamark, and Terje Johansen

Molecular Cancer Research Group, Department of Medical Biology, University of Tromsø – The Arctic University of Norway, 9037 Tromsø, Norway

Corresponding author: terje.johansen@uit.no

Running title: Acetylation regulates TP53INP2 localization

Keywords: Acetylation, autophagy, DOR, LC3B, nuclear localization, TP53INP2

Abstract

TP53INP2/DOR (tumor protein p53 inducible nuclear protein 2)/ (diabetes and obesity-related) is a multifunctional protein acting as a coactivator of thyroid receptor-mediated transcription in the nucleus, as a facilitator of ribosome biogenesis in the nucleolus, and as an enhancer of starvation-induced autophagy. In this study, we uncover novel mechanisms for regulation of the subcellular localization and stability of TP53INP2. TP53INP2 is a nuclear protein under normal cellular conditions. Here, we identified a nuclear localization signal (NLS) and nucleolar localization signal (NoLS) in the C terminal part of TP53INP2. Upon mTOR inactivation such as starvation, TP53INP2 was stabilized and accumulated strongly in the cytoplasm. FRAP experiments revealed that this redistribution of TP53INP2 was due to cytoplasmic retention combined with an enhanced nuclear degradation rate. This result was supported by the lack of functional NES motifs in TP53INP2. Interestingly, the cytoplasmic retention of TP53INP2 during starvation was mediated by acetylation of lysine 187, impairing its interaction with importins. Furthermore, the rapid nuclear degradation of TP53INP2 was regulated by lysine's 165 and 204. Starvation-induced acetylation of these residues led to proteasomal degradation of TP53INP2. Hence, here we provide novel evidence that the subcellular localization of TP53INP2 is regulated by its three C-terminal lysine residues. mTOR inhibition mediated their acetylation leading to impaired nuclear import and proteasomal degradation in the nucleus, effectively switching TP53INP2 localization from nuclear to cytoplasmic.

Introduction

Lysine acetylation has been extensively studied in the context of transcription regulation. In the past decade, it has become clear that non-histone proteins are frequently acetylated regulating key cellular processes such as gene transcription, DNA damage repair, cell division, signal transduction, protein folding, autophagy, and metabolism. Acetylation may affect protein function through various mechanisms, including impact on protein stability, subcellular localization and by controlling protein-protein interactions¹. Several studies have reported that acetylation plays an important role in the regulation of autophagy. Acetyltransferase TIP60 acetylates and thereby stimulates the activity of ULK1, required for autophagy induction². Acetyltransferase CBP/p300 mediates acetylation of the autophagy proteins ATG5, ATG7, ATG8 and ATG12, and thereby inhibits autophagy activity³. The ATG8 family protein LC3B is reported to shuttle between the nucleus and the cytoplasm^{4,5}. Upon nutrient deprivation, nuclear LC3B becomes deacetylated at K49 and K52 by Sirt1. This is reported to allow LC3B to bind to nuclear TP53INP2/DOR (tumor protein p53 inducible nuclear protein 2)/(diabetes and obesity-related), which then mediates transport of LC3B out of the nucleus⁵. Cytoplasmic LC3B binds to ATG7, undergoes lipidation that converts soluble LC3B to the membrane-bound form and thereby recruits LC3B interacting proteins to the growing phagophore. Recently it was reported that cytoplasmic localized TP53INP2 is recruited to early autophagic membranes by LC3B, where it promotes the interaction between LC3B and ATG7 thereby facilitating autophagosome formation⁶.

TP53INP2 was originally identified as a nuclear protein highly expressed in tissues with high metabolism level. In addition to its role in autophagy, it acts as a transcription coactivator of thyroid hormone receptor and regulates thyroid hormone function⁷. In a transgenic mouse model, muscle-specific overexpression of TP53INP2 led to reduced muscle mass and deletion of it led to muscle hypertrophy⁸. TP53INP2 is also linked to adipose cell differentiation. It acts as a negative regulator of adipogenesis by promoting sequestration of GSK3 β in an ESCRT dependent pathway⁹. Nuclear TP53INP2 is enriched in the nucleolus, where it facilitates the formation of the RNA polymerase I preinitiation complex on rDNA promoters, and thereby promotes ribosome biogenesis when mTOR is active¹⁰. The complete redistribution of TP53INP2 from the nucleus to the cytoplasm upon mTOR inhibition has raised the question of whether TP53INP2 has dual roles in cell anabolism and catabolism determined by its subcellular localization.

In this study, we mapped the amino acid residues directing nuclear (NLS) and nucleolar (NoLS) localization of TP53INP2. Using CRISPR/Cas9, we established TP53INP2 knock out (KO) cells reconstituted with inducible expression of various EGFP-TP53INP2 constructs. To our surprise, we found that TP53INP2 is not exported out of the nucleus upon mTOR inhibition. In contrast, nuclear import of newly synthesized TP53INP2 is inhibited while the nuclear-localized TP53INP2 is degraded by the proteasome. Mass spectrometry analyses showed that three C-terminal lysine residues, K187, K165, and K204, were acetylated upon amino acid starvation. Acetylation of K187 impaired importin binding and nuclear import, while acetylation of K165 and K204 facilitated nuclear degradation. Autophagy flux was not affected by TP53INP2 KO, and TP53INP2 was not degraded by autophagy. However, over-expression of TP53INP2 in the cytoplasm leads to recruitment to LC3B dots and degradation by autophagy.

Materials and methods

Plasmids

The Gateway entry clones used in this study are listed in the table below. QuickChange site-directed mutagenesis kit (Stratagene) were used to create desired point mutation which was verified by DNA sequencing (BigDye sequencing kits, Applied Biosystems). For a generation of Gateway destination plasmid, Gateway LR and BP recombination kit from Invitrogen was used.

Gateway entry vectors

| Plasmid | Source |
|-----------------------------|------------|
| pENTR -TP53INP2 | Ref. 11 |
| pENTR -TP53INP2 W35A/I38A | Ref. 11 |
| pENTR -TP53INP2 K165R | This study |
| pENTR -TP53INP2 K187R | This study |
| pENTR -TP53INP2 K204R | This study |
| pENTR -TP53INP2 K165R/K204R | This study |

| | |
|------------------------------------|------------|
| pENTR -TP53INP2 K165R/K187R/K204R | This study |
| pENTR -TP53INP2 E97K/D98K | Ref. 11 |
| pENTR -TP53INP2 Δ24-40 | This study |
| pENTR -TP53INP2 Δ189-211 | This study |
| pENTR -TP53INP2 Δ201-204 | This study |
| pENTR -TP53INP2 Δ201-204 | This study |
| pENTR -TP53INP2 W35A/I38A/Δ189-211 | This study |
| pENTR -TP53INP2 1-143 | This study |
| pENTR -TP53INP2 1-165 | This study |
| pENTR -TP53INP2 1-189 | This study |
| pENTR -TP53INP2 1-211 | This study |
| pENTR -TP53INP2 143-211 | This study |
| pENTR -TP53INP2 143-165 | This study |
| pENTR -TP53INP2 165-189 | This study |
| pENTR -TP53INP2 189-211 | This study |
| pENTR -TP53INP2 Δ6-14 | This study |
| pENTR -TP53INP2 Δ43-65 | This study |
| pENTR -TP53INP2 Δ70-80 | This study |
| pENTR -TP53INP2 Δ93-114 | This study |
| pENTR -TP53INP2 Δ121-141 | This study |
| pENTR -TP53INP2 S185A | This study |
| pENTR -TP53INP2 S198A | This study |
| pENTR -TP53INP2 S207A/S208A | This study |

| | |
|-----------------------|------------|
| pENTR -TP53INP2 S203A | This study |
|-----------------------|------------|

Gateway expression plasmids

| Plasmid | Source |
|--|------------|
| pDest EGFP-Flp-In-TP53INP2 | This study |
| pDest EGFP-Flp-In-TP53INP2 W35A/I38A | This study |
| pDest EGFP-Flp-In-TP53INP2 K165R | This study |
| pDest EGFP-Flp-In-TP53INP2 K187R | This study |
| pDest EGFP-Flp-In-TP53INP2 K204R | This study |
| pDest EGFP-Flp-In-TP53INP2 K165R/K204R | This study |
| pDest EGFP-Flp-In-TP53INP2 K165R/K187R/K204R | This study |
| pDest EGFP-Flp-In-TP53INP2 E97K/D98K | This study |
| pDest EGFP-Flp-In-TP53INP2 Δ 24-40 | This study |
| pDest EGFP-Flp-In-TP53INP2 Δ 189-211 | This study |
| pDest EGFP-Flp-In-TP53INP2 Δ 201-204 | This study |
| pDest EGFP-Flp-In-TP53INP2 Δ 201-204 | This study |
| pDest EGFP-Flp-In-TP53INP2 W35A/I38A/ Δ 189- 211 | This study |
| pDest EGFP -TP53INP2 1-143 | This study |
| pDest EGFP -TP53INP2 1-165 | This study |
| pDest EGFP -TP53INP2 1-189 | This study |
| pDest EGFP -TP53INP2 1-211 | This study |
| pDest EGFP -TP53INP2 143-211 | This study |

| | |
|--|------------|
| pDest EGFP -TP53INP2 143-165 | This study |
| pDest EGFP -TP53INP2 165-189 | This study |
| pDest EGFP -TP53INP2 189-211 | This study |
| pDest EGFP-Flp-In-TP53INP2 Δ6-14 | This study |
| pDest EGFP-Flp-In-TP53INP2 Δ43-65 | This study |
| pDest EGFP-Flp-In-TP53INP2 Δ70-80 | This study |
| pDest EGFP-Flp-In-TP53INP2 Δ93-114 | This study |
| pDest EGFP-Flp-In-TP53INP2 Δ121-141 | This study |
| pDest EGFP-Flp-In-TP53INP2 S185A | This study |
| pDest EGFP-Flp-In-TP53INP2 S198A | This study |
| pDest EGFP-Flp-In-TP53INP2 S207A/S208A | This study |
| pDest EGFP-Flp-In-TP53INP2 S203A | This study |

Additional plasmids

| Plasmid | Source |
|----------------------------|------------|
| Rev 1.4 EGFP | Ref. 12 |
| Rev 1.4 NES EGFP | Ref. 12 |
| Rev 1.4 TP53INP2 NES1 EGFP | This study |
| Rev 1.4 TP53INP2 NES1 EGFP | This study |

Cell culture

HeLa Flp-In T-Rex cells (Invitrogen, R714-07) were cultured in Eagle's minimum essential medium with 10% serum (Biochrom, S0615) and 1% streptomycin-penicillin (Sigma-Aldrich, P4333). All HeLa FlpIn cell lines with EGFP-TP53INP2 integrated at FRT site were maintained

in the same medium with additional selection antibiotics 100 µg/ml hygromycin (Calbiochem, 400051) and 7.5 µg/ml blasticidin S (Invitrogen, R210-01).

Generation of stable cell lines

HeLa FlpIn T-Rex cells were used to make stable TP53INP2 cell lines. The N-terminal EGFP-tagged TP53INP2 cDNAs were cloned into pcDNA 3.1 FRT/TO plasmid. The generation of stable cell lines was performed in accordance with the manufacturer's instructions (Invitrogen, V6520-20). Briefly, 48 hours after transfection of different mutants of TP53INP2 cloned into pcDNA 3.1 FRT/TO plasmids, colonies of cells with the gene of interest integrated into FRT site were selected with 200 ng/ml of hygromycin (Calbiochem, 400051). Gene expression was induced with 1µg/ml of tetracycline for 24 hours.

MEF ATG5 KO and WT cells were kindly provided by N. Mizushima¹³. Stable MEF cell lines expressing EGFP-TP53INP2 cell line were made by retroviral transfer. First, Platinum Retroviral Packaging Cell Line-E (Cell Biolabs, RV-101) was transfected with a pMXs retroviral plasmid containing EGFP-TP53INP2 cDNA. After 24 hours of transfection, viral supernatant was harvested, filtered through a 0.45 µM filter and mixed with 8 µg/ml of Polybrene (Sigma-Aldrich, H9268) before being added to cells. The viral transduction procedure was repeated again for the next 48 and 72 hours posts transfection. After the last viral transduction, MEF cells were selected with 5 µg/ml of blasticidin S HCL (Thermo Fisher Scientific R2210-01).

CRISPR/Cas9

To construct the specific TP53INP1/TP53INP2 guide RNAs the CRISPR/Cas9 plasmid, sense- and antisense oligonucleotides encoding the selection guide sequence were annealed and then inserted into plasmid pSpCas9(BB)-2A-Puro (PX459). For a generation of CRISPR/Cas9 KO cells, approximately 30,000 of HeLa Flp-In T-Rex cells were seeded into 24 well plates and then 500 ng of plasmid PX459 per well were transfected using Metafectene Pro (Biontex, T040). The clonal selection was achieved by 500 ng/ml puromycin treatment, 24 hours after transfection for 48-72 hours. Later, single cells were sorted into 96 well plates via FACS

sorting. The clones were allowed to grow for 7-10 days and each clone was screened for KO by DNA sequencing of PCR products amplified from the targeted region in the genome.

Fluorescence Recovery After Photobleaching (FRAP)

HeLa Flp-In cells expressing EGFP-TP53INP2 WT or various mutants were grown on Lab-Tek chambered cover glass (Thermo Scientific, Cat.no. 155411,) and imaged at 37° C and 5% CO₂ on an LSM780 confocal microscope (Carl Zeiss Microscopy) equipped with a 40X 1.2NA water immersion lens. FRAP analysis was performed by drawing regions of interest (ROIs) around the nucleus and photobleaching the GFP signal inside the ROI to 100% of its initial value using 5 iterations of unattenuated 488 nm laser light. Fluorescence recovery was then monitored. An ROI placed inside a neighboring cell was monitored to control for photobleaching during image acquisition.

Antibodies and reagents

The following antibodies were used: Rabbit anti-LC3B (Novus, NB100-2220) mouse anti-GABARAP (MBL, M135-3), mouse anti-p62 (BD Bioscience, 610833), rabbit anti-NDP52 (Sigma, HPA023195), mouse anti-NBR1 (Santa Cruz Biotechnology, sc-130380), rabbit anti-GFP (Abcam, AB290), rabbit anti-ACTIN (Sigma-Aldrich, A2066), mouse anti-GABARAP(MBL, M135-3), horseradish peroxidase-conjugated goat anti-mouse- (BD Biosciences, 554002) and anti-rabbit (BD Biosciences, 554021) secondary antibodies. For confocal imaging following antibodies were used: rabbit anti LC3B (Sigma, L7543), guinea pig anti p62 (Progen, GP62-C), rabbit anti-Fibrillarin (Santa Cruz Biotechnology, sc-25397), Alexa Fluor® 555-conjugated goat anti-rabbit IgG (Life Technologies, A-21428), Alexa Fluor® 647-conjugated goat anti-guinea pig IgG (Life Technologies, A-21450), DAPI (Thermo Scientific, Cat.no. 62248,).

Chemicals

Bafilomycin A1 (Sigma, B1793), MG132 (Sigma, C2211), Cycloheximide (Sigma, C7698), C646 (Sigma, C646), Torin 1 (Santa Cruz Biotechnology, sc-396760), Trichostatin A (Sigma,

T9033), Nicotinamide (Sigma, N3376), (Leptomycin B (Sigma, L2913), [³⁵S]-methionine (PerkinElmer, NEG709A500UC).

Real-Time PCR

The total RNA was isolated using GenElute Mammalian Total RNA Miniprep Kit (Sigma, RTN70) and reverse transcribed using Transcriptor Universal cDNA master mix (Roche, Cat.no. 05893151001). The Realtime-PCR was performed using FastStart Universal SYBR Green Master Mix (Roche, Cat.no. 04913850001) on a LightCycler® 96 Real-Time PCR system (Roche). The primers used were as follows: 47S rRNA: forward primer TGTCAGGCGTTCTCGTCTC, reverse primer GAGAGCACGACGTCACCAC and Actin: forward primer TGACGGTCAGGTCATCACTATCGGCAATGA, Reverse primer TTGATCTTCATGGTGATAGGAGCGAGGGCA.

Cell proliferation assay

HeLa FlpIn TP53INP2 KO cells and HeLa FlpIn T-Rex control cells were seeded with four different concentrations (2000, 4000, 5000 and 6000 cells), two parallels of each concentration, in 100 µl DMEM (Sigma, D6046) on E-Plate L16 PET readers (ACEA Biosciences Inc, #2801185). xCELLigence® Real-Time Cell Analysis (RTCA) (ACEA Biosciences) were used to measure the cell proliferation over a time of 96 hours with recording at 1hr intervals.

Protein purification and GST affinity isolation experiments

GST-tagged proteins were expressed in *Escherichia coli* BL21 (DE3). GST fusion proteins were purified on glutathione-Sepharose 4 Fast Flow beads (GE Healthcare, 17513201) followed by washing with NET-N buffer (100 mM NaCl, 1 mM EDTA, 0.5% Nonidet P-40 (Sigma-Aldrich, 74385), 50 mM Tris-HCl, pH 8) supplemented with cOmplete Mini EDTA-free protease inhibitor mixture tablets (Roche Applied Science, 11836170001). GST-tagged proteins were eluted with 50 mM Tris-HCl pH 8, 200 mM NaCl, 5 mM reduced L-glutathione (Sigma-Aldrich, G425). GST affinity isolation assays were performed with ³⁵S-labeled proteins co-transcribed and translated using the TNT Coupled Reticulocyte Lysate System (Promega, L4610) as described previously¹⁴. For quantifications, gels were vacuum dried and ³⁵S-labeled proteins detected on a Fujifilm bioimaging analyzer BAS-5000 (Fujifilm, Tokyo, Japan).

Acetylation modification and mass Spectrometry

The total level of TP53INP2 acetylation under starvation and nutrient-rich condition was detected by Signal Seeker Acetyl-Lysine Detection Kits (Cat. # BK163, Cytoskeleton, Inc). The cells were harvested, and immunoprecipitations performed using manufacturer protocols. For mass spectrometry, cells were lysed with lysis buffer containing 20 mM Tris-HCl, pH 7.4, 1% NP-40, 137 mM NaCl, 1 mM MgCl₂, 1 mM CaCl₂, 10% Glycerol, 1 μM Trichostatin A (TSA), 5 mM nicotinamide (NAM) and cOmplete Mini EDTA-free protease inhibitor mixture tablets. The inhibitors were added just before the lysis of cells. The μMACS GFP isolation kits (Miltenyi Biotec) was used for immunoprecipitation of EGFP-TP53INP2 from cell lysate. The gel band containing EGFP-TP53INP2 was precisely cut and subjected to in-gel reduction, alkylation, and endopeptidase digestion using 4 ng/μl of Arg-C, sequencing grade (cat. no 11370 529001, Roche) protease. OMIX C18 tips (Varian) were used for sample cleanup and concentration. Peptide mixtures containing 0.1% formic acid were loaded onto a Thermo Fisher Scientific EASY-nLC1200 system. Samples were injected to a trap column (Acclaim PepMap 75 μm × 2 cm, C18, 3 μm, 100 Å; ThermoFisher) for desalting before elution to the separation column (EASY-Spray column, C18, 2 μm, 100 Å, 50 μm, 50 cm; ThermoFisher). Peptides were fractionated using a 4–40 % gradient of increasing amounts of 80% acetonitrile in water over 60 min at a flow rate of 300 ml/min. The mobile phases contained 0.1% formic acid. Separated peptides were analyzed using an Orbitrap Fusion Lumos mass spectrometer. The mass spectrometer was operated in a data-dependent mode with the precursor scan in the orbitrap over the range m/z 350–1500. The most intense ions were selected for ETD or CID fragmentation using 3 sec between each master scan. Dynamic exclusion was set to 30s. The Orbitrap AGC target was set to 4E5 and the MS2 scans in the Ion Trap were set to 1E4 with maximum injection times 50 and 100 ms, respectively. Precursor ions with charge 3+ in the m/z range 350-650 and 4+ or 5+ ions in the m/z range 350-900 was fragmented with ETD. All ions with 6+ or higher were also fragmented using ETD. The rest of the precursor ions were fragmented using CID. Protein identification and PTM mapping were done using the Proteome Discoverer 2.2 software (ThermoFisher).

Western blot and immunoprecipitation experiments

For western blotting experiments, cells were washed in PBS (137 mM NaCl, 2.7 mM KCl, 4.3 mM Na₂HPO₄, 1.47 mM KH₂PO₄, pH 7.4.) followed by lysis directly in SDS-PAGE loading

buffer (2% SDS, 10% glycerol 50 mM Tris-HCl, pH 6.8) and boiled for 10 min. Protein concentration was measured followed by addition of bromophenol blue (0.1%) and DTT (100 mM). Samples (20 µg) were run on 10-16% gradient- or 10%- SDS-polyacrylamide gels and blotted on Hybond nitrocellulose membranes (GE Healthcare, 10600003) followed by Ponceau S staining. Blocking was performed in 5% nonfat dry milk in PBS-Tween 20 (0.1%). Primary antibody was diluted in PBS-Tween 20 containing 5% nonfat dry milk and incubation was performed overnight at 4°C. Secondary antibody incubation was performed at room temperature for 1 h in PBS-Tween 20 containing 5% nonfat dry milk. Membranes were washed 3 times prior to the addition of secondary antibody and development using LAS-300 (Fujifilm, Tokyo, Japan).

Bioinformatics and statistics

The prediction of nucleolar localization signal (NoLS) and Nuclear export signal was performed using online servers: <http://www.compbio.dundee.ac.uk/www-nod/> and (<http://www.cbs.dtu.dk/services/NetNES/>), respectively. Secondary structure predictions were performed using the PSIPRED server: <http://bioinf.cs.ucl.ac.uk/>. Helical wheel projections were made using HeliQuest: <http://heliquest.ipmc.cnrs.fr/>. Data in all figures are from experiments performed at least twice unless otherwise stated.

Results

The autophagic flux is unaffected by CRISPR/CAS9-mediated knock-out of TP53INP2 in HeLa cells

The multifaceted roles of TP53INP2, acting as a transcriptional coactivator in the cell nucleus, as a promoter of rRNA transcription in the nucleolus, and as a regulator of autophagy in the cytoplasm, seem to be regulated by subcellular localization^{10,15}. In order to reveal the molecular mechanisms regulating TP53INP2 localization and autophagic activity, we first established CRISPR/Cas9 mediated HeLa FlpIn knock-out (KO) cells of TP53INP2 and its homologue TP53INP1. KO of the genes was verified by genomic DNA sequencing since their expression levels in the HeLa FlpIn cells were too low to be detected by commercial antibodies (**Fig. S1A and B**). To measure the autophagic flux in the KO cells, the level of the autophagy receptors

p62, NBR1 and NDP52, and the lipidation of LC3B and GABARAP, under normal and starved conditions, were analyzed by Western blotting (**Fig. S2A and B**). Surprisingly, no differences were observed in the KO cell lines compared to wild type (WT) cells. This suggests that TP53INP2, and its homologue TP53INP1, does not have a detectable impact on the regulation of autophagy flux during normal and starved conditions in the HeLa cells applied in this study. However, we cannot rule out that they are redundant in function, and that knocking out both TP53INP1 and TP53INP2 might have affected the autophagy pathway. Recently, TP53INP2 was shown to have a role in ribosomal biogenesis and cell proliferation¹⁰. In order to, confirm that the TP53INP2 KO cells have a similar phenotype, the cell proliferation of the KO cells was analyzed and compared to wild type cells (**Fig. S2C**). In line with previous reports, we observed that the TP53INP2 KO cells have a slower proliferation rate than the wild type cells and a decreased transcription of 47S rRNA (**Fig. S2D**).

TP53INP2 is degraded by the proteasome in the nucleus and accumulates in the cytoplasm upon inhibition of mTOR

Previous studies have shown that TP53INP2 redistributes to the cytoplasm upon mTOR inhibition. To determine which factors or modifications of TP53INP2 that mediates this redistribution, we reconstituted the HeLa FlpIn TRex TP53INP2 KO cells with EGFP-TP53INP2. The expression of EGFP-TP53INP2 was induced by tetracycline treatment and kept at a low level to obtain a situation as close to endogenous as possible. Confocal fluorescence microscopy analysis of the reconstituted cells under normal conditions and upon mTOR inhibition by starvation or Torin 1 treatment, revealed that redistribution of EGFP-TP53INP2 from the nucleus to the cytoplasm is regulated by mTOR activity (**Fig. 1A and Fig. S2E**). Surprisingly, EGFP-TP53INP2 retained diffusible cytoplasmic staining and did not form any puncta structures in the cytoplasm during starvation. The autophagy receptor p62 and the autophagosome marker protein LC3B formed punctate structures that increased upon starvation and treatment with the lysosomal inhibitor Bafilomycin A1 (BafA1), indicating that the autophagy process acts as normal in the cell line. In contrast, when we over-expressed EGFP-TP53INP2 in the KO cells by transient transfection, EGFP-TP53INP2 formed punctate structures in the cytoplasm upon starvation (**Fig. S3**). This suggests that overexpression of TP53INP2 may impair its normal subcellular localization pattern. To determine whether EGFP-TP53INP2 is an autophagic substrate, the level of EGFP-TP53INP2 upon starvation and BafA1

treatment was measured by Western blotting. To our surprise, the expression level of EGFP-TP53INP2 was strongly increased upon starvation and unaffected by BafA1 treatment (**Fig. 1B**). In contrast, inhibition of the proteasomal degradation pathway by MG132 treatment led to increased expression of EGFP-TP53INP2 (**Fig. 1B**). Furthermore, confocal microscopy imaging showed accumulation of EGFP-TP53INP2 in the nucleolus (**Fig. 1C**). Proteins are degraded by ubiquitin-dependent and -independent pathways. To test this, we mutated all three lysines (K) residues in TP53INP2 to arginines (R) and reconstituted KO cells with the K3R triple mutant. Interestingly, also the K3R mutant displayed increased accumulation of TP53INP2 in the nucleoli upon MG132 treatment indicating ubiquitin-independent degradation (**Fig. 1D and E**). Similar to our result, PICT1, a nucleolar ribosomal protein is also degraded inside the nucleolus in a ubiquitin-independent manner¹⁶. Altogether, these results show that mTOR inhibition leads to cytoplasmic accumulation of EGFP-TP53INP2 and that the nuclear pool of TP53INP2 is degraded by the proteasome.

Partial overlapping NLS and NoLS signals are located in the C-terminal region of TP53INP2

To facilitate the nuclear pore complex (NPC) mediated import of a protein requires a nuclear localization signal (NLS) that interacts with importin proteins. The first described NLS motif was identified in SV40 T antigen (PKKKRKV)¹⁷. To map the NLS directing nuclear import of TP53INP2 we made several deletions constructs of TP53INP2 fused to EGFP (**Fig. 2A**). These expression constructs were transfected into HeLa cells and the subcellular localization of the various constructs was analyzed by confocal fluorescence microscopy (**Fig. 2B**). The N-terminal part of TP53INP2 (amino acids 1-143, 1-165 and 1-189) displayed a localization pattern similar to EGFP alone (**Fig. 2B**). However, extending the expression construct to include the region 189-211 resulted in a dominant nuclear localization. This suggested the presence of an NLS motif within the region 189-211. The localization of an NLS in this region was further validated by deleting this region from full-length TP53INP2. This led to reduced nuclear localization compared to the WT protein (**Fig. 2B**). Moreover, fusing the 189-211 region to EGFP resulted in complete nuclear localization of EGFP (**Fig. 2B**). Together with bioinformatics tools and a recent publication that predicted an NLS within the 144-221 region of TP53INP2⁶, our results clearly have identified the 189-211 region of TP53INP2 to direct nuclear localization.

A recent report showed that endogenous TP53INP2 is enriched in the nucleoli where it plays a role in ribosome biogenesis¹⁰, and that the 191-211 region constitutes a nucleolar localization signal (NoLS)¹⁰. In line with this, we observed nucleolar enrichment of EGFP-TP53INP2 both upon transient transfection and in the EGFP-TP53INP2 reconstituted KO cell line (**Fig. 1A, C and Fig. 2B**). The consensus sequence based on several proteins with NoLS is designated as R/K-R/K-X-R/K¹⁸. Sequence analysis predicted a putative NoLS sequence in the 201-204 region, partially overlapping the NLS. Deletion of the 201-204 region from full-length TP53INP2 prevented localization of TP53INP2 in the nucleolus (**Fig. 2B**) and clearly identified the NoLS of TP53INP2. Together with our results and previously published data identify partial overlapping NLS and NoLS signals in the C-terminal region of TP53INP2.

Deletion of the TP53INP2 NLS motif leads to protein accumulation and partial autophagic degradation

Exogenously over-expressed TP53INP2 forms punctate structures in the cytoplasm co-localized with ATG8s upon induction of autophagy by starvation¹⁵(**Fig. S3**) . However, confocal fluorescence microscopy analysis of our TP53INP2 KO cell line reconstituted with EGFP-TP53INP2 expressed at a low level, did not display any puncta formation in the cytoplasm during starvation (**Fig. 1A**). Moreover, treatment of the cell line with the lysosomal inhibitor BafA1 did not stabilize EGFP-TP53INP2, while the proteasomal inhibitor MG132 caused strong stabilization (**Fig. 1B**). This suggests that over-expression of TP53INP2 may overload the regulation mechanisms for nuclear import of TP53INP2 leading to cytoplasmic accumulation and may potentiate TP53INP2 as an autophagic substrate. To clarify this, we generated a HeLa FlpIn cell line with inducible expression of EGFP-TP53INP2 lacking the NLS and NoLS sequences (Δ 189-211). Interestingly, deletion of the NLS-NoLS motif led to the formation of cytoplasmic puncta that co-localized with LC3B under basal conditions. The number of cytoplasmic puncta co-localizing with LC3B increased upon inhibition of lysosomal degradation and even more upon starvation (**Fig. 3A**). Monitoring the expression level of EGFP-TP53INP2(Δ 189-212) by Western blotting revealed that there was no significant stabilization upon starvation of the NLS-NoLS mutant (**Fig. 3B**) as found for WT TP53INP2 (**Fig. 1B**). There was a small stabilization by BafA1 while proteasomal inhibition gave a profound stabilization. Together this suggests that the nuclear pool of TP53INP2 is degraded by the proteasome while the smaller cytoplasmic pool may be degraded by autophagy. Mutation

of the LIR motif in the TP53INP2(Δ 189-211) constructs impaired the recruitment of TP53INP2 to the cytoplasmic LC3B dots (EGFP-TP53INP2 Δ NLS+ Δ LIR in **Fig 3A**), confirming previous studies based on transient over-expression¹⁵. These results suggest that TP53INP2 is more stable when localized in the cytoplasm than in the nucleus. This is consistent with previously published data showing that TP53INP2 is very unstable with a half-life of about 4 hours¹⁹. TP53INP2 which has accumulated in the cytoplasm is recruited to LC3B-positive structures via its LIR motif and can undergo degradation via the autophagic-lysosomal pathway as published for TP53INP1²⁰. However, normally TP53INP2 is a substrate for proteasomal degradation in the nucleolus.

The starvation-induced cytoplasmic localization of TP53INP2 is independent of ATG5 and NES motifs

TP53INP2 is reported to mediate transport of nuclear LC3B to the cytoplasm to promote autophagy under starvation⁵. Translocation of TP53INP2 from the nucleus to the cytoplasm upon starvation required a functional LIR motif¹¹. A nuclear export sequence (NES) was identified in the region amino acids 25-47 encompassing the LIR motif at positions 35-38¹¹. Together these studies indicate a mutual role of ATG8s and TP53INP2 in facilitating each other's export out of nucleus upon mTOR inactivation. Furthermore, it is reported that autophagy-deficient cells lacking ATG5 display impaired nucleocytoplasmic shuttling of TP53INP2¹⁵. To study this more closely as we first applied bioinformatics tools to predict putative NES motifs in TP53INP2. In addition to the published NES1 (25-VSEEDVDGWLIIIDLPSYAAP-47), another NES2 motif (87 GPARLQSSPLEDLLIEH 104) was predicted. To test their functionality in mediating nuclear export in isolation, both motifs were cloned into the Rev 1.4 plasmid vector²¹. The positive control REV NES motif directed REV-EGFP out of the nucleus (**Fig. 4A**). However, both the NES1 and the NES2 motifs failed to export the REV-EGFP protein out of the nucleus (**Fig. 4B**). Furthermore, when the HeLa FlpIn EGFP-TP53INP2 cells were starved and treated with leptomycin B (LMB) for 2 hours, EGFP-TP53INP2 was still localized in the cytoplasm and not retained in the nucleus as p62 (**Fig. 4C**). p62 is continuously shuttling between the nucleus and the cytoplasm²¹. LMB inhibits CRM1-mediated export from the nucleus to the cytoplasm. These results indicate that NES1 and NES2 in TP53INP2 are not functional NES motifs and that TP53INP2 nuclear export is not mediated by CRM1 (also called exportin 1). Interestingly, similar to TP53INP2, LMB

treatment is not able to restrict LC3B to the nucleus⁴, suggesting that the two proteins use a similar mechanism for directing cytoplasmic localization. Therefore, we analyzed the importance of the LIR motif in TP53INP2 for nucleocytoplasmic shuttling by establishing a HeLa FlpIn EGFP-TP53INP2 W35A/I38A (LIR mutant) expressing cell line. Surprisingly, and in contrast to previous studies¹¹, we found that the mutation of the LIR motif did not impact TP53INP2 localization (**Fig. 4D**). Deletion of the complete NES1 encompassing the LIR motif (TP53INP2 Δ 24-40) (**Fig. S4A**), or mutation of the residues E97 and D98 previously reported to be important for TP53INP2 shuttling¹¹, did not affect localization either (**Fig. S4B**). Hence, the nuclear export of TP53INP2 seems not to be mediated by the previous published NES motif or by interaction with the ATG8 proteins. Our next question was therefore whether ATG5 and autophagy activity had any impact on TP53INP2 localization. To this end, we generated WT MEF and ATG5 KO MEF cell lines constitutively expressing EGFP-TP53INP2. In contrast to previous reports¹⁵, we found that the ATG5 KO MEF EGFP-TP53INP2 cell line showed similar nuclear-cytoplasmic shuttling as the MEF wild type cells (**Fig. 5A and B**). This suggests that the autophagy process does not impact directly on the TP53INP2 nuclear-cytoplasmic shuttling.

mTOR inactivation mediates acetylation and cytoplasmic retention of TP53INP2

Our failure to identify a functional NES in TP53INP2 together with the lack of nuclear retention upon LMB treatment raised the question whether the cytoplasmic accumulation of TP53INP2 is regulated by inhibition of nuclear import and not a consequence of nuclear export. To investigate this, we performed fluorescence recovery after photobleaching (FRAP) on the FlpIn TP53INP2 KO cell line reconstituted with EGFP-TP53INP2. The nuclear EGFP-TP53INP2 was completely photoed bleached and then the cells were starved in HBSS for 1 hour. During this period, the localization of EGFP-TP53INP2 was followed by live cell imaging. Despite photobleaching of the entire nuclear pool of EGFP-TP53INP2, we still observed cytoplasmic accumulation similar to the unbleached cells, upon starvation (**Fig. 6A**). This shows that the cytoplasmic accumulation takes place without contribution from the nuclear EGFP-TP53INP2 fraction. Thus, the newly synthesized EGFP-TP53INP2 is restricted to the cytoplasm upon mTOR inhibition while the nuclear EGFP-TP53INP2 fraction is degraded by nuclear proteasomes. To test this further, we checked if the interaction between TP53INP2 and the importin family of proteins is modulated upon starvation. For nuclear import, proteins interact with the nuclear pore complex whereby the importin family of proteins plays an essential role.

First, we assayed the interaction of TP53INP2 with importin family proteins by GST pulldown assay (**Fig. 6B**). Since TP53INP2 bound best to importin α 1, GST-Importin α 1 was applied in a GST-pulldown assay with cell lysates from the HeLa FlpIn EGFP-TP53INP2 cell line exposed to normal medium or starvation medium (HBSS) for 2 hours. Interestingly, EGFP-TP53INP2 from cells exposed to full medium interacted strongly with GST-Importin α 1 while EGFP-TP53INP2 from cells exposed to HBSS did not (**Fig. 6C**). This indicates that mTOR inhibition affects the binding of TP53INP2 to Importin and thereby restricts TP53INP2 to the cytoplasm. Acetylation of proteins can regulate their subcellular localization¹. Importantly, nuclear localization of LC3B is shown to be regulated via acetylation of the lysine residues K49/K51⁵. This prompted us to investigate if starvation could change the acetylation pattern of TP53INP2, and thereby inhibit Importin binding and nuclear translocation. To this end, we monitored acetylated EGFP-TP53INP2 in cell extracts from the HeLa FlpIn EGFP-TP53INP2 cell line exposed to normal or starvation conditions using an acetylation enrichment assay. In contrast to what is reported for LC3B, we found that starvation induces strong acetylation of TP53INP2 (**Fig. 6D**). To verify this further, we immunoprecipitated EGFP-TP53INP2 from the cells and analyzed post-translational modifications by mass spectrometry. Notably, we found that all three residues within the C terminal part of TP53INP2 undergo acetylation upon exposure to starvation media (**Fig. 6E and Fig. S5A-F**). Secondary structure predictions²² suggest the presence of two helices in the C-terminal region of TP53INP2. The second helix is part of the NLS and projects K187 and two arginines (R191 and R194) on the same side of the helix suggesting they may constitute an interaction surface for importin α . Acetylation of K187 may then inhibit this interaction and thereby inhibit the nuclear import of TP53INP2. Taken together, and in contrast to previous reports, our results show that starvation-induced mTOR inhibition leads to increased acetylation of the three C terminal lysine residues in TP53INP2 inhibiting binding to the importins and blockage of nuclear translocation of TP53INP2.

Acetylation of TP53INP2 at K187 inhibits nuclear import upon starvation

To determine the importance of each of the three lysine residues (K165, K187, K204) for regulating nuclear localization of TP53INP2, we generated HeLa FlpIn cells expressing each of the TP53INP2 mutants EGFP-TP53INP2 K165R, EGFP-TP53INP2 K187R, and EGFP-TP53INP2 K204R. HeLa FlpIn cells expressing EGFP-TP53INP2 K165R and EGFP-TP53INP2 K204R displayed a similar localization pattern as wild type EGFP-TP53INP2 (**Fig.**

1A, Fig. 7A, and C). However, cells expressing EGFP-TP53INP2 K187R did not display any cytoplasmic retention upon starvation and TP53INP2 K187R remained completely nuclear (**Fig. 7B**). This indicates that K187 regulates the nuclear import of TP53INP2. To rule out the possibility of phosphorylation regulating nuclear-cytoplasmic shuttling, we made several cell lines expressing EGFP-TP53INP2 with deletions (**Fig. S6A-F**) or point mutations of serine-threonine phosphorylatable residues (**Fig. S6G-K**), but we could not see any effect of any of these mutations on subcellular localization.

Inhibition of CBP leads to dysregulated expression of TP53INP2

Since the MS data showed acetylation of all the three C-terminal lysine residues in TP53INP2, we next analyzed the localization of an EGFP-TP53INP2 mutant with all three lysine residues mutated, K3R. In a normal medium, the K3R mutant displayed a nuclear localization similar to the WT protein (**Fig. 8A**). However, exposure to starvation conditions led to strong nuclear accumulation in addition to the cytoplasmic accumulation typical for the WT protein (**Fig. 8A and Fig. 1A**). This combined phenotype was a surprise because the K3R has the K187R mutation allowing unregulated nuclear import. This result clearly suggests that K165 and/or K204 also are involved in regulating the localization and/or stability of TP53INP2. To further confirm that acetylation of these three lysine residues is important for regulation of subcellular localization and degradation, we next exposed the HeLa FlpIn EGFP-TP53INP2 cell line to the CBP/p300 inhibitor C646. CBP/p300 is localized both in the cytoplasm and in the nucleus and is previously shown to regulate autophagy via acetylation of autophagy-related proteins such as ATG5 and LC3B^{3,5}. Notably, starvation of HeLa FlpIn EGFP-TP53INP2 cells that had been treated with C646 led to a similar nuclear and cytoplasmic accumulation as the EGFP-TP53INP2(K3R) mutant (**Fig. 8B**). This clearly suggests that acetylation of the three C-terminal lysine residues in TP53INP2 is important for regulating its subcellular localization and the degradation rate upon starvation.

Acetylation of K165 and K240 facilitates nuclear degradation of TP53INP2 upon starvation

Our results so far have shown that the expression of TP53INP2 is strongly enhanced upon starvation. At the same time, the nuclear import is inhibited due to acetylation of

TP53INP2(K187) and the subcellular localization of TP53INP2 switches from nuclear to cytoplasmic. Our FRAP analyses suggested that there is no significant translocation of TP53INP2 from the nucleus to the cytoplasm during this period. Hence, the next question was if the localization switch was caused by cytoplasmic retention and stabilization of newly synthesized TP53INP2, while the nuclear pool of TP53INP2 proteins was directed to degradation via the proteasome. To this end, we exposed the EGFP-TP53INP2 wild type and mutant cell lines for starvation while we inhibited protein synthesis with cycloheximide and followed the localization of the EGFP-TP53INP2 proteins. The subcellular localization of the wild type protein was completely switched from nuclear to cytoplasmic within 80 minutes of starvation. Inhibition of protein synthesis leads to a strong reduction in the accumulation of cytoplasmic EGFP-TP53INP2 protein (**Fig. 9A**). This shows that the accumulation of cytoplasmic TP53INP2 is due to increased synthesis and stabilization by cytoplasmic retention. The EGFP-TP53INP2 K187R mutant displayed complete nuclear localization even after 120 minutes of starvation. Inhibition of protein synthesis led to a strong reduction in the amount of TP53INP2 K187R (**Fig. 9B**). This confirms that acetylation of K187 directs inhibition of nuclear import. Furthermore, it shows that newly synthesized EGFP-TP53INP2 K187R is continuously imported to the nucleus where it undergoes nuclear degradation. Addition of cycloheximide to the EGFP-TP53INP2 K3R mutant, which normally accumulated both in the nucleus and in the cytoplasm upon starvation, led to the disappearance of the cytoplasmic proteins while the nuclear proteins remained unchanged (**Fig. 9C**). This confirms that the cytoplasmic accumulation upon starvation is due to enhanced protein synthesis of TP53INP2. Interestingly, also p53 is stabilized upon starvation in certain cell lines²³. Hence, enhanced TP53INP2 expression may be mediated by p53. Moreover, it shows that modification of the lysine residues K165 and K204 facilitates nuclear degradation upon starvation. When they are mutated, TP53INP2 is still expressed in the nucleus under starvation conditions. Altogether, our results show that the localization of TP53INP2 is regulated by its three C-terminal lysine residues K165, K187, and K204. K187 regulates the nuclear import of the protein, while K165 and K204 regulate its nuclear degradation rate. Upon starvation, these three residues are acetylated, leading to cytoplasmic retention and nuclear degradation, and hence a switch in its subcellular localization from nuclear to cytoplasmic.

Discussion

The major conclusion of this study is that the localization switch of TP53INP2 upon mTOR inhibition from the nucleus to the cytoplasm, is regulated by acetylation of three lysine residues in its C-terminal region. By establishing TP53INP2 KO cell lines with low expression levels of EGFP-TP53INP2, we found that EGFP-TP53INP2 does not shuttle from the nucleus to the cytoplasm. Instead, mTOR inhibition led to impairment of nuclear import combined with facilitated degradation of nuclear TP53INP2 proteins. A previous study showed data to suggest that TP53INP2 shuttles between the cytoplasm and nucleus. During this shuttling, it passes through the nucleolus²⁴. Furthermore, TP53INP2 has also been reported to act as a mediator of nucleocytoplasmic shuttling of LC3B, binding to deacetylated LC3B in the nucleus and facilitating its export to the cytoplasm upon nutrient deprivation⁵. Our data do not oppose that nuclear export of LC3B occurs upon mTOR inhibition, but TP53INP2 is not exported together with LC3B. This finding was supported by the lack of a functional NES in TP53INP2, the inability of a CRM1 inhibitor to restrict TP53INP2 to the nucleus, and by FRAP data showing that TP53INP2 does not move out of the nucleus.

Under full media conditions, TP53INP2 is localized in the nucleus, and enriched in the nucleolus. It serves roles both as a transcriptional coactivator of the thyroid hormone receptor and as a facilitator of RNA polymerase I transcription, respectively^{7,10}. These findings were supported by our analysis of the TP53INP2 KO cells, which displayed a lower proliferation rate and less rDNA transcription than the wild type cells. We mapped the region encompassing amino acids 189-211 to constitute the NLS of TP53INP2, and within this region, we mapped the NoLS to be represented by amino acids 201 to 204. Interestingly, immediately preceding the mapped NLS we identified the K187 residue that regulated the nuclear import of TP53INP2. Starvation-induced acetylation of K187 restricted TP53INP2 to the cytoplasm. K187 is predicted to be located on a helix that also projects two R191 and R194 on the same side. Acetylation of K187 may compromise binding of the helix with R191 and R194 to importin α and inhibit nuclear import of TP53INP2. When the nuclear import of TP53INP2 is inhibited under nutrient deprivation its stimulating effects on cell proliferation and ribosome biogenesis is consequently blocked. Moreover, we also identified the K204 residue within the NoLS and K165 to be acetylated under cellular starvation. Acetylation of these residues facilitated nuclear degradation of TP53INP2, and hence further ensured that the anabolic roles of TP53INP2 are switched off during starvation.

In this study, we found that p300/CBP can mediate acetylation of the three regulatory lysine residues in the C-terminal of TP53INP2 with acetylation of K187 inhibiting nuclear import. Regulation of subcellular localization by acetylation is already known in the literature¹. Acetylation of the NLS of S phase kinase-associated protein 2 (SKP2) by p300 promotes its cytoplasmic retention and inhibits its degradation²⁵. This is essentially the same mechanism as we here report for TP53INP2. Also, acetylation of the NLS of the viral- DNA sensor γ -interferon-inducible protein 16 (IFI16) leads to its cytoplasmic localization²⁶. Furthermore, AMPK-dependent p300-mediated acetylation of importin α 1 is associated with regulation of nuclear import of RNA binding protein, Hu-antigen R²⁷. Also, p300 is shown to acetylate histone deacetylase 6 (HDAC6) leading to inhibition of interaction with importin α and subsequent inhibition of nuclear import²⁸.

We found the expression of TP53INP2 to strongly increase upon starvation. Treatment with cycloheximide showed that this increase is dependent on protein synthesis, and hence not only due to protein stabilization. This shows that TP53INP2 escapes the global downregulation of translation that occurs upon mTOR inhibition. Importantly, p53 is shown to be stabilized by starvation in hepatic tissue²³. The stabilization was obtained by post-transcriptional mechanisms and was required for gluconeogenesis and amino acid catabolism in a starved state. The role of starvation-induced TP53INP2 expression upon mTOR inhibition will be an important question to address in future studies.

One suggested a role of cytoplasmic TP53INP2 is the reported role in facilitating autophagosome formation, thus acting as a positive regulator of autophagy¹⁵. Whether TP53INP2, via binding to the vacuole membrane protein 1 (VMP1), functions as a scaffold for LC3B recruitment to autophagosomes, or if LC3B recruits TP53INP2 to the phagophore structures, has not been clarified^{5,15,24,29}. However, a recent report shows that LC3B recruits TP53INP2 to autophagic membranes⁶, which is in line with our results. Our data suggest that cytoplasmic degradation of TP53INP2 is regulated by modifications of the C-terminal lysine residues. This regulation is overridden when TP53INP2 is over-expressed by transient transfection. Then it is recruited to LC3B-positive structures in a LIR-dependent manner. However, when the expression of TP53INP2 is kept at a level closer to the endogenous level, TP53INP2 is stabilized in the cytoplasm upon starvation and not detected in LC3B-positive structures. Normally, TP53INP2 is degraded by the proteasome¹⁹, which we show occurs in the nucleus, most likely in the nucleolus, by an ubiquitin-independent pathway. This degradation pathway is not much studied and not well understood. Recently, Protein interacting with the

carboxyl terminus (PICT), a regulator of p53, was found to be degraded by a nucleolar ubiquitin-independent proteasomal pathway¹⁶. It is interesting that TP53INP2 may be degraded by the same pathway.

Our measurements of autophagic flux in the TP53INP2 KO out cells revealed no difference from WT cells. LC3B lipidation upon starvation was completely normal, and the autophagy receptors were not accumulated. This suggests that at least in these cell lines loss of TP53INP2 does not affect autophagy flux detectably. This cannot rule out the possibility of functional redundancy between TP53INP1 and TP53INP2. Another recent study reported that TP53INP2 interaction with ATG7 enhanced LC3-ATG7 interaction but did not affect the formation of autophagosomes on knockdown of TP53INP2⁶. Consistent with this, TP53INP2-deficient 3T3-L1 cells did not display any changes in autophagy flux during adipogenesis relative to control cells⁹. Taken together, this raises the question if TP53INP2 may have other roles in the cytoplasm than being a regulator of autophagy activity. Interestingly, a recent paper shows that TP53INP2 sensitizes cells to apoptosis induced by death receptor ligands³⁰. TP53INP2 was found to bind to caspase-8 and the ubiquitin ligase TRAF6, and thereby regulate TRAF6-mediated activation of caspase-8. Hence, an important role of TP53INP2 in the cytoplasm may be to regulate this death receptor pathway. To conclude, TP53INP2 serves important roles in the cytoplasm, nucleus, and nucleolus. We now show that its subcellular localization is tightly regulated by acetylation of specific lysine residues in its C-terminal part.

Acknowledgments

We are grateful to the proteomics and imaging core facilities at UiT, Faculty of Health Sciences for valuable assistance. This work was funded by grants from the FRIBIOMED (grant number 214448) and the TOPPFORSK (grant number 249884) programs of the Research Council of Norway, and the Norwegian Cancer Society (grant number 71043-PR-2006-0320) to T.J.

References

- 1 Narita, T., Weinert, B. T. & Choudhary, C. Functions and mechanisms of non-histone protein acetylation. *Nat Rev Mol Cell Biol* **20**, 156-174, doi:10.1038/s41580-018-0081-3 (2019).
- 2 Lin, S. Y. *et al.* GSK3-TIP60-ULK1 signaling pathway links growth factor deprivation to autophagy. *Science (New York, N.Y.)* **336**, 477-481, doi:10.1126/science.1217032 (2012).
- 3 Lee, I. H. & Finkel, T. Regulation of autophagy by the p300 acetyltransferase. *J Biol Chem* **284**, 6322-6328, doi:10.1074/jbc.M807135200 (2009).
- 4 Drake, K. R., Kang, M. & Kenworthy, A. K. Nucleocytoplasmic distribution and dynamics of the autophagosome marker EGFP-LC3. *PLoS one* **5**, e9806, doi:10.1371/journal.pone.0009806 (2010).
- 5 Huang, R. *et al.* Deacetylation of nuclear LC3 drives autophagy initiation under starvation. *Mol Cell* **57**, 456-466, doi:10.1016/j.molcel.2014.12.013 (2015).
- 6 You, Z. *et al.* TP53INP2 contributes to autophagosome formation by promoting LC3-ATG7 interaction. *Autophagy*, 1-13, doi:10.1080/15548627.2019.1580510 (2019).
- 7 Baumgartner, B. G. *et al.* Identification of a novel modulator of thyroid hormone receptor-mediated action. *PLoS one* **2**, e1183, doi:10.1371/journal.pone.0001183 (2007).
- 8 Sala, D. *et al.* Autophagy-regulating TP53INP2 mediates muscle wasting and is repressed in diabetes. *The Journal of clinical investigation* **124**, 1914-1927, doi:10.1172/jci72327 (2014).
- 9 Romero, M. *et al.* TP53INP2 regulates adiposity by activating beta-catenin through autophagy-dependent sequestration of GSK3beta. *Nat Cell Biol* **20**, 443-454, doi:10.1038/s41556-018-0072-9 (2018).
- 10 Xu, Y. *et al.* TP53INP2/DOR, a mediator of cell autophagy, promotes rDNA transcription via facilitating the assembly of the POLR1/RNA polymerase I preinitiation complex at rDNA promoters. *Autophagy* **12**, 1118-1128, doi:10.1080/15548627.2016.1175693 (2016).
- 11 Sancho, A. *et al.* DOR/Tp53inp2 and Tp53inp1 Constitute a Metazoan Gene Family Encoding Dual Regulators of Autophagy and Transcription. *PLoS one* **7**, e34034, doi:10.1371/journal.pone.0034034 (2012).
- 12 Pankiv, S. *et al.* Nucleocytoplasmic shuttling of p62/SQSTM1 and its role in recruitment of nuclear polyubiquitinated proteins to promyelocytic leukemia bodies. *J Biol Chem* **285**, 5941-5953, doi:M109.039925 [pii]10.1074/jbc.M109.039925 (2010).
- 13 Hosokawa, N., Hara, Y. & Mizushima, N. Generation of cell lines with tetracycline-regulated autophagy and a role for autophagy in controlling cell size. *FEBS Lett* **580**, 2623-2629 (2006).
- 14 Pankiv, S. *et al.* p62/SQSTM1 binds directly to Atg8/LC3 to facilitate degradation of ubiquitinated protein aggregates by autophagy. *J Biol Chem* **282**, 24131-24145, doi:M702824200 [pii]10.1074/jbc.M702824200 (2007).
- 15 Nowak, J. *et al.* The TP53INP2 protein is required for autophagy in mammalian cells. *Mol Biol Cell* **20**, 870-881, doi:10.1091/mbc.E08-07-0671 (2009).
- 16 Maehama, T., Kawahara, K., Nishio, M., Suzuki, A. & Hanada, K. Nucleolar stress induces ubiquitination-independent proteasomal degradation of PICT1 protein. *The Journal of biological chemistry* **289**, 20802-20812, doi:10.1074/jbc.M114.571893 (2014).
- 17 Kalderon, D., Richardson, W. D., Markham, A. F. & Smith, A. E. Sequence requirements for nuclear location of simian virus 40 large-T antigen. *Nature* **311**, 33-38 (1984).
- 18 Weber, J. D. *et al.* Cooperative signals governing ARF-mdm2 interaction and nucleolar localization of the complex. *Molecular and cellular biology* **20**, 2517-2528, doi:10.1128/mcb.20.7.2517-2528.2000 (2000).
- 19 Mauvezin, C. *et al.* The nuclear cofactor DOR regulates autophagy in mammalian and *Drosophila* cells. *EMBO Rep* **11**, 37-44, doi:10.1038/embor.2009.242 (2010).
- 20 Seillier, M. *et al.* TP53INP1, a tumor suppressor, interacts with LC3 and ATG8-family proteins through the LC3-interacting region (LIR) and promotes autophagy-dependent cell death. *Cell Death Differ* **19**, 1525-1535, doi:10.1038/cdd.2012.30 (2012).

- 21 Pankiv, S. *et al.* Nucleocytoplasmic shuttling of p62/SQSTM1 and its role in recruitment of nuclear polyubiquitinated proteins to promyelocytic leukemia bodies. *The Journal of biological chemistry* **285**, 5941-5953, doi:10.1074/jbc.M109.039925 (2010).
- 22 Jones, D. T. Protein secondary structure prediction based on position-specific scoring matrices. *J Mol Biol* **292**, 195-202, doi:10.1006/jmbi.1999.3091 (1999).
- 23 Prokesch, A. *et al.* Liver p53 is stabilized upon starvation and required for amino acid catabolism and gluconeogenesis. *FASEB journal : official publication of the Federation of American Societies for Experimental Biology* **31**, 732-742, doi:10.1096/fj.201600845R (2017).
- 24 Mauvezin, C., Sancho, A., Ivanova, S., Palacin, M. & Zorzano, A. DOR undergoes nucleocytoplasmic shuttling, which involves passage through the nucleolus. *FEBS letters* **586**, 3179-3186, doi:10.1016/j.febslet.2012.06.032 (2012).
- 25 Inuzuka, H. *et al.* Acetylation-dependent regulation of Skp2 function. *Cell* **150**, 179-193, doi:10.1016/j.cell.2012.05.038 (2012).
- 26 Li, T., Diner, B. A., Chen, J. & Cristea, I. M. Acetylation modulates cellular distribution and DNA sensing ability of interferon-inducible protein IFI16. *Proc Natl Acad Sci U S A* **109**, 10558-10563, doi:10.1073/pnas.1203447109 (2012).
- 27 Wang, W. *et al.* AMP-activated protein kinase-regulated phosphorylation and acetylation of importin alpha1: involvement in the nuclear import of RNA-binding protein HuR. *The Journal of biological chemistry* **279**, 48376-48388, doi:10.1074/jbc.M409014200 (2004).
- 28 Liu, Y., Peng, L., Seto, E., Huang, S. & Qiu, Y. Modulation of histone deacetylase 6 (HDAC6) nuclear import and tubulin deacetylase activity through acetylation. *J Biol Chem* **287**, 29168-29174, doi:10.1074/jbc.M112.371120 (2012).
- 29 Ropolo, A. *et al.* The pancreatitis-induced vacuole membrane protein 1 triggers autophagy in mammalian cells. *The Journal of biological chemistry* **282**, 37124-37133, doi:10.1074/jbc.M706956200 (2007).
- 30 Ivanova, S. *et al.* Regulation of death receptor signaling by the autophagy protein TP53INP2. *The EMBO journal*, doi:10.15252/embj.201899300 (2019).

FIGURE LEGENDS

Figure 1. TP53INP2 is degraded by the proteasome in the nucleolus but accumulates in the cytoplasm upon inhibition of mTOR. (A) TP53INP2 does not co-localize with p62 or LC3B puncta upon starvation. TP53INP2 KO cells reconstituted with EGFP-TP53INP2 were treated with doxycycline for 24 h to induce expression. Cells were then kept in full medium (FM) or treated as indicated, before staining with p62 and LC3B antibodies and analysis by confocal fluorescence microscopy. (B) TP53INP2 is mainly degraded by the proteasome but is strongly stabilized upon starvation. After induction of EGFP-TP53INP2 with doxycycline, cells were treated as indicated and cell extracts analyzed by western blotting using the indicated antibodies. (C) EGFP-TP53INP2 accumulates in the nucleolus upon proteasomal inhibition. After induction of EGFP-TP53INP2 with doxycycline, cells were treated with MG132 for 8 h, stained with fibrillarin antibodies, and analyzed by confocal imaging. (D) Mutation of all lysines in TP53INP2 does not prevent its degradation by the proteasome nor its stabilization in response to starvation. Cells expressing EGFP-TP53INP2 K3R were treated as in B and cell extracts analyzed by western blotting as in B. (E) Mutation of all lysines in TP53INP2 does not affect its accumulation in the nucleolus upon proteasomal inhibition. Cells expressing EGFP-TP53INP2 K3R were treated and analyzed by confocal fluorescence microscopy as in C. Scale bars, 10 μm .

Figure 2. Partial overlapping NLS and NoLS signals are located in the C-terminal region of TP53INP2. (A) Schematic diagram of TP53INP2, showing the extension of deletion constructs used to identify nuclear localization signal (NLS) and nucleolar localization signal (NoLS) in TP53INP2. The localization of different deletion constructs in the nucleus (N) or cytoplasm (C) of transfected cells is indicated to the right. (B) HeLa cells transiently transfected with the indicated EGFP-TP53INP2 constructs were analyzed by confocal imaging 24 h post transfection. Scale bars, 10 μm . (C) Mapping of NLS and NoLS motifs in TP53INP2. The extent of the motifs are shown above a sequence alignment indicating evolutionary conservation of the NLS and NoLS motifs in higher vertebrates. The green dots indicate the positions of the three lysine residues in human TP53INP2. Basic residues are indicated in blue and acidic ones in red. The amino acid numbering below the alignment is based on the human TP53INP2 sequence. * indicate identical residues in all sequences, : indicate identical residues in almost all sequences.

Figure 3. Deletion of the TP53INP2 NLS motif leads to cytoplasmic protein accumulation and partial autophagic degradation. (A) TP53INP2 Δ 189-211 is partially cytoplasmic and co-localizes with LC3B puncta. After induction of expression of EGFP-TP53INP2 Δ 189-211 with doxycycline, cells were treated as indicated and stained with LC3B or Fibrillarin antibodies, before analysis by confocal fluorescence microscopy. Scale bars, 10 μ m. (B) TP53INP2 Δ 189-211 is partially degraded by autophagy. After induction of EGFP-TP53INP2 Δ 189-211 with doxycycline, cells were treated as indicated and cell extracts analyzed by western blotting using the indicated antibodies.

Figure 4. The starvation-induced cytoplasmic localization of TP53INP2 is independent of NES and LIR motifs. (A and B) Predicted NES1 and NES2 motifs in TP53INP2 are unable to mediate export of the NES reporter REV-EGFP out of the nucleus. HeLa cells were transfected with the indicated REV-EGFP constructs and analyzed by confocal fluorescence microscopy. REV1.4 EGFP is a negative control without any NES motif. REV1.4 NES EGFP is a positive control containing the NES from the REV protein. (C) Treatment of cells with the nuclear export inhibitor leptomycin B (LMB) does not inhibit a redistribution of TP53INP2 in response to starvation. HeLa FlpIn cells expressing EGFP-TP53INP2 were treated as indicated and stained for endogenous p62 as a positive control for LMB treatment, before analysis by confocal imaging. (D) EGFP-TP53INP2 with the LIR motif mutated (W35A/I38A) shows similar nuclear cytoplasmic shuttling as wild type in response to starvation. HeLa FlpIn cells expressing EGFP-TP53INP2 W35A/I38A were treated as indicated and stained with LC3B antibodies, before analysis by confocal imaging. Scale bars, 10 μ m.

Figure 5. The starvation-induced cytoplasmic localization of TP53INP2 is independent of ATG5. (A and B) Stable WT MEFs (A) and ATG5^{-/-} MEFs cell lines expressing EGFP-TP53INP2 made by retroviral transfer were treated with tetracycline for 24 h to induce expression of EGFP-TP53INP2. Cells were then treated as indicated and stained with p62 and LC3B antibodies, before analysis by confocal fluorescence microscopy. Scale bars, 10 μ m.

Figure 6. mTOR inactivation mediates acetylation and cytoplasmic retention of TP53INP2. (A) Cytoplasmic accumulation of TP53INP2 upon starvation does not depend on the nuclear pool of TP53INP2. Confocal fluorescence microscopy live cell imaging of HeLa FlpIn cells expressing EGFP-TP53INP2 under starvation. The nucleus of one of the representative cells was photobleached while another cell was left unbleached. After complete photobleaching of nuclear EGFP-TP53INP2, cells were treated with HBSS and live cell imaging performed. Scale bars, 10 μ m. (B) TP53INP2 interacts with Importin α 1. GFP-tagged TP53INP2 was *in vitro* translated in the presence of [³⁵S]-methionine and tested in GST pulldown assays for binding to the indicated recombinant Importin family proteins fused to GST. Bound proteins were detected by autoradiography (AR), and immobilized GST fusion proteins by Coomassie brilliant blue staining. (C) The binding of TP53INP2 to Importin α 1 is reduced upon starvation. HeLa FlpIn cells expressing EGFP-TP53INP2 were starved or not for 2 h, and cell lysates tested in GST pulldown assays for binding of EGFP-TP53INP2 to GST-Importin α 1. Bound EGFP-TP53INP2 was detected with EGFP antibodies and immobilized GST-Importin α 1 by Coomassie brilliant blue staining. (D) TP53INP2 is acetylated upon starvation. HeLa FlpIn cells expressing EGFP-TP53INP2 were starved or not for 2 h, before immunoprecipitation of EGFP-TP53INP2 from cell lysates. Total EGFP-TP53INP2 was detected by western blotting with EGFP antibodies, while acetylated TP53INP2 was detected with the anti-acetylated lysine antibody supplied in the Signal Seeker Acetyl Lysine Detection Kit (Cytoskeleton, Inc). (E) Sequence of the C-terminal region encompassing amino acids 161-220 of TP53INP2 showing PSIPRED secondary structure prediction²², location of NLS and NoLS and the three lysine (K) residues that were shown by mass spectrometry to become acetylated upon starvation. A helical wheel projection shows the location of the K187 and the two arginine (R) residues to be located on the same side of the helix. Blue squares indicate basic residues and red one's acidic residues.

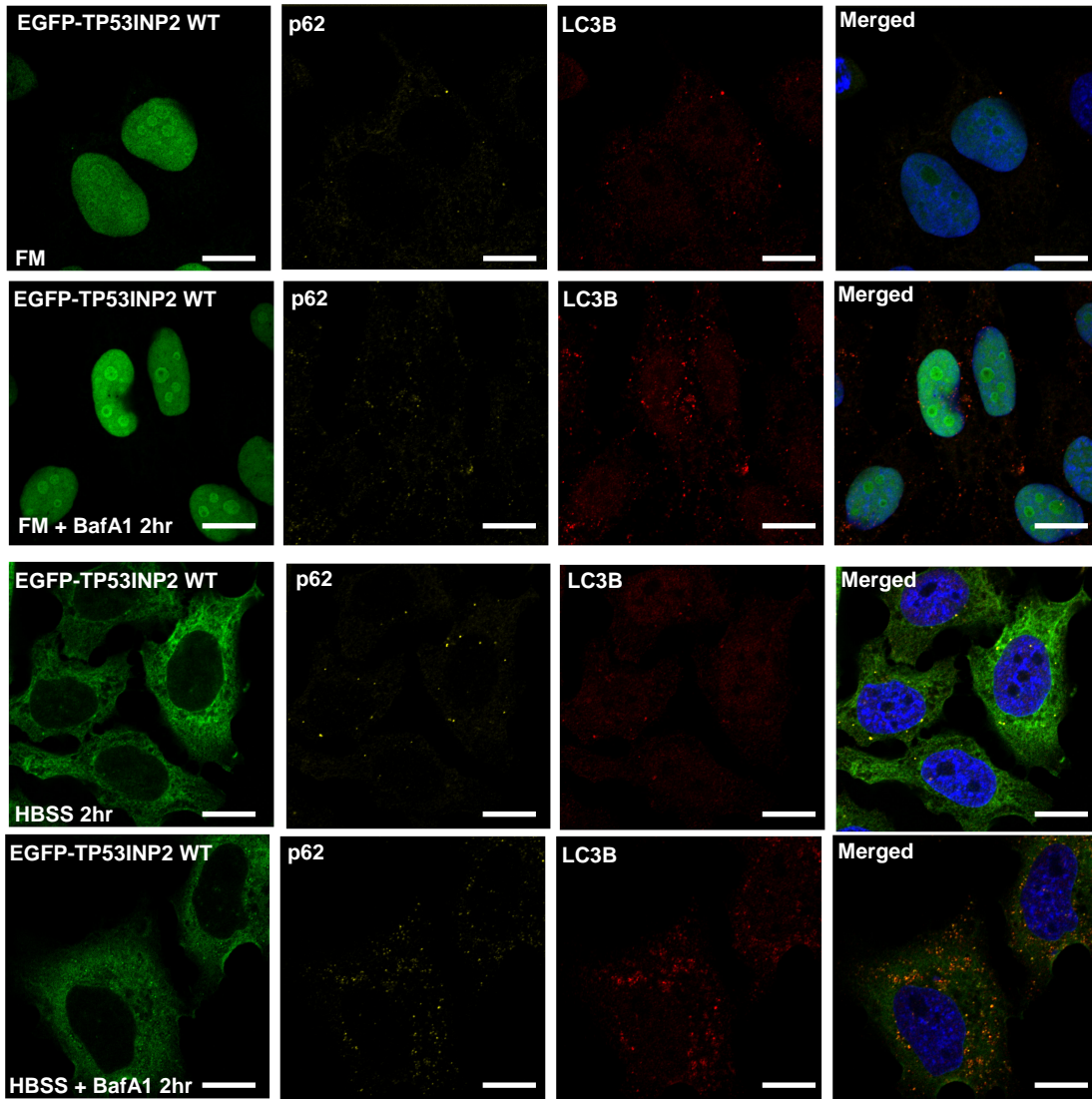
Figure 7. Acetylation of TP53INP2 at K187 inhibits nuclear import upon starvation. (A, B and C) HeLa FlpIn cells expressing EGFP-TP53INP2 with the indicated K to R mutations were treated as indicated, stained with LC3B antibodies and analyzed by confocal fluorescence microscopy. Scale bars, 10 μ m.

Figure 8. Inhibition of CBP/p300 leads to dysregulated expression of TP53INP2. (A) TP53INP2 with all three lysines mutated to arginines (K3R) is nuclear in full medium (FM) but displays a partial and dysregulated nuclear cytoplasmic shuttling upon starvation. HeLa FlpIn cells expressing EGFP-TP53INP2 K3R were treated as indicated, stained with LC3B antibodies and analyzed by confocal fluorescence microscopy. (B) TP53INP2 treated with CBP/P300 inhibitor is nuclear in full medium but displays a partial and dysregulated nuclear cytoplasmic shuttling upon starvation. HeLa FlpIn cells expressing EGFP-TP53INP2 were treated as indicated with CBP/P300 inhibitors and analyzed by confocal fluorescence microscopy. Scale bars, 10 μ m.

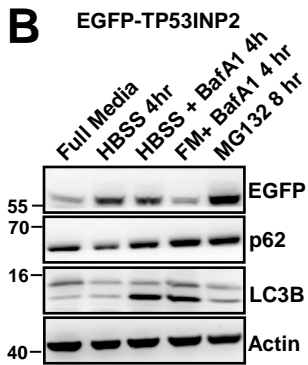
Figure 9. Acetylation of K165 and K240 facilitates nuclear degradation of TP53INP2 upon starvation. (A, B and C) HeLa FlpIn cells expressing the indicated EGFP-TP53INP2 constructs were starved in HBSS with or without cycloheximide (CHX) to block protein synthesis, and cells were imaged at 80, 90 and 120-mins post treatment. Scale bars, 10 μ m.

Figure 1

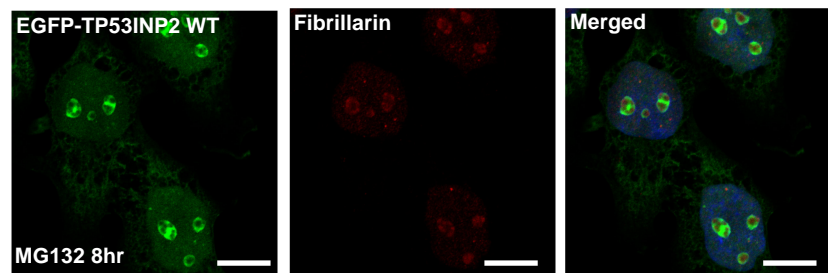
A



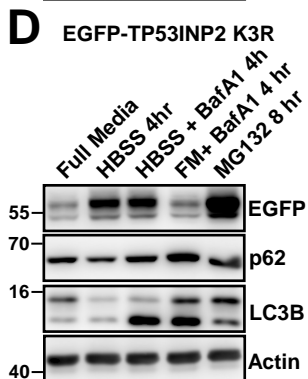
B



C



D



E

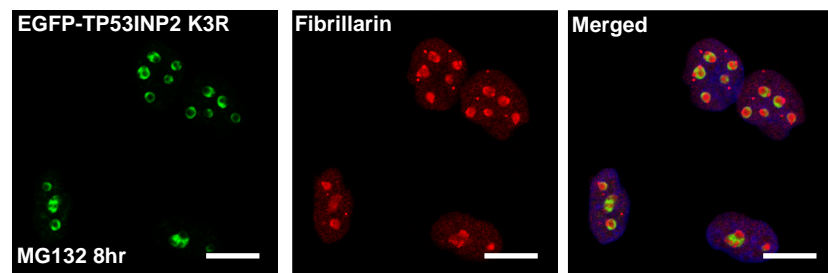
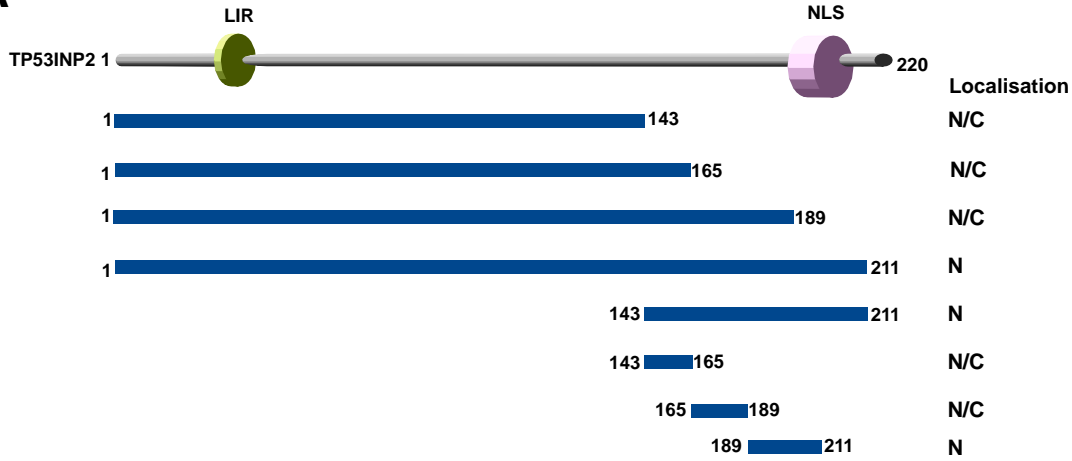
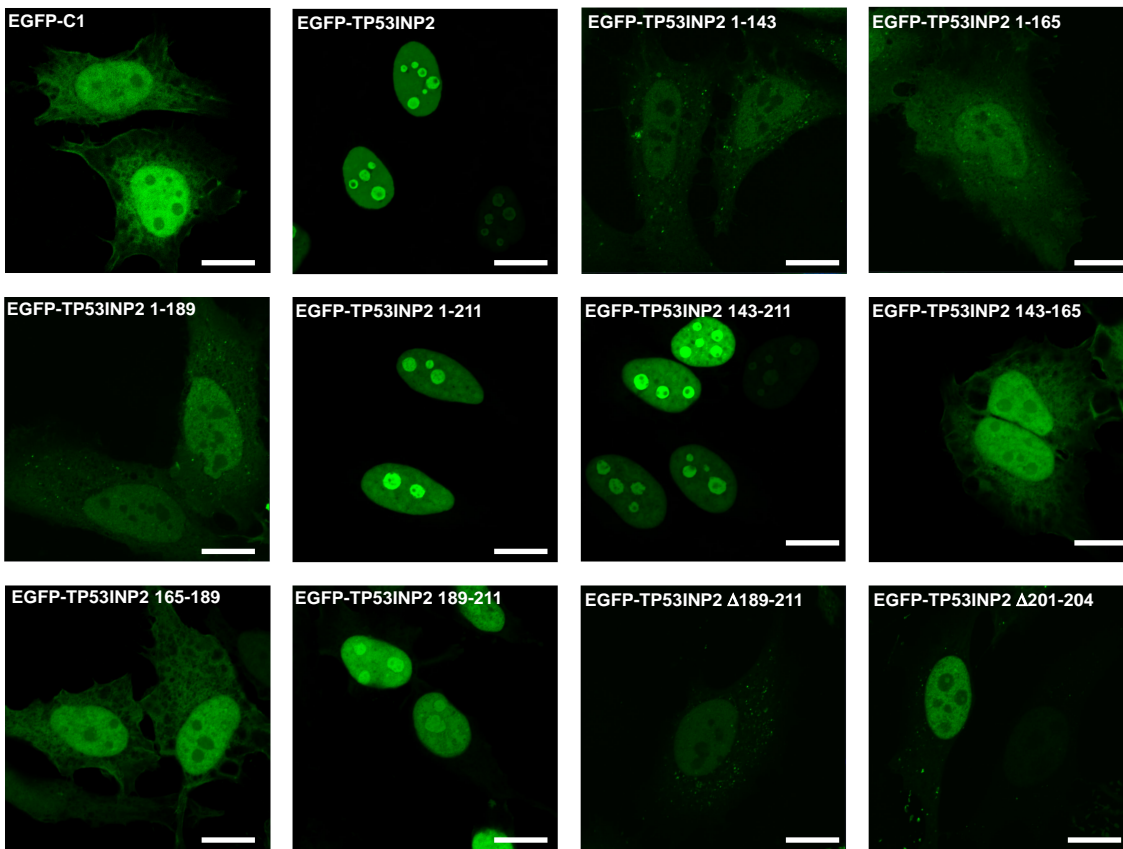


Figure 2

A



B



C

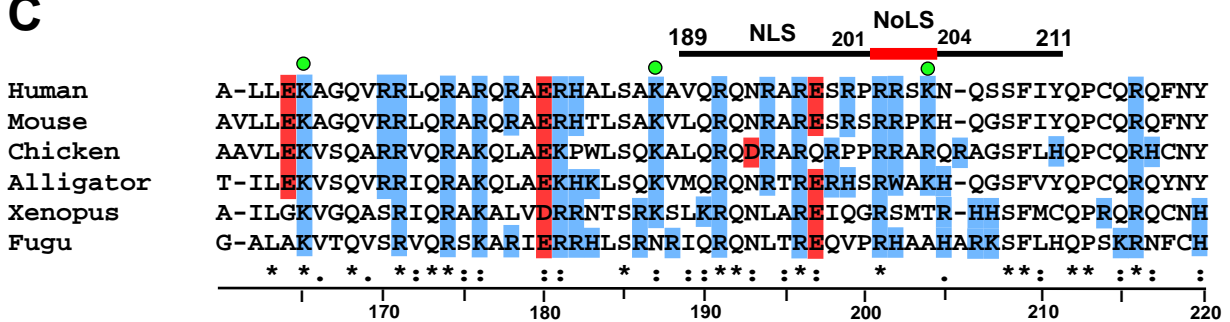
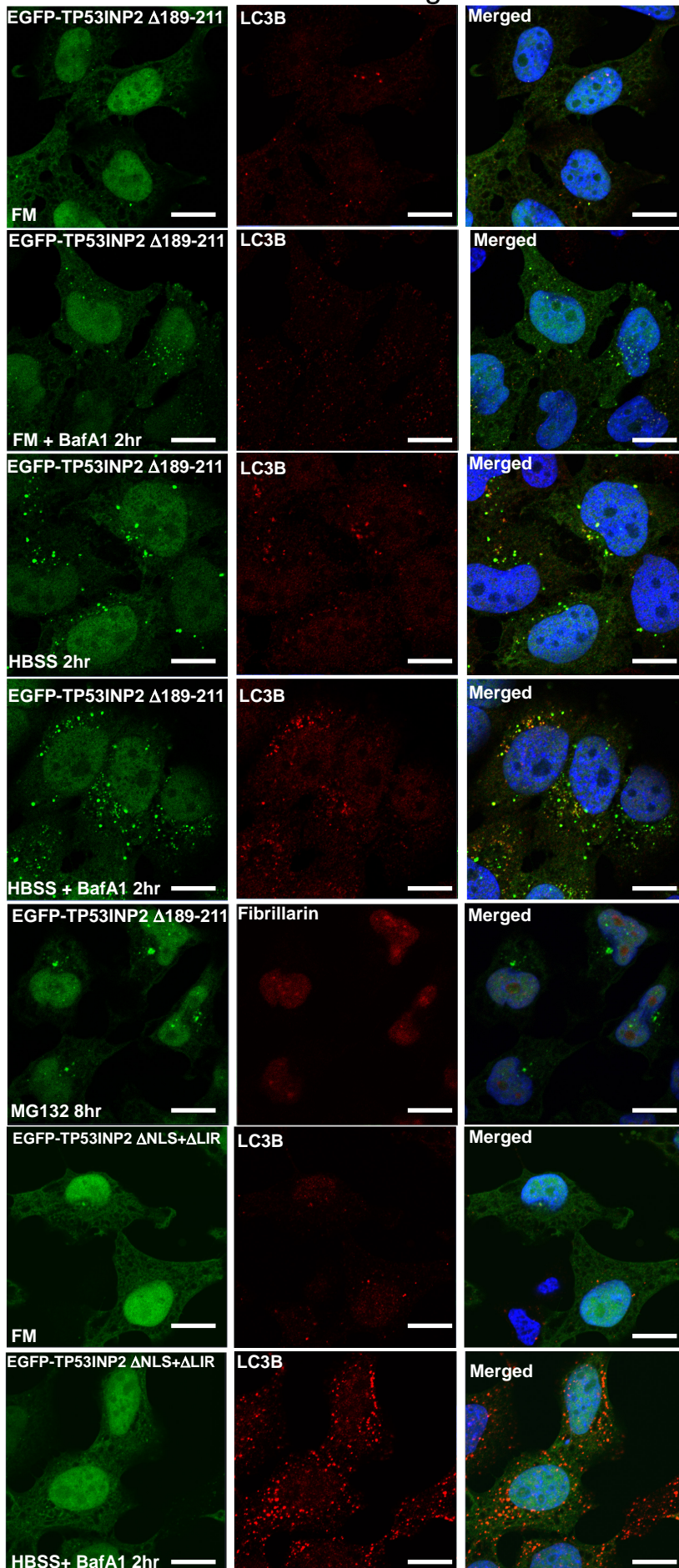


Figure 3

A



B

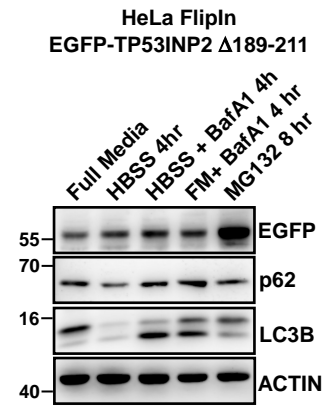


Figure 4

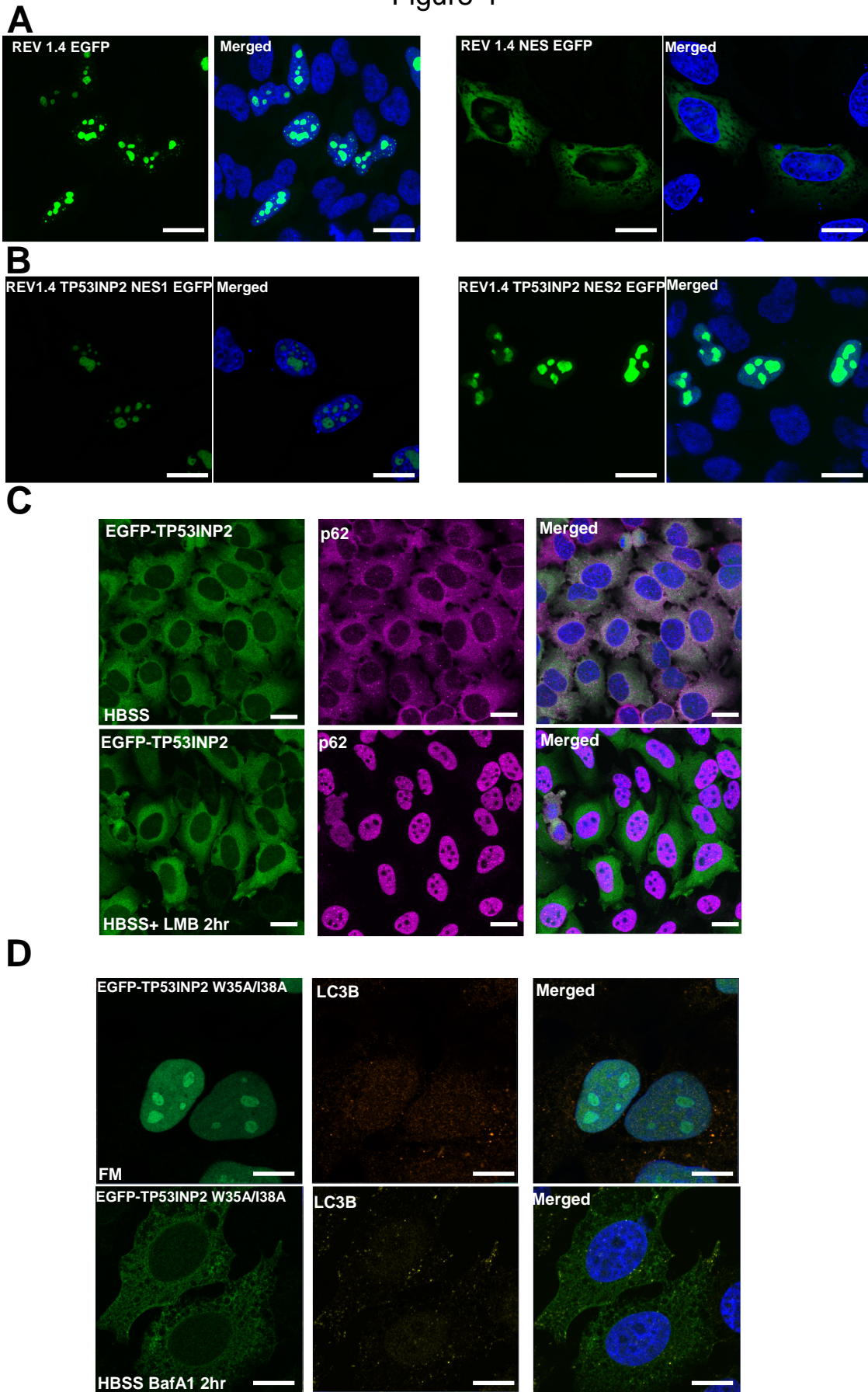


Figure 5

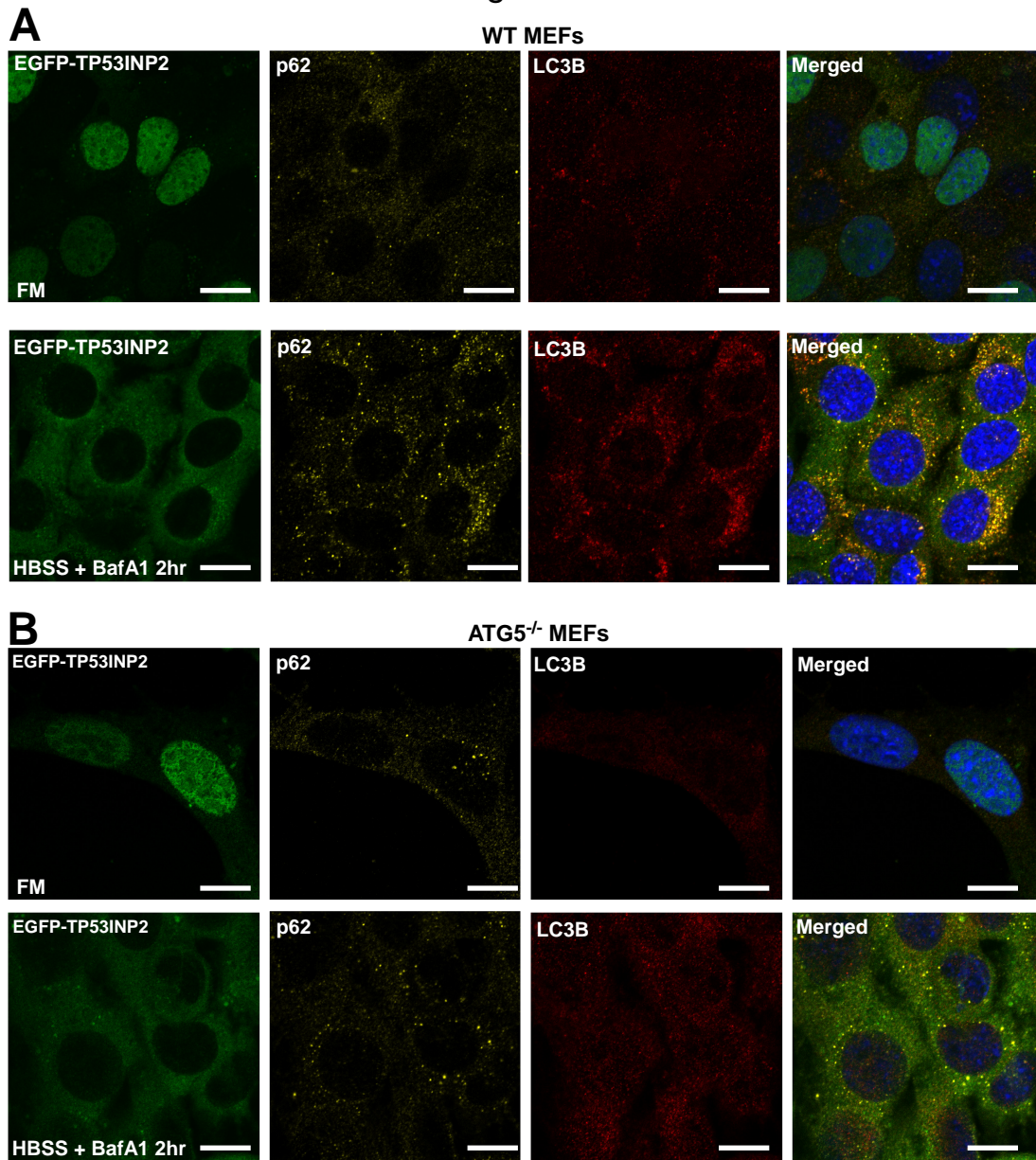


Figure 6

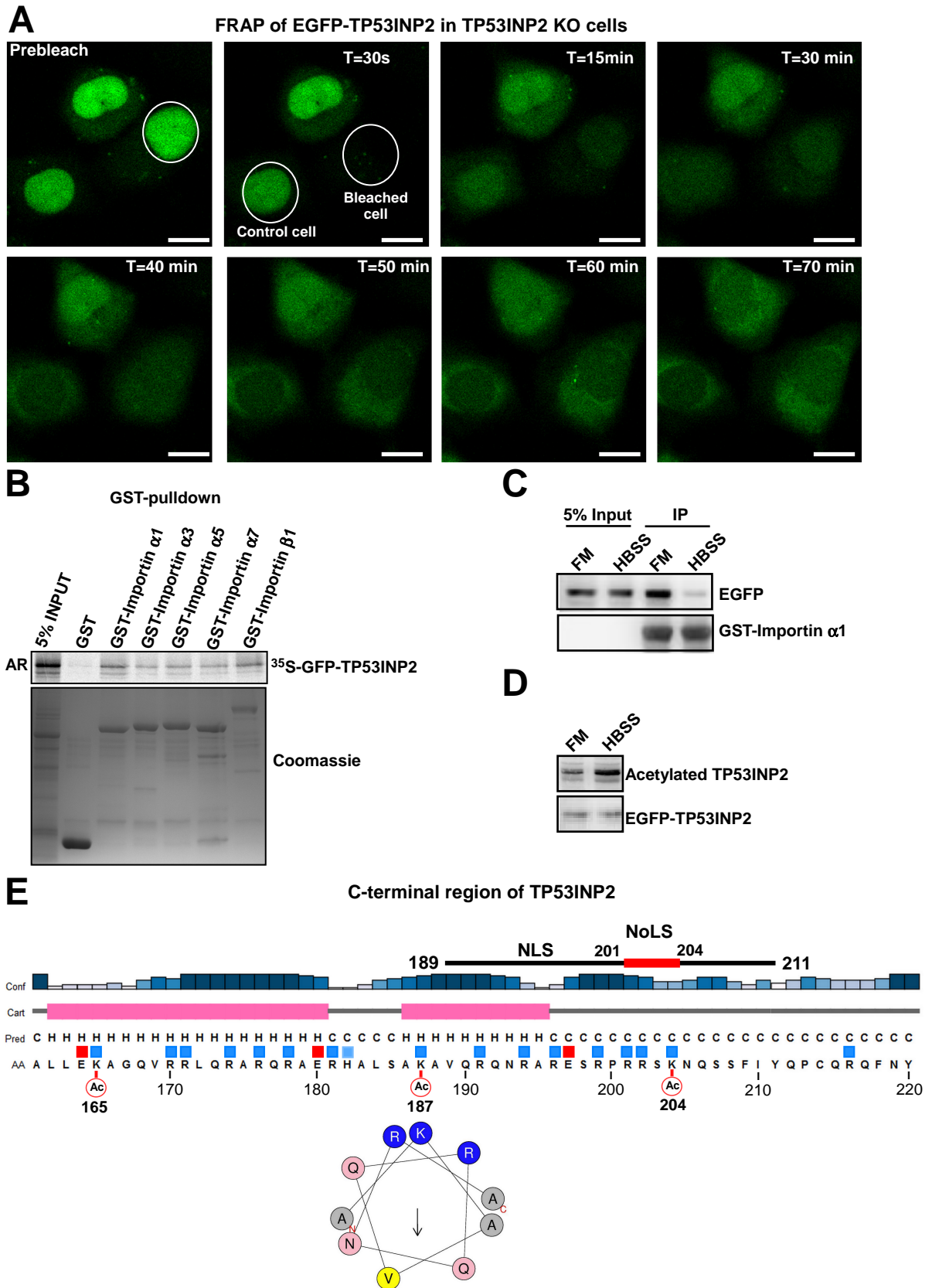
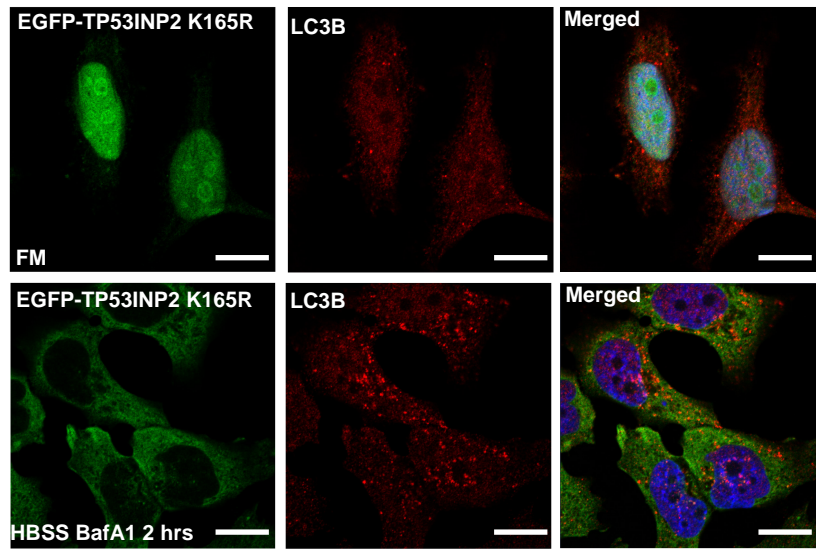
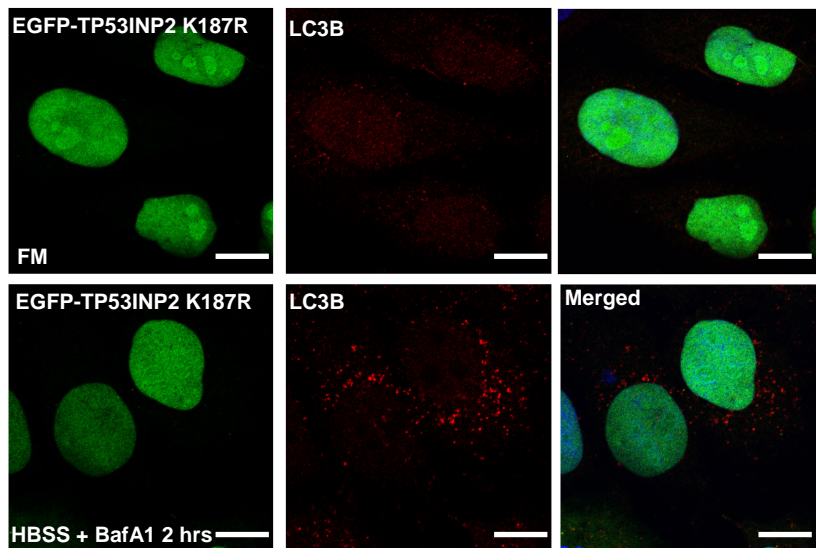


Figure 7

A



B



C

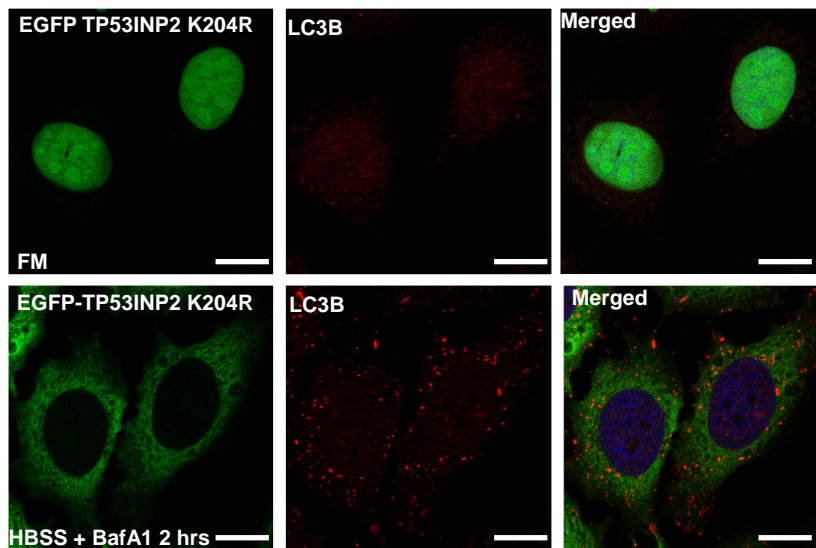
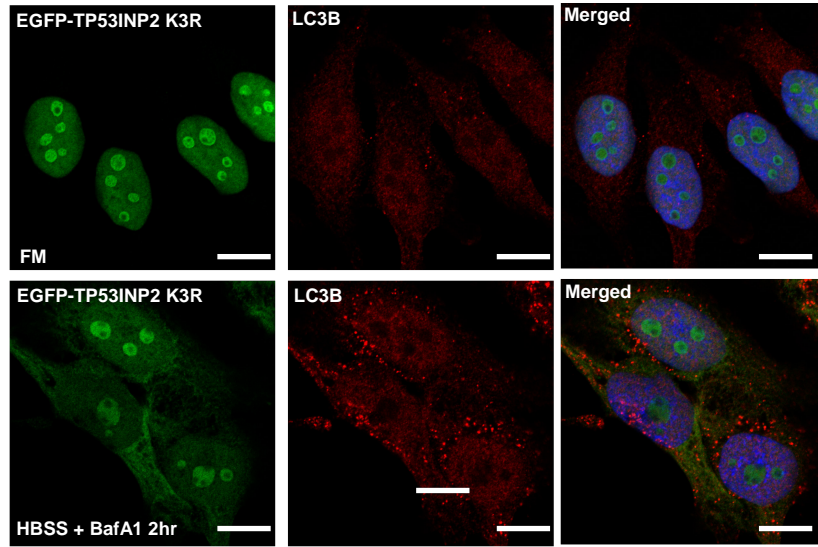


Figure 8

A



B

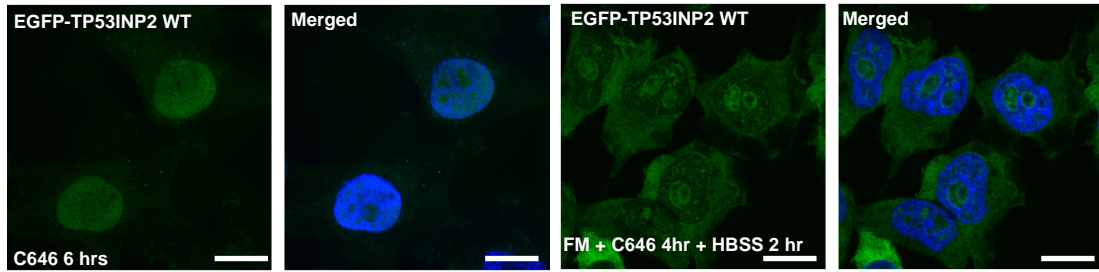
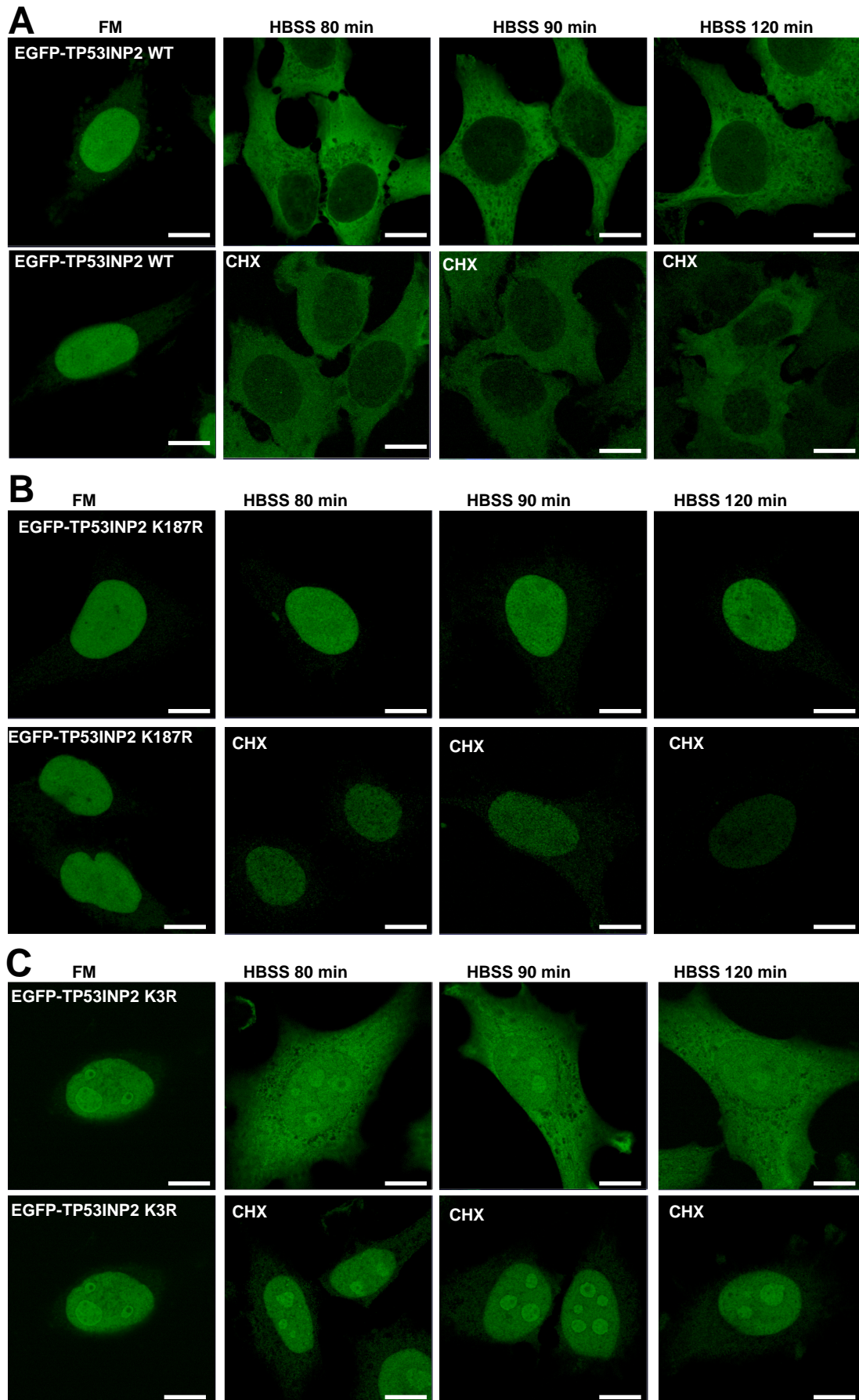


Figure 9



SUPPLEMENTAL FIGURE LEGENDS

Supplementary Figure S1: Generation of CRISPR/CAS9-mediated HeLa FlpIn TP53INP1 and TP53INP2 KO cells: (A and B) Genomic sequences of indicated TP53INP1 and TP53INP2 exons targeted by guide RNAs. Shown are the sequences of two mutated alleles in TP53INP1 KO clone 19 (A) and two mutated alleles in TP53INP2 clone 10 (B). For each clone, more than 10 sequences were analyzed, and only two different alleles were identified.

Supplementary Figure S2: Effects on autophagic flux and cell proliferation by knock-out of TP53INP1 or TP53INP2 in HeLa FlpIn cells: (A and B) Western blot analysis of NBR1, p62, NDP52, GABARAP and LC3B in lysates from the indicated cell lines treated or not with HBSS and/or bafilomycin A1 (Baf.) as indicated. (C) Proliferation curves of WT and TP53INP2 KO cell lines (number of analyzed cells seeded are indicated). The diagram represents one of three biological replicates. (D) Relative level of 47S rRNA in WT and TP53INP2 KO cell lines. (E) Confocal fluorescence microscopy analysis of EGFP-TP53INP2 in reconstituted HeLa FlpIn TP53INP2 KO cells after treatment with the mTOR inhibitor Torin 1 for 6 h. Endogenous p62 and LC3B were detected by immuno-fluorescence. Scale bars, 10 μm .

Supplementary Figure S3: Transiently transfected EGFP-TP53INP2 co-localize with LC3B in puncta: HeLa FlpIn cells transiently transfected with EGFP-TP53INP2 were subjected to the indicated treatments and analyzed by confocal fluorescence microscopy 24 h after transfection. LC3B was detected with LC3B antibodies. Scale bars, 10 μm .

Supplementary Figure S4: The nucleocytoplasmic redistribution of TP52INP2 upon starvation is independent of its LIR and predicted NES motifs: (A and B) HeLa FlpIn TP53INP2 KO cells stably reconstituted with the indicated EGFP-TP53INP2 constructs were treated as indicated, stained with LC3B antibodies, and analyzed by confocal fluorescence microscopy. Scale bars, 10 μm .

Supplementary Figure S5: Mass spectrometry spectra showing acetylation. HeLa FlpIn cells stably expressing EGFP-TP53INP2 cells were treated with HBSS for 2 hours. Cells were lysed and EGFP-TP53INP2 immunoprecipitated using EGFP magnetic beads. Following SDS-PAGE the bands corresponding to EGFP-TP53INP2 were precisely cut out and subjected to in-gel reduction, alkylation, and endopeptidase digestion using 4 ng/ μ l of Arg-C before sample clean up and MS analyses (see Materials and methods). **(A-F)** Tables of MS2 fragment matches and MS2 spectra of the acetylated peptides showing acetylation on K165, K187 and K204. **(A, B)** ETD fragmented 3+ m/z 399.908 peptide showing the K165 acetylation. **(C, D)** CID fragmented 2+ m/z 561.822 peptide showing the K187 acetylation. **(E, F)** CID fragmented 2+ m/z 892.922 peptide showing the K204 acetylation.

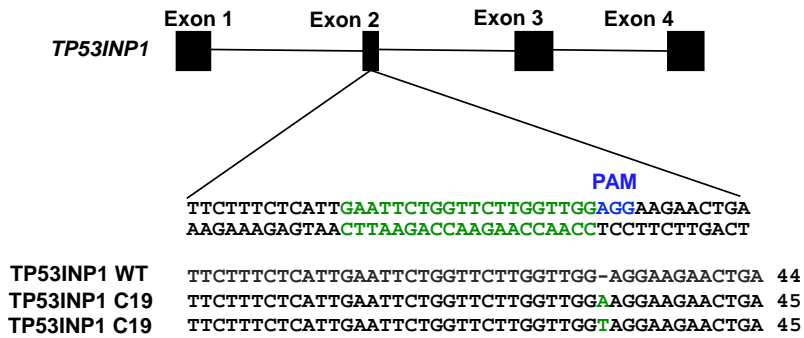
Supplementary Figure S6: Deletion of serine-threonine residues have no effect on nucleocytoplasmic shuttling of TP53INP2. **(A)** TP53INP2 amino acid sequence indicating mutated serine residues and the extension of systematic deletions done to identify essential serine or threonine residues. **(B-J)** Confocal fluorescence microscopy of HeLa FlpIn TP53INP2 KO cells stably expressing the indicated EGFP-TP53INP2 point mutant or deletion constructs, treated as indicated and stained with p62 and LC3B antibodies. Scale bars, 10 μ m.

Supplementary Figure S7: Model explaining the observed regulation of subcellular localization and degradation of TP53INP2. **(A)** In full medium TP53INP2 is completely nuclear and degraded by a nucleolar proteasomal pathway. **(B)** In response to starvation or mTOR inactivation, acetylation of K187 in TP53INP2 by CBP/p300 inhibits the nuclear import and this results in a stabilization and cytoplasmic accumulation of the protein. Simultaneously there is a rapid degradation of nuclear TP53INP2.

Supplementary Figure S1

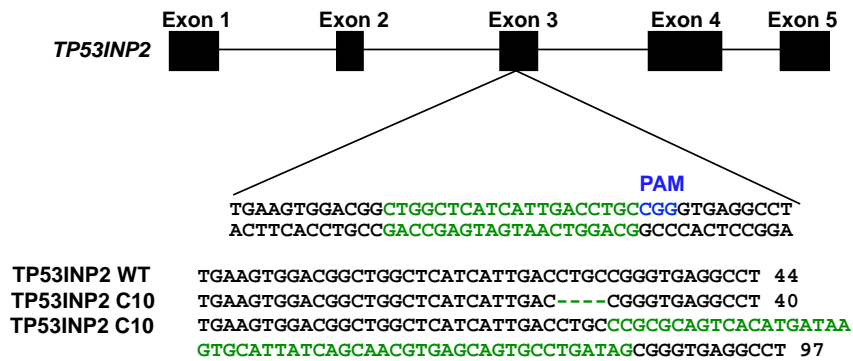
A

CRISPR/CAS9 KO of *TP53INP1* in HeLa FlpIn cells

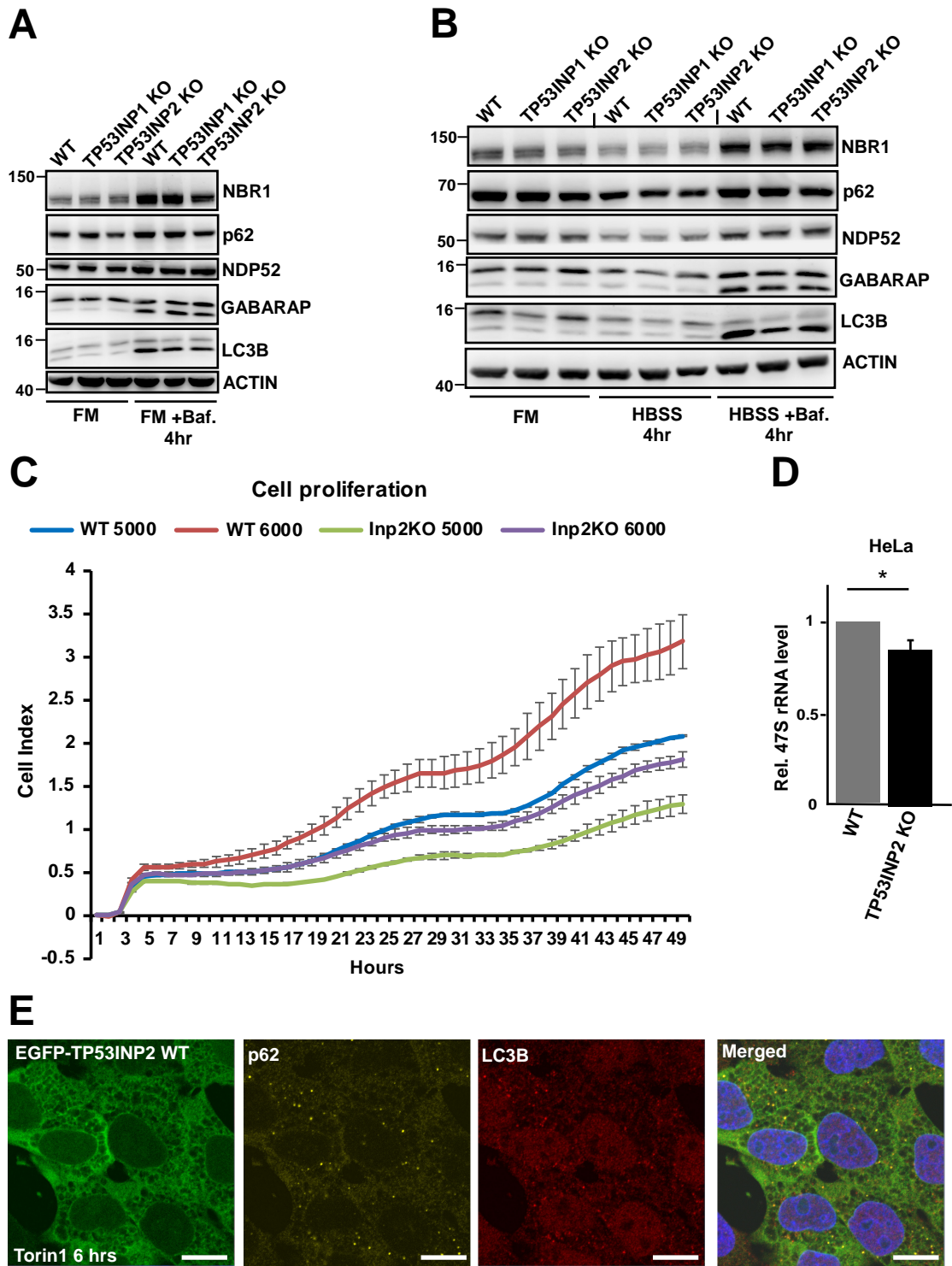


B

CRISPR/CAS9 KO of *TP53INP2* in HeLa FlpIn cells

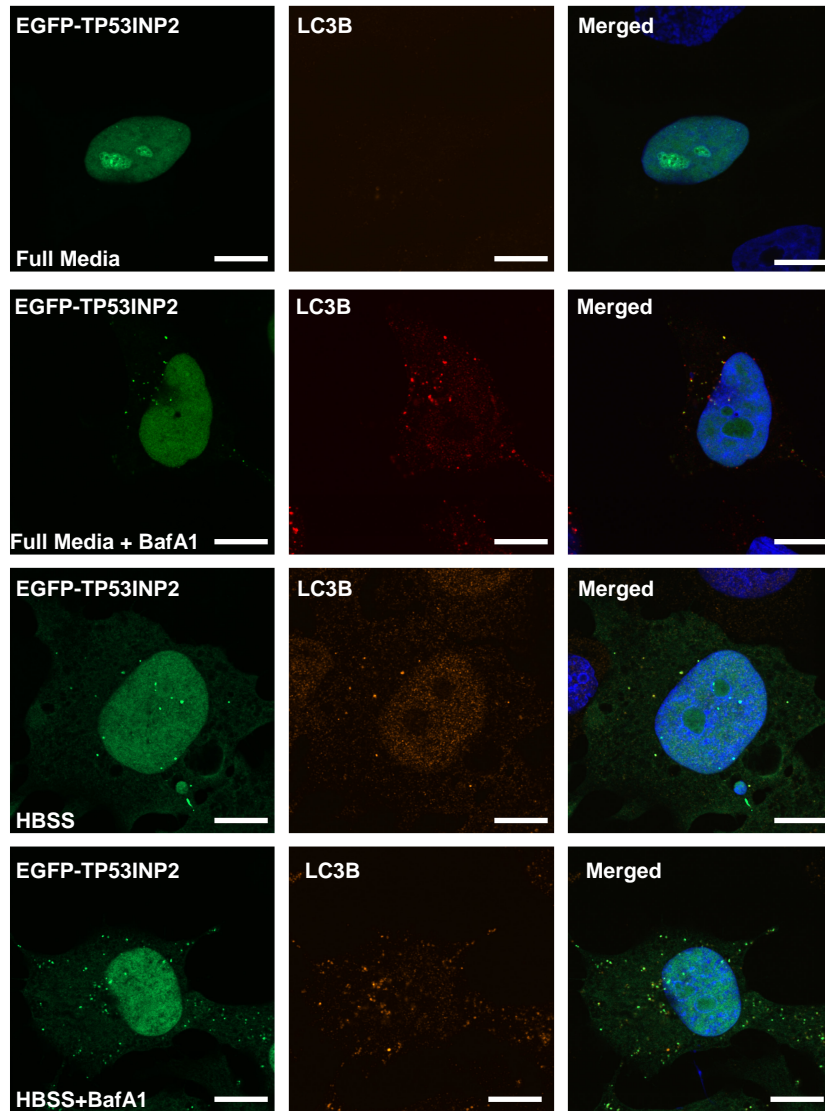


Supplementary Figure S2



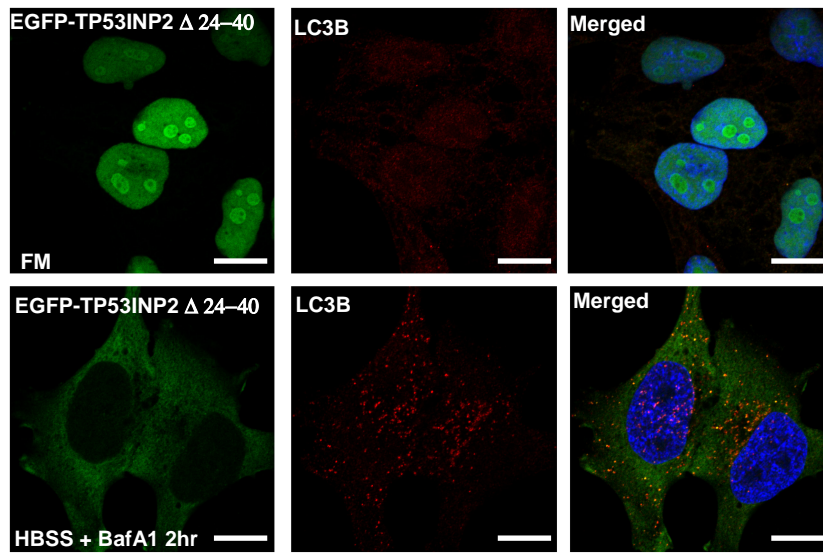
Supplementary Figure S3

Transient over-expression of EGFP-TP53INP2 in HeLa cells

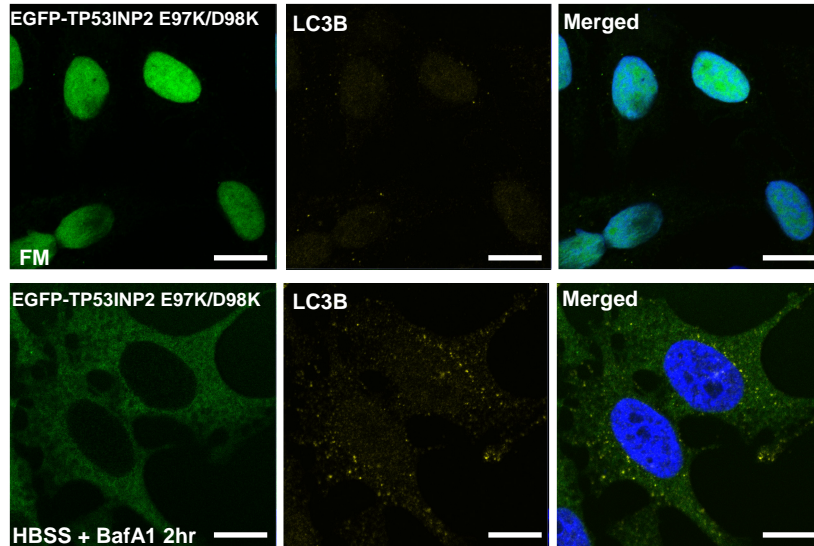


Supplementary Figure S4

A



B



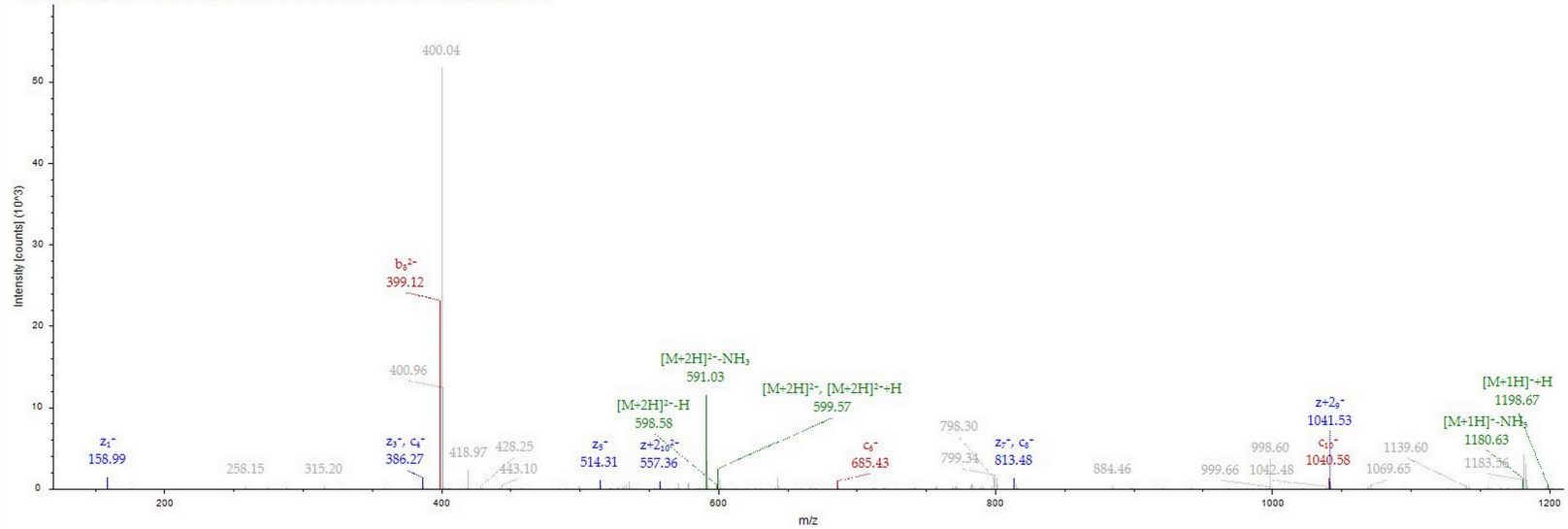
Supplementary Figure S5

A

| #1 | a ⁺ | a ²⁺ | b ⁺ | b ²⁺ | c ⁺ | c ²⁺ | Seq. | y ⁺ | y ²⁺ | z ⁺ | z ²⁺ | z+2 ⁺ | z+2 ²⁺ | #2 |
|----|----------------|-----------------|----------------|-----------------|----------------|-----------------|----------|----------------|-----------------|----------------|-----------------|------------------|-------------------|----|
| 1 | 44.04948 | 22.52838 | 72.04439 | 36.52583 | 89.07094 | 45.03911 | A | | | | | | | 11 |
| 2 | 115.08659 | 58.04693 | 143.08150 | 72.04439 | 160.10805 | 80.55766 | A | 1126.65788 | 563.83258 | 1110.63916 | 555.82322 | 1112.65481 | 556.83104 | 10 |
| 3 | 228.17065 | 114.58897 | 256.16557 | 128.58642 | 273.19212 | 137.09970 | L | 1055.62077 | 528.31402 | 1039.60205 | 520.30466 | 1041.61770 | 521.31249 | 9 |
| 4 | 341.25472 | 171.13100 | 369.24963 | 185.12845 | 386.27618 | 193.64173 | L | 942.53671 | 471.77199 | 926.51798 | 463.76263 | 928.53363 | 464.77045 | 8 |
| 5 | 470.29731 | 235.65229 | 498.29223 | 249.64975 | 515.31877 | 258.16303 | E | 829.45264 | 415.22996 | 813.43392 | 407.22060 | 815.44957 | 408.22842 | 7 |
| 6 | 640.40284 | 320.70506 | 668.39775 | 334.70251 | 685.42430 | 343.21579 | K-Acetyl | 700.41005 | 350.70866 | 684.39132 | 342.69930 | 686.40697 | 343.70713 | 6 |
| 7 | 711.43995 | 356.22361 | 739.43487 | 370.22107 | 756.46142 | 378.73435 | A | 530.30452 | 265.65590 | 514.28580 | 257.64654 | 516.30145 | 258.65436 | 5 |
| 8 | 768.46142 | 384.73435 | 796.45633 | 398.73180 | 813.48288 | 407.24508 | G | 459.26741 | 230.13734 | 443.24868 | 222.12798 | 445.26433 | 223.13580 | 4 |
| 9 | 896.51999 | 448.76363 | 924.51491 | 462.76109 | 941.54146 | 471.27437 | Q | 402.24594 | 201.62661 | 386.22722 | 193.61725 | 388.24287 | 194.62507 | 3 |
| 10 | 995.58841 | 498.29784 | 1023.58332 | 512.29530 | 1040.60987 | 520.80857 | V | 274.18737 | 137.59732 | 258.16864 | 129.58796 | 260.18429 | 130.59578 | 2 |
| 11 | | | | | | | R | 175.11895 | 88.06311 | 159.10023 | 80.05375 | 161.11588 | 81.06158 | 1 |

B

181129_1209_BS_HBSS_EDT.raw #20194 RT: 49.7710 min
 ITMS: 399.9022@eld52.36, z=3, Mono m/z=399.90222 Da, MH+=1197.69211 Da, Match Tol.=0.6 Da



Supplementary Figure S5

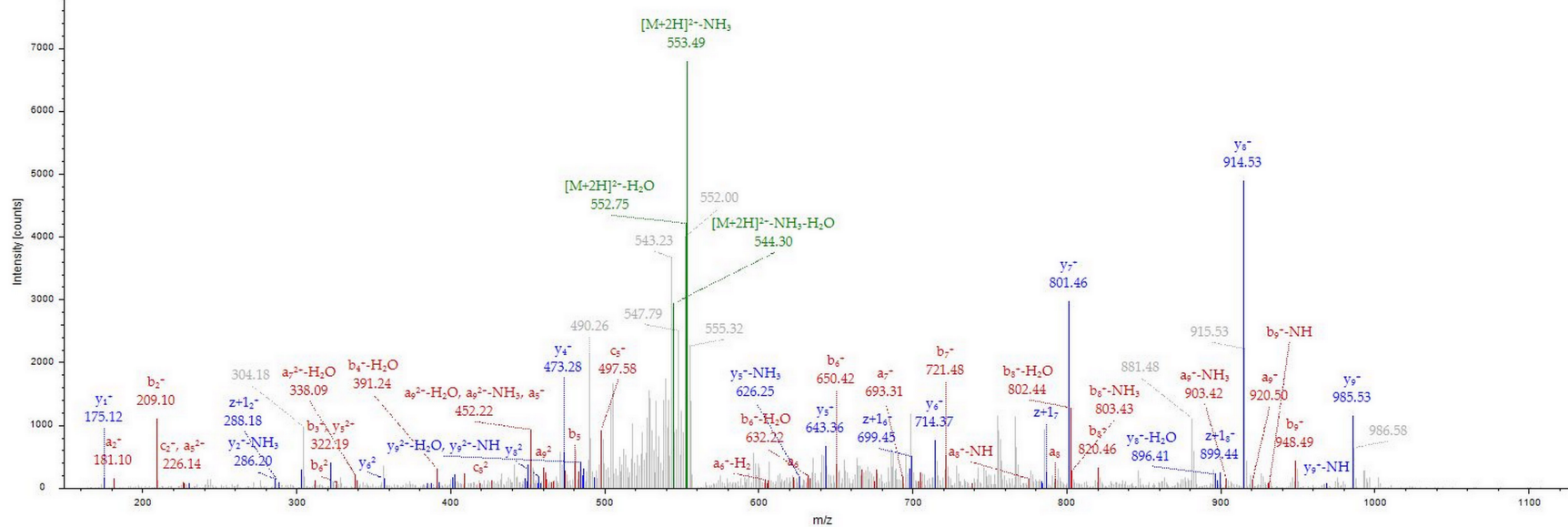
C

| #1 | a ⁺ | a ²⁺ | b ⁺ | b ²⁺ | c ⁺ | c ²⁺ | Seq | y ⁺ | y ²⁺ | z+1 ⁺ | z+1 ²⁺ | #2 |
|----|----------------|-----------------|----------------|-----------------|----------------|-----------------|--------------|----------------|-----------------|------------------|-------------------|----|
| 1 | 60.04439 | 30.52583 | 88.03930 | 44.52329 | 105.06585 | 53.03657 | S | | | | | 14 |
| 2 | 230.14992 | 115.57860 | 258.14483 | 129.57605 | 275.17138 | 138.08933 | K-Acetyl | 1697.80642 | 849.40685 | 1682.79552 | 841.90140 | 13 |
| 3 | 344.19285 | 172.60006 | 372.18776 | 186.59752 | 389.21431 | 195.11079 | N | 1527.70089 | 764.35408 | 1512.68999 | 756.84863 | 12 |
| 4 | 472.25142 | 236.62935 | 500.24634 | 250.62681 | 517.27289 | 259.14008 | Q | 1413.65796 | 707.33262 | 1398.64706 | 699.82717 | 11 |
| 5 | 559.28345 | 280.14536 | 587.27837 | 294.14282 | 604.30492 | 302.65610 | S | 1285.59938 | 643.30333 | 1270.58848 | 635.79788 | 10 |
| 6 | 646.31548 | 323.66138 | 674.31039 | 337.65884 | 691.33694 | 346.17211 | S | 1198.56735 | 599.78732 | 1183.55645 | 592.28187 | 9 |
| 7 | 793.38389 | 397.19559 | 821.37881 | 411.19304 | 838.40536 | 419.70632 | F | 1111.53533 | 556.27130 | 1096.52443 | 548.76585 | 8 |
| 8 | 906.46796 | 453.73762 | 934.46287 | 467.73507 | 951.48942 | 476.24835 | I | 964.46691 | 482.73709 | 949.45601 | 475.23164 | 7 |
| 9 | 1069.53129 | 535.26928 | 1097.52620 | 549.26674 | 1114.55275 | 557.78001 | Y | 851.38285 | 426.19506 | 836.37195 | 418.68961 | 6 |
| 10 | 1197.58986 | 599.29857 | 1225.58478 | 613.29603 | 1242.61133 | 621.80930 | Q | 688.31952 | 344.66340 | 673.30862 | 337.15795 | 5 |
| 11 | 1294.64263 | 647.82495 | 1322.63754 | 661.82241 | 1339.66409 | 670.33568 | P | 560.26094 | 280.63411 | 545.25004 | 273.12866 | 4 |
| 12 | 1454.67328 | 727.84028 | 1482.66819 | 741.83773 | 1499.69474 | 750.35101 | Carbamidomet | 463.20818 | 232.10773 | 448.19728 | 224.60228 | 3 |
| 13 | 1582.73185 | 791.86956 | 1610.72677 | 805.86702 | 1627.75332 | 814.38030 | Q | 303.17753 | 152.09240 | 288.16663 | 144.58695 | 2 |
| 14 | | | | | | | R | 175.11895 | 88.06311 | 160.10805 | 80.55766 | 1 |

D

190108_0201_PTM2_ETD.raw #3083 RT: 12.7838 min
 ITMS, 561.8216@cid30.00, z=+2, Mono m/z=561.82159 Da, MH+=1122.63591 Da, Match Tol.=0.6 Da

K187-Acetyl

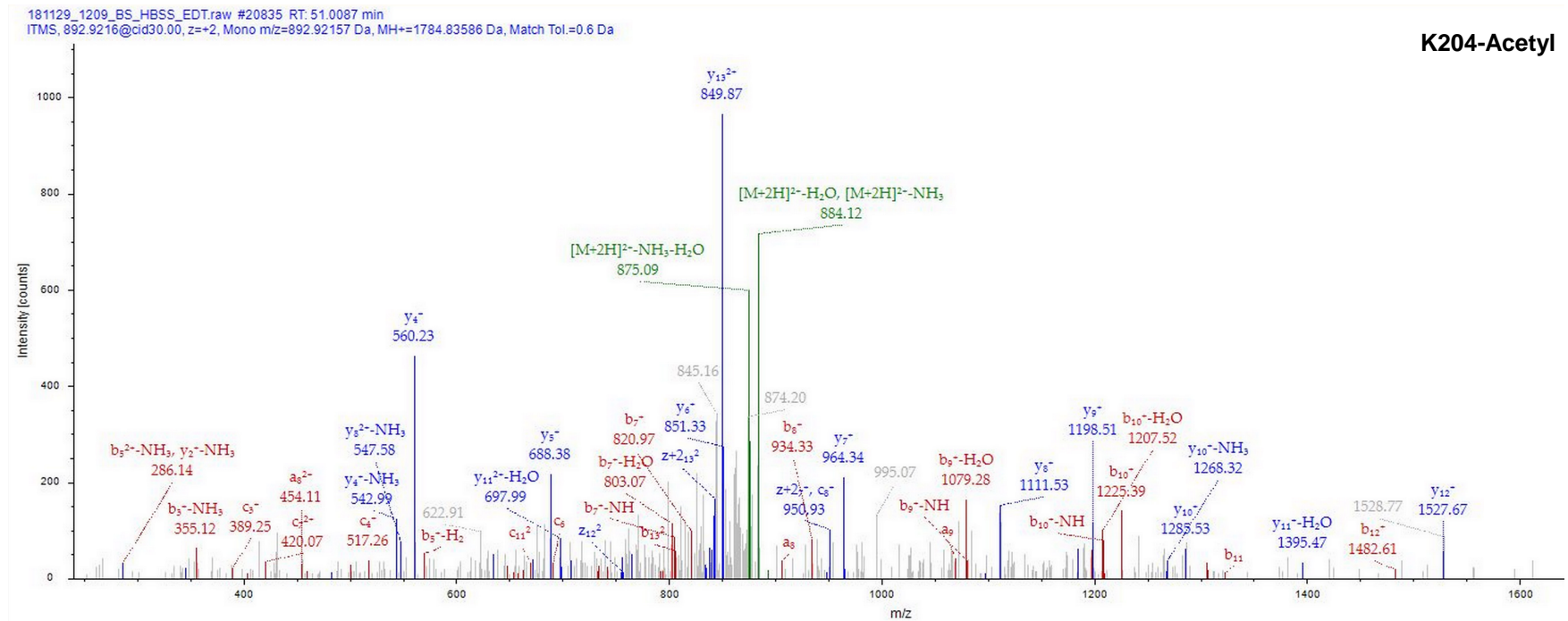


Supplementary Figure S5

E

| #1 | a ⁺ | a ²⁺ | b ⁺ | b ²⁺ | c ⁺ | c ²⁺ | Seq. | y ⁺ | y ²⁺ | z ⁺ | z ²⁺ | z+2 ⁺ | z+2 ²⁺ | #2 |
|----|----------------|-----------------|----------------|-----------------|----------------|-----------------|--------------|----------------|-----------------|----------------|-----------------|------------------|-------------------|----|
| 1 | 60.04439 | 30.52583 | 88.03930 | 44.52329 | 105.06585 | 53.03657 | S | | | | | | | 14 |
| 2 | 230.14992 | 115.57860 | 258.14483 | 129.57605 | 275.17138 | 138.08933 | K-Acetyl | 1697.80642 | 849.40685 | 1681.78769 | 841.39748 | 1683.80334 | 842.40531 | 13 |
| 3 | 344.19285 | 172.60006 | 372.18776 | 186.59752 | 389.21431 | 195.11079 | N | 1527.70089 | 764.35408 | 1511.68216 | 756.34472 | 1513.69781 | 757.35254 | 12 |
| 4 | 472.25142 | 236.62935 | 500.24634 | 250.62681 | 517.27289 | 259.14008 | Q | 1413.65796 | 707.33262 | 1397.63924 | 699.32326 | 1399.65489 | 700.33108 | 11 |
| 5 | 559.28345 | 280.14536 | 587.27837 | 294.14282 | 604.30492 | 302.65610 | S | 1285.59938 | 643.30333 | 1269.58066 | 635.29397 | 1271.59631 | 636.30179 | 10 |
| 6 | 646.31548 | 323.66138 | 674.31039 | 337.65884 | 691.33694 | 346.17211 | S | 1198.56735 | 599.78732 | 1182.54863 | 591.77795 | 1184.56428 | 592.78578 | 9 |
| 7 | 793.38389 | 397.19559 | 821.37881 | 411.19304 | 838.40536 | 419.70632 | F | 1111.53533 | 556.27130 | 1095.51660 | 548.26194 | 1097.53225 | 549.26976 | 8 |
| 8 | 906.46796 | 453.73762 | 934.46287 | 467.73507 | 951.48942 | 476.24835 | I | 964.46691 | 482.73709 | 948.44819 | 474.72773 | 950.46384 | 475.73556 | 7 |
| 9 | 1069.53129 | 535.26928 | 1097.52620 | 549.26674 | 1114.55275 | 557.78001 | Y | 851.38285 | 426.19506 | 835.36412 | 418.18570 | 837.37977 | 419.19353 | 6 |
| 10 | 1197.58986 | 599.29857 | 1225.58478 | 613.29603 | 1242.61133 | 621.80930 | Q | 688.31952 | 344.66340 | 672.30080 | 336.65404 | 674.31645 | 337.66186 | 5 |
| 11 | 1294.64263 | 647.82495 | 1322.63754 | 661.82241 | 1339.66409 | 670.33568 | P | 560.26094 | 280.63411 | 544.24222 | 272.62475 | 546.25787 | 273.63257 | 4 |
| 12 | 1454.67328 | 727.84028 | 1482.66819 | 741.83773 | 1499.69474 | 750.35101 | Carbamidomet | 463.20818 | 232.10773 | 447.18945 | 224.09837 | 449.20510 | 225.10619 | 3 |
| 13 | 1582.73185 | 791.86956 | 1610.72677 | 805.86702 | 1627.75332 | 814.38030 | Q | 303.17753 | 152.09240 | 287.15881 | 144.08304 | 289.17446 | 145.09087 | 2 |
| 14 | | | | | | | R | 175.11895 | 88.06311 | 159.10023 | 80.05375 | 161.11588 | 81.06158 | 1 |

F



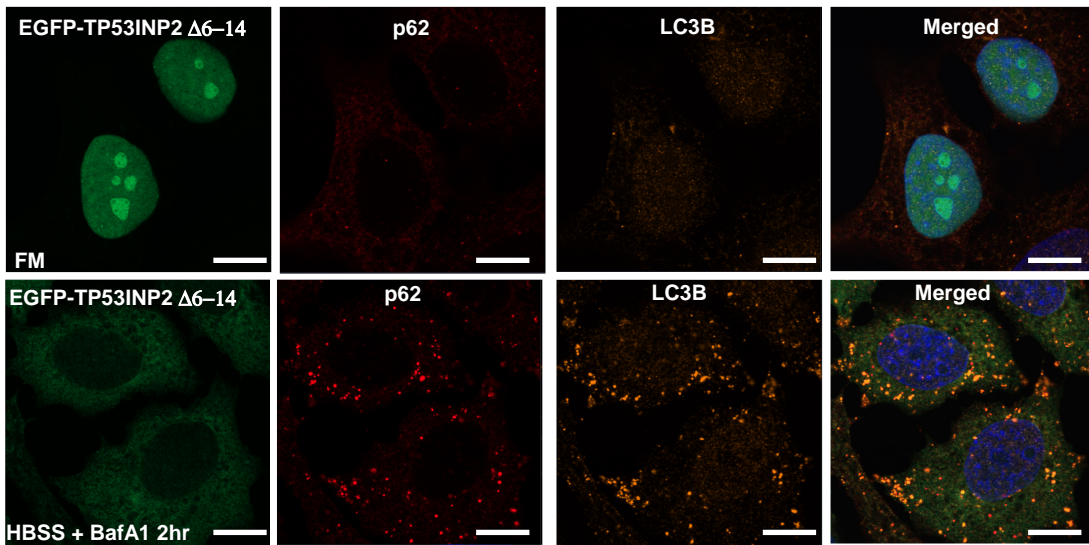
Supplementary Figure S6

A Deletions and point mutations of S and T residues in TP53INP2

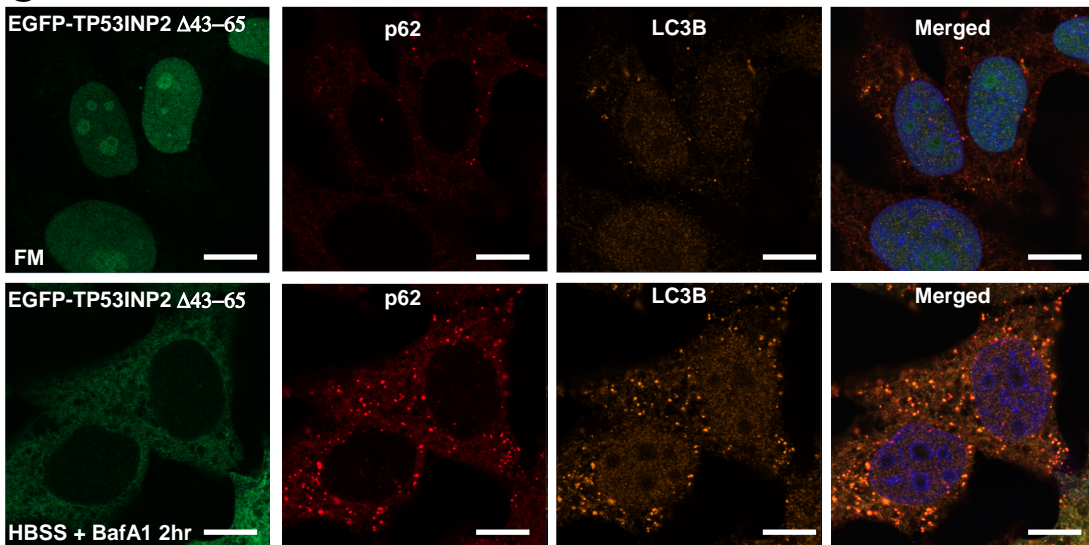
```

TP53INP2_HUMAN  MFQRLSSLFF STPSPPEDPD CPRAFVSEED EVDGWL IIDL PDSYAAPPSP
                Δ 6-14      20      Δ 24-40      40      Δ 43-65
TP53INP2_HUMAN  GAAPAPAGRP PPAPSLMDES WFTTPACFT AEGPGLGPAR LQSSPLEDLL
                Δ 43-65      80      Δ 70-80      80      Δ 93-114      100
TP53INP2_HUMAN  IEHPSMSVYV TGSTIVLEPG SPSPLPDAAL PDGDLSEGE LTPARREPRAA
                Δ 93-114      120      Δ 121-141      140
TP53INP2_HUMAN  RHAAPL PARA ALLEKAGQVR RLQRRARQRAE RHALSAKAVQ RQNRARESRP
                160      180      A      200
TP53INP2_HUMAN  RRSKNQSSF I YQPCQRQFN Y
                A AA      220
    
```

B

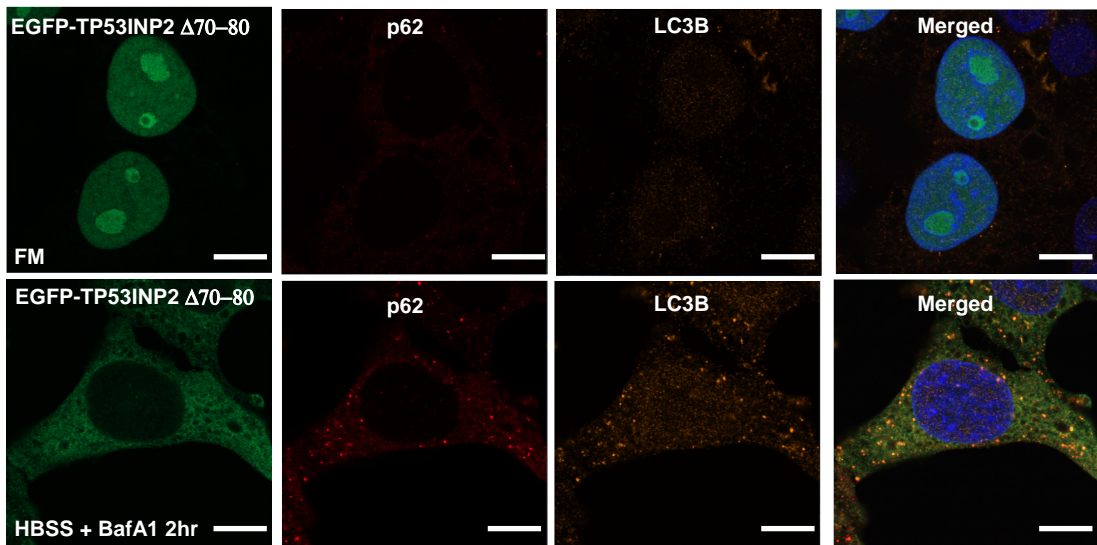


C

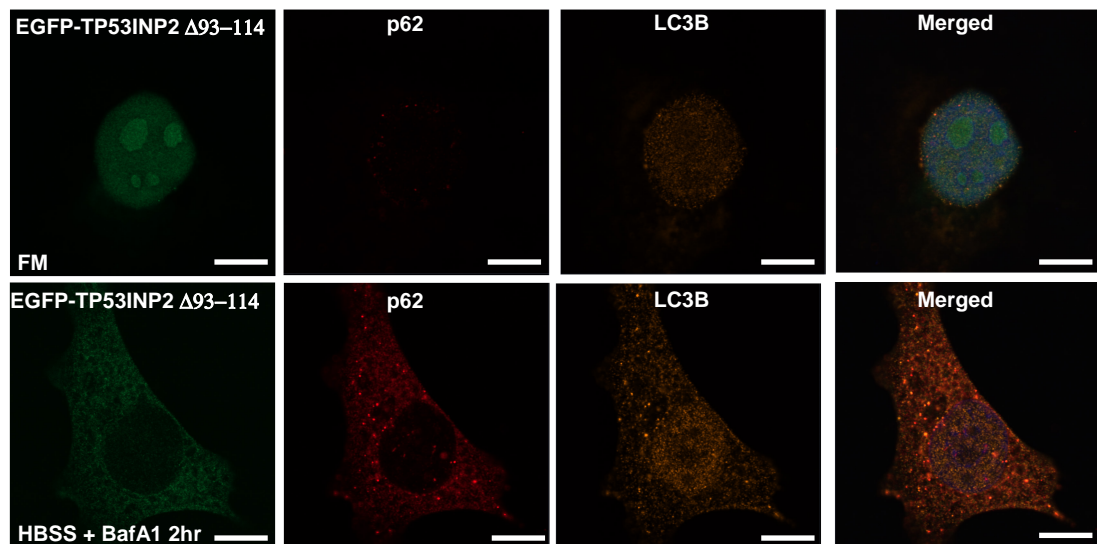


Supplementary Figure S6 - continued

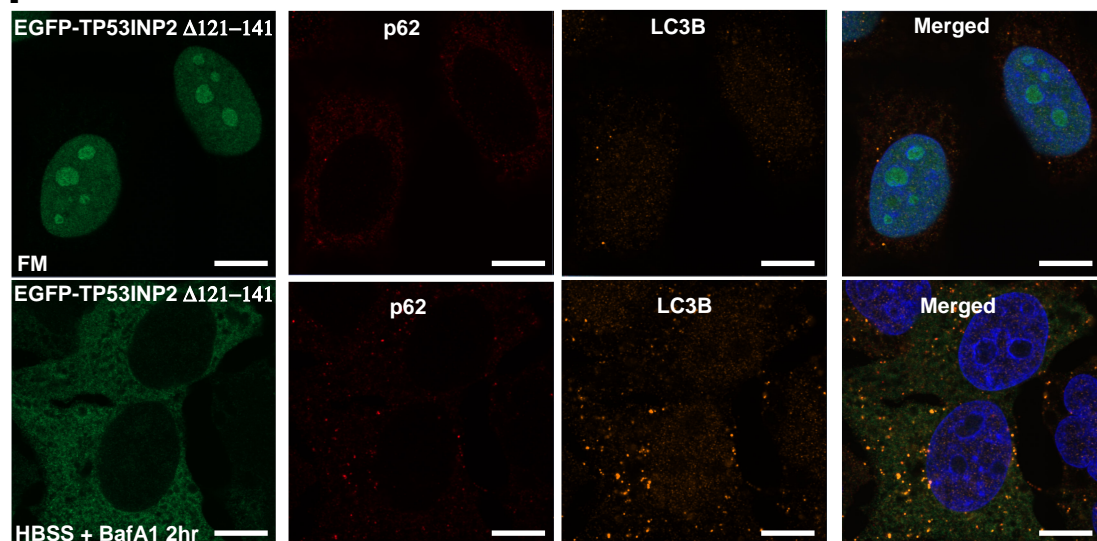
D



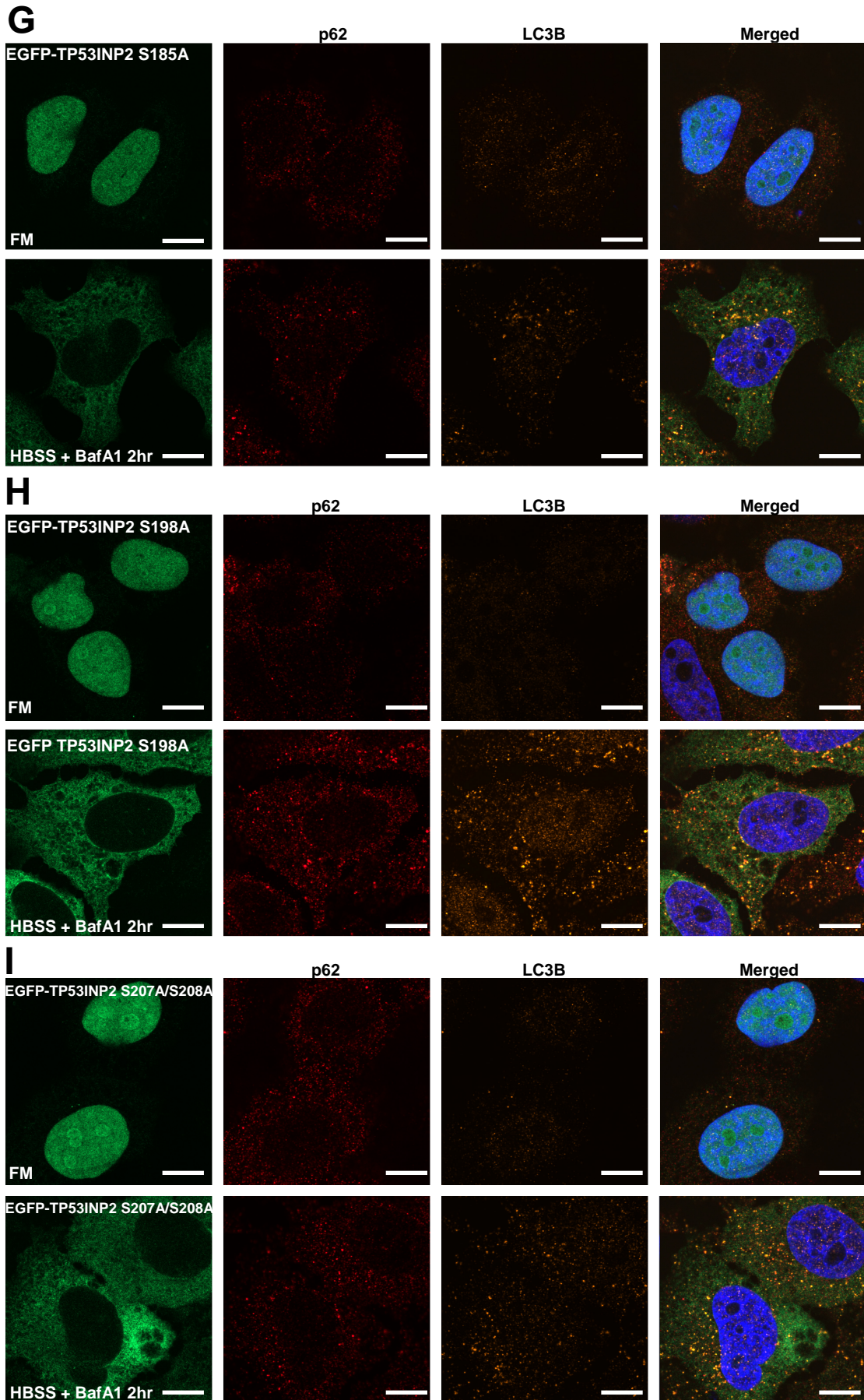
E



F

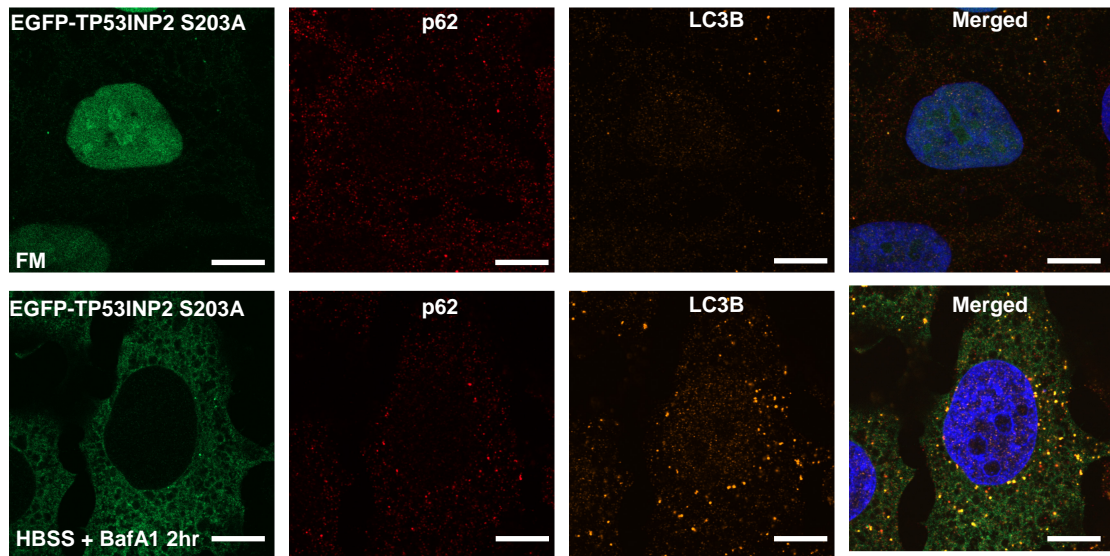


Supplementary Figure S6 - continued

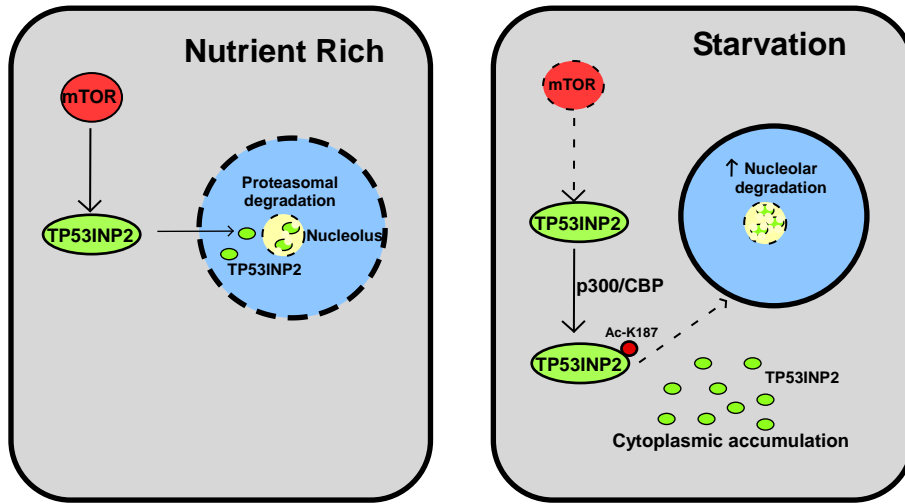


Supplementary Figure S6 - continued

J



Supplementary Figure S7



BASIC RESEARCH PAPER

ATG4B contains a C-terminal LIR motif important for binding and efficient cleavage of mammalian orthologs of yeast Atg8

Mads Skytte Rasmussen^a, Stéphane Mouilleron^b, Birendra Kumar Shrestha^a, Martina Wirth^c, Rebecca Lee^b, Kenneth Bowitz Larsen^a, Yakubu Abudu Princely^a, Nicola O'Reilly^d, Eva Sjøttem^a, Sharon A. Tooze^{ib,c}, Trond Lamark^a, and Terje Johansen^{id,a}

^aMolecular Cancer Research Group, Department of Medical Biology, University of Tromsø – The Arctic University of Norway, Tromsø, Norway; ^bStructural Biology, The Francis Crick Institute, London, UK; ^cMolecular Cell Biology of Autophagy Laboratory, The Francis Crick Institute, London, UK; ^dPeptide Chemistry Science Technology Platform, The Francis Crick Institute, London, UK

ABSTRACT

The cysteine protease ATG4B cleaves off one or more C-terminal residues of the inactive proform of proteins of the ortholog and paralog LC3 and GABARAP subfamilies of yeast Atg8 to expose a C-terminal glycine that is conjugated to phosphatidylethanolamine during autophagosome formation. We show that ATG4B contains a C-terminal LC3-interacting region (LIR) motif important for efficient binding to and cleavage of LC3 and GABARAP proteins. We solved the crystal structures of the GABARAP1-ATG4B C-terminal LIR complex. Analyses of the structures and in vitro binding assays, using specific point mutants, clearly showed that the ATG4B LIR binds via electrostatic-, aromatic HP1 and hydrophobic HP2 pocket interactions. Both these interactions and the catalytic site-substrate interaction contribute to binding between LC3s or GABARAPs and ATG4B. We also reveal an unexpected role for ATG4B in stabilizing the unlipidated forms of GABARAP and GABARAP1. In mouse embryonic fibroblast (MEF) *atg4b* knockout cells, GABARAP and GABARAP1 were unstable and degraded by the proteasome. Strikingly, the LIR motif of ATG4B was required for stabilization of the unlipidated forms of GABARAP and GABARAP1 in cells.

ARTICLE HISTORY

Received 24 June 2016
Revised 10 January 2017
Accepted 23 January 2017

KEYWORDS





ATG4; autophagy; GABARAP; GABARAP1; LC3B; LIR; peptide arrays; X-ray structure


Introduction

Macroautophagy (hereafter referred to as autophagy) is an evolutionarily conserved pathway for lysosome-mediated degradation of cytosolic components.¹ The autophagic pathway begins morphologically with formation of a crescent shaped double-membrane structure, the phagophore,² which expands and wraps around the cytoplasmic content targeted for degradation closing upon itself to form the autophagosome.³ The content may either be bulk cytoplasm or protein aggregates, specific macromolecules or organelles specifically recruited via selective autophagy receptors.^{4,5} The autophagosomes may fuse with late endosomes, forming amphisomes,⁶ before ultimately maturing by fusion with lysosomes.⁷ Pioneering genetic studies in yeast revealed 14 AuTophagy-related (*ATG*) genes (*ATG1* to *ATG14*) essential for autophagy.⁸ The list has grown to 18 *Atg* proteins essential for autophagosome formation.³ These *Atg* proteins are classified into 5 functional groups including: the *Atg1* kinase complex, the autophagy-specific phosphatidylinositol 3-kinase complex, the *Atg8*-lipid- and *Atg12*-*Atg5* conjugation systems, the *Atg2*-*Atg18* complex and the transmembrane protein *Atg9*.⁹ Please note that *Atg8* follows yeast nomenclature in the description of proteins. In other models and species, there are several other orthologs and

paralogs of yeast *Atg8*. However, for the sake of simplicity we use the term “*Atg8*-family” to denote orthologs and paralogs of yeast *Atg8*, in other species. Over 40 *Atg* proteins are now known in yeast, most of which have orthologs in higher eukaryotes.⁹ Except for some regulatory components, these are conserved during evolution from yeast to man.

The mammalian *Atg8*-family proteins contain a ubiquitin-like core and a distinct N-terminal arm with 2 short α -helices. The mammalian orthologs of yeast *Atg8* have 7 members divided into 2 major subfamilies: MAP1LC3/LC3 (microtubule-associated protein 1 light chain 3) A, B, B2 and C and GABARAP (gamma-aminobutyric acid receptor associated protein), GABARAP1 (gamma-aminobutyric acid [GABA] A receptor-associated protein-like 1) and GABARAP2.¹⁰ The LC3-subfamily and GABARAP-subfamily proteins are anchored to the inner and outer membrane of the phagophore through lipidation to phosphatidylethanolamine (PE).^{11,12} The *Atg8*-family proteins are involved in recruitment of cargo proteins,^{4,5} proteins involved in the autophagy pathway, and regulatory proteins.¹³ The *Atg8* family is also involved in the expansion,¹⁴ and closure of the phagophore.¹⁵ Newly synthesized mammalian *Atg8*-family proteins contain a C-terminal

CONTACT Trond Lamark  trond.lamark@uit.no  Molecular Cancer Research Group, Department of Medical Biology, University of Tromsø - The Arctic University of Norway, 9037 Tromsø, Norway; Terje Johansen  terje.johansen@uit.no  Molecular Cancer Research Group, Department of Medical Biology, University of Tromsø - The Arctic University of Norway, 9037 Tromsø, Norway

 Supplemental data for this article can be accessed on the publisher's website.

stretch of residues shielding a C-terminal glycine essential for lipidation. The glycine is exposed by cleavage of the LC3 and GABARAP proteins of the Atg8-family through the action of the cysteine protease ATG4, forming the active form-I variants (LC3-I and GABARAP-I).¹¹ Through interaction with ATG7 (E1-like enzyme), ATG3 (E2-like enzyme) and finally the ATG12-ATG5-ATG16L1 complex (E3-like), the LC3-I and GABARAP-I proteins undergo a covalent conjugation to PE, resulting in lipidated species (form-II) of the Atg8-family, tethered to the phagophore (e.g., LC3-II and GABARAP-II). ATG4 can subsequently cleave LC3-II or GABARAP-II proteins off the outer membrane, stripping the autophagosome of its coat of Atg8-family proteins and in the process restoring the LC3-I or GABARAP-I forms.^{16,17}

A growing number of proteins have been shown to interact with the LC3 and GABARAP subfamilies through the sequence motif named the LC3-interacting region (LIR).^{5,13,18} The core LIR motif, [W/F/Y]xx[L/I/V], is often preceded by a stretch of acidic residues.^{13,19} The region immediately N-terminal to the core LIR may also harbor phosphorylatable serine or threonine residues. Phosphorylation of such residues has been shown to regulate binding of optineurin and several mitophagy receptors.^{20,21} The LIR motif provides specificity for the autophagic process and can mediate binding with cargo proteins or proteins important for the regulation of autophagy.¹³ Proteins harboring an LIR motif interact with proteins of the Atg8 family through interactions with the LIR docking site (LDS). The LDS consists of 2 hydrophobic pockets, which can envelop the aromatic and aliphatic residues of the LIR. Furthermore, the N-terminal arm of Atg8-family proteins is able to make electrostatic interactions with the acidic residues (if any) preceding the LIR.^{13,22,23}

The mammalian Atg4-family consists of 4 different members (ATG4 isoforms A,B,C and D).²⁴ ATG4B, the main human ortholog, acts efficiently in both the initial cleavage and the delipidation of all proteins of the Atg8 family.²⁵⁻²⁷ ATG4A has been shown to cleave GABARAPL2 *in vitro* and *in vivo*, but does not cleave LC3B,^{26,28,29} whereas ATG4D has been reported to be important for GABARAPL1 processing *in vivo* following caspase-mediated activation.³⁰ A clear role for ATG4C has yet to be determined but a function during starvation has been reported.³¹ The cleavage of Atg8-family proteins by ATG4, and subsequent conjugation to PE provide 2 opportunities for regulating autophagy. The delipidation of Atg8-family proteins by ATG4 from the autophagosomal membrane has also been suggested as a possible regulatory step, as delipidation of the Atg8 family bound to the outer membrane may function as a prerequisite for both efficient autophagosome formation and maturation.^{16,32-34} Reactive oxygen species can directly inhibit the delipidating activity of ATG4A and ATG4B by oxidation of a noncatalytic residue near the active site.³⁵ Knockout of *Atg4b* or expression of the catalytically inactive mutant (C74S) arrests autophagy as measured by higher basal SQSTM1/p62 levels and the lack of form-II of Atg8-family proteins. On the other hand, overexpression of ATG4B also leads to arrested autophagy judged by the same measures,³⁶ indicating an inhibitory role for ATG4B in autophagy.

The crystal structure of both processed and unprocessed LC3B bound to a C-terminally truncated catalytically inert

ATG4B has been solved.³⁷ In free ATG4B, the regulatory loop masks the entrance and the N-terminal tail masks the exit to the active site. Both the regulatory loop of the active site and the N-terminal tail of ATG4B undergo large conformational changes upon binding the substrate, LC3B. This exposes the active site and allows ATG4B to access membrane bound, lipidated LC3B. Consistent with a negative regulatory role deletion of the N-terminal tail increased the *in vitro* cleavage efficiency of ATG4B. The N-terminal tail contains a putative LIR motif that in the X-ray structures was found to interact with adjacent, nonsubstrate LC3B molecules via the LDS site. This could be part of an activation mechanism to unmask the exit of the active site.³⁷

Here we show that ATG4B harbors a C-terminal LIR motif important for binding and cleavage of Atg8-family proteins with a particular role in stabilizing the unlipidated forms of GABARAP and GABARAPL1. Crystal structures of the complex of GABARAPL1 with 2 LIR peptides at 1.55- and 1.75-Å resolution reveal canonical LIR-LDS interactions with important contributions from electrostatic interactions involving residues both N-terminal to, and within, the core LIR.

Results

ATG4B contains a C-terminal LIR motif important for a strong interaction with Atg8-family orthologs

We have previously identified functional LIR motifs preferentially interacting with GABARAP subfamily proteins in ULK1 and ULK2, ATG13 and RB1CC1 of the human ULK complex.¹⁹ Hence, we asked if other important regulatory components of the autophagy machinery, in particular the LC3- and GABARAP-activating protease ATG4B contained functional LIR motifs. In an unbiased approach we used the iLIR³⁸ server to predict LIR motifs, and a peptide array screen to map GABARAP-binding motifs in human ATG4B. iLIR returned 3 top hits, 2 of which reside at the extreme N- and C-termini which are predicted to be disordered by the PONDR-FIT algorithm (Fig. 1A).³⁹ Strikingly, the peptide array (overlapping 20-mer peptides shifted by a window of 3 amino acids along the entire sequence of ATG4B) also identified the same 3 putative LIR motifs; a putative N-terminal LIR motif (YDTL), another putative motif (FELV) just C-terminal to the protease domain, and a third motif (FEIL) located in the very C terminus (Fig. 1B).

The published crystal structure for a C-terminally truncated ATG4B and full-length LC3B reveals an interactions mainly located around the active site of ATG4B (C74) with the critical C-terminal glycine of LC3B interacting with these residues.³⁷ Regarding the putative LIRs we identified, the side chains of the FELV motif are hidden in the reported crystal structure, suggesting that it may not act as a functional LIR motif in the full-length protein. However, as the YDTL and the FEIL are both placed in disordered regions of ATG4B (Fig. 1A), they are more likely to engage in interactions with Atg8-family proteins. Interestingly, the C-terminal FEIL LIR motif clearly displayed the strongest binding to GST-GABARAP. Notably, a weak interaction was also observed with a peptide containing only the first 2 residues of the core LIR motif (Fig. 1B). The N-

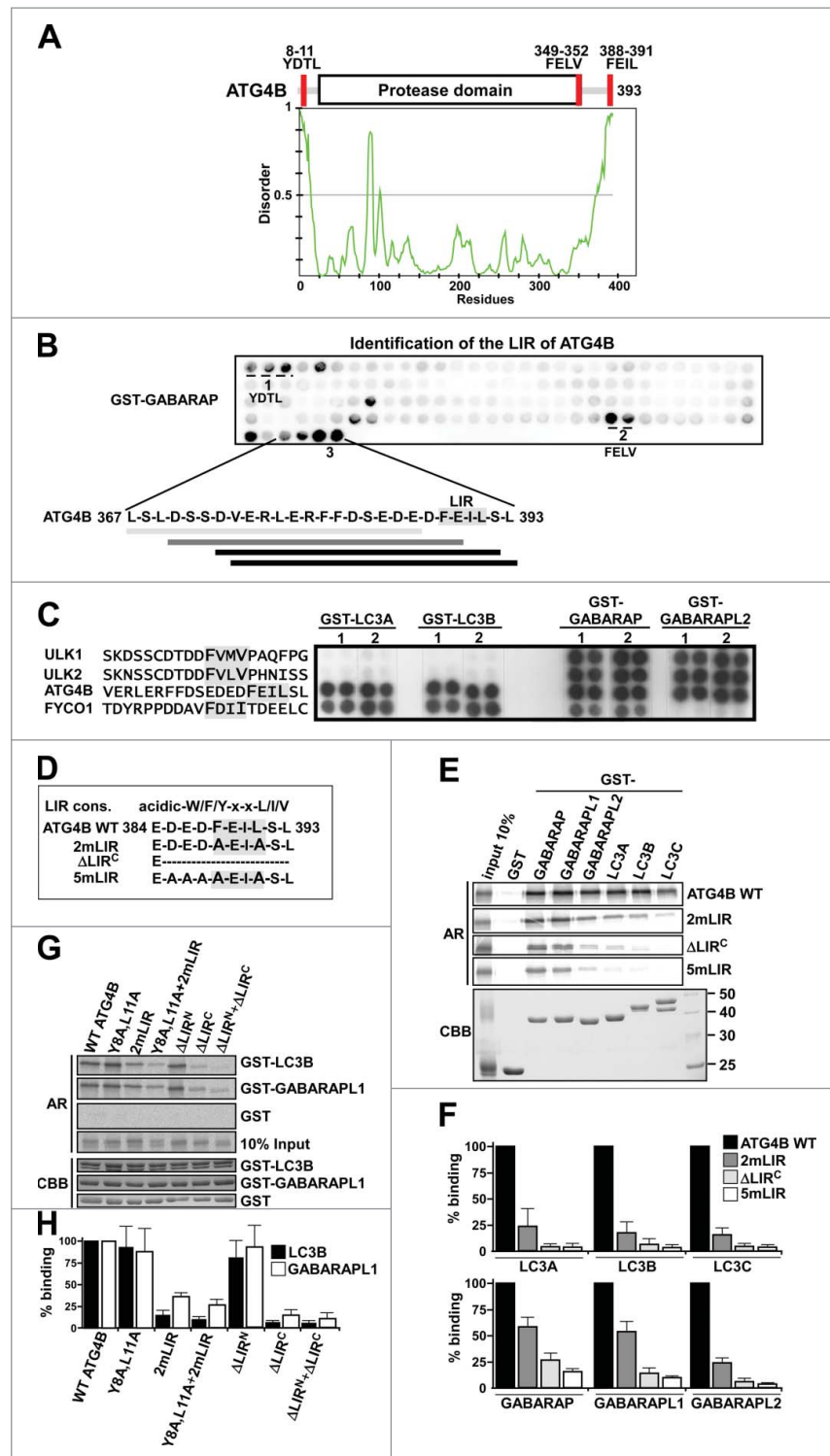


Figure 1. ATG4B contains a C-terminal LIR motif important for a strong interaction with Atg8-family orthologs. (A) Schematic overview of ATG4B indicating disordered regions and LIR motifs predicted by the iLIR and PONDR-FIT servers. (B) Identification of a C-terminal LIR motif. An array of 20-mer peptides covering full-length ATG4B (each peptide shifted 3 amino acids relative to the previous) was mixed with GST-GABARAP (1 μ g/ml) and binding detected with GST antibodies. The extension of the most strongly interacting peptides is indicated below in black. (C) The C-terminal LIR in ATG4B interacts with the LC3 and GABARAP subfamilies. The indicated peptides from ULK1, ULK2, ATG4B and FYCO1 (synthesized in duplicates marked 1 and 2) were examined as in B in a peptide array for binding to GST-tagged Atg8-family orthologs. (D) C-terminal sequences of ATG4B constructs carrying mutations affecting the C-terminal LIR motif. (E) The C-terminal LIR motif is important for the interaction of full-length ATG4B with Atg8-family orthologs. Myc-tagged ATG4B constructs were in vitro translated in the presence of [³⁵S]methionine, and tested in GST affinity isolation experiments for binding to the indicated Atg8-family orthologs fused to GST. Bound proteins were detected by autoradiography (AR), and immobilized GST or GST-tagged proteins by Coomassie brilliant blue staining (CBB). (F) Quantification of E, % binding relative to WT ATG4B based on 3 independent experiments. (G) A putative N-terminal LIR is not important for the interaction of ATG4B with LC3B or GABARAPL1. MYC-tagged ATG4B constructs were in vitro translated and tested for binding to GST-LC3B and GST-GABARAPL1 as in (E). (H) Quantification of (G) from 3 independent experiments.

terminal YDTL and the internal FELV LIR motifs displayed a weaker interaction with GST-GABARAP (Fig. 1B). Note, in the reported structure of the ATG4B-LC3B complex,³⁷ the N-terminal YDTL motif is bound at the LIR docking site (LDS) of a LC3B molecule adjacent to the LC3B molecule bound to the active site of ATG4B.

The strong GABARAP interaction with the C-terminal LIR in ATG4B prompted us to focus on this unstudied LIR motif. To determine its specificity for the various Atg8-family proteins, we first tested a peptide containing this LIR for interaction with GST-LC3A, GST-LC3B, GST-GABARAP and GST-GABARAPL2 (Fig. 1C). A strong interaction was observed with all 4 members of the Atg8 family, indicating the C-terminal LIR has a broad specificity. Next, a series of mutant ATG4B constructs, either deleted for the C-terminal LIR region (Δ LIR^C) or carrying 2 (2mLIR) or 5 (5mLIR) point mutations affecting the motif (Fig. 1D), were *in vitro* translated and tested for interaction with Atg8-family orthologs fused to GST. Mutation of 2 residues in the core LIR^C motif (F388A and L391A) reduced the interaction of ATG4B with LC3A, LC3B, LC3C and GABARAPL2 to 25% residual binding, and the interactions with GABARAP or GABARAPL1 to 60% (Fig. 1E and F). However, mutation of 5 residues in the LIR^C region, or deletion of the LIR^C motif, reduced the interactions with GABARAP and GABARAPL1 to 10% to 15% (Fig. 1E and F). The 5 point-mutations included the 3 negatively charged residues located immediately N-terminal to the core LIR^C motif (Fig. 1D), in addition to the F388A and L391A mutations. In contrast to mutation of the C-terminal LIR, mutation or deletion of the N-terminal YDTL LIR (LIR^N) had only a very minor effect on the interaction with LC3B or GABARAPL1 (Fig. 1G and H). Thus, we identified a LIR motif in the C terminus of ATG4B that contributed strongly to the interaction between ATG4B and Atg8-family proteins. The finding that LIR^N of ATG4B is not important for the interaction is entirely consistent with published structural data showing that the catalytic core of ATG4B and LIR^N interact with 2 adjacent LC3B molecules.³⁷ We propose that the LIR in the C terminus of ATG4B strongly increases the affinity of the interaction because it can adopt a *cis*-type interaction where the catalytic core and this LIR interact with the same Atg8-family molecule.

Structure of the GABARAPL1-ATG4B LIR^C complex

To evaluate the interaction between the C-terminal LIR-motif of ATG4B with Atg8-family proteins in more detail, we determined the X-ray structure of GABARAPL1 in complex with a peptide containing the C-terminal 10-amino acid LIR^C motif of ATG4B (Fig. S1A). The crystal structure of the ATG4B peptide-bound GABARAPL1 is similar to the previously reported structures of GABARAPL1 alone (PDB code 2PQR) and GABARAPL1 in complex with the LIR of NBR1.⁴⁰ These structures have an average 0.74 and 0.78 Å root mean square deviation for the C- α positions, respectively. ATG4B C-terminal FEIL LIR binds GABARAPL1 in an extended conformation with the core residues ATG4B (F388) and ATG4B (L391) deeply bound into the 2 hydrophobic pockets HP1 and HP2, as described previously for canonical LIR interactions (Fig. 2A).¹³ The structure displays 4 additional interactions: 1) Electrostatic

interactions between the acidic N-terminal LIR^C residues ³⁸⁴Glu-Asp-Glu-Asp³⁸⁷ of ATG4B and the basic residues GABARAPL1 (K46), GABARAPL1 (K24), GABARAPL1 (K20) and GABARAPL1 (K48), respectively; 2) a salt bridge between ATG4B (E389) and GABARAPL1 (R67); 3) some hydrophobic interactions between ATG4B (I390) in position +2 and GABARAPL1 (L50) as well as GABARAPL1 (Y25); 4) 3 hydrogen bonds between the carbonyls of ATG4B (L391), ATG4B (S392) and the guanidinium group of GABARAPL1 (R28). Except for the C-terminal ATG4B (L393), all residues in the LIR^C are contributing to the interaction. Two sulfate ions are bound to the basic groove formed between GABARAPL1 N-terminal arm (helix α 1 and α 2) and the β strand β 2 (Fig. 2A and D). This basic patch is reported to interact with the N-terminal acidic residues of LIR motifs.¹³ Hence, the presence of sulfate ions might therefore interfere with ATG4B LIR^C binding to GABARAPL1 under these crystallization conditions. Phosphorylation of S392, located just C-terminal to the core FEIL LIR^C motif of ATG4B (Fig. 1A to D), is recently reported to increase cleavage of LC3B.⁴¹ To evaluate the importance of this phosphorylation for its interaction with the Atg8-family proteins, the X-ray structure of GABARAPL1 bound to the ATG4B LIR^C peptide phosphorylated on residue S392 of ATG4B (hereafter referred to as phosphorylated ATG4B LIR^C) (Fig. 2B and Fig. S1B) was solved. Interestingly, the N-terminal acidic amino-acids of phosphorylated ATG4B LIR^C interact with the basic patch of GABARAPL1 where the sulfate anions were binding in the wild-type GABARAPL1-ATG4B LIR^C complex (Fig. 2C and D). Indeed, ATG4B (E386) forms an important electrostatic interaction with GABARAPL1 (H9) and GABARAPL1 (R47), while the rest of the LIR^C binds similarly except for the phospho-serine 392 (p-S392), which points toward the solvent, and is not engaged in any contact with GABARAPL1 (Fig. 2B and C). This complex crystallized in absence of ammonium sulfate and is therefore very likely more physiological representative for the interactions of the ATG4B residues ³⁸⁴Glu-Asp-Glu-Asp³⁸⁷. The residues GABARAPL1 (H9) and GABARAPL1 (R47) binding to ATG4B (E386) are conserved in all GABARAP isoforms but not in LC3 proteins (Fig. 2E). Similarly, arginine residue GABARAPL1 (R28) observed in all GABARAP isoforms is a lysine in all LC3 isoforms. The shorter lysine side chain may not be able to engage in an interaction similar to the arginine GABARAPL1 (R28) (Fig. 2C and E). These differences may provide an explanation for the stronger binding of ATG4B LIR^C to GABARAP isoforms compared with LC3 isoforms.

Interestingly, ATG4B (F388) adopts different conformations in the 2 structures. In the ATG4B LIR^C-GABARAPL1 complex the 2 sulfate anions form a network of hydrogen bonds with the GABARAPL1 (K48) side chain (Fig. 2D). GABARAPL1 (K48) is a key component of the hydrophobic pocket HP1 critical for the binding of the aromatic hydrophobic residue F/W/Y in position 0 of a LIR motif.⁴² GABARAPL1 (K48) is usually adopting an extended conformation and is held in place by a hydrogen bond with the GABARAPL1 (E17) side chain to form one side of the HP1 (Fig. 2D and S2). GABARAPL1 (K48) adopts this conformation in complex with the phosphorylated ATG4B LIR^C. However, in the complex between GABARAPL1 and wild-type ATG4B LIR^C, GABARAPL1

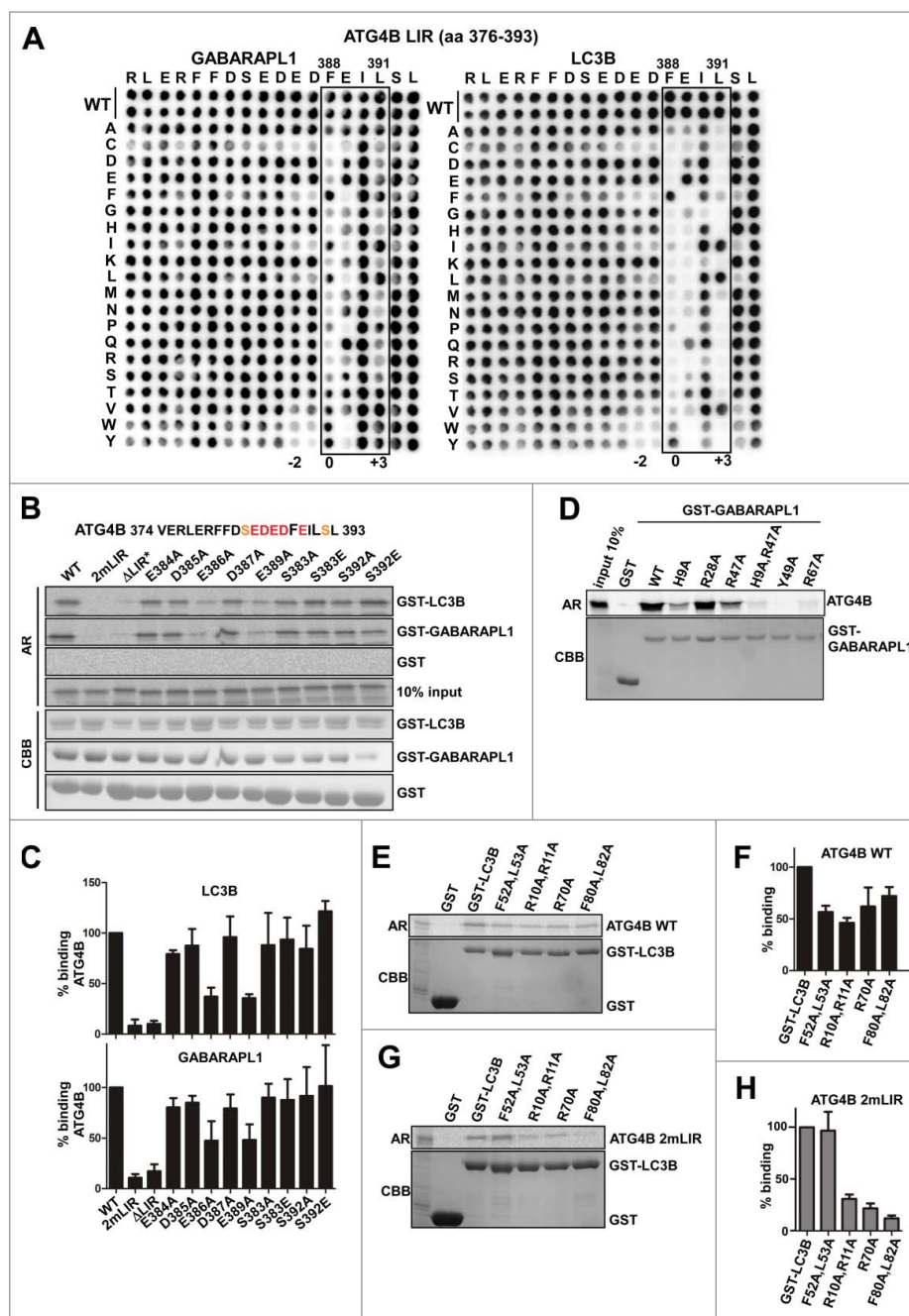


Figure 3. The C-terminal LIR in ATG4B relies both on electrostatic interactions, as well as aromatic and hydrophobic pocket interactions for efficient binding. (A) Two-dimensional peptide array scan analyzing the effects of single amino acid substitutions at all positions of the indicated 20-mer peptide from the C terminus of ATG4B. Arrays were probed with GST-GABARAPL1 or GST-LC3B. (B) E386 and E389 in the LIR^C of ATG4B form important electrostatic interactions with both LC3B and GABARAPL1. A C-terminal ATG4B peptide (amino acids 374 to 393), fused to GFP and carrying the indicated point mutations, were in vitro translated and tested in GST affinity isolation assays for binding to LC3B and GABARAPL1. The Δ LIR^C construct is indicated with an asterisk because it comprises amino acids 365 to 384 of ATG4B (LNLSLDSSDVERLERFFDSE) and 2mLIR harbors the F388A and L391A double mutation of the canonical aromatic and hydrophobic core LIR^C residues. (C) Quantification of the experiment shown in B, based on 3 independent experiments. The binding to the WT peptide is set to 100%. (D) H9 and R47 are crucial for binding of GABARAP or GABARAPL1 to the ATG4B LIR^C. The C-terminal ATG4B peptide (amino acids 374 to 393), fused to GFP was in vitro translated and tested in GST affinity isolation assays for binding to specific point mutants of GABARAPL1 fused to GST and bound to GST beads. ((E) and G) Both LIR^C-LDS interactions and catalytic site-substrate interactions contribute to ATG4B-LC3B binding. MYC-ATG4B (E) and MYC-ATG4B 2mLIR (G) were in vitro translated and tested in GST affinity isolation assays for binding to GST-LC3B with or without mutations affecting the LIR^C-LDS interaction (F52A and L53A, R10A and R11A, as well as R70A) or the catalytic site-substrate interaction (F80A and L82A). (F) Quantification of (E), the % binding relative to the binding of WT GST-LC3B to WT ATG4B based on 3 independent experiments. (H) Quantification of (G), % binding relative to the binding of WT GST-LC3B to ATG4B 2mLIR based on 3 independent experiments.

(Fig. 1E and F). Notably, the +1 position of ATG4B LIR^C is the second most vulnerable to mutations for GABARAPL1 binding. Here, substitution of E389 in the +1 position to N, D, Q, S, T and A does not impair binding, while all other substitutions decrease binding. Any amino acid can

be placed in the +2 position. Aromatic and hydrophobic residues are counterselcted at the -1 and -2 positions (Fig. 3A). For the ATG4B LIR^C interaction with GST-LC3B we see a classical binding pattern where substitutions of the core LIR amino acids strongly affect the binding. Only the

F and Y in the 0 position, and I, V and L in the hydrophobic +3 position are tolerated for significant binding (Fig. 3A). The negatively charged E389 at position +1 is critical also for the interaction with LC3B. Any other amino acid in this position negatively affects the interaction. Mutations of residues outside the core LIR^C have a very similar effect on LC3B and GABARAPL1 binding, including the counterselection of aromatic or hydrophobic substitutions at positions -1 and -2. However, the LC3B interaction is additionally intolerant to aromatic or hydrophobic substitutions affecting S392 at position +4.

The single point mutations were further analyzed by GST affinity isolation assays in which the C terminus of ATG4B (amino acids 373 to 393) fused to GFP was in vitro translated and tested for interaction with GST-LC3B or GST-GABARAPL1 (Fig. 3B and C). For selected single point mutants, the effect on the full-length ATG4B interaction was additionally tested (Fig. S3). We chose to use the C-terminal ATG4B fragment in this assay, since the effects of single point mutations on the LIR^C interactions are more easily detected when there is no compensatory catalytic site interaction. The 2mLIR (F388A,L391A) double mutation strongly inhibited the interaction of the C-terminal ATG4B fragment with GST-GABARAPL1 and GST-LC3B (about 10% residual binding) (Fig. 3B and C).

To identify important acidic residues in the ATG4B LIR^C, the effect of single point mutations affecting negatively charged residues within the core ATG4B LIR^C motif (E389) or N-terminal to the core ATG4B LIR^C motif (E384, D385, E386, D387) were analyzed. The E386A (-2) and E389A (+1) mutations strongly reduced binding of the LIR^C peptide of ATG4B to both GST-LC3B and GST-GABARAPL1 (Fig. 3B and C), although their effect was less pronounced when tested in full-length ATG4B (Fig. S3). This is entirely consistent with the crystal structure showing the electrostatic interactions between ATG4B (E389) and GABARAPL1 (R67) as well as between ATG4B (E386) and GABARAPL1 (H9 and R47) (Fig. 2). The crucial roles of these electrostatic interactions for binding was also shown by GST affinity isolation assays where Ala (A) substitutions of H9, R47 and R67 abolished the binding of GABARAPL1 to the ATG4B LIR^C (Fig. 3D). The R28A mutation did not have any effect (Fig. 3D). This is consistent with the modest effect of mutating the core LIR^C hydrophobic Leu residue for binding to GABARAPL1 (Fig. 3A).

Cleavage of LC3B by ATG4B has been recently reported to be regulated by phosphorylation of S383 and S392.⁴¹ These residues flank the core LIR^C region. We therefore analyzed the effect of mutations of S383 or S392 to alanine (A) or glutamic acid (E) on the binding of the LIR^C fragment and full-length ATG4B to GST-GABARAPL1 or GST-LC3B. None of these mutations affected the LIR^C interactions significantly. However, the S392E mutation increased binding between the ATG4B LIR^C fragment and LC3B by 20% (Fig. 3B and C). The S392E mutation also had a weak, although not significant, positive effect on the interaction of full-length ATG4B with LC3B (Fig. S3).

Both catalytic site-substrate interactions and LIR-LDS interactions contribute to the binding between LC3B and ATG4B

The ATG4B-LC3B crystal structure revealed that the F80 and L82 residues in LC3B are important for ATG4B binding and processing.³⁷ The LC3B surface involved in this catalytic interaction is distinct from the LDS involved in the LIR interaction.³⁷ To analyze the relative importance of the catalytic site interaction for binding, selected mutants of LC3B located on different binding surfaces were tested in GST affinity isolation assays for binding to WT ATG4B. We found that the F80A and L82A double mutation (affecting the catalytic site interaction) had a negative effect on ATG4B binding comparable to mutations affecting the LIR^C interaction (Fig. 3E and F). This strongly supports the conclusion that catalytic site-substrate interaction and the LIR-LDS interaction both contribute to the binding between ATG4B and LC3B. When the same experiment was repeated with the 2mLIR mutant of ATG4B, the F52A and L53A LDS mutation in LC3B had no effect (Fig. 3G and H). This is as expected since the 2mLIR mutation and the F52A and L53A double mutation both impair the hydrophobic LIR-LDS interactions. However, LC3B mutations affecting electrostatic LIR-LDS interactions or the catalytic site-substrate interaction, all strongly impaired the interaction between ATG4B 2mLIR and LC3B (Fig. 3G and H). This corroborates the dual importance of catalytic site-substrate interactions and LIR^C-LDS interactions for binding. The strong effect of the R10A and R11A double mutation is also notable, since it supports an important role for the N-terminal arm of LC3B in stabilizing the LIR^C-LDS interaction.

Theoretically, the C-terminal LIR-LDS interaction may act both in *cis* and *trans*. To investigate whether the *cis* interaction is sterically hindered, the structure of the phosphorylated ATG4B LIR^C motif bound to GABARAPL1 was superposed on the ATG4B (1 to 354)-LC3B complex (PDB ID: 2ZZP) to generate a model of full-length ATG4B bound to LC3B (Fig. 4A and Fig. S4). The model clearly supports that a *cis*-mediated LIR-LDS interaction is possible.

The ATG4 family shows differential binding to LC3B and GABARAP

The C-terminal LIR (FEIL) found in ATG4B is completely conserved in ATG4A, while the other 2 human ATG4 orthologs have the sequences ATG4C (FVLL) or ATG4D (FVFL) (Fig. 4B and C). When tested in GST affinity isolation assays, in vitro translated ATG4A interacted strongly with GST-LC3B and GST-GABARAP, and both interactions were strongly impaired by a deletion of the C-terminal LIR motif (Fig. 4D and E). The C terminus is only partially conserved in ATG4C and ATG4D. In these proteins, the critical acidic residue in position +1 is substituted with a hydrophobic V and the core LIR motif has no C-terminal extension (Fig. 4C). When tested in GST affinity isolation assays, these proteins interacted well, but more weakly than ATG4B, with GST-GABARAP. However, they displayed a very weak interaction with LC3B. Deletion of the C terminus had a negative effect on interactions

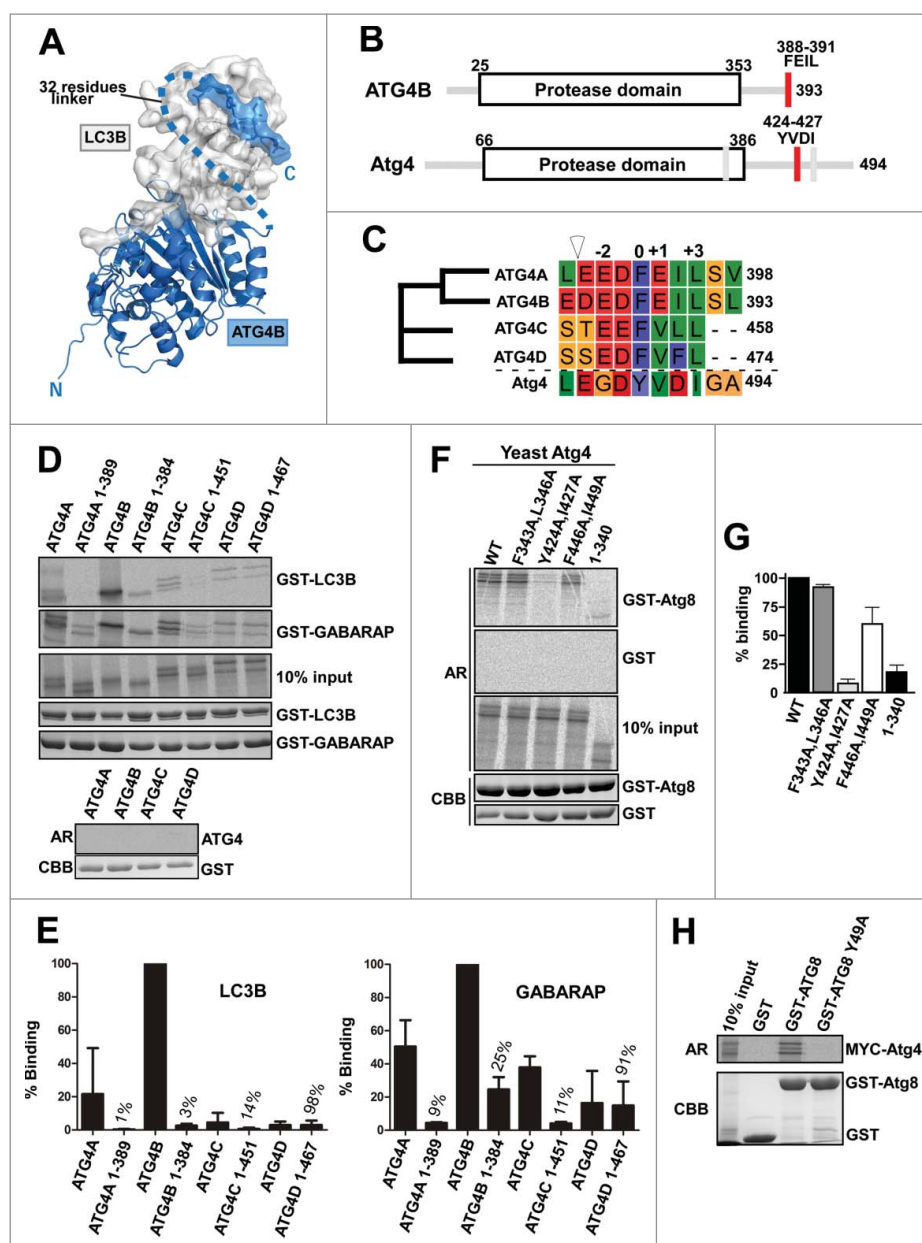


Figure 4. ATG4A and ATG4B harbor a C-terminal LIR, binding efficiently to LC3B and GABARAP, while ATG4C and ATG4D do not. (A) Model of full-length ATG4B bound to LC3B. The structure of the phosphorylated ATG4B LIR^C motif bound to GABARAP1 was superposed to the ATG4B (1 to 354)-LC3B complex (PDB ID: 2ZZP) to generate a model of the full-length ATG4B bound to LC3B. ATG4B is displayed in blue cartoons and LC3B is displayed in white cartoons and transparent surface. The 32 missing residues connecting ATG4B C-terminal LIR motif to Q354 are represented by a dashed line. (B) Schematic illustration of human ATG4B and yeast Atg4 indicating the protease domain and the functional LIRs (red bar) with the location of 2 candidate LIRs in yeast Atg4 tested in F indicated as gray bars. (C) A phylogenetic tree (left), and alignment of the far C-terminal sequence of the 4 different mammalian ATG4s and yeast Atg4 LIR (referred to in yeast as the Atg8-interacting motif). (D) MYC-tagged human ATG4 orthologs (WT and LIR^C-deleted) were in vitro translated and tested in GST affinity isolation assays for binding to GST-LC3B and GST-GABARAP. The region deleted in the LIR^C-deleted constructs is indicated by an open arrowhead in (C). The affinity isolation with the respective GST controls is shown below. (E) Quantification of the experiment shown in (D), based on 3 independent experiments. Bars indicate relative binding, and the interaction with ATG4B is set to 100%. For LIR^C-deleted constructs, % binding relative to the corresponding full-length construct is indicated. (F) Yeast Atg4 has predicted LIR motifs binding to yeast Atg8 at a similar C-terminal distance to the protease domain as human ATG4B. Yeast Atg4 (WT and candidate LIR mutants) were in vitro translated and analyzed by GST affinity isolation assays for binding to GST-Atg8 (yeast). (G) Quantification of the experiment shown in (F), based on 3 independent experiments. WT was set to 100% binding. (H) Yeast MYC-tagged Atg4 was in vitro translated and analyzed by GST affinity isolation assays for binding to GST-Atg8 (WT and LDS mutated).

mediated by ATG4C, but it did not affect interactions mediated by ATG4D (Fig. 4D and E). Hence, the canonical LIR motif in the C terminus of ATG4B is conserved also functionally in ATG4A, while the more divergent motifs in ATG4C and ATG4D play a minor, or no, role in the binding to LC3B and GABARAP. To check for evolutionary conservation of the LIR-mediated interaction between ATG4 and the Atg8 family we looked at yeast (*S. cerevisiae*). By mutagenesis of 3

candidate LIR motifs (mutating the aromatic HP1 and hydrophobic HP2 residues to Ala) we identified a single LIR motif (YVDI; Fig. 4C) crucial for binding to yeast Atg8 (Fig. 4F and G). Although not at the extreme C terminus, strikingly, this motif is located in a similar distance C-terminal to the protease domain as the LIR motif in ATG4B (Fig. 4B). Mutation of LDS in yeast Atg8 (Y49A) abolished the interaction between yeast Atg8 and yeast Atg4 (Fig. 4H), further supporting the

conclusion that the LIR interaction is essential for binding also in yeast.

The C-terminal LIR motif of ATG4B is important for efficient cleavage of Atg8-family proteins in vitro and in vivo

The importance of the LIR^C motif for ATG4B-mediated cleavage was tested in an in vitro cleavage assay using recombinant proteins. Hence, WT, Δ LIR^C or catalytically inactive (C74S) ATG4B was added to GABARAP or LC3B fused to a C-terminal GST tag. Cleavage was measured as reduction in the amount of the full-length fusion protein. WT ATG4B had the highest cleavage activity, while only a partial cleavage was seen with ATG4B Δ LIR^C. During the 1-h time frame of the experiment, no cleavage activity was measured for the catalytically inactive ATG4B (C74S) mutant (Fig. 5A).

To analyze the effect of ATG4B C-terminal LIR mutants in cells, we established stable cell lines expressing GFP-tagged ATG4B WT, catalytic inactive C74S- or LIR^C mutants. *atg4b* knockout (KO) mouse embryo fibroblasts (MEFs)⁴³ were stably reconstituted with WT or the selected mutants of ATG4B using a doxycycline inducible retroviral vector. The induced expression levels of the various GFP-ATG4B fusion proteins were similar. All constructs were expressed at a low level in uninduced cells due to promoter leakage (Fig. 5B and Fig. S5A). The expression level of GFP-ATG4B without induction was 5-fold higher than that of endogenous ATG4B (Fig. S5B). It has been shown that overexpression of ATG4B inhibits lipidation of Atg8-family orthologs by preventing their delivery to ATG7.³⁶ Hence, we chose to use the uninduced cell lines for our experiments. To probe the requirements for ATG4B-mediated cleavage of Atg8-family proteins in cells, we used transiently transfected LC3B and GABARAP1 fused to ACTB and Gaussia luciferase (Fig. 5C). Cleavage is measured by assaying the activity of Gaussia luciferase released into the growth medium following *in cellulo* cleavage.⁴⁴ Cells expressing WT ATG4B clearly displayed more effective cleavage (measured 18 to 24 h after transfection) than cells expressing ATG4B Δ LIR^C or 5 point mutations in the LIR motif (5mLIR). Cells expressing ATG4B (C74S) showed background levels (Fig. 5C). Strikingly, this was also the case when a LDS mutated (F52A and L53A) LC3B was used as reporter (Fig. 5C). Taken together, these results strongly support our finding that the LIR^C interaction is important for efficient cleavage by ATG4B.

To compare the relative importance of the N-terminal and C-terminal LIR motifs in ATG4B for cleavage, another series of *atg4b* KO MEFs stably reconstituted with selected ATG4B mutants fused to GFP were made (Fig. 5D). Reconstituted cells were transiently transfected with LC3B and GABARAP1 fused to ACTB and Gaussia luciferase, and assayed for *in vivo* cleavage activity. Deletion of the N-terminal LIR (Δ LIR^N) of ATG4B had a consistent, weak, but statistically insignificant, positive effect on GABARAP1 cleavage while deletion of the C-terminal LIR (Δ LIR^C) strongly reduced cleavage of both LC3B and GABARAP1 (Fig. 5E). When both LIRs were deleted there was a slight positive effect relative to deletion of the C-terminal LIR. This is consistent with the data of Satoo et al.,³⁷ showing

that deletion of LIR^N resulted in more active cleavage in vitro. Taken together, our results support the conclusion that the C-terminal LIR is important for binding and required for effective cleavage of LC3B and GABARAP1.

Next, we looked at subcellular distribution of endogenous LC3B in *atg4b* KO MEFs reconstituted with GFP, GFP-ATG4B WT, -C74S or - Δ LIR^C mutants. We observed a much higher number of LC3B dots in cells expressing catalytically active ATG4B constructs (WT and - Δ LIR^C) than in cells lacking ATG4B or expressing the C74S mutant (Fig. 6A and B). The presence of LC3B dots correlated with the detection of LC3B-II in western blot experiments (Fig. 5B), indicating autophagosome formation occurs in *atg4b* KO cells expressing active forms of ATG4B. There was no striking difference in the number of LC3B positive dots between cells expressing WT ATG4B or ATG4B Δ LIR^C (Fig. 6A). However, this number was consistently slightly higher in cells expressing the ATG4B Δ LIR^C construct than in cells expressing WT ATG4B (Fig. 6B).

To look at the importance of the LIR^C motif in ATG4B for autophagosome formation, cell lines stably expressing GFP-ATG4B WT or GFP-ATG4B Δ LIR^C were transiently transfected with mCherry-GFP-LC3B. Using this marker, autophagosomes emit green and red (yellow) fluorescence due to the recruitment of LC3B, while autolysosomes are only red because the green fluorescence is lost within acidic structures.¹⁸ Expression of GFP-ATG4B in the stably expressing cell lines was not induced with doxycycline, therefore the fluorescent signals were only detected from the mCherry-GFP-LC3B construct. While cells expressing mCherry-GFP-LC3B but lacking ATG4B contained no yellow dots and few red only dots, cells expressing GFP-ATG4B WT or GFP-ATG4B Δ LIR^C contained many red only dots and also numerous yellow dots indicating autophagosome formation (Fig. 6C). Interestingly, cells expressing the ATG4B Δ LIR^C construct often contained mCherry- and GFP-positive ring structures larger than 1 μ m. Such structures were rarely seen in cells expressing WT ATG4B (Fig. 6C). Given these results, we suggest that delipidation is impaired, resulting in a deregulated growth of phagophores and thereby a larger size of autophagosomes.

The LIR^C motif of ATG4B is required for stabilization of GABARAP and GABARAP1 in vivo

Transient transfection of WT ATG4B has previously been shown to stabilize the unlipidated form of LC3B, and thereby inhibit the delivery of LC3B to ATG7.³⁶ We similarly observed that doxycycline-induced overexpression of WT ATG4B reduced lipidation of LC3B (Fig. 5B). However, when we compared uninduced cells with low expression of the various GFP-ATG4B constructs, there was no apparent sequestration of unlipidated LC3 or GABARAP2 (Fig. 5B and Fig. 7A). The cellular pools of LC3B-I were basically similar in all the reconstituted cell lines, and affected neither by the presence or absence of ATG4B nor by the expression of a LIR^C mutated construct (Fig. 7A). The formation of LC3B-II clearly depends on the expression of catalytically active ATG4B, but unless highly overexpressed,³⁶ there was no apparent difference in LC3B-II formation between cell lines expressing WT or LIR^C mutated ATG4B constructs.

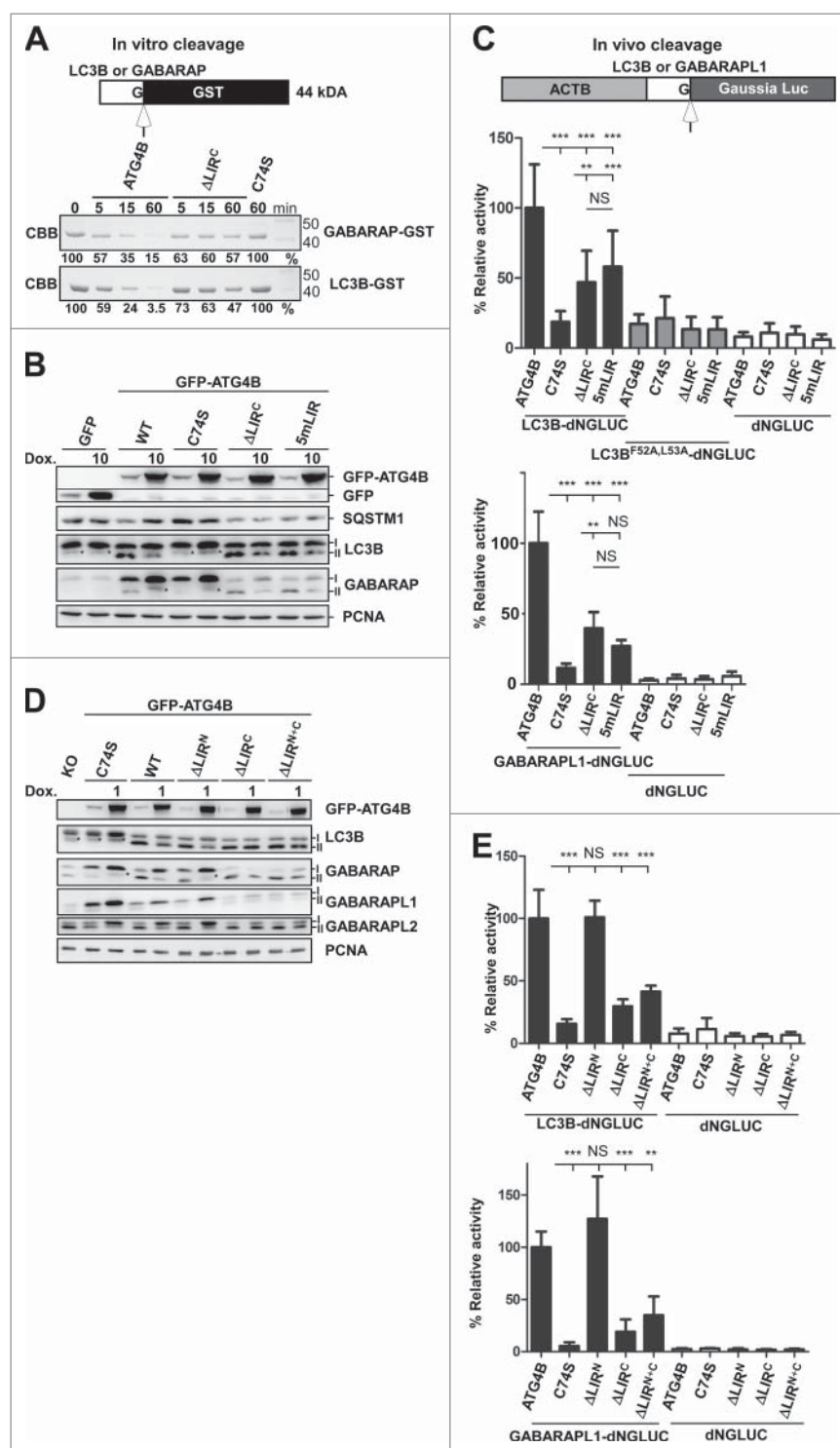


Figure 5. The C-terminal LIR motif of ATG4B is important for efficient cleavage of Atg8-family proteins. (A) GST-ATG4B Δ LIR^C displays reduced ability to cleave off a C-terminal GST tag on both LC3B and GABARAP. The GST-tagged substrates were incubated with recombinant ATG4B (WT or mutated) for 0, 5, 15 or 60 min. The rate of cleavage was measured after SDS-PAGE as a loss of the band corresponding to the GST-tagged substrate. The % of uncleaved substrate remaining is indicated. (B) Lipidation of LC3 and GABARAP is functional in *atg4b* knockout cells rescued with WT or LIR^C mutated GFP-ATG4B. Cells rescued with GFP-ATG4B constructs were treated or not with doxycycline (10 μ g/ml) for 24 h to induce expression and cell lysates analyzed by western blotting. (C) Reduced ability of LIR^C mutated ATG4B constructs to cleave transiently transfected LC3B or GABARAP1 fused to the Gaussia luciferase. Cells reconstituted with the indicated ATG4B constructs were transiently transfected with the indicated LC3B or GABARAP1 Gaussia luciferase constructs or vector control. Cleavage was measured by release of Gaussia luciferase over a period of 18 to 24 h for cells expressing the indicated LC3B or GABARAP1 Gaussia luciferase constructs or vector control. Mean \pm SD of 4 independent experiments, wild type set to 100%, $n \geq 6$, NS $P > 0.05$, * $P \leq 0.05$, ** $P \leq 0.01$, *** $P \leq 0.001$. One-way ANNOVA followed by the Tukey multiple comparison test. (D) Deletion of LIR^N in ATG4B has no effect on lipidation of LC3B, GABARAP, GABARAP1 or GABARAP2 in *atg4b* knockout cells rescued with GFP-ATG4B. Cells rescued with WT or mutated GFP-ATG4B were treated or not with doxycycline (1 μ g/ml) for 24 h to induce expression and cell lysates analyzed by western blotting. (E) Deletion of LIR^N has a slightly positive effect on cleavage of transiently transfected LC3B or GABARAP1 fused to the Gaussia luciferase. Cells reconstituted with the indicated ATG4B constructs were transiently transfected with the indicated constructs and in vivo cleavage measured as in (C). Mean \pm SD of 3 independent experiments, wild type set to 100%, $n \geq 6$, NS $P > 0.05$, * $P \leq 0.05$, ** $P \leq 0.01$, *** $P \leq 0.001$. One-way ANNOVA followed by the Tukey multiple comparison test.

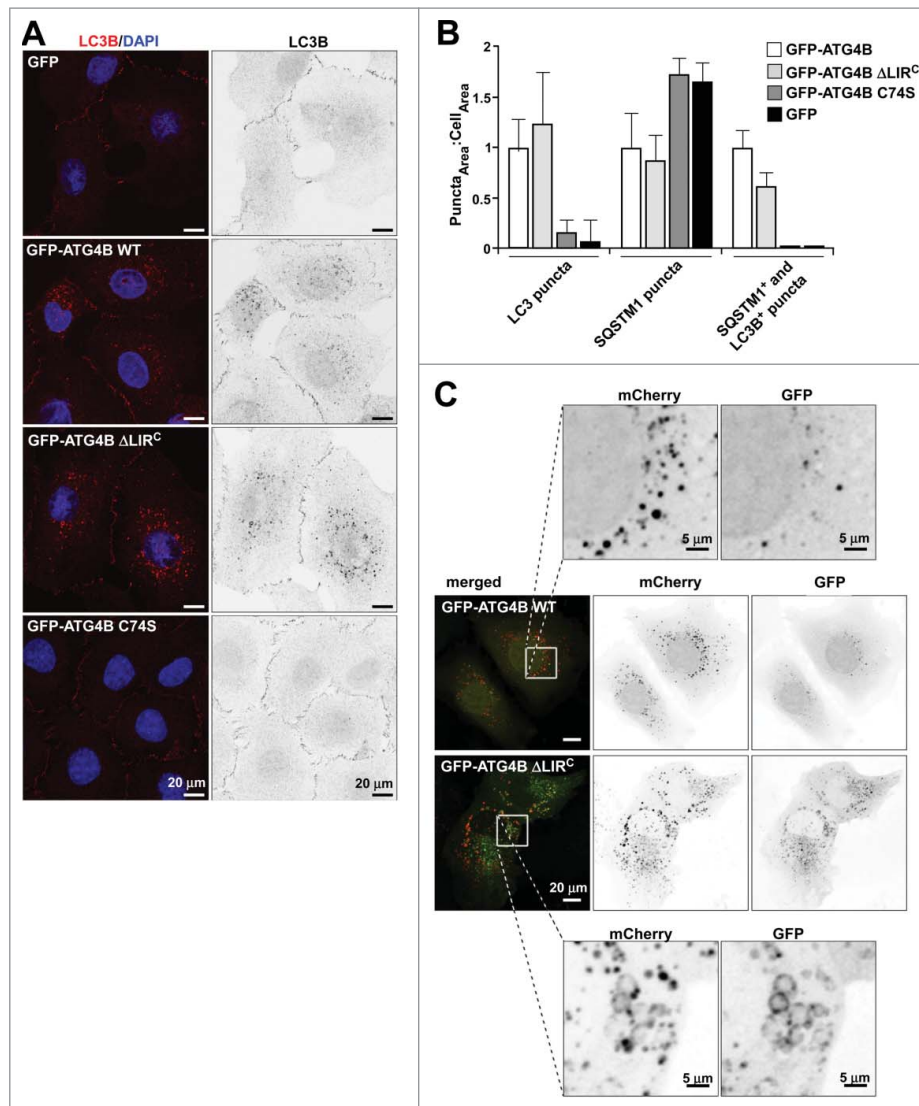


Figure 6. LC3B puncta formation is similar in *atg4b* KO MEFs expressing WT or LIR^C-deleted GFP-ATG4B. (A) Cells were stained with LC3B antibodies and analyzed by confocal imaging. (B) Quantification of fractions of cells containing LC3B puncta, SQSTM1 puncta, or puncta positive for both LC3B and SQSTM1. (C) *atg4b* KO MEFs reconstituted with WT or LIR^C-deleted GFP-ATG4B were transiently transfected with mCherry-GFP-LC3B, and analyzed by confocal imaging 16 h after transfection. There was no difference in yellow or red only structures between the cell lines, but cells expressing the LIR^C-deleted construct contained large ring structures rarely seen in cells expressing WT ATG4B. Note that cells were not treated with doxycycline, and expression of GFP-ATG4B was therefore below detection level in these studies.

In sharp contrast to LC3B and GABARAPL2, the cellular pools of unlipidated GABARAP and GABARAPL1 were strongly affected both by the presence of ATG4B and by a mutation of the LIR^C motif (Fig. 7A). As previously noted,⁴³ loss of ATG4B results in a severe reduction of unlipidated GABARAP and GABARAPL1 (Fig. 7A, lanes 1,2). A similar reduction in unlipidated LC3B was not seen in cells lacking ATG4B (Fig. 7A). Furthermore, while cells expressing WT or GFP-ATG4B (C74S) contained unlipidated GABARAP and GABARAPL1 (Fig. 7A, lanes 3,4), these pools of unlipidated GABARAP and GABARAPL1 were strongly reduced in cells expressing LIR^C mutated GFP-ATG4B constructs (Fig. 7A, lanes 5,6). Thus, ATG4B stabilizes GABARAP and GABARAPL1, and this stabilization is dependent on the C-terminal LIR motif. Mutation of the putative phosphorylated p-S392 residue,⁴¹ to A or E, had no apparent effect on the stabilization or lipidation of Atg8-family orthologs (Fig. 7A, lanes 7 to 9), neither did the expression of a LIR^N deleted ATG4B (Fig. 5D).

Surprisingly, elevated expression of ATG4A or ATG4C could not compensate for the lack of ATG4B (Fig. 7A, lanes 10 to 12). Treatment of *atg4b* KO cells with the proteasomal inhibitor MG132 resulted in accumulation of unlipidated GABARAP and GABARAPL1 (Fig. 7B, lanes 1,2 and 7,8), while inhibition of lysosomal degradation with bafilomycin A₁ (BafA1) only very weakly increased the level of GABARAP (Fig. 7C, lanes 2 and 7, and Fig. S6A). Hence, unlipidated GABARAP and GABARAPL1 are efficiently degraded by the proteasome in cells lacking ATG4B. In contrast, in cells expressing ATG4B WT, C74S or Δ LIR^C, both forms of GABARAP accumulated in BafA1-treated cells, and not in the MG132-treated cells (Fig. 7B, C). This suggests that ATG4B directs GABARAP to lysosomal degradation pathways.

To further demonstrate a correlation between the level of WT ATG4B and the levels of unlipidated and lipidated GABARAP, we analyzed cells expressing increasing amounts of ATG4B (Fig. 7D). We used cells treated or not with

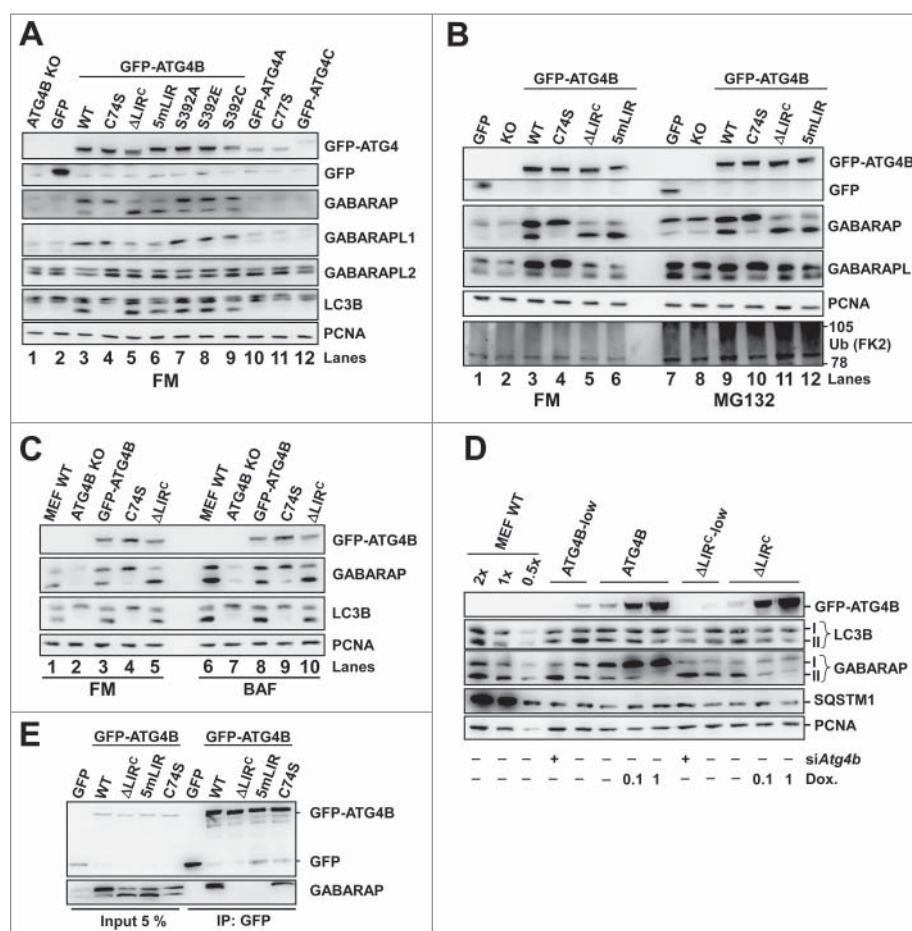


Figure 7. The LIR^C motif of ATG4B is required for stabilization of GABARAP and GABARAPL1. (A) The endogenous level of GABARAP is severely diminished in cells that do not express ATG4B. Extracts of *atg4b* KO cells reconstituted with the indicated GFP-ATG4 constructs were analyzed by western blotting. (B) GABARAP is degraded by the proteasome in cells that do not express ATG4B. Cells reconstituted with GFP or indicated GFP-ATG4B constructs were treated or not with the proteasomal inhibitor MG132 (10 μ M) for 4 h and analyzed by western blotting. The FK2 anti-ubiquitin antibody was used as a positive control for proteasomal inhibition. (C) In cells that do not express ATG4B, or inactive ATG4B, there is very little, if any, accumulation of GABARAP in response to lysosomal inhibition by BafA1. Cells were treated with or without BafA1 (0.2 μ M) for 8 h, and cell lysates analyzed by western blotting. (D) GABARAP, but not LC3B, is stabilized by an elevated expression of WT ATG4B, and stabilization is LIR^C dependent. Cell lysates from cells expressing different amounts of GFP-ATG4B or GFP-ATG4B Δ LIR^C were analyzed by western blotting. To increase or reduce the expression of GFP-ATG4B, cells were treated as indicated with doxycycline (0.1 or 1 μ M) or *Atg4b* siRNA for 48 h, respectively. (E) Endogenous GABARAP is efficiently immunoprecipitated by ATG4B in a LIR^C-dependent manner. Lysates of *atg4b* KO cells reconstituted with the indicated GFP-ATG4B constructs were immunoprecipitated with GFP antibodies and analyzed by western blotting.

doxycycline. To increase the sensitivity of the assay we also used flow cytometry to select cells with lower expression of ATG4B than our initial clones (ATG4B-low and Δ LIR^C-low). In addition, these cells were transfected with siRNA against *Atg4b* to further reduce expression levels. The level of unlipidated GABARAP-I gradually increased when the level of WT ATG4B increased, reflecting stabilization of unlipidated GABARAP by ATG4B. No stabilization of GABARAP-I was seen in cells expressing increasing amounts of ATG4B Δ LIR^C (Fig. 7D). Thus, the ability of ATG4B to stabilize unlipidated GABARAP strongly depends on its LIR^C motif. In a similar type of experiment performed with cells expressing LIR^N-deleted constructs, it appeared that a deletion of LIR^N had no effect on the stabilization of GABARAP (Fig. S6B).

For cells expressing ATG4B WT, we observed a gradual decrease in the level of lipidated GABARAP (II form) correlating with the level of ATG4B (Fig. 7D). The high amount of GABARAP-II in cells expressing very little ATG4B indicates that the initial cleavage is efficient even with low ATG4B concentrations. Presumably, elevated ATG4B may reduce the

amount of lipidated GABARAP both because it stabilizes the unlipidated form and because it increases delipidation from the phagophore. For cells expressing ATG4B Δ LIR^C, the II form was reduced in response to high overexpression, but the effect was weaker than seen for WT ATG4B (Fig. 7D).

The LIR^C dependent stabilization of GABARAP and GABARAPL1 by ATG4B indicates that these proteins form a stable complex in cells. To test this, GFP or GFP-tagged ATG4B proteins (WT or mutated) were immunoprecipitated from KO cells reconstituted with these constructs and coprecipitated endogenous GABARAP was detected by western blotting. Interestingly, GABARAP was efficiently coprecipitated with WT GFP-ATG4B and the catalytic inactive GFP-ATG4B (C74S), but not with the LIR^C mutated GFP-ATG4B proteins (Fig. 7E). This supports the conclusion that ATG4B forms a stable interaction with GABARAP that depends on the LIR^C motif. Without induction of GFP-ATG4B expression, no detectable coprecipitation of LC3B was seen. However, after induction of GFP-ATG4B expression with doxycycline, a weak and LIR^C dependent coprecipitation of endogenous LC3B was also seen (Fig. S6C). The

coprecipitation of LC3B was much less efficient than coprecipitation of GABARAP (Fig. S6C). The strongest LC3B interaction was consistently seen with the GFP-ATG4B (C74S) construct.

Next, the intracellular location of endogenous GABARAP in the *atg4b* KO MEFs reconstituted with different GFP-ATG4B constructs was studied by confocal imaging. In the cell lines reconstituted with catalytically active ATG4B GABARAP accumulated in dots dispersed throughout the cytoplasm, as well as in centrosomes identified as distinct TUBG/ γ -tubulin positive dots (Fig. S7). The dots represent autophagic structures as some colocalize with LC3B and some with the early autophagosome marker WIPI2. This is in line with previous results suggesting a scaffolding role for GABARAP in autophagosome formation.^{19,45} Surprisingly, in contrast to the western blot results (Fig. 5B), there was no significant increase in endogenous GABARAP staining in the cell lines reconstituted with WT or catalytically inactive ATG4B. We tested several antibodies with the same results. We therefore think that there is a problem with exposure of the epitope(s) recognized by the antibodies in the heterodimeric ATG4B-GABARAP complex. Consistent with the observed destabilization of endogenous GABARAP (Fig. 5B), ectopically expressed mCherry-GABARAP was not detected by confocal microscopy in *atg4b* KO cells. Reconstitution of the KO cells with low levels of WT GFP-ATG4B or GFP-ATG4B Δ LIR^C resulted in accumulation of mCherry-GABARAP dots similarly to the WT cells (Fig. 8A). Interestingly, induction of a high level WT GFP-ATG4B expression redistributed mCherry-GABARAP into a highly diffuse localization pattern (Fig. 8B), whereas high-level expression of GFP-ATG4B Δ LIR^C did not (Fig. 8B). Furthermore, cells reconstituted with the catalytically inactive C74S mutant redistributed mCherry-GABARAP into a diffuse localization pattern (Fig. 8A to C). Presumably, the dots represent phagophores and autophagosomes, while the diffuse mCherry-GABARAP constitutes the ATG4B associated pool of unlipidated GABARAP. Taken together, all our data clearly demonstrate a strong LIR^C-dependent interaction between ATG4B and GABARAP in cells. As depicted (Fig. 8D), a pool of unlipidated GABARAP may be stabilized by a LIR^C-dependent direct interaction between ATG4B and GABARAP. This may negatively regulate autophagosome formation by inhibiting the delivery of the cleaved product to ATG7, or may be required for the maintenance of an unlipidated pool of GABARAP that can be used upon autophagy induction.

Discussion

In this study, we identified a canonical LIR motif in the C terminus of ATG4B required for efficient binding of ATG4B to Atg8-family proteins, and for efficient cleavage of Atg8-family proteins both in vitro and in vivo. Previous structural studies of complexes formed between LC3B and ATG4B have been performed with C-terminally truncated ATG4B lacking the LIR^C motif because the high flexibility of the C-terminal residues (355 to 393) of human (*Homo sapiens*/Hs) ATG4 precluded crystallization.³⁷ The C-terminal LIR interaction was therefore not detected. Our results

show that a strong interaction with LC3s and GABARAPs depends on simultaneous interactions with the catalytic domain and the LIR^C motif of ATG4B. Molecular modeling suggests that the linker between the catalytic domain and the LIR^C motif is long enough to adopt into a structure connecting the catalytic domain attached to LC3B with the LIR^C motif attached to LDS on the opposite side of LC3B. Since the LIR^C motif was equally important for binding as for cleavage, we have no evidence that the C terminus of ATG4B directly participates in the catalytic reaction. We therefore think that the increase in cleavage seen with LIR^C-containing constructs primarily is caused by a more efficient binding to Atg8-family proteins. In agreement with this view, the C-terminal region of *Xenopus laevis* ATG4B is reported to be important for in vitro cleavage of Atg8-family orthologs.⁴⁶

LIR-LDS interaction may be regulated by phosphorylation.¹³ A recent study reports that 2 sites in the C-terminal region of ATG4B (S383 and S392) are regulated in vivo by phosphorylation, and the phosphorylation of these sites increases after treatment of cells with the MTORC1 inhibitor rapamycin.⁴¹ These sites flank the LIR^C motif. However, in our crystal structure, phosphorylated S392 pointed toward the solvent and the phosphomimetic mutation of these residues (S383E or S392E) did not significantly affect LIR^C binding. Further studies are needed to evaluate the regulatory importance of these sites in vivo.

The cleavage of proteins of the Atg8-family by ATG4B provides the primed conjugation-ready form (the I form) and is an essential step in phagophore formation. ATG4B also regulates the delipidation of Atg8-family proteins from the outer membrane of the phagophore.^{16,32–34} A continuous lipidation and delipidation of Atg8-family proteins on the phagophore may act as a cyclical proofreading event to control the fidelity of growth of autophagosomes.³² In yeast, Atg4 removes Atg8-PE from nonPAS organelle membranes. This may be critical for maintaining a pool of unlipidated Atg8 during autophagosome formation.^{33,34} The lipidation and delipidation of yeast Atg8 has been reconstituted in vitro on giant unilamellar vesicles.¹⁶ On these structures, Atg8-PE associated with Atg12-Atg5-Atg16 into a mesh-like membrane scaffold. Atg4 first disrupts the scaffold before delipidating Atg8. Our finding of a very efficient C-terminal LIR in ATG4B suggests that ATG4B may use the LIR^C to compete out GABARAP and LC3 interactions with ATG12-ATG5 and disrupt the membrane scaffold before delipidating. It is therefore tempting to speculate that the LIR^C motif is particularly important in the delipidation step, and even more so under endogenous conditions with limiting amounts of ATG4B. Delipidation occurs on membrane surfaces where Atg8-family molecules are enriched, and the process is therefore likely to involve both *cis* and *trans* type LIR-LDS interactions (Fig. 8D and E). The C-terminal LIR-LDS interaction may potentially act in *cis* or *trans*, but *trans*-interactions are most likely mediated by the N-terminal LIR motif which can only act in *trans*.³⁷ While the *cis*-interaction is necessary for the formation of a stable complex and for the maintenance of cellular pools of GABARAP and GABARAPL1, *trans*-interactions may be

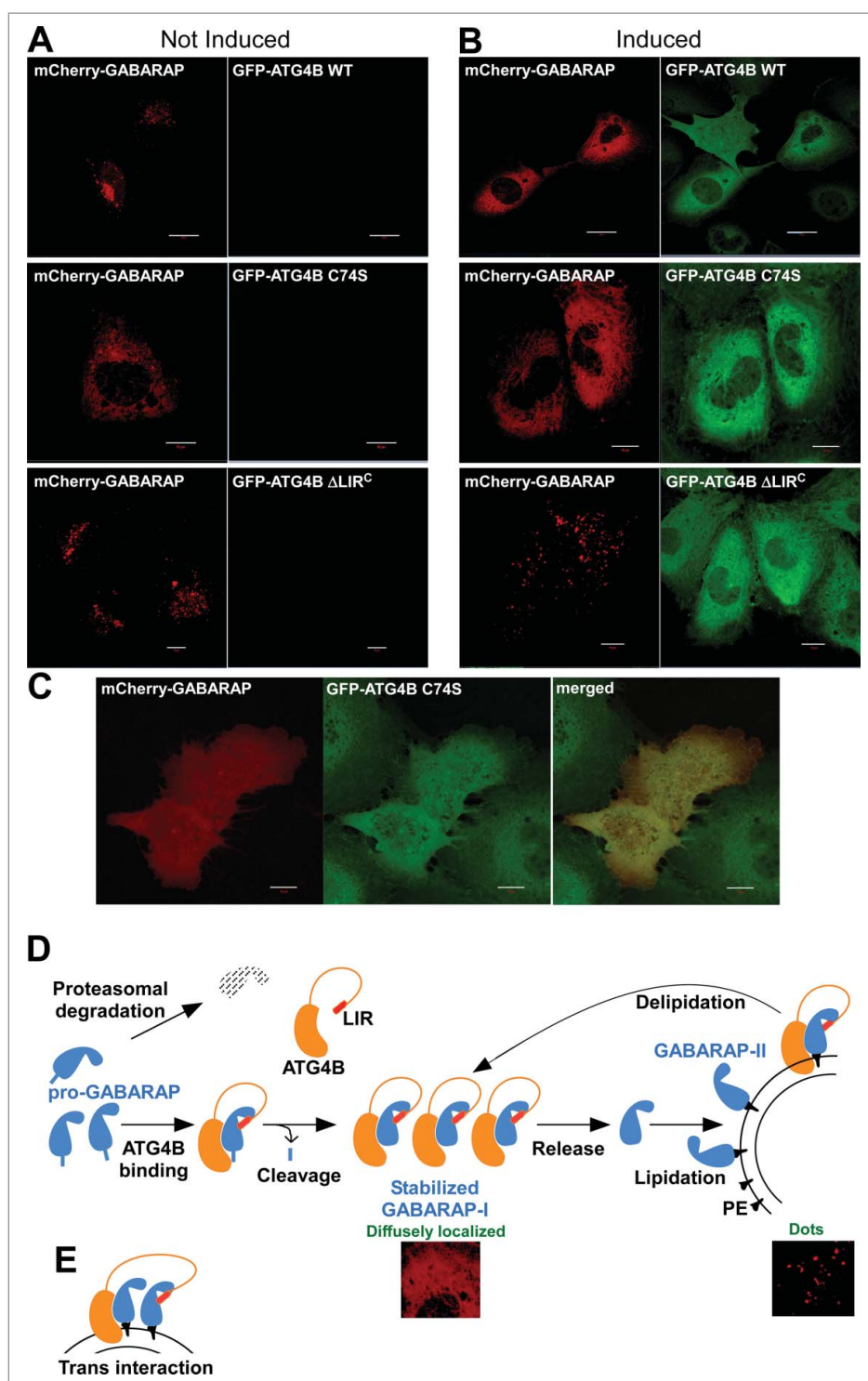


Figure 8. ATG4B stabilizes GABARAP in a LIR-dependent manner. (A) GABARAP stabilized by catalytic inactive ATG4B has a diffuse localization pattern in cells. *atg4b* KO cells reconstituted with GFP-ATG4B WT, C74S or Δ LIR^C mutant were transiently transfected with mCherry-GABARAP and analyzed by confocal microscopy 24 h post transfection. (B) High-level expression of ATG4B WT and catalytic inactive, but not ATG4B Δ LIR^C, stabilizes and redistributes ectopically expressed mCherry-GABARAP into a diffuse localization pattern. *atg4b* KO cells reconstituted with GFP-ATG4B WT, C74S or Δ LIR^C mutant were transiently transfected with mCherry-GABARAP, induced with doxycycline (1 μ g/ml), and analyzed by confocal microscopy 24 h post transfection. (C) GFP-ATG4B (C74S) and ectopically expressed mCherry-GABARAP display an almost completely overlapping localization pattern, both in the cytoplasm and in the cell nucleus. *atg4b* KO cells reconstituted with GFP-ATG4B (C74S) were transiently transfected with mCherry-GABARAP, induced by doxycycline (1 μ g/ml), and analyzed by confocal microscopy 24 h post transfection. Representative images are shown. Bars: 10 μ m. (D) Illustration of functional activities of ATG4B, indicating how the C-terminal LIR stabilizes the interaction between ATG4B and GABARAP and thereby contributes to the maintenance of a pool of unlipidated GABARAP. In (E) a potential *trans*-mediated interaction of the C-terminal LIR with an adjacent Atg8-family molecule conjugated to the same membrane is illustrated.

more important during dynamic processes such as delipidation. Structural data show that is sterically possible that a single ATG4B molecule may be engaged in 3 interactions

with 2 neighboring molecules of the Atg8 family. The substrate Atg8-family molecule is bound in *cis* by the C-terminal LIR and at the catalytic site, and the neighbor molecule

of the Atg8 family is bound in *trans* by the N-terminal LIR. This may facilitate efficient activation and delipidation on membrane surfaces.

The most dramatic effect seen in cells expressing a mutated LIR^C or a LIR^C-deleted GFP-ATG4B was a strong reduction in the cellular pools of unlipidated GABARAP and GABARAPL1, while the levels of LC3B and GABARAPL2 were unaffected. Previous studies have shown that the presence of unlipidated pools of Atg8-family proteins at least in part relies on their recycling from membranes by ATG4-dependent delipidation.^{30–32} However, other studies have revealed that overexpressed ATG4B stabilizes unlipidated LC3B by preventing its delivery to ATG7.³⁶ Our study indicates that the formation of stable complexes between ATG4B and GABARAP or GABARAPL1 may be equally important as delipidation for the maintenance of unlipidated pools of these Atg8-family proteins.

Intriguingly, we observed that GABARAP and GABARAPL1 were degraded and virtually absent in cells lacking ATG4B. Consistently, the levels of these 2 proteins were highly elevated in cells overexpressing WT ATG4B. We propose that binding to ATG4B stabilizes these proteins. Without this stabilization they are rapidly degraded by the proteasome and unavailable for autophagosome formation. Hence, direct binding of ATG4B to GABARAP and GABARAPL1, depending on the C-terminal LIR motif, plays an important role in maintaining unlipidated pools of these 2 Atg8-family proteins. Potentially, the direct binding of ATG4B to proteins of the Atg8-family may also inhibit their delivery to ATG7 and thereby have a negative effect on autophagosome formation. Given that the presence of the LIR^C motif positively affects binding and cleavage of Atg8-family proteins, but negatively affects their release from ATG4B, the full complexity of these interactions are not easily reconstituted in a system based on ectopic overexpression of ATG4B mutants. Despite numerous attempts, we were unable to reconstitute *atg4b* KO MEFs at an endogenous expression level. In line with a previous report,³⁶ we show here that an elevated cellular pool of WT ATG4B has a negative effect on autophagosome formation: This is presumably because its inhibitory effect on the release of Atg8-family proteins then becomes dominant. However, at an endogenous expression level, the relative impact of binding and cleavage becomes crucial. Very likely, the LIR^C motif may then have a positive effect on autophagosome formation due to an increased rate of binding and cleavage of proteins of the Atg8 family.

Importantly, the C-terminal LIR motif in ATG4B increases the complexity of ATG4B interactions and thereby adds another layer of regulation of autophagosome biogenesis. This may have important regulatory consequences. In *C. elegans* GABARAP (LGG-1) acts upstream of LC3 (LGG-2) in removal of paternally inherited mitochondria in embryos,⁴⁷ and nonredundantly in autophagic degradation of PGL granules during embryogenesis.⁴⁸ LGG-1 and LGG-2 differentially interact with autophagy substrates and Atg proteins. Excess lipidated LGG-1 inhibited LGG-2 puncta formation, and UNC-51 (Atg1/ULK1 ortholog) interacted with LGG-1, but not LGG-2.⁴⁸ We have previously shown that the ULK complex members ULK1/2, RB1CC1, and ATG13 bind GABARAP preferentially via LIR motifs,¹⁹ and that knockdown of GABARAP specifically attenuates ULK1 activation.⁴⁵ Hence, GABARAP may be involved in scaffolding this complex on autophagic structures. WAC (WW domain-containing adaptor with

coiled-coil), a positive regulator of autophagy,⁴⁹ inhibits binding of GABARAP to the vesicle tethering GOLGA2/golgin A2/GM130 (golgi autoantigen, golgin subfamily a, 2) to release unlipidated GABARAP from the centrosome enabling its transport to autophagosome formation sites.⁴⁵ We show here that in addition to the centrosomal pool of GABARAP there is also a large pool of diffusely localized, unlipidated GABARAP bound to ATG4B. Further studies are needed to elucidate the regulatory roles of the ATG4B-GABARAP interaction, particularly during starvation and other stress conditions inducing autophagy.

Materials and methods

Plasmids

The Gateway entry clones used in this study were pENTR-ATG4A (Harvard PlasmID Repository, HsCD00372535), pENTR-ATG4B, pDONR-ATG4C (Harvard PlasmID Repository, HsCD00044545), pENTR-ATG4D (Harvard PlasmID Repository, HsCD00383159), pENTR-ATG4, pENTR-GABARAP, pENTR-GABARAPL1, pENTR-GABARAPL2, pENTR-LC3A, pENTR-LC3B, pENTR-LC3C, pENTR-Atg8. Point mutants of pENTR-ATG4A (1 to 389, C77S), pENTR-ATG4B [1 to 384, 12 to 393, 12 to 384, (Y8A and L11A), (F388A and L391A), (Y8A, L11A, F388A and L391A), C74S, (D385A, E386A, D387A, F388A and L391A), S383E, E386A, E389A, (E386A and E389A), S392A, S392E, (S392E and S383E), and S392C], pENTR-ATG4B 374 to 393 [(F388A and L391A), E384A, D385A, E386A, D387A, E389A, S383A, S383E, S392A and S392E], pENTR-ATG4C (1 to 451), pENTR-ATG4D (1 to 467), pENTR-ATG4 [1 to 340, (F343A and L346A), (Y424A and I427A), (F446A and I449A)], pENTR-LC3B [(R10A and R11A), (F52A and L53A), R70A and (F80A and L82A)], pENTR-GABARAPL1 [H9A, R28A, R47A, (H9A and R47A), Y49A and R67A], and pENTR-Atg8 (Y49A) were made using the QuikChange site-directed mutagenesis kit (Agilent Technologies, 210515). pENTR-ATG4B were made by subcloning of ATG4B into pENTR1A (Thermo Fisher Scientific, A10462) from pOTB7-ATG4B (Harvard PlasmID Repository, HsCD00324503). Generation of constructs containing the C-terminal region of ATG4B (374 to 393 or 365 to 384) were made by subcloning into pENTR1A. ACTB-LC3B (F52A,L53A)-dNGLUC and ACTB-GABARAPL1-dNGLUC were established by mutagenesis and subcloning into the ACTB-LC3-dNGLUC plasmid (kind gifts from Robin Ketteler and Bryan Seed, Medical Research Council, Laboratory for Molecular and Cell Biology, University College London). The plasmid for recombinant expression of yeast Atg4 fused to GST was a kind gift of Sascha Martens (Department of Biochemistry and Cell Biology, Max F. Perutz Laboratories, University of Vienna). Yeast Atg4 was inserted into pENTR1A by subcloning. Gateway destination vectors used were pDEST15 (bacterial expression of N-terminal GST fusion proteins; Thermo Fisher Scientific, 11802014), pDEST24 (bacterial expression of C-terminal GST fusion proteins) (Thermo Fisher Scientific, 12216016), pDESTmyc (mammalian expression of N-terminal MYC-tagged proteins), pDEST-EGFP (mammalian expression of N-terminal EGFP-tagged proteins), and pDEST53 (mammalian expression of N-terminal GFP-tagged proteins; Thermo Fisher Scientific, 12288015). pDEST-LTR-EGFP (mammalian transfection vector for stable

and doxycycline controlled inducible expression of N-terminal-EGFP tagged fusion constructs under the control of a truncated CMV promoter) conferring blasticidin resistance was made by subcloning of EGFP and the GATEWAY cassette as a PCR product from pDEST-EGFP-C1 into the reverse Tetracycline retrovirus vector pLRT-X (a kind gift from Dr. Masaaki Komatsu, School of Medicine, Niigata University, Japan). Transfer of pENTR constructs to destination vectors was performed using the Gateway LR reaction (Thermo Fisher Scientific, 11791020).

Cell culture

MEFs were cultured in DMEM (Sigma-Aldrich, D6046) supplemented with 10% fetal bovine serum (Biochrom, S 0615) and 1% streptomycin-penicillin (Sigma-Aldrich, P4333). Knockdown of ATG4B was achieved by transfection of *Atg4b* siRNA (GAUUGGAGGUGGACACAAA, 50 nM) with Lipofectamine[®] RNAiMAX (Thermo Fisher Scientific, 13778030).

Generation of stable cell lines

ATG4B wild-type and knockout MEFs were obtained from Dr. Carlos López-Otín.⁴³ Cell lines stably expressing different GFP-ATG4 variants and GFP were made by transfection of Platinum Retroviral Packaging Cell Line-E (Cell Biolabs, RV-101) with pDEST-LTR plasmids containing the different GFP-ATG4 constructs or GFP. Viral supernatant was harvested, filtered through a 0.45- μ m filter, supplemented with 8 μ g/ml of polybrene (Sigma-Aldrich, H9268) and added to the *atg4b* knockout MEFs 24, 48 and 72 h post transfection. Immediately after viral transfection the MEFs were split and reseeded in medium containing 5 μ g/ml blasticidin S HCl (Thermo Fisher Scientific, R210-01). Induction of GFP-tagged proteins was achieved by treatment of the stable cell lines with the indicated amounts of Doxycycline (Sigma-Aldrich, D9891) for 24 h unless otherwise stated.

Peptide arrays

Peptides were synthesized on cellulose membranes using a MultiPep automated peptide synthesizer (INTAVIS Bioanalytical Instruments AG, Cologne, Germany), as described previously.⁵⁰ Membranes were blocked using 5% nonfat dry milk in Tris-buffered saline (10 mM Tris-HCl, pH 7.4, 150 mM NaCl) containing 0.1% Tween 20 (Sigma-Aldrich, P1379). The membrane was probed by overlaying with 1 μ g/ml of either GST, GST-LC3B or GST-GABARAPL1 for 2 h at RT. Membranes were washed 3 times in Tris-buffered saline containing 0.1% Tween 20. Bound protein were detected with HRP-conjugated anti-GST antibody (GE Healthcare, RPN1236)

Antibodies and reagents

The following antibodies were used: Rabbit anti-LC3B (Sigma-Aldrich, L7543), mouse anti-GABARAP (MBL, M135-3), rabbit anti-GABARAPL1 (Proteintech Group, 18723-1-AP), rabbit anti-GABARAPL2 (MBL, PM038) guinea pig anti-SQSTM1 (Progen, GP62-C), rabbit anti-GFP (Abcam, AB290), mouse anti-PCNA (DAKO, M0829), rabbit anti-ATG4B (Santa Cruz

Biotechnology, SC-130968), mouse anti-ubiquitin (FK2; Enzo Life Sciences, PW8810), horseradish peroxidase-conjugated goat anti-mouse (BD Biosciences, 554002), anti-rabbit (BD Biosciences, 554021) and goat anti-guinea pig (Santa Cruz Biotechnology, sc-2438) secondary antibodies. Other reagents used were BafA1 (Santa Cruz Biotechnology, sc-201550) and L-[³⁵S] methionine (PerkinElmer, NEG709A500UC).

Protein purification and GST affinity isolation experiments

GST-tagged proteins were expressed in *Escherichia coli* BL21 (DE3). GST-(Atg8-family proteins) and (Atg8-family proteins)-GST fusion proteins were purified on glutathione-Sepharose 4 Fast Flow beads (GE Healthcare, 17513201) followed by washing with NET-N buffer (100 mM NaCl, 1 mM EDTA, 0.5% Nonidet P-40 (Sigma-Aldrich, 74385), 50 mM Tris-HCl, pH 8) supplemented with cComplete Mini EDTA-free protease inhibitor mixture tablets (Roche Applied Science, 11836170001). GST-ATG4Bs fusion proteins were purified on GSTrap Fast Flow columns (GE Healthcare, 17-5130-01). GST-tagged proteins were eluted with 50 mM Tris, pH 8, 200 mM NaCl, 5 mM L-gluthathione reduced (Sigma-Aldrich, G425). GST affinity isolation assays were performed with ³⁵S-labeled proteins cotranscribed and translated using the TnT Coupled Reticulocyte Lysate System (Promega, L4610) as described previously.¹⁸ For quantifications gels were vacuum dried and ³⁵S-labeled proteins detected on a Fujifilm bioimaging analyzer BAS-5000 (Fujifilm, Tokyo, Japan).

Expression and purification of GABARAPL1 for crystallization

GABARAPL1 full-length sequence was inserted between the BamHI and NotI sites of a pGEX-6P2 plasmid (GE Healthcare, 28-9546-50) containing a cleavable glutathione S-transferase tag. Protein expression was at 30°C in *E. coli* Rosetta (DE3) pLysS. Bacteria were harvested by centrifugation and resuspended in lysis buffer (50 mM Tris-HCl, pH 8.0, 500 mM NaCl, 0.1% Triton X-100 (Sigma-Aldrich, T8787), 0.5 mM TCEP (Melford Laboratories, T2650), 0.5 mM AEBSF (AppliChem, A1421) and 15 μ g/ml benzamidine (Melford Laboratories, B4101). The fusion protein was batch-adsorbed onto a glutathione-Sepharose affinity matrix and GABARAPL1 recovered by cleavage with 3C protease (made in house) at 4°C overnight in 50 mM Tris-HCl, pH 8.0, 100 mM NaCl, 0.5 mM TCEP. GABARAPL1 was then purified by size exclusion chromatography using a Superdex 75 column equilibrated and run in 25 mM Tris-HCl, pH 8.0, 150 mM NaCl and 0.5 mM TCEP. Peptides were synthesized by the Francis Crick Institute Peptide Chemistry Science Technology Platform.

Crystallization of ATG4B LIR

GABARAPL1-ATG4B LIR complexes were prepared by mixing purified full-length GABARAPL1 and ATG4B peptide (residues 384 to 393, defined hereafter as wild-type ATG4B LIR; EDEDFEILSL) at a 1:3 molar ratio. The complex of the ATG4B peptide phosphorylated on residue S392 (residues 384 to 393, defined hereafter as phosphorylated ATG4B LIR;

EDDFEIL-pS-L) was prepared by mixing GABARAPL1 and the phosphorylated ATG4B peptide at a 1:3 molar ratio. The complexes were dialyzed overnight in 25 mM Tris-HCl, pH 8.0, 150 mM NaCl and 0.5 mM TCEP buffer, using a 500- to 1000-Da MWCO dialysis tubing for both complexes. The wild-type ATG4B complex was crystallized at 20°C using the sitting-drop vapor diffusion method with a protein concentration of 20 mg/ml. Sitting drops of 1 μ l consisted of a 1:1 (vol:vol) mixture of protein and a well solution containing 0.17 M (NH₄)₂SO₄ (Hampton Research, HR2-541), 40% PEG 4000 (Sigma-Aldrich, 95904), 15% glycerol (Sigma-Aldrich, G5516). Crystals appeared after 10 d and reached their maximum size after 20 d (0.05 mm \times 0.05 mm). Crystals were flash-frozen in liquid nitrogen, and X-ray data sets were collected at 100 K at the I02 beamline of the Diamond Light Source Synchrotron (Oxford, UK).

The phosphorylated ATG4B complex was crystallized at 20°C using the sitting-drop vapor diffusion method with a protein concentration of 20 mg/ml. Sitting drops of 1 μ l consisted of a 1:1 (vol:vol) mixture of protein and a well solution containing 0.1 M MgCl₂, 24.6% PEG 400, 29.5% PEG 8000 (Sigma-Aldrich, 89510), 0.1M Tris, pH 8.5. Crystals appeared after 5 d and reached their maximum size after 10 d (0.2 mm \times 0.05 mm). Crystals were flash-frozen in liquid nitrogen, and X-ray data sets were collected at 100 K at the I03 beamline of the Diamond Light Source Synchrotron (Oxford, UK).

Data collection and refinement statistics are summarized in Table 1. The data sets were indexed and scaled with xia2.⁵¹ Molecular replacement was achieved by using the atomic

coordinates of the peptide-free GABARAPL1 (PDB code: 2R2Q) in PHASER.⁵² Refinement was performed using Phenix.⁵³ Model building was performed in COOT.⁵⁴ Model validation used PROCHECK,⁵⁵ and figures were prepared using the graphics program PYMOL (<http://www.pymol.org>). The asymmetric units contain 3 identical copies of the complex for the wild-type ATG4B-GABARAPL1 structure and 2 identical copies of the complex for the phosphorylated ATG4B-GABARAPL1 structure. In both structures the difference electron density map covering ATG4B shows unambiguous density for residues 484 to 493.

In vitro assay of ATG4B cleavage activity

LC3B-GST- and GABARAP-GST proteins expressed and purified from E. coli were washed 5 times to remove excess protease inhibitor. 2.5 μ g/ml of GST-ATG4B, GST-ATG4B (C74S), or GST-ATG4B Δ LIR^C proteins were incubated together with 0.5 to 1.5 μ g of LC3B-GST or GABARAP-GST at 30°C for the indicated time points in 20 μ l buffer (200 mM NaCl, 1 mM EDTA, 5 mM DTT, 20 mM Tris-HCl, pH 7.4). Reactions were stopped by addition of 5xSDS-loading buffer (500 mM DTT, 10% SDS, 0.5% bromophenol blue, 50% glycerol, 250 mM Tris-HCl, pH 6.8), resolved by SDS-PAGE and visualized by Coomassie brilliant blue staining.

Western blot and immunoprecipitation experiments

For western blotting experiments, cells were washed in PBS (137 mM NaCl, 2.7 mM KCl, 4.3 mM Na₂HPO₄, 1.47 mM KH₂PO₄, pH 7.4.) followed by lysis directly in SDS-PAGE loading buffer (2% SDS, 10% glycerol 50 mM Tris-HCl, pH 6.8) and boiled for 10 min. Protein concentration was measured followed by addition of bromophenol blue (0.1%) and DTT (100 mM). Samples (20 μ g) were run on 10–16% gradient- or 10%-SDS-polyacrylamide gels and blotted on Hybond nitrocellulose membranes (GE Healthcare, 10600003) followed by Ponceau S staining. Blocking was performed in 5% nonfat dry milk in PBS-Tween 20 (0.1%). Primary antibody was diluted in PBS-Tween 20 containing 5% nonfat dry milk and incubation was performed overnight at 4°C. Secondary antibody incubation was performed at room temperature for 1 h in PBS-Tween 20 containing 5% nonfat dry milk. Membranes were washed 3 times before addition of secondary antibody and development using either Amersham Hyperfilm ECL (GE Healthcare, 28906836) or LAS-300 (Fujifilm, Tokyo, Japan). Immunoprecipitations were performed by use of GFP-trap_A system in accordance with the manufacturer's instructions (Chromotek, gta-20).

Luciferase assay to monitor in vivo cleavage activity of ATG4B

In vivo ATG4B activity was assayed by measuring cellular export of Gaussia luciferase as described previously.⁴⁴ Reconstituted *atg4b* KO MEFs were seeded in 24-well plates and cotransfected with 50 ng pGL3 promoter (Firefly luciferase) (Promega, E1761) and 200 ng of either ACTB-LC3B-dNGLUC/ACTB-LC3B F52A L53A-dNGLUC/ACTB-GABARAPL1-dNGLUC or ACTB-dNGLUC using Metafectene Pro

Table 1. Data collection and refinement statistics.

| PDB ID | WT ATG4B-GABARAPL1 5LXH | ATG4B (p-S392)-GABARAPL1 5LXI |
|---|--|---------------------------------------|
| Data collection | | |
| Space group | P 2 ₁ 2 ₁ 2 ₁ | C 2 |
| Cell dimensions a, b, c (Å) α , β , γ (°) | 51.5, 79.89, 97.64 90.0, 90.0, 90.0 | 124.9, 78.4, 30.6 90.0, 99.2, 90.0 |
| Resolution (Å) (Outer resolution shell) Å | 51 – 1.58 (1.66 – 1.58) | 35 – 1.44 (1.48 – 1.44) |
| R _{pim} | 3.0 (49.4) | 2.9 (50.9) |
| R _{sym} (%) | 5.6 (87.9) | 3.8 (59.0) |
| CC(1/2) | 99.9 (60.5) | 99.8 (74.6) |
| I/ σ I | 10.7 (1.3) | 10.1 (1.3) |
| Completeness (%) | 100 (99.9) | 96.0 (93.7) |
| Redundancy | 5.1 (4.9) | 3.1 (3.0) |
| Refinement | | |
| Resolution (Å) (Outer resolution shell) Å | 48 – 1.58 (1.60 – 1.58) | 31 – 1.44 (1.47 – 1.44) |
| No. unique reflections | 55 946 | 46 217 |
| R _{work} | 20.5 (39.1) | 19.6 (36.3) |
| R _{free} ^a | 23.7 (45.6) | 22.9 (41.7) |
| No. atoms | 3 467 | 2 290 |
| Average isotropic B-factors (Å ²) | 25.8 | 30.7 |
| GABARAPL1 | 24.3 | 30.1 |
| ATG4B peptide | 43.6 | 35.0 |
| Water | 34.7 | 34.6 |
| R.m.s. deviations | | |
| bonds (Å) | 0.017 | 0.014 |
| angles (°) | 1.42 | 1.15 |
| Ramachandran plot (%) (favored, allowed, disallowed) | 98.9/1.1/0 | 97.3/2.7/0 |

^a A total of 5% of the data were set aside to compute R_{free}.

(Biont, T040). Media was changed 24 h post-transfection, and Gaussia luciferase was allowed to accumulate in the media for 18 to 24 h. Media and cells were harvested for measurements of Gaussia and Firefly luciferase, respectively, using the Dual luciferase reporter assay system (Promega, E1910) and a CLARIOstar (BMG labtech, Ortenberg, Germany) in accordance with the manufacturer's instructions. For ACTB-dNGLUC and ACTB-LC3B (F52A,L53A)-dNGLUC, single sampling tests were conducted on the cell lysate to verify that functional Gaussia luciferase was retained inside the cells.

Bioinformatics and statistics

Data in all figures are shown as mean \pm SD from at least 3 independent experiments. Statistical significance was evaluated with one-way ANOVA followed by the Tukey multiple comparison test performed in PRISM (Graphpad) (ns $P > 0.05$, * $P \leq 0.05$, ** $P \leq 0.01$, *** $P \leq 0.001$). Alignment of ATG4 isoform homologs was performed in CLC Main workbench (Qiagen).

Abbreviations

| | |
|---|---|
| 2mLIR, F388A and L391A | double mutation of LIR |
| 5mLIR, D385A, E386A, D387A, F388A and L391A | multiple mutation of LIR |
| ATG | AuTophagy-related |
| BafA1 | Bafilomycin A ₁ |
| GABARAP | gamma-aminobutyric acid receptor associated protein |
| GFP | enhanced green fluorescent protein |
| KO | knockout |
| LDS | LIR docking site |
| LIR | LC3-interacting region |
| MAP1LC3/LC3 | microtubule-associated protein 1 light chain 3 |
| MEF | mouse embryonic fibroblast |
| PE | phosphatidylethanolamine |

Disclosure of potential conflicts of interest

No potential conflicts of interest were disclosed.

Acknowledgments

We are indebted to Carlos López-Otín for the generous gift of the *atg4b* KO MEFs, to Robin Ketteler and Bryan Seed for the ACTB-LC3-dNGLUC and ACTB-dNGLUC plasmids, Dr. Masaaki Komatsu for the pLRT-X retrovirus vector, and to Sascha Martens for the yeast GST-Atg4 plasmid. The technical assistance of Gry Evjen and Roy André Lyså is greatly appreciated. We thank the Advanced Microscopy Core Facility (AMCF) at the Institute of Medical Biology (UiT – The Arctic University of Norway) for the use of instrumentation and expert assistance. We thank the Francis Crick Institute Structural Biology Science Technology Platform for technical support.

Funding

This work was funded by grants from the FRIBIOMED program of the Norwegian Research Council (grant number 214448), and the Norwegian Cancer Society (grant number 71043-PR-2006-0320) to T.J., S.M., N. O'R., M.W. and S.A.T. were supported by the Francis Crick Institute

(FC001187; M.W. and S.A.T.) which receives its core funding from Cancer Research UK, the UK Medical Research Council, and the Wellcome Trust.

ORCID

Sharon A. Tooze  <http://orcid.org/0000-0002-2182-3116>
Terje Johansen  <http://orcid.org/0000-0003-1451-9578>

References

- [1] Mizushima N, Komatsu M. Autophagy: renovation of cells and tissues. *Cell* 2011; 147:728-41; PMID:22078875; <http://dx.doi.org/10.1016/j.cell.2011.10.026>
- [2] Seglen PO. Regulation of autophagic protein degradation in isolated liver cells. In: Glaumann H, Ballard FJ, ed. *Lysosomes: Their Role in Protein Breakdown*. London: Academic Press, 1987:371-414
- [3] Wen X, Klionsky DJ. An overview of macroautophagy in yeast. *J Mol Biol* 2016; 428:1681-99; PMID:26908221; <http://dx.doi.org/10.1016/j.jmb.2016.02.021>
- [4] Johansen T, Lamark T. Selective autophagy mediated by autophagic adapter proteins. *Autophagy* 2011; 7:279-96; PMID:21189453; <http://dx.doi.org/10.4161/auto.7.3.14487>
- [5] Rogov V, Dotsch V, Johansen T, Kirkin V. Interactions between autophagy receptors and ubiquitin-like proteins form the molecular basis for selective autophagy. *Mol Cell* 2014; 53:167-78; PMID:24462201; <http://dx.doi.org/10.1016/j.molcel.2013.12.014>
- [6] Gordon PB, Seglen PO. Prelysosomal convergence of autophagic and endocytic pathways. *Biochem Biophys Res Commun* 1988; 151:40-7; PMID:3126737; [http://dx.doi.org/10.1016/0006-291X\(88\)90556-6](http://dx.doi.org/10.1016/0006-291X(88)90556-6)
- [7] Shen HM, Mizushima N. At the end of the autophagic road: an emerging understanding of lysosomal functions in autophagy. *Trends Biochem Sci* 2014; 39:61-71; PMID:24369758; <http://dx.doi.org/10.1016/j.tibs.2013.12.001>
- [8] Tsukada M, Ohsumi Y. Isolation and characterization of autophagy-defective mutants of *Saccharomyces cerevisiae*. *FEBS Lett* 1993; 333:169-74; PMID:8224160; [http://dx.doi.org/10.1016/0014-5793\(93\)80398-E](http://dx.doi.org/10.1016/0014-5793(93)80398-E)
- [9] Mizushima N, Yoshimori T, Ohsumi Y. The role of Atg proteins in autophagosome formation. *Annu Rev Cell Dev Biol* 2011; 27:107-32; PMID:21801009; <http://dx.doi.org/10.1146/annurev-cellbio-092910-154005>
- [10] Shpilka T, Weidberg H, Pietrokovski S, Elazar Z. Atg8: an autophagy-related ubiquitin-like protein family. *Genome Biol* 2011; 12:226; PMID:21867568; <http://dx.doi.org/10.1186/gb-2011-12-7-226>
- [11] Ichimura Y, Kirisako T, Takao T, Satomi Y, Shimonishi Y, Ishihara N, Mizushima N, Tanida I, Kominami E, Ohsumi M, et al. A ubiquitin-like system mediates protein lipidation. *Nature* 2000; 408:488-92; PMID:11100732; <http://dx.doi.org/10.1038/35044114>
- [12] Kabeya Y, Mizushima N, Ueno T, Yamamoto A, Kirisako T, Noda T, Kominami E, Ohsumi Y, Yoshimori T. LC3, a mammalian homologue of yeast Apg8p, is localized in autophagosome membranes after processing. *EMBO J* 2000; 19:5720-8; PMID:11060023; <http://dx.doi.org/10.1093/emboj/19.21.5720>
- [13] Birgisdottir AB, Lamark T, Johansen T. The LIR motif - crucial for selective autophagy. *J Cell Sci* 2013; 126:3237-47; PMID:23908376
- [14] Xie Z, Nair U, Klionsky DJ. Atg8 controls phagophore expansion during autophagosome formation. *Mol Biol Cell* 2008; 19:3290-8; PMID:18508918; <http://dx.doi.org/10.1091/mbc.E07-12-1292>
- [15] Weidberg H, Shvets E, Shpilka T, Shimron F, Shinder V, Elazar Z. LC3 and GATE-16/GABARAP subfamilies are both essential yet act differently in autophagosome biogenesis. *EMBO J* 2010; 29:1792-802; PMID:20418806; <http://dx.doi.org/10.1038/emboj.2010.74>
- [16] Kaufmann A, Beier V, Franquelim HG, Wollert T. Molecular mechanism of autophagic membrane-scaffold assembly and disassembly. *Cell* 2014; 156:469-81; PMID:24485455; <http://dx.doi.org/10.1016/j.cell.2013.12.022>
- [17] Kirisako T, Ichimura Y, Okada H, Kabeya Y, Mizushima N, Yoshimori T, Ohsumi M, Takao T, Noda T, Ohsumi Y. The reversible modification regulates the membrane-binding state of Apg8/Aut7

- essential for autophagy and the cytoplasm to vacuole targeting pathway. *J Cell Biol* 2000; 151:263-76; PMID:11038174; <http://dx.doi.org/10.1083/jcb.151.2.263>
- [18] Pankiv S, Clausen TH, Lamark T, Brech A, Bruun JA, Outzen H, Overvatn A, Bjorkoy G, Johansen T. p62/SQSTM1 binds directly to Atg8/LC3 to facilitate degradation of ubiquitinated protein aggregates by autophagy. *J Biol Chem* 2007; 282:24131-45; PMID:17580304; <http://dx.doi.org/10.1074/jbc.M702824200>
- [19] Alemu EA, Lamark T, Torgersen KM, Birgisdottir AB, Larsen KB, Jain A, Olsvik H, Overvatn A, Kirkin V, Johansen T. ATG8 family proteins act as scaffolds for assembly of the ULK complex: Sequence Requirements For LC3-Interacting Region (LIR) Motifs. *J Biol Chem* 2012; 287:39275-90; PMID:23043107; <http://dx.doi.org/10.1074/jbc.M112.378109>
- [20] Hamacher-Brady A, Brady NR. Mitophagy programs: mechanisms and physiological implications of mitochondrial targeting by autophagy. *Cell Mol Life Sci* 2016; 73:775-95; PMID:26611876; <http://dx.doi.org/10.1007/s00018-015-2087-8>
- [21] Wild P, McEwan DG, Dikic I. The LC3 interactome at a glance. *J Cell Sci* 2014; 127:3-9; PMID:24345374; <http://dx.doi.org/10.1242/jcs.140426>
- [22] Ichimura Y, Kumanomidou T, Sou YS, Mizushima T, Ezaki J, Ueno T, Kominami E, Yamane T, Tanaka K, Komatsu M. Structural basis for sorting mechanism of p62 in selective autophagy. *J Biol Chem* 2008; 283:22847-57; PMID:18524774; <http://dx.doi.org/10.1074/jbc.M802182200>
- [23] Noda NN, Kumeta H, Nakatogawa H, Satoo K, Adachi W, Ishii J, Fujioka Y, Ohsumi Y, Inagaki F. Structural basis of target recognition by Atg8/LC3 during selective autophagy. *Genes Cells* 2008; 13:1211-8; PMID:19021777; <http://dx.doi.org/10.1111/j.1365-2443.2008.01238.x>
- [24] Fernandez AF, Lopez-Otin C. The functional and pathologic relevance of autophagy proteases. *J Clin Invest* 2015; 125:33-41; PMID:25654548; <http://dx.doi.org/10.1172/JCI73940>
- [25] Hemelaar J, Lelyveld VS, Kessler BM, Ploegh HL. A single protease, Apg4B, is specific for the autophagy-related ubiquitin-like proteins GATE-16, MAP1-LC3, GABARAP, and Apg8L. *J Biol Chem* 2003; 278:51841-50; PMID:14530254; <http://dx.doi.org/10.1074/jbc.M308762200>
- [26] Li M, Hou Y, Wang J, Chen X, Shao ZM, Yin XM. Kinetics comparisons of mammalian Atg4 homologues indicate selective preferences toward diverse Atg8 substrates. *J Biol Chem* 2011; 286:7327-38; PMID:21177865; <http://dx.doi.org/10.1074/jbc.M110.199059>
- [27] Tanida I, Ueno T, Kominami E. Human light chain 3/MAP1LC3B is cleaved at its carboxyl-terminal Met121 to expose Gly120 for lipidation and targeting to autophagosomal membranes. *J Biol Chem* 2004; 279:47704-10; PMID:15355958; <http://dx.doi.org/10.1074/jbc.M407016200>
- [28] Kabeya Y, Mizushima N, Yamamoto A, Oshitani-Okamoto S, Ohsumi Y, Yoshimori T. LC3, GABARAP and GATE16 localize to autophagosomal membrane depending on form-II formation. *J Cell Sci* 2004; 117:2805-12; PMID:15169837; <http://dx.doi.org/10.1242/jcs.01131>
- [29] Scherz-Shouval R, Sagiv Y, Shorer H, Elazar Z. The COOH terminus of GATE-16, an intra-Golgi transport modulator, is cleaved by the human cysteine protease HsApg4A. *J Biol Chem* 2003; 278:14053-8; PMID:12473658; <http://dx.doi.org/10.1074/jbc.M212108200>
- [30] Betin VM, Lane JD. Caspase cleavage of Atg4D stimulates GABARAP-L1 processing and triggers mitochondrial targeting and apoptosis. *J Cell Sci* 2009; 122:2554-66; PMID:19549685; <http://dx.doi.org/10.1242/jcs.046250>
- [31] Marino G, Salvador-Montoliu N, Fueyo A, Knecht E, Mizushima N, Lopez-Otin C. Tissue-specific autophagy alterations and increased tumorigenesis in mice deficient in Atg4C/autophagin-3. *J Biol Chem* 2007; 282:18573-83; PMID:17442669; <http://dx.doi.org/10.1074/jbc.M701194200>
- [32] Nair U, Yen WL, Mari M, Cao Y, Xie Z, Baba M, Reggiori F, Klionsky DJ. A role for Atg8-PE deconjugation in autophagosome biogenesis. *Autophagy* 2012; 8:780-93; PMID:22622160; <http://dx.doi.org/10.4161/auto.19385>
- [33] Nakatogawa H, Ishii J, Asai E, Ohsumi Y. Atg4 recycles inappropriately lipidated Atg8 to promote autophagosome biogenesis. *Autophagy* 2012; 8:177-86; PMID:22240591; <http://dx.doi.org/10.4161/auto.8.2.18373>
- [34] Yu ZQ, Ni T, Hong B, Wang HY, Jiang FJ, Zou S, Chen Y, Zheng XL, Klionsky DJ, Liang Y, et al. Dual roles of Atg8-PE deconjugation by Atg4 in autophagy. *Autophagy* 2012; 8:883-92; PMID:22652539; <http://dx.doi.org/10.4161/auto.19652>
- [35] Scherz-Shouval R, Shvets E, Fass E, Shorer H, Gil L, Elazar Z. Reactive oxygen species are essential for autophagy and specifically regulate the activity of Atg4. *EMBO J* 2007; 26:1749-60; PMID:17347651; <http://dx.doi.org/10.1038/sj.emboj.7601623>
- [36] Fujita N, Hayashi-Nishino M, Fukumoto H, Omori H, Yamamoto A, Noda T, Yoshimori T. An Atg4B mutant hampers the lipidation of LC3 paralogues and causes defects in autophagosome closure. *Mol Biol Cell* 2008; 19:4651-9; PMID:18768752; <http://dx.doi.org/10.1091/mbc.E08-03-0312>
- [37] Satoo K, Noda NN, Kumeta H, Fujioka Y, Mizushima N, Ohsumi Y, Inagaki F. The structure of Atg4B-LC3 complex reveals the mechanism of LC3 processing and delipidation during autophagy. *EMBO J* 2009; 28:1341-50; PMID:19322194; <http://dx.doi.org/10.1038/emboj.2009.80>
- [38] Kalvari I, Tsompanis S, Mulakkal NC, Osgood R, Johansen T, Nezis IP, Promponas VJ. iLIR: A web resource for prediction of Atg8-family interacting proteins. *Autophagy* 2014; 10:913-25; PMID:24589857; <http://dx.doi.org/10.4161/auto.28260>
- [39] Xue B, Dunbrack RL, Williams RW, Dunker AK, Uversky VN. PONDR-FIT: a meta-predictor of intrinsically disordered amino acids. *Biochim Biophys Acta* 2010; 1804:996-1010; PMID:20100603; <http://dx.doi.org/10.1016/j.bbapap.2010.01.011>
- [40] Rozenknop A, Rogov VV, Rogova NY, Lohr F, Guntert P, Dikic I, Dotsch V. Characterization of the interaction of GABARAP-1 with the LIR motif of NBRL. *J Mol Biol* 2011; 410:477-87; PMID:21620860; <http://dx.doi.org/10.1016/j.jmb.2011.05.003>
- [41] Yang Z, Wilkie-Graham RP, Yanagi T, Shu CW, Matsuzawa S, Reed JC. ATG4B (Autophagin-1) phosphorylation modulates autophagy. *J Biol Chem* 2015; 290:26549-61; PMID:26378241; <http://dx.doi.org/10.1074/jbc.M115.658088>
- [42] Rogov VV, Suzuki H, Fiskin E, Wild P, Kniss A, Rozenknop A, Kato R, Kawasaki M, McEwan DG, Lohr F, et al. Structural basis for phosphorylation-triggered autophagic clearance of Salmonella. *Biochem J* 2013; 454:459-66; PMID:23805866; <http://dx.doi.org/10.1042/BJ20121907>
- [43] Marino G, Fernandez AF, Cabrera S, Lundberg YW, Cabanillas R, Rodriguez F, Salvador-Montoliu N, Vega JA, Germana A, Fueyo A, et al. Autophagy is essential for mouse sense of balance. *J Clin Invest* 2010; 120:2331-44; PMID:20577052; <http://dx.doi.org/10.1172/JCI42601>
- [44] Ketteler R, Sun Z, Kovacs KF, He WW, Seed B. A pathway sensor for genome-wide screens of intracellular proteolytic cleavage. *Genome Biol* 2008; 9:R64; PMID:18387192; <http://dx.doi.org/10.1186/gb-2008-9-4-r64>
- [45] Joachim J, Jefferies HB, Razi M, Frith D, Snijders AP, Chakravarty P, Judith D, Tooze SA. Activation of ULK kinase and autophagy by GABARAP trafficking from the centrosome is regulated by WAC and GM130. *Mol Cell* 2015; 60:899-913; PMID:26687599; <http://dx.doi.org/10.1016/j.molcel.2015.11.018>
- [46] Frey S, Gorlich D. The *Xenopus laevis* Atg4B Protease: Insights into substrate recognition and application for tag removal from proteins expressed in Pro- and Eukaryotic hosts. *PloS One* 2015; 10:e0125099; PMID:25923686; <http://dx.doi.org/10.1371/journal.pone.0125099>
- [47] Manil-Segalen M, Lefebvre C, Jenzer C, Trichet M, Boulogne C, Satiat-Jeunemaitre B, Legouis R. The *C. elegans* LC3 acts downstream of GABARAP to degrade autophagosomes by interacting with the HOPS subunit VPS39. *Dev Cell* 2014; 28:43-55; PMID:24374177; <http://dx.doi.org/10.1016/j.devcel.2013.11.022>
- [48] Wu F, Watanabe Y, Guo XY, Qi X, Wang P, Zhao HY, Wang Z, Fujioka Y, Zhang H, Ren JQ, et al. Structural Basis of the Differential Function of the Two *C. elegans* Atg8 Homologs, LGG-1 and LGG-2,

- in Autophagy. *Mol Cell* 2015; 60:914-29; PMID:26687600; <http://dx.doi.org/10.1016/j.molcel.2015.11.019>
- [49] McKnight NC, Jefferies HB, Alemu EA, Saunders RE, Howell M, Johansen T, Tooze SA. Genome-wide siRNA screen reveals amino acid starvation-induced autophagy requires SCOC and WAC. *EMBO J* 2012; 31:1931-46; PMID:22354037; <http://dx.doi.org/10.1038/emboj.2012.36>
- [50] Kramer RM, Roberts EF, Um SL, Borsch-Haubold AG, Watson SP, Fisher MJ, Jakubowski JA. p38 mitogen-activated protein kinase phosphorylates cytosolic phospholipase A2 (cPLA2) in thrombin-stimulated platelets. Evidence that proline-directed phosphorylation is not required for mobilization of arachidonic acid by cPLA2. *J Biol Chem* 1996; 271:27723-9; PMID:8910365; <http://dx.doi.org/10.1074/jbc.271.44.27723>
- [51] Winter G, Lobley CM, Prince SM. Decision making in xia2. *Acta Crystallogr D Biol Crystallogr* 2013; 69:1260-73; PMID:23793152; <http://dx.doi.org/10.1107/S0907444913015308>
- [52] McCoy AJ, Grosse-Kunstleve RW, Adams PD, Winn MD, Storoni LC, Read RJ. Phaser crystallographic software. *J Appl Crystallogr* 2007; 40:658-74; PMID:19461840; <http://dx.doi.org/10.1107/S0021889807021206>
- [53] Adams PD, Afonine PV, Bunkoczi G, Chen VB, Davis IW, Echols N, Headd JJ, Hung LW, Kapral GJ, Grosse-Kunstleve RW, et al. PHENIX: a comprehensive Python-based system for macromolecular structure solution. *Acta Crystallogr D Biol Crystallogr* 2010; 66:213-21; PMID:20124702; <http://dx.doi.org/10.1107/S0907444909052925>
- [54] Emsley P, Lohkamp B, Scott WG, Cowtan K. Features and development of Coot. *Acta Crystallogr D Biol Crystallogr* 2010; 66:486-501; PMID:20383002; <http://dx.doi.org/10.1107/S0907444910007493>
- [55] Vaguine AA, Richelle J, Wodak SJ. SFCHECK: a unified set of procedures for evaluating the quality of macromolecular structure-factor data and their agreement with the atomic model. *Acta Crystallogr D Biol Crystallogr* 1999; 55:191-205; PMID:10089410; <http://dx.doi.org/10.1107/S0907444998006684>
- [56] Robert X, Gouet P. Deciphering key features in protein structures with the new ENDscript server. *Nucleic Acids Res* 2014; 42:W320-4; PMID:24753421; <http://dx.doi.org/10.1093/nar/gku316>

Figure S1

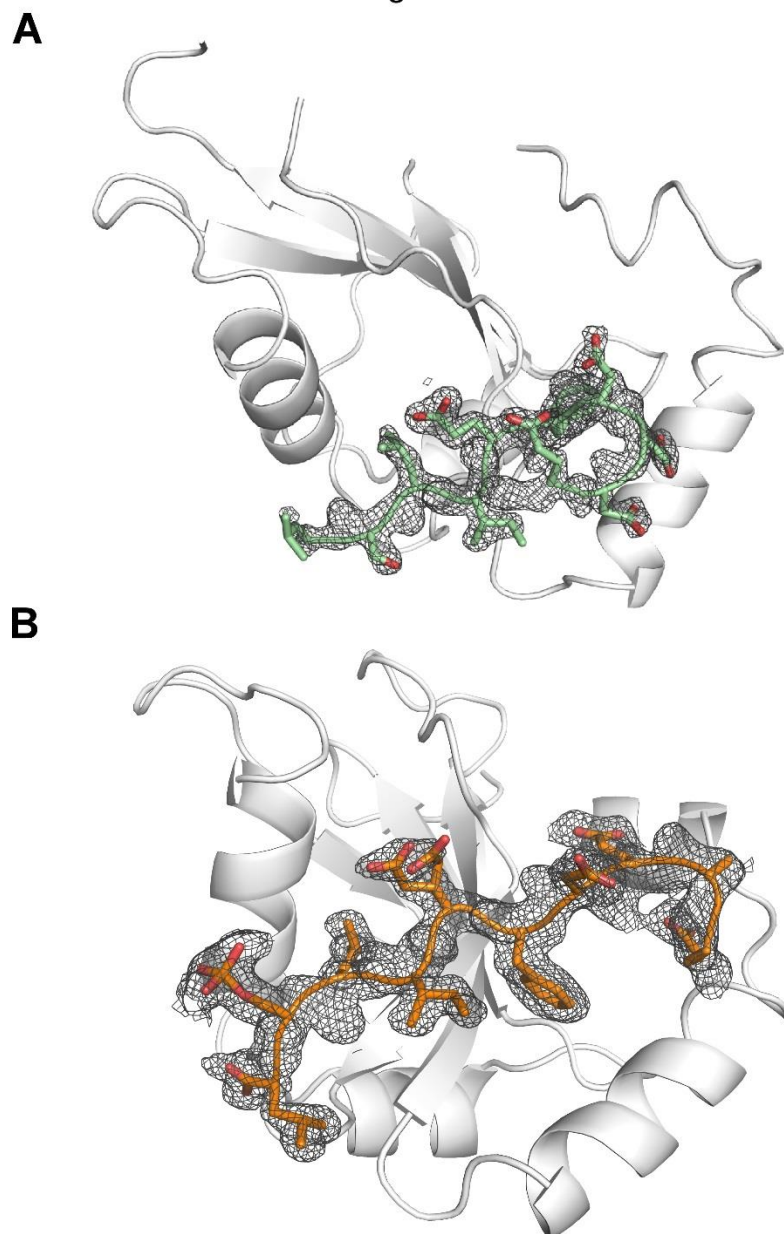


Figure S1. Electron density map of ATG4B LIR^C bound to GABARAPL1. **(A)** Electron density map of wild-type ATG4B LIR^C peptide bound to GABARAPL1. The Fo-Fc omit map of the ATG4B peptide is contoured at 0.8 σ . GABARAPL1 is displayed in white cartoon and the ATG4B peptide in pale green cartoon with its side chains drawn in sticks. **(B)** Electron density map of phosphorylated ATG4B LIR^C peptide bound to GABARAPL1. The Fo-Fc omit map of the ATG4B peptide is contoured at 0.8 σ . GABARAPL1 is displayed in white cartoon and ATG4B peptide in orange cartoon.

Figure S2

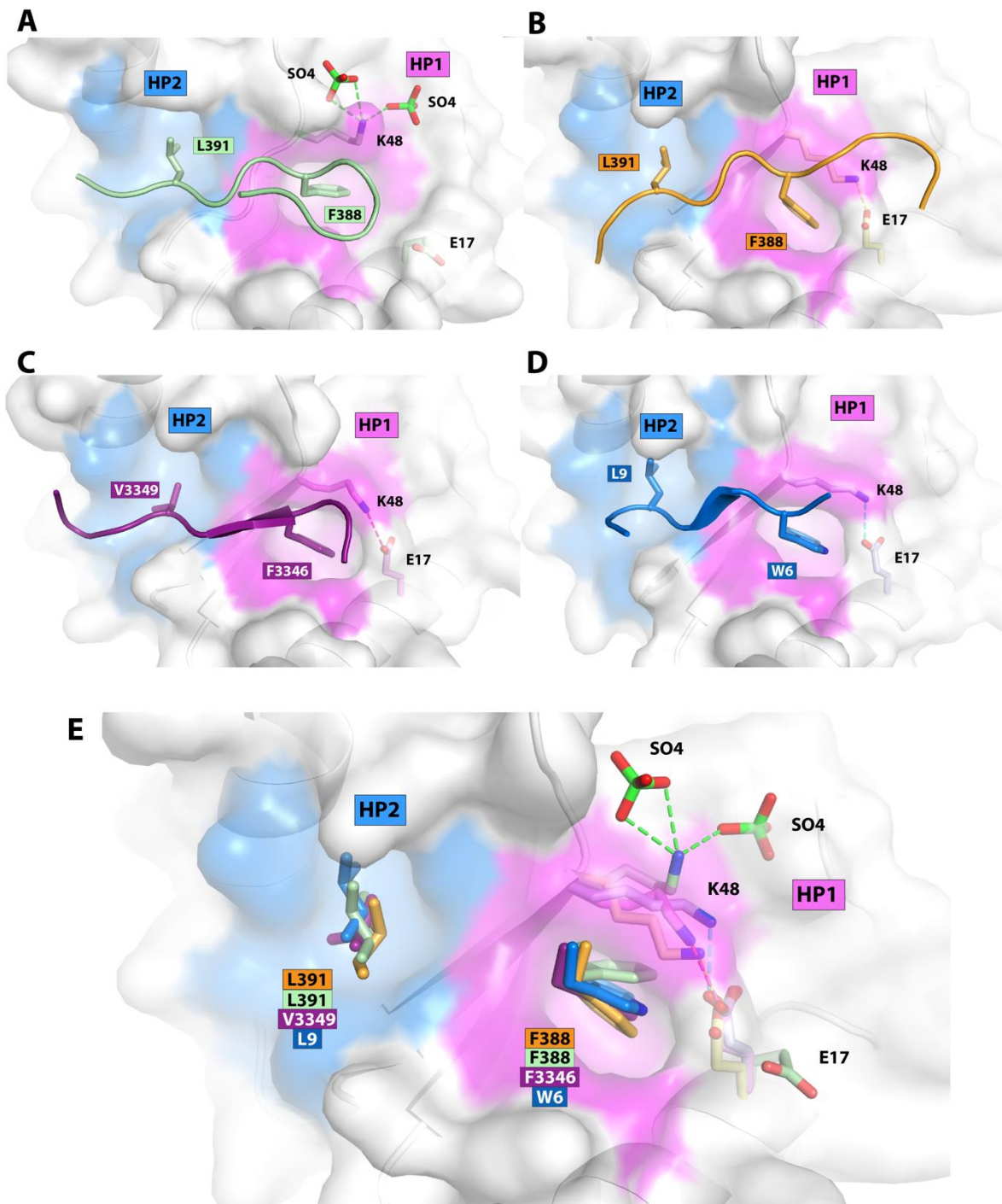


Figure S2. Comparison of the structures of the ATG4B LIR^C-GABARAPL1 complexes with published F- and W-type LIR-GABARAP crystal structures. Close-up of LDS for: (A) ATG4B LIR^C motif crystallized in the presence of ammonium sulphate bound to

GABARAPL1, **(B)** p-S392 (phosphorylated) ATG4B LIR^C motif bound to GABARAPL1, **(C)** WDFY3/ALFY LIR motif bound to GABARAP (PDB ID 3WIM), **(D)** CALR (calreticulin) LIR motif bound to GABARAP (PDB ID 3DOW). GABARAPL1 is displayed in white cartoon and transparent surface with the hydrophobic pocket 1 and 2 colored in pink and blue surfaces, respectively. Only the side chains of the 2 highly conserved hydrophobic residues binding to the GABARAP and GABARAPL1 hydrophobic pocket 1 and 2 are displayed in stick. The side chains of GABARAP and GABARAPL1 residues K48 and E17 are also displayed in stick. They are engaged in a hydrogen bond forming one side of the hydrophobic pocket 1 (HP1). In the ATG4B LIR^C structure crystallized in the presence of ammonium sulphate, K48 and E17 adopt a different conformation. K48 interacts with 2 sulphate anions and the resulting HP1 is much wider and allows ATG4B residue F388 to adopt a different conformation. **(E)** Superposition of **(A-D)**. For clarity, only the side chains of the 2 conserved hydrophobic residues from each LIR motif are displayed, as well as the surface and cartoon of the p-S392 (phosphorylated) ATG4B LIR^C-GABARAPL1 complex.

Figure S3

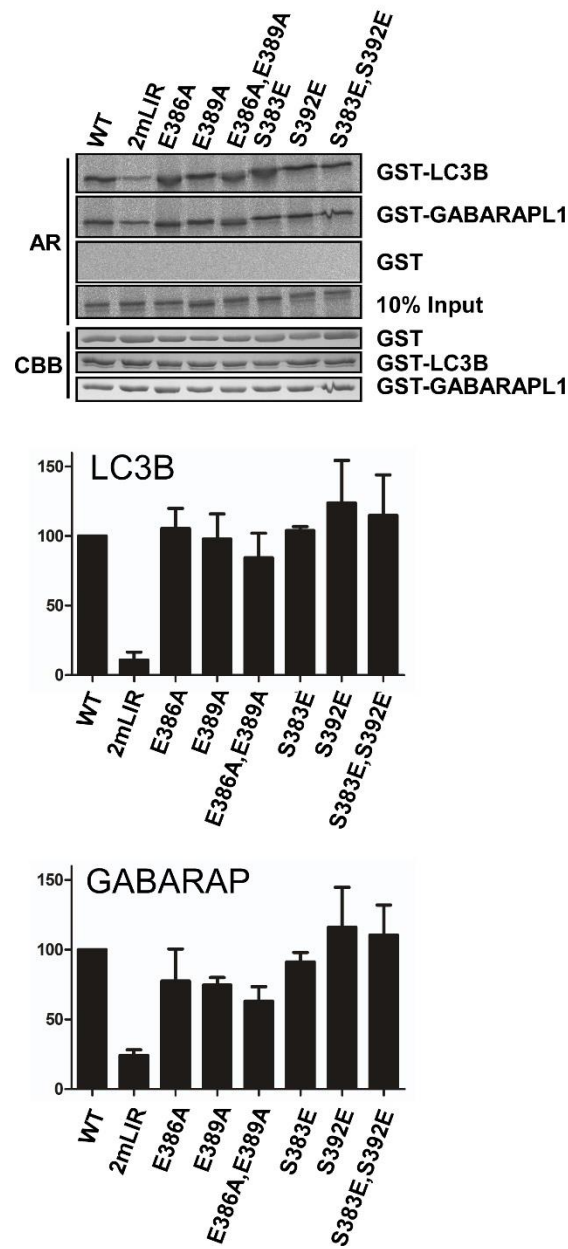


Figure S3. Full-length ATG4B (WT and indicated mutants) were in vitro translated and tested in GST affinity isolation assays for binding to GST-LC3B, GST-GABARAPL1 or GST. The quantification is based on 3 independent experiments.

Figure S4

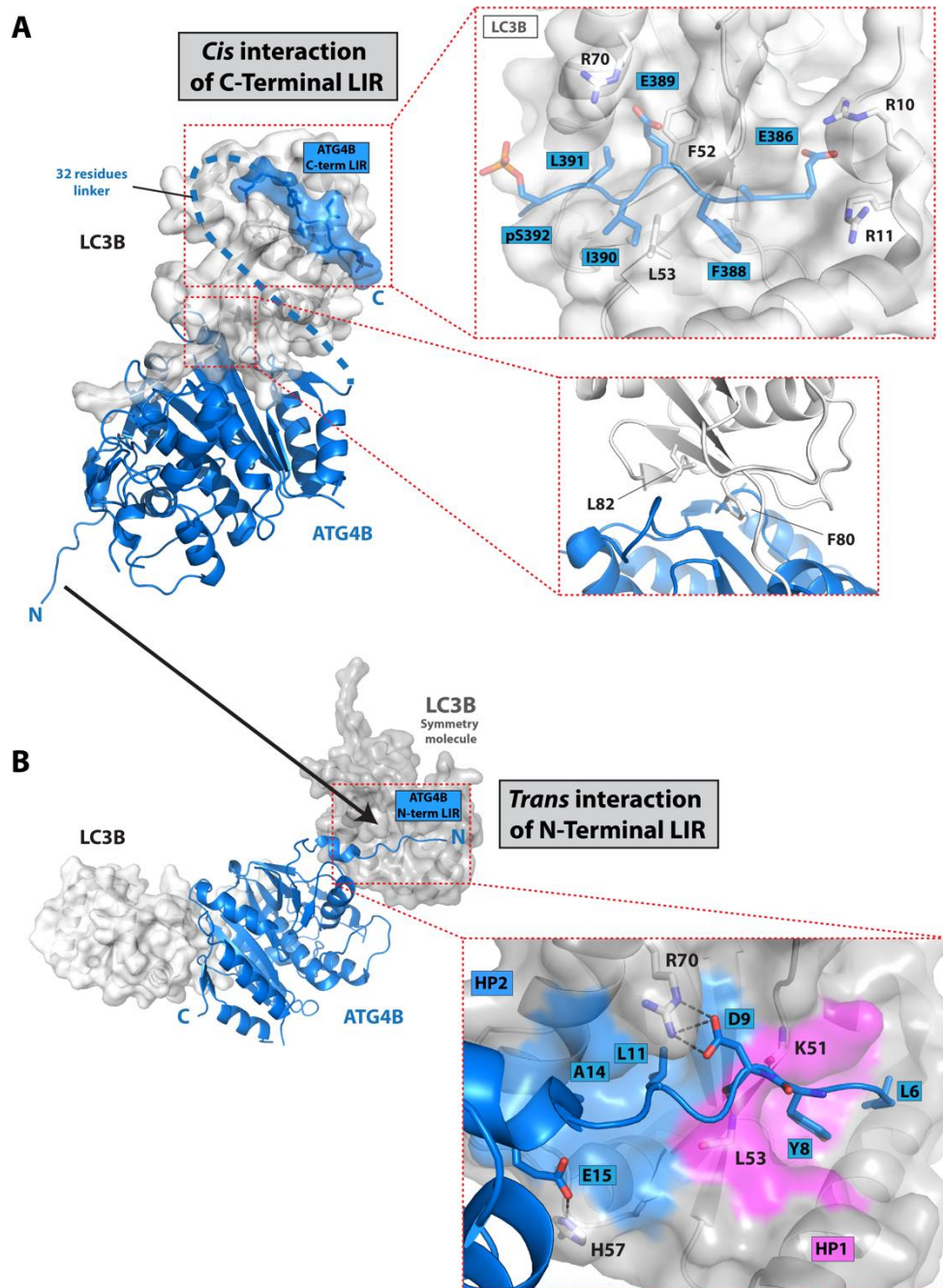


Figure S4. Model of full-length ATG4B bound to LC3B in *cis* and *trans*. (A) The structure of the phosphorylated ATG4B LIR^C motif bound to GABARAPL1 was superposed to the ATG4B (1 to 354)-LC3B complex (PDB ID: 2ZZP) in order to generate a model of the full-length ATG4B bound to LC3B. ATG4B is displayed in transparent blue cartoons and LC3B is displayed in white cartoons and transparent surface. The 32 missing residues connecting ATG4B C-terminal LIR motif to Q354 are represented by a dash line. (Top panel) View of

LC3B LDS. The superposed ATG4B LIR^C motif is displayed in transparent stick in the cartoon. (Bottom panel) View of the ATG4B catalytic site-substrate interaction. **(B)** *Trans* interaction of ATG4B N-terminal LIR motif with a symmetry related LC3B molecule. ATG4B is displayed in transparent blue cartoons and LC3B is displayed in white cartoons and transparent surface. The LC3B symmetry molecule interacting with ATG4B N-terminal LIR motif is displayed in gray.

Figure S5

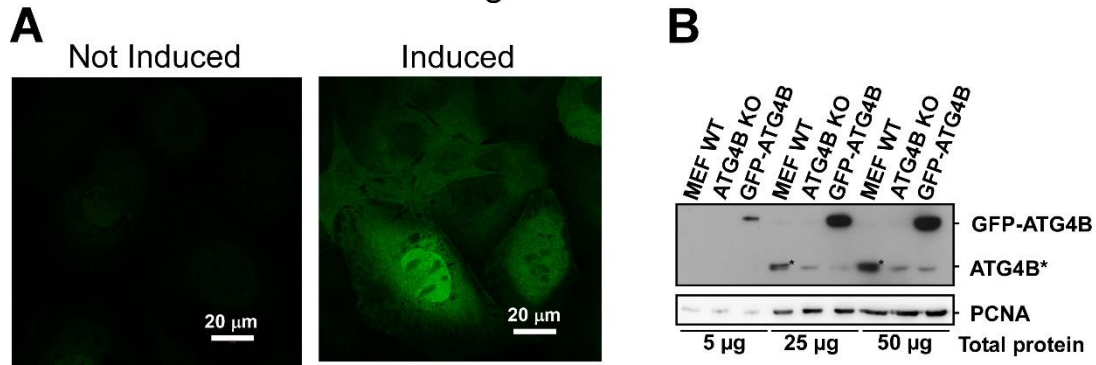


Figure S5. Expression of WT GFP-ATG4B in reconstituted *atg4b* KO MEFs. **(A)** Confocal images illustrating doxycycline induced expression of WT GFP-ATG4B. A nuclear localization of GFP-ATG4B were seen in about 10% of cells treated with doxycycline. **(B)** Dilution series comparing the level of GFP-ATG4B versus endogenous level of ATG4B. A sample of 5 μg of protein from GFP-ATG4B lysate is similar to 25 μg of sample from wild-type MEFs indicating a 5-fold higher level in the reconstituted cell line.

Figure S6

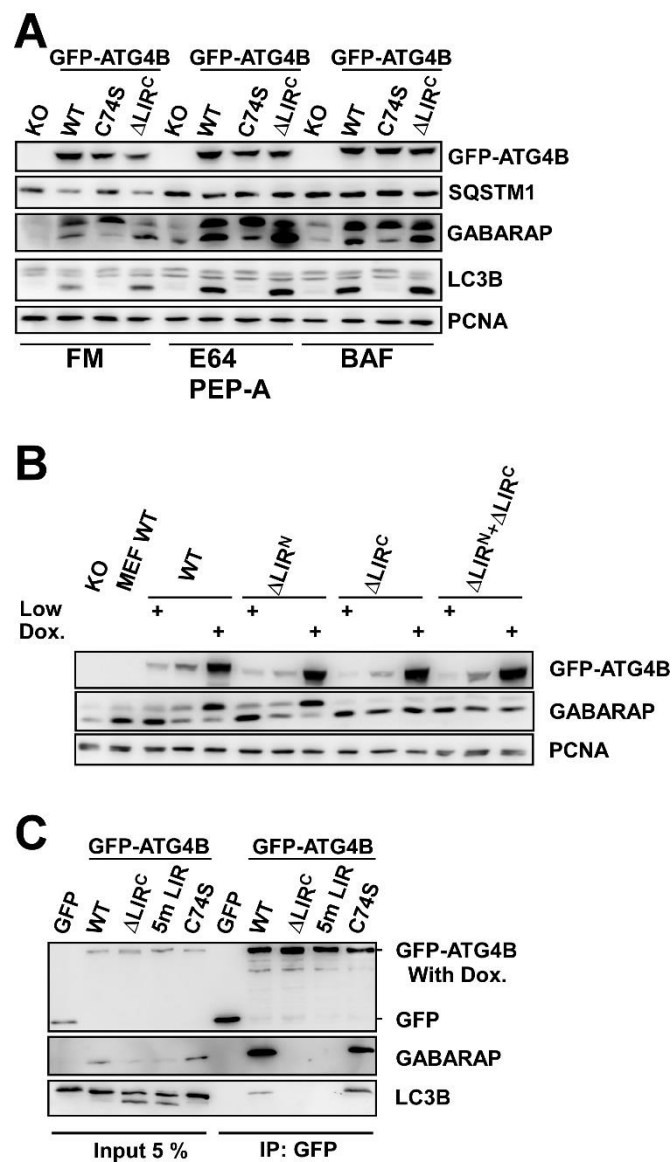


Figure S6. The C-terminal LIR in ATG4B is required for stabilization of GABARAP. **(A)** Inhibition of lysosomal proteases has a similar effect as BafA1 in *atg4b* KO cells or *atg4b* KO cells reconstituted with GFP-ATG4B, ATG4B^{C74S} or ΔLIR^C. Cells were treated or not with BafA1 (0.2 μM) or E64/Pepstatin A (5 μM and 10 μg/ml) for 8 h, and cell lysates analyzed by western blotting using the shown antibodies. **(B)** Deletion of the N-terminal LIR in ATG4B has no effect on stabilization or lipidation of GABARAP. *atg4b* KO cells, reconstituted with the indicated GFP-ATG4B constructs, were treated or not with doxycycline (1 μg/ml) for 24 h to induce expression, and cell lysates analyzed by western blotting. Low indicates selected

pools of cells with reduced expression of GFP-ATG4B. (C) Endogenous LC3 is less efficiently immunoprecipitated with GFP-ATG4B than GABARAP. *atg4b* KO cells reconstituted with the indicated GFP-ATG4B constructs were treated with 1 µg/ml doxycycline for 24 h before lysates were immunoprecipitated with GFP antibodies and analyzed by western blotting.

Figure S7

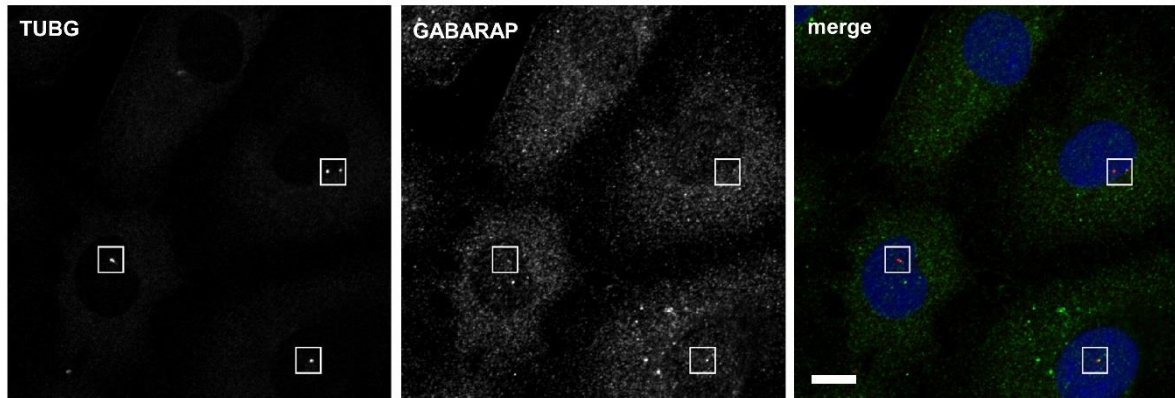


Figure S7. Endogenous GABARAP localizes to TUBG/ γ -tubulin-positive centrosomes and to perinuclear, cytoplasmic dots in *atg4b* KO MEFs reconstituted with WT GFP-ATG4B. The MEFs were immunostained using antibodies to TUBG/ γ -tubulin (red in merged image), to visualize centrosomes, and to GABARAP (green in merged image). Squares are used to indicate the colocalization between GABARAP and TUBG/ γ -tubulin in centrosomes. Scale bar: 20 μ m.